

SYNTHESES AND EVALUATION OF
^{99m}Tc(CO)₃ COMPLEXES OF DIFFERENTLY SUBSTITUTED
NITROIMIDAZOLES AS AGENTS FOR TARGETING TUMOR HYPOXIA

By

MADHAVA B. MALLIA

(Enrolment No. CHEM01200604036)

BHABHA ATOMIC RESEARCH CENTRE

A thesis submitted to the

Board of Studies in Chemical Science Discipline

In partial fulfillment of requirements

For the Degree of

DOCTOR OF PHILOSOPHY

of

HOMI BHABHA NATIONAL INSTITUTE



February, 2013

Homi Bhabha National Institute
Recommendations of the Viva Voce Board

As members of the Viva Voce Board, we certify that we have read the dissertation prepared by **Madhava B. Mallia** entitled “**Syntheses and Evaluation of $^{99m}\text{Tc}(\text{CO})_3$ Complexes of Differently Substituted Nitroimidazoles as Agents for Targeting Tumor Hypoxia**” and recommend that it may be accepted as fulfilling the dissertation requirement for the Degree of Doctor of Philosophy.

Chairman- Prof. K. L. Ramakumar

Date:

Member 1- Prof. M. R. A. Pillai

Date:

Member 2- Prof. S. Chattopadhyay

Date:

Convener- Prof. Sharmila Banerjee

Date:

Final approval and acceptance of this dissertation is contingent upon the candidates' submission of the final copies of the dissertation to HBNI.

I hereby certify that I have read this dissertation prepared under my direction and recommend that it may be accepted as fulfilling the dissertation requirement.

Date:

Place: Mumbai-400085

Guide - Prof. Sharmila Banerjee

STATEMENT BY AUTHOR

This dissertation has been submitted in partial fulfillment of requirement for an advanced degree at Homi Bhabha National Institute (HBNI) and is deposited in the Library to be made available to borrowers under rules of the HBNI.

Brief quotations from this dissertation are allowable without special permission, provided that accurate acknowledgement of source is made. Requests for permission for extended quotation from or reproduction of this manuscript in whole or in part may be granted by the Competent Authority of HBNI when in his or her judgment the proposed use of the material is in the interests of scholarship. In all other instances, however, permission must be obtained from the author.

Madhava B Mallia

DECLARATION

I, hereby declare that the investigation presented in the thesis has been carried out by me. The work is original and has not been submitted earlier as a whole or in part for a degree / diploma at this or any other Institution / University.

Madhava B Mallia

Dedicated to

My parents,

For the hardships they took to bring me up and educate me...

My wife,

For her inspiring criticism, encouragement and moral support...

And to all those who taught me something,

For making me who I am.

ACKNOWLEDGEMENTS

As I complete my PhD thesis, it is time to express my gratitude to all those people without whom this work would not have been possible. Research is truly an uncharted territory where one can easily get lost unless guided by a truly capable master, who has already explored it. I keep on record my sincere and heartfelt gratitude to my guide **Prof. Sharmila Banerjee**, who, like a beacon, showed me the right direction, when required, till I reached my destination. Frankly, as a student of science what I am today is because of my guide. She let me find my own ways to tackle the problems I faced in my work, but always kept a vigil on me and intervened when it was necessary. She made me self-reliant and nurtured my faculty of thinking. I learned from her the art of writing manuscript and continue to learn.

Now, I would like to express my sincere gratitude to **Prof. M. R. A. Pillai**, Head, Radiopharmaceuticals Division. It was Dr. Pillai, who initially suggested technetium tricarbonyl chemistry, when I joined Radiopharmaceuticals Division. Though his direct involvement in my research work has been minimal, he helped me realize my scientific capabilities by assigning scientific projects with steep deadlines. I am confident that this exercise will certainly help me in my career ahead. His suggestions during the preparation of this thesis were worthy and his advice worth remembering. Though my association with him was relatively short, this period in my career is something which I will cherish life-long.

It is my pleasure to thank **Prof. Meera Venkatesh**, former Head, Radiopharmaceuticals Division, and presently the Director, Division of Physical and Chemical Sciences, International Atomic Energy Agency (IAEA), Vienna, for her help in facilitating my work in Radiopharmaceuticals Division as well as for her inputs and suggestions during the preparation of some of the manuscripts included in my thesis.

I cannot forget **Dr. Kanchan Kothari (Retd.)**, for she initiated me into technetium tricarbonyl chemistry. Sincerity towards work and hard working attitude are virtues which I adopted from her. I thank her deep from my heart for all the help she has provided. I also thank **Dr. Grace Samuel**, Head, Radiopharmaceuticals Evaluation Section, for her help related to quality control of compounds reported in this thesis. It is a great pleasure for me to thank **Dr. H. D. Sarma**, Head, Laboratory animal facility and radioisotope laboratory, for helping me carrying out biological evaluations of all the compounds reported in this thesis. This work would not have been possible without his help.

I am grateful to **Prof. Roger Alberto**, the pioneer in the field of technetium tricarbonyl chemistry, for his invaluable suggestions and encouragement. I also thank him for arranging lyophilized kits for the preparation of technetium tricarbonyl precursor complex for my work. He was and he is my inspiration.

I am also grateful to the chairman, **Prof. K. L. Ramakumar** (Director, Radiochemistry and Isotope Group, BARC), former chairman, **Prof. V. Venugopal** (Former Director, Radiochemistry and Isotope Group, BARC), and member **Prof. S. Chattopadhyaya**, (Head, Bio-Organic Division, BARC) of the doctoral committee, for their critical assessment and suggestions provided during review of my work and pre-synopsis viva-voce.

Now, I would like to express my sincere thanks to my colleagues and intellectual partners **Dr. Anupam Mathur** and **Mr. Suresh Subramanian**. Work related discussions with them, irrespective of place and time, was a pleasure to remember and enriched my knowledge on diverse scientific topics. I also thank **Mr. Viju Chirayil** and **Mr. Vimalnath Nair** for their moral support, encouraging words and for posing questions related to my work which forced me search the literature.

I thank my colleagues in Radiopharmaceuticals Chemistry Section **Dr. Drishty Satpati, Dr. Tapas Das** and **Dr. Sudipta Chakraborty** for the help rendered to me whenever necessary. I also thank all the members of Radiopharmaceuticals Evaluation Section, especially **Dr. Aruna Korde**, who enlightened me on quality control aspects of radiopharmaceuticals. I thank **Dr. P. V. Joshi**, Head, Radiochemicals Section and all its members for regularly providing ^{99}Mo isotope for my work.

Finally, I gratefully acknowledge the help rendered by the technical staff Mr. A. D. Kadam, Mr. G. Gandhale, Mr. Umesh Kumar and Mr. U. Sukhale of RPhD, BARC.

February, 2013

Madhava B Mallia

CONTENTS		Page No.
SYNOPSIS		xiv
LIST OF FIGURES		xxvi
LIST OF TABLES		xxxviii
CHAPTER 1		
INTRODUCTION		
1.1.	Background	2
1.2.	Hypoxia and its causes	2
1.3.	Problems posed by hypoxia	2
1.4.	Measuring tumor hypoxia	4
1.4.1.	Invasive techniques	4
1.4.1.1.	Polarographic oxygen electrode	4
1.4.1.2.	Immuno-histochemical markers	5
1.4.2.	Non-invasive methods	6
1.4.2.1.	MRI	6
1.4.2.2.	Imaging using radiopharmaceuticals	7
1.5.	Radiopharmaceuticals	7
1.6.	Diagnostic radiopharmaceuticals	8
1.7.	Essential characteristics of a diagnostic radiopharmaceutical	9
1.8.	Radiopharmaceuticals for the detection of tumor hypoxia	11
1.8.1.	Non-nitroimidazole radiopharmaceuticals for the detection of hypoxia	11
1.8.2.	Nitroimidazole radiopharmaceuticals for the detection of hypoxia	12
1.8.2.1.	Evolution	12
1.8.2.2.	Nitroimidazole reduction process and hypoxia selectivity	13
1.8.2.3.	An overview of nitroimidazole radiopharmaceuticals	14
1.9.	Need for a SPECT radiopharmaceutical for detecting hypoxia	15
1.10.	Technetium-99m in nuclear medicine	16
1.10.1.	⁹⁹ Mo- ^{99m} Tc generator	17
1.10.2.	Radiolabeling with ^{99m} Tc: Available options	18

1.10.2.1.	Radiolabeling with $[\text{}^{99\text{m}}\text{TcO}]^{3+}$ and $[\text{}^{99\text{m}}\text{TcO}_2]^+$ core	19
1.10.2.2.	Radiolabeling with $[\text{}^{99\text{m}}\text{TcN}]^{2+}$ core	21
1.10.2.3.	Radiolabeling with $^{99\text{m}}\text{Tc-HYNIC}$ core	23
1.10.2.4.	Radiolabeling with $^{99\text{m}}\text{Tc}(\text{CO})_3$ core	24
1.11.	Quality control of radiopharmaceuticals	27
1.12.	Evaluation of radiopharmaceuticals	27
1.13.	Brief overview of present thesis	28
1.14.	Common materials and methods	29
1.14.1.	Solvents and chemicals	30
1.14.2.	Characterization of the ligands and intermediate compounds	30
1.14.3.	Preparation of $[\text{}^{99\text{m}}\text{Tc}(\text{CO})_3(\text{H}_2\text{O})_3]^+$ precursor complex	31
1.14.4.	Characterization of $[\text{}^{99\text{m}}\text{Tc}(\text{CO})_3(\text{H}_2\text{O})_3]^+$ precursor complex and various $^{99\text{m}}\text{Tc}(\text{CO})_3/\text{Re}(\text{CO})_3$ complexes	31
1.14.5.	Determination of partition coefficient ($\text{LogP}_{\text{o/w}}$)	32
1.14.6.	Serum stability studies	32
1.14.7.	Biological evaluation	33
1.14.7.1.	Tumor model	33
1.14.7.2.	Biodistribution studies	33
1.14.8.	Statistical analysis	34

CHAPTER 2

ANALYSIS OF THE EFFECT OF DIFFERENT PROPERTIES OF NITROIMIDAZOLE- $^{99\text{m}}\text{Tc}(\text{CO})_3$ COMPLEXES ON THEIR IN VIVO UPTAKE AND RETENTION IN HYPOXIC TUMOR

2.1.	Introduction	36
2.2.	Materials and methods	37
2.3.	Synthesis	37
2.3.1.	Synthesis of IDA derivatives of 2-, 4- and 5-nitroimidazole	37
2.3.1.1.	Synthesis of N,N-bis(<i>tert</i> -butoxycarbonyl)methyl -3-bromopropylamine (2a)	38
2.3.1.2.	Synthesis of N,N-bis(<i>tert</i> -butoxycarbonyl)methyl -3-(2-nitro-1H-imidazol-1-yl)-propane-1-amine (2b)	38
2.3.1.3.	Synthesis of N,N-bis(<i>tert</i> -butoxycarbonyl)methyl -3-	38

	(4-nitro-1H-imidazol-1-yl)-propane-1-amine (2c) and N,N-bis(<i>tert</i> -butoxycarbonyl)methyl)-3-(5-nitro-1H- imidazol-1-yl)-propane-1-amine (2d)	
2.3.1.4.	Synthesis of ligands 2L1 – 2L3	40
2.3.1.5.	Preparation of Re(CO) ₃ complex of ligand 2L1 (2e)	41
2.3.2.	Synthesis of DETA derivatives of 2-, 4- and 5-nitroimidazole	50
2.3.2.1.	Synthesis of <i>tert</i> -butyl 2-(2-(<i>tert</i> -butoxycarbonyl) aminoethyl)aminoethyl carbamate (2f)	50
2.3.2.2.	Synthesis of <i>tert</i> -butyl 2-((2-(<i>tert</i> -butoxycarbonyl) aminoethyl)(3-bromopropyl)amino)ethyl carbamate (2g)	51
2.3.2.3.	Synthesis of <i>tert</i> -butyl 2-((2-(<i>tert</i> -butoxycarbonyl) aminoethyl)(3-(2-nitro-1H-imidazol-1-yl)propyl) amino)ethyl carbamate (2h)	52
2.3.2.4.	Synthesis of <i>tert</i> -butyl 2-((2-(<i>tert</i> -butoxycarbonyl) aminoethyl)(3-(4-nitro-1H-imidazol-1-yl)propyl) amino)ethyl carbamate (2i)	52
2.3.2.5.	Synthesis of <i>tert</i> -butyl 2-((2-(<i>tert</i> -butoxycarbonyl) aminoethyl)(3-(5-nitro-1H-imidazol-1-yl)propyl) amino)ethyl carbamate (2j)	53
2.3.2.6.	Synthesis of ligands 2L4 – 2L6	54
2.3.2.7.	Preparation of Re(CO) ₃ complex of 2L6 (2l)	55
2.3.3.	Synthesis of AEG derivatives of 2-, 4- and 5-nitroimidazole	64
2.3.3.1.	Synthesis of <i>tert</i> -butyl 2-((<i>tert</i> -butoxycarbonyl) methylamino)ethyl carbamate (2m)	64
2.3.3.2.	Synthesis of <i>tert</i> -butyl 2-(((<i>tert</i> -butoxycarbonyl) methyl)(3-bromopropyl)amino)ethyl carbamate (2n)	65
2.3.3.3.	Synthesis of <i>tert</i> -butyl 2-(((<i>tert</i> -butoxycarbonyl) methyl)(3-(2-nitro-1H-imidazol-1-yl)propyl) amino)ethyl carbamate (2o)	65
2.3.3.4.	Synthesis of <i>tert</i> -butyl 2-(((<i>tert</i> -butoxycarbonyl) methyl)(3-(4-nitro-1H-imidazol-1-yl)propyl) amino)ethyl carbamate (2p)	66

2.3.3.5.	Synthesis of <i>tert</i> -butyl 2-(((<i>tert</i> -butoxycarbonyl) methyl)(3-(5-nitro-1H-imidazol-1-yl)propyl) amino)ethyl carbamate (2q)	67
2.3.3.6.	Synthesis of ligands 2L7 – 2L9	67
2.3.3.9.	Preparation of Re(CO) ₃ complex of 2L8 (2r)	69
2.3.4.	General work-up procedure for compounds 2a-2d, 2g-2k and 2m-2q	77
2.3.5.	General procedure for the hydrolysis of Boc- and <i>tert</i> -butyl ester groups in compounds 2b – 2d, 2h – 2j and 2o – 2q	77
2.4.	Radiolabeling	77
2.4.1.	General procedure for the preparation of ^{99m} Tc(CO) ₃ complexes of ligands 2L1-2L9	77
2.5.	Quality control	77
2.6.	Biological evaluation	77
2.7.	Results and discussion	78
2.7.1.	Synthesis	78
2.7.2.	Radiolabeling, quality control and characterization	81
2.7.3.	Biological evaluation	85
2.7.4.	Conclusions	98

CHAPTER 3

MODIFIED 2-NITROIMIDAZOLE-^{99m}Tc(CO)₃ COMPLEX WITH IMPROVED PHARMACOKINETICS FOR TARGETING TUMOR HYPOXIA

3.1.	Introduction	101
3.2.	Materials and methods	102
3.3.	Synthesis	103
3.3.1.	Synthesis of 1-(2-(2-bromoethoxy)ethyl)-2-nitro-1H-imidazole (3a)	103
3.3.2.	Synthesis of 2-(2-(2-(2-nitro-1H-imidazol-1-yl)ethoxy)ethyl) isoindoline-1,3-dione (3b)	104
3.3.3.	Synthesis of 1-(2-(2-aminoethoxy)ethyl)-2-nitro-1H-imidazole (3c)	104
3.3.4.	Synthesis of 1-(N,N-bis(<i>tert</i> -butoxycarbonylmethyl)-2-(2-(2-	105

	nitroimidazolyl)ethoxy) ethane (3d)	
3.3.5.	Synthesis of 2-(carboxymethyl(2-(2-nitroimidazolyl ethoxy)ethyl)amino)acetic acid (3e)	105
3.3.6	Synthesis of Re(CO) ₃ complex of ligand 3e (3f)	106
3.4.	Results and discussion	111
3.4.1.	Synthesis	111
3.4.2.	Radiolabeling, quality control and characterization	111
3.4.3.	Biological studies	113
3.5.	Conclusions	117

CHAPTER 4

PREPARATION OF ^{99m}Tc(CO)₃-ANALOGUE OF [¹⁸F]FLUOROMISONIDAZOLE

4.1.	Introduction	120
4.2.	Materials and methods	122
4.3.	Synthesis	122
4.3.1.	Synthesis of 2-(2-hydroxy-3-(2-nitro-1H-imidazol-1-yl)propyl) isoindoline-1,3-dione (4a)	122
4.3.2.	Synthesis of 1-amino-3-(2-nitro-1H-imidazol-1-yl)propan-2-ol hydrochloride (4b)	123
4.3.3.	Synthesis of N, N-bis(<i>tert</i> -butoxycarbonylmethyl)-((2-hydroxy)-3-(2-nitroimidazolyl))propyl amine (4c)	123
4.3.4.	Synthesis of 2-(N-carboxymethyl, N-((2-hydroxy)-3-(2-nitroimidazolyl)propyl)amino)acetic acid (4d)	124
4.3.5.	Preparation of Re(CO) ₃ complex of compound 4d (4e)	124
4.4.	Results and discussion	127
4.4.1.	Synthesis	127
4.4.2.	Radiolabeling, quality control and characterization	128
4.4.3.	Biological studies	129
4.5.	Conclusions	133
	EPILOGUE	136
	REFERENCES	138
	LIST OF PUBLICATIONS	153

SYNOPSIS

Cancer is one of the most dreaded diseases which cause about 12% of all deaths worldwide, and an estimated 2.5 million people suffer from this disease in India. Therefore, an effort to develop new drugs and strategies to control or cure this disease is a priority. While planning treatment strategy, an accurate assessment of the clinical status of the disease is essential to ensure the expected clinical outcome. Thus, the choice of the clinical probe and its ability to provide the required information itself becomes a major consideration. In this context, development of effective probes to obtain clinical status of a disease becomes as important as the development of new drugs and strategies.

A major cause for the cancerous lesions to be resistant to the treatment modalities such as chemotherapy and radiotherapy is hypoxia. It is a pathological condition where a certain region in the body has inadequate levels of oxygen. There are several causes for hypoxia,¹ including pathological conditions such as oncology, cardiovascular disease, cerebrovascular disease, diabetes, infection and wound healing.² However, it is hypoxia in cancerous lesions that is more detrimental as it has direct implications on the prognosis and therapeutic outcome of the disease. Experimental and clinical evidence has clearly established the negative influence of hypoxia in tumor propagation, malignant progression and resistance to radiation therapy and chemotherapy.³⁻⁹

The resistance of hypoxic cells to radiation therapy and chemotherapy was known as early as 1953, when well oxygenated tumor cells were found to exhibit three-fold greater response to radiotherapy compared to anoxic cells.¹⁰ Potential issues posed by hypoxia in cancerous lesions are extensively reviewed.^{10, 11} Hypoxia posed significant problems to the clinical oncologists compelling them to assess the hypoxic status of the cancerous lesions so that appropriate alterations can be made to the therapeutic strategy. Knowledge on hypoxic status of the cancer can also help the physicians to isolate patients who may be benefited

from hypoxia-directed treatment from those who will not, thereby avoiding unnecessary discomfort to latter group of patients already in a state of deteriorated health conditions. These factors adequately substantiate the significance of detection of hypoxia in cancer and the relevance of developing efficient techniques to achieve this objective.

There are several methods to detect and quantify hypoxia in tumor which can be broadly classified into invasive and non-invasive. However, invasive methods have several drawbacks and most of these techniques are applicable only to superficial tumors.¹² Therefore, non-invasive techniques are preferred over invasive techniques.

Currently, imaging using radiopharmaceuticals and Magnetic Resonance Imaging (MRI) are the two non-invasive modalities available for the detection and quantification of hypoxia. MRI combines morphological imaging with limited functional imaging. Though the spatial resolution of the images obtained using MRI technique is high, sensitivity is low and, it often requires appreciable quantity of contrast agents, which may be toxic to the body, to obtain images of acceptable quality. On the other hand, radiopharmaceuticals with their high sensitivity and ability to provide functional information of organs/tissue are considered superior to MRI.

Radiopharmaceuticals are defined as radioactive drugs that can be used in vivo for the diagnosis or monitoring of a disease or its manifestation as well as for therapy of a disease in a body. Diagnostic and therapeutic radiopharmaceuticals essentially differ in the nature of radioisotope contained in the radiopharmaceutical. While diagnostic radioisotopes are preferably pure gamma or positron emitters, therapeutic radioisotopes invariably emits particulate radiations with or without accompanying gamma emissions.

The radiopharmaceutical for the detection of hypoxia relies on the oxygen dependent chemical change of the tracer molecule, which results in the accumulation of the radiotracer in the hypoxic cells, thereby enabling the detection and delineation of hypoxic tissue from

oxygenated tissue. Majority of radiopharmaceuticals developed and evaluated for the detection of hypoxia are based on nitroimidazoles. The two prominent non-nitroimidazole radiopharmaceuticals are $^{62/64}\text{Cu-ATSM}^{13,14}$ and $^{99\text{m}}\text{Tc-HL-91}^{15}$.

Nitroimidazoles undergo selective reduction, mediated by nitroreductase enzyme, and gets subsequently trapped in viable hypoxic cells. This selectivity could be utilized to detect hypoxic cells in vivo, if a suitable radioisotope is tagged to nitroimidazole. Following this approach, several nitroimidazole-based molecules labeled with positron emitting¹⁶⁻¹⁹ or gamma emitting^{12,20,21} radioisotopes are evaluated for their potential to target tumor hypoxia. Positron Emission Tomography (PET) is employed for imaging positron emitting radiopharmaceuticals and Single Photon Emission Computed Tomography (SPECT) is used for gamma emitting radiopharmaceuticals. ^{18}F -fluoromisonidazole (FMISO), a PET-radiopharmaceutical, is probably the most widely used radiopharmaceutical for detection of tumor hypoxia.²² However, due to high lipophilicity, FMISO shows uptake in brain and clears slowly through hepatobiliary route.^{23,24} Slow clearance of activity from the body required delayed imaging to obtain images of acceptable quality. However, relatively short half-life of ^{18}F (109.8 min) imposed a limit to the delay in imaging. In general, availability of a cyclotron for the production of positron emitting radioisotopes, necessity of automated modules for the preparation of PET-radiopharmaceuticals and the requirement of a PET camera makes PET-based radiopharmaceuticals far from being cost-effective. On the other hand, SPECT machines are relatively economical and recent advances in SPECT technology have tremendously reduced the gap between SPECT and PET in terms of image resolution.²⁵ Hence, a SPECT-based radiopharmaceutical for imaging hypoxia that can provide diagnostic information comparable to that obtained using a PET-based radiopharmaceutical, such as [^{18}F]-FMISO, will be preferred and may find wider applicability. Among different SPECT isotopes, $^{99\text{m}}\text{Tc}$ with its ideal decay characteristics, optimal half-life, versatile chemistry, cost-

effectiveness and availability is still the irrefutable leader, which earned it the name “work horse of nuclear medicine”.

Technetium belongs to group VIIB of the periodic table with electronic configuration $[\text{Kr}]4d^65s^1$ (neutral atom). It shows variable oxidation states ranging from +7 to -1, +7 being the most stable oxidation. This oxidation state is encountered in technetium obtained as pertechnetate ($^{99m}\text{TcO}_4^-$) from $^{99}\text{Mo}/^{99m}\text{Tc}$ generator.²⁶ Technetium in +7 oxidation state being least reactive, its reduction from +7 oxidation state is necessary to bind it with suitable organic ligands to obtain the required radiopharmaceutical. In aqueous solution, reduction of $^{99m}\text{TcO}_4^-$ in the absence of any stabilizing ligands leads to the formation of colloidal $^{99m}\text{TcO}_2$. Hence, to obtain the required radiopharmaceutical in good yield, it is often necessary to have large excess of ligand (large ligand to metal ratio) in solution, especially when the kinetics of complex formation is slow compared to the kinetics of reduction of ^{99m}Tc .²⁷ Use of excess ligand is a drawback in the case of receptor targeting radiopharmaceuticals, since the free ligand also competes with the radiolabeled ligand for the limited number of receptors available on the cancerous cells. The competition significantly decreases the binding of the radiolabeled ligand compromising the quality of the image to a great extent.

The introduction of the radiosynthetic precursor $[\text{}^{99m}\text{Tc}(\text{CO})_3(\text{H}_2\text{O})_3]^+$ by Alberto et al., which can be prepared in aqueous solution under mild conditions, opened up the possibility of radiolabeling ligands with high specific activity (low ligand to metal ratio).²⁸ Unlike ^{99m}Tc -oxo core ($[\text{}^{99m}\text{Tc}(\text{V})\text{O}]^{3+}$) and ^{99m}Tc -dioxo core ($[\text{}^{99m}\text{Tc}(\text{V})\text{O}_2]^+$), the $[\text{}^{99m}\text{Tc}(\text{CO})_3(\text{H}_2\text{O})_3]^+$ core is stable over a wide range of pH (1-13)²⁸ and immune to re-oxidation to $^{99m}\text{TcO}_4^-$. Since ^{99m}Tc is already stabilized in +1 oxidation state, use of excess ligand can be avoided while radiolabeling with $[\text{}^{99m}\text{Tc}(\text{CO})_3(\text{H}_2\text{O})_3]^+$ core. Ligands containing donor atoms like N, O, S etc. are suitable for replacing the three labile water molecules in $[\text{}^{99m}\text{Tc}(\text{CO})_3(\text{H}_2\text{O})_3]^+$ core to form octahedral complexes. The

$[\text{}^{99\text{m}}\text{Tc}(\text{CO})_3(\text{H}_2\text{O})_3]^+$ core is lipophilic with an overall charge of +1. However, through appropriate selection of the donor ligands, the lipophilicity and charge on the resulting complex could be altered thereby opening up the possibility of fine tuning the in vivo pharmacokinetics of the molecule.

In the present thesis, several $^{99\text{m}}\text{Tc}(\text{CO})_3$ -labeled nitroimidazole complexes are envisaged, synthesized and an attempt has been made to study the effect of different parameters, such as single electron reduction potential (SERP), lipophilicity as well as overall charge on the nitroimidazole- $^{99\text{m}}\text{Tc}(\text{CO})_3$ complex, which decides the in vivo efficacy of these agents to target tumor hypoxia. The logical conclusions derived from the in vivo evaluation of these complexes in suitable tumor bearing animal models were further utilized to develop new/modified hypoxia targeting agents.

The thesis consists of four chapters and the contents of each of the chapters are briefly mentioned below.

CHAPTER 1: INTRODUCTION

This chapter highlights the role played by ‘Hypoxia’ in the clinical management of cancer and the necessity to develop methods to detect and quantify hypoxia in cancerous lesions. Various techniques that are presently available for the detection of hypoxia are discussed and the advantages of non-invasive imaging methods using radiopharmaceuticals are emphasized. Brief account of different radiopharmaceuticals for imaging hypoxia, including those which are in clinical use, is provided with particular mention on nitroimidazole based radiopharmaceuticals. This chapter also brings to light the importance of $^{99\text{m}}\text{Tc}$, a SPECT isotope, in the era of PET and also discusses different labeling approaches with this isotope, with emphasis on labeling with $[\text{}^{99\text{m}}\text{Tc}(\text{CO})_3(\text{H}_2\text{O})_3]^+$ core. A short account of quality control methods, biological study protocols etc., which will be common for evaluating different labeled molecules mentioned throughout the thesis, is provided.

CHAPTER 2: ANALYSIS OF THE EFFECT OF DIFFERENT PROPERTIES OF NITROIMIDAZOLE-^{99m}Tc(CO)₃-COMPLEXES ON THEIR IN VIVO UPTAKE AND RETENTION IN HYPOXIC TUMOR

Prediction of the in vivo behavior of foreign agents designed for a specific task in biological systems is extremely difficult, owing to different factors involved in deciding the overall pharmacokinetics. Nevertheless, by systematic experimentation and careful evaluation of the results, certain logical conclusions can be derived which can provide insights while tailoring of new molecules.

For nitroimidazole-^{99m}Tc(CO)₃ complexes, three important properties viz. lipophilicity, SERP and overall charge of the complex, could be linked to the hypoxia targeting efficacy as well as the pharmacokinetic behavior in vivo. Lipophilicity is essential for any complex to enter the cell by passive diffusion, especially when active transport mechanism is not available for crossing the cell membrane. Once the complex enters a viable hypoxic cell, the efficiency of reduction and subsequent trapping of the complex is decided by SERP. The overall charge on the complex plays a role in deciding the clearance of the complex from the body.

To study the effect of these properties on the uptake and retention of the complex in vivo, several nitroimidazole-^{99m}Tc(CO)₃ complexes which differ in their lipophilicity, SERP and overall charge are prepared. As the SERP of the nitroimidazole depends on the position of nitro group in the imidazole ring, a set of ^{99m}Tc(CO)₃ complexes with different SERP could be prepared from appropriately functionalized 2-, 4- and 5-nitroimidazole ligands. Different ligands synthesized to achieve this objective are shown in Fig. 1. The choice of tridentate ligands viz. iminodiacetic acid (IDA), aminoethylglycine (AEG) and diethylenetriamine (DETA) was made keeping in mind the objective of achieving -1, 0 and +1 overall charge on the complexes of 2-, 4- and 5-nitroimidazole. The [^{99m}Tc(CO)₃(H₂O)₃]⁺

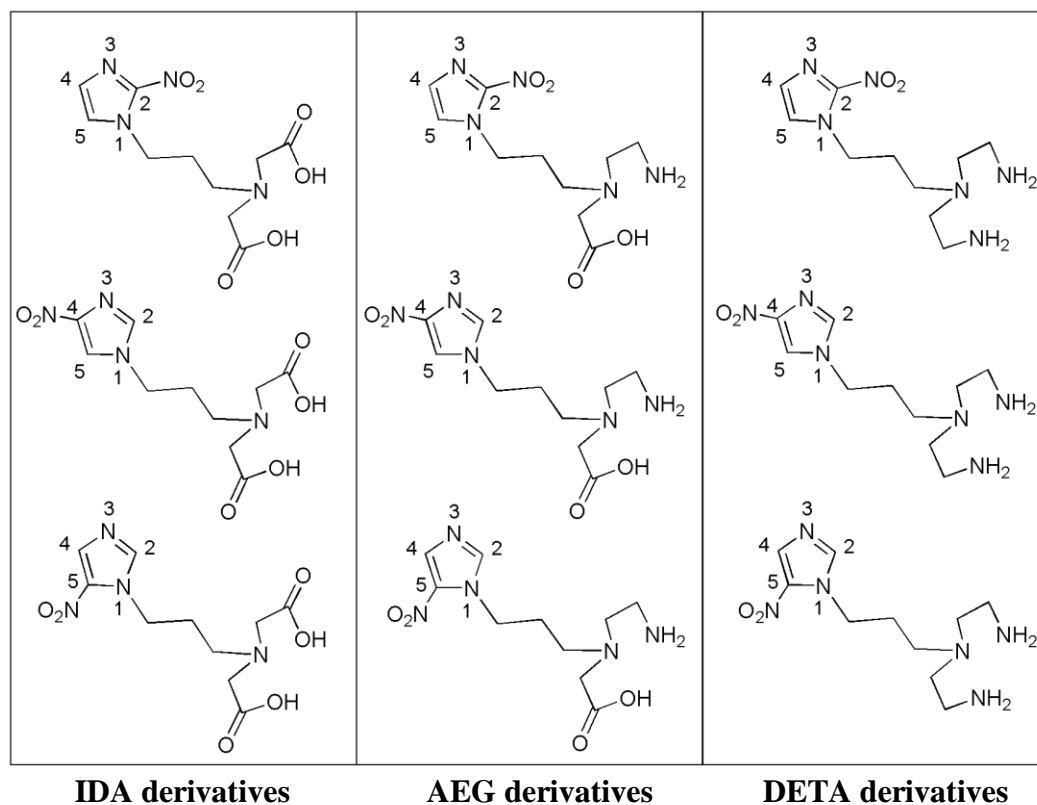


Fig. 1. Nitroimidazole ligands synthesized to prepare $^{99m}\text{Tc}(\text{CO})_3$ complexes with different SERP, lipophilicity and overall charge

core which has an overall charge of +1, on complexation with iminodiacetic acid (IDA) ligand forms a complex with an overall charge of -1. Similarly, aminoethylglycine (AEG) and diethylenetriamine (DETA) forms neutral and positively charged complexes respectively on complexation with the $[\text{}^{99m}\text{Tc}(\text{CO})_3(\text{H}_2\text{O})_3]^+$ core. Typical structures of differently substituted nitroimidazole- $^{99m}\text{Tc}(\text{CO})_3$ complexes are shown in Fig. 2.

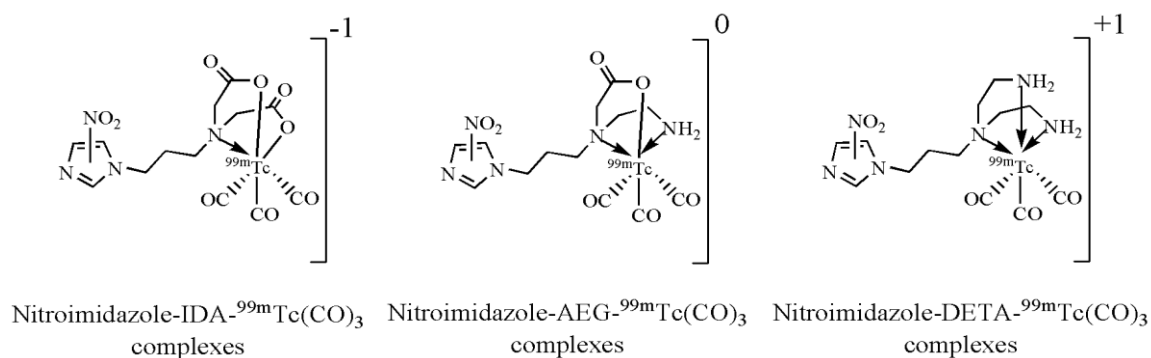


Fig. 2. Typical structures of nitroimidazole- $^{99m}\text{Tc}(\text{CO})_3$ complexes

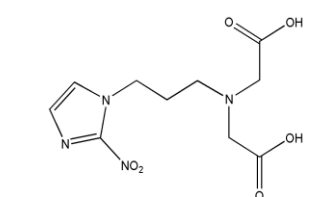
The synthetic modifications made to 2-, 4- and 5-nitroimidazole itself leads to variations in lipophilicity of the corresponding $^{99m}\text{Tc}(\text{CO})_3$ -complexes. To establish the structure of the nitroimidazole- $^{99m}\text{Tc}(\text{CO})_3$ complexes formed in the tracer level, corresponding $^{185/187}\text{Re}(\text{CO})_3$ complex of 2-nitroimidazole from each series viz. IDA, AEG and DETA are prepared and characterized by $^1\text{H-NMR}$.

The preparation and biological evaluation of a set of nine nitroimidazole- $^{99m}\text{Tc}(\text{CO})_3$ complexes, with different SERP, overall charge and lipophilicity, forms the core content of this chapter. The results obtained are analyzed and logical conclusions are drawn which can serve as guidelines for future work on identification and development of suitable nitroimidazoles.

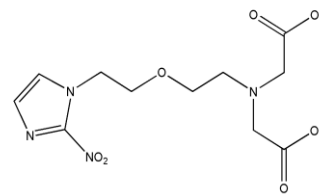
CHAPTER 3: MODIFIED 2-NITROIMIDAZOLE- $^{99m}\text{Tc}(\text{CO})_3$ COMPLEX WITH IMPROVED PHARMACOKINETICS FOR TARGETING TUMOR HYPOXIA

In this chapter, re-designing of 2-nitroimidazole-IDA- $^{99m}\text{Tc}(\text{CO})_3$ complex, which has emerged as the best candidate as far as the tumor uptake and retention is concerned, was attempted to improve its pharmacokinetics.

The complex showed uptake and slow clearance from liver which limited its utility to image tumors in abdominal region. For faster clearance from liver, the propylene spacer in the original complex was replaced with an ether spacer



Original 2-nitroimidazole-IDA derivative



Modified 2-nitroimidazole-IDA derivative with ether spacer

Fig. 3.

(Fig. 3) which supposedly hydrolyses in liver leading to faster clearance of activity from the organ. The synthesis involved five steps starting with the synthesis of 1-(2-(2-bromoethoxy)ethyl)-2-nitro-1H-imidazole from 2-nitroimidazole and 2-bromoethylether. The 2-nitroimidazole bromo derivative was subsequently converted to corresponding amine, 2-(2-(2-nitro-1H-imidazol-1-yl)ethoxy)ethanamine hydrochloride, via Gabriel phthalimide

synthesis. The amine is then converted to di-*tert*-butylester derivative which upon hydrolysis gave the target ligand.

The ligand was radiolabeled with $[^{99m}\text{Tc}(\text{CO})_3(\text{H}_2\text{O})_3]^+$ core following optimized protocol. Corresponding $^{185/187}\text{Re}(\text{CO})_3$ complex was also prepared in macroscopic scale to establish the structure of the $^{99m}\text{Tc}(\text{CO})_3$ -complex prepared at the tracer level.

The biological evaluation of the complex was carried out in suitable tumor bearing animal model. As per the expectation, while retaining its favorable tumor uptake characteristics, results clearly indicated faster clearance of activity from liver in case of the present complex compared to that of the 2-nitroimidazole-IDA- $^{99m}\text{Tc}(\text{CO})_3$ complex.

CHAPTER 4: PREPARATION OF $^{99m}\text{Tc}(\text{CO})_3$ -ANALOGUE OF [^{18}F]FLUORO MISONIDAZOLE

This chapter deals with the synthesis, radiolabeling and biological evaluation of ^{99m}Tc analogue of [^{18}F]-fluoromisonidazole which is a PET based radiopharmaceutical currently being used in the clinic for imaging tumor hypoxia. Here, an attempt was made to combine the favorable hypoxia targeting property of misonidazole with the favorable nuclear characteristics of ^{99m}Tc . To achieve this, an IDA derivative of misonidazole was synthesized to facilitate radiolabeling using

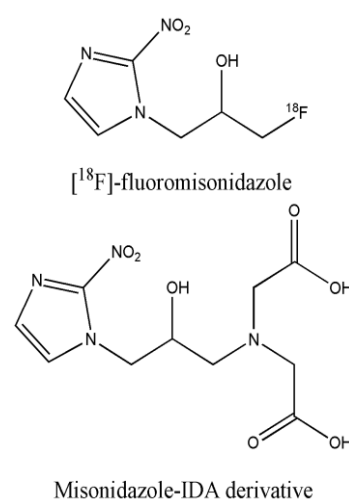


Fig. 4.

fluoromisonidazole as shown in Fig. 4.

The target ligand was synthesized in four steps starting with 2-nitroimidazole and 2,3-epoxypropylphthalimide. The intermediate compound, 2-(2-hydroxy-3-(2-nitro-1H-imidazol-1-yl)propyl)isoindoline-1,3-dione, was purified and hydrolyzed to obtain corresponding amine which was subsequently converted into di-*tert*-ester derivative by

reacting with *tert*-butylbromoacetate. The ester derivative was hydrolyzed to obtain the target ligand.

The ligand was radiolabeled with [$^{99m}\text{Tc}(\text{CO})_3(\text{H}_2\text{O})_3$] $^+$ core following the optimized protocol. Corresponding $^{185/187}\text{Re}(\text{CO})_3$ complex was also prepared in macroscopic level for further characterization by ^1H -NMR. The radiolabeled complex as well as [^{18}F]-fluoromisonidazole was evaluated in vivo in fibrosarcoma tumor bearing animal model. The results are thoroughly analyzed and discussed.

References

1. Hockel M., Vaupel P. *J. Natl. cancer Inst.*, **2001**, 93(4), 266.
2. Weibe L. I., Machulla H. J. *Imaging Hypoxia. Netherlands: Kluwer Academic Publishers (Ed. Machulla H. J.)*, **1999**, 1.
3. Höckel M., Schlenger K., Aral B., Mitze M., Schäffer U., Vaupel P. *Eur. J. Nucl. Med. Mol. Imaging*, **2009**, 36, 1674.
4. Fyles A. W., Milosevic M., Wong R., Kavanagh M. C., Pintilie M., Sun A., Chapman W., Levin W., Manchul L., Keane T. J., Hill R. P. *Radiother. Oncol.*, **1998**, 48, 149.
5. Nordsmark M., Overgaard M., Overgaard J. *Radiother. Oncol.*, **1996**, 41, 31.
6. Brizel D. M., Sibley G. S., Prosnitz L. R., Scher R. L., Dewhirst M. W. *Int. J. Radiat. Oncol. Biol. Phys.*, **1997**, 38, 285.
7. Nordsmark M., Bentzen S. M., Rudat V., Brizel D., Lartigau E., Stadler P., Becker A., Adam M., Molls M., Dunst J., Terris D. J., Overgaard J. *Radiother. Oncol.*, **2005**, 77, 18.
8. Duffy J. P., Eibl G., Reber H. A., Hines O. J. *Molecular Cancer*, **2003**, 2, 12.
9. Brizel D. M., Scully S. P., Harrelson J. M., Layfield L. J., Bean J. M., Prosnitz L. R., Dewhirst M. W. *Cancer Res.*, **1996**, 56, 941.
10. Gray L. H., Conger A. D., Ebert M. *Br. J. Radiol.*, **1953**, 26, 683.

11. McKeown S. R., Cowen R. L., Williams K. J. *Clin. Oncol.*, **2007**, *19*(6), 427.
12. Mallia M. B., Banerjee S., Venkatesh M. *Technetium-99m Radiopharmaceuticals: Status and Trends. Vienna: IAEA*, **2009**, 295.
13. Fujibayashi Y., Taniuchi H., Yonekura Y., Ohtani H., Konishi J., Yokoyama A. *J. Nucl. Med.*, **1997**, *38*, 1155.
14. Dearling J. L. D., Lewis J. S., Mullen G. E. D., Rae M. T., Zweit J., Blower P. J. *Eur. J. Nucl. Med.*, **1998**, *25*, 788.
15. Honess D. J., Hill S. A., Collingridge D. R., Edwards B., Brauers G., Powell N. A., Chaplin D. J. *Int. J. Radiat. Oncol. Biol. Phys.*, **1998**, *42*(4), 731.
16. Lee S. T., Scott A. M. *Semin. Nucl. Med.*, **2007**, *37*, 451.
17. Piert M., Machulla H. J., Picchio M., Reischl G., Ziegler S., Kumar P., Wester H. J., Beck R., McEwan A. J., Wiebe L. I., Schwaiger M. *J. Nucl. Med.*, **2005**, *46*, 106.
18. Reischl G., Dorow D. S., Cullinane C., Katsifis A., Roselt P., Binns D., Hicks R. J. *J. Pharm. Pharm. Sci.*, **2007**, *10*, 203.
19. Yang D. J., Wallace S., Cherif A., Li C., Gretzer M. B., Kim E. E., Podoloff D. A. *Radiology.*, **1995**, *194*: 795.
20. Rumsey W. L., Cyr, J. E., Raju N., Narra R. K. *Biochem. Biophys. Res. Commun.*, **1993**, *193*(3), 1239.
21. Melo T., Duncan J., Ballinger J. R., Rauth A. M. *J. Nucl. Med.*, **2000**, *41*, 169.
22. Lee S. T., Scott A. M. *Semin Nucl Med.*, **2007**, *37*, 451.
23. Koh W. J., Rasey J. S., Evans M. L., Grierson J. R., Lewellen T. K., Graham M. M., Krohn K. A., Griffin T. W.. *Int. J. Radiat. Oncol. Biol. Phys.*, **1992**, *22*, 199.
24. Valk P. E., Mathis C. A., Prados M. D., Gilbert J. C., Budinger T. F. *J. Nucl. Med.*, **1992**, *33*, 2133.
25. Rahmim A., Zaidi H. *Nucl. Med. Comm.*, **2008**, *29*(3), 193.

26. Boyd R. E. *Int. J. Appl. Radiat. Isot.*, **1982**, 33(10), 801.
27. Level S. Z., *Principles of Nuclear Medicine. Philadelphia: Saunders (Eds. Wagner H. N. Jr, Szabo S., Buchanan J. W.)*, **1995**, 213.
28. Alberto R., Schibli R., Egli A., Schubiger, A. P. *J. Am. Chem. Soc.*, **1998**, 120, 7987.

LIST OF FIGURES

Fig. 1.1.

Typical design of a radiopharmaceutical using bifunctional chelator approach

Fig. 1.2.

Different steps involved in the nitroimidazole reduction process in hypoxic cell

Fig. 1.3.

Few clinically evaluated nitroimidazole radiopharmaceuticals for detecting hypoxia in cancerous lesions

Fig. 1.4.

Simplified ^{99}Mo decay scheme

Fig. 1.5.

Structure of (a) technetium oxo core $[\text{}^{99\text{m}}\text{Tc}(\text{V})\text{O}]^{3+}$ and (b) technetium dioxo core $[\text{}^{99\text{m}}\text{Tc}(\text{V})\text{O}_2]^+$. **L** represents the ligands

Fig. 1.6.

Some clinically useful radiopharmaceuticals having $^{99\text{m}}\text{Tc}$ -oxo or $^{99\text{m}}\text{Tc}$ -dioxo core

Fig. 1.7.

Structure of technetium nitrido ($[\text{}^{99\text{m}}\text{Tc}(\text{V})\text{N}]^{2+}$) core

Fig. 1.8.

Structure of two potential myocardial perfusion imaging agents based on $[\text{}^{99\text{m}}\text{TcN}]^{2+}$ core

Fig. 1.9.

Typical structure of radiopharmaceutical containing $^{99\text{m}}\text{TcN}(\text{PNP})$ core

Fig. 1.10.

Typical structure $^{99\text{m}}\text{Tc}$ -HYNIC-biomolecule complex using (a) EDDA/tricine as co-ligand and (b) TPPTS/tricine co-ligand

Fig. 1.11.

Typical structure of (a) $[\text{}^{99\text{m}}\text{Tc}(\text{CO})_3(\text{H}_2\text{O})_3]^+$ precursor complex and (b) a complex formed with ligand **L**

Fig. 1.12.

Lyophilized kit vial for the preparation of $[\text{}^{99\text{m}}\text{Tc}(\text{CO})_3(\text{H}_2\text{O})_3]^+$ precursor complex

Fig. 1.13.

Different approaches of radiolabeling ligands with $^{99\text{m}}\text{Tc}(\text{CO})_3$ core

Fig. 2.1.

Synthesis of IDA derivatives of nitroimidazole (i) *tert*-butyl bromoacetate, DIEA, acetonitrile, 25°C (ii) 4-nitroimidazole, anhyd. K_2CO_3 , acetonitrile, reflux (iii) 2-nitroimidazole, anhyd. K_2CO_3 , acetonitrile, reflux (iv) 6N HCl, 25°C

Fig. 2.2.

$^1\text{H-NMR}$ spectrum of N,N-bis(*tert*-butoxycarbonyl)methyl)-3-bromopropyl amine (**2a**)

Fig. 2.3.

$^1\text{H-NMR}$ spectrum of N,N-bis(*tert*-butoxycarbonyl)methyl)-3-(2-nitro-1H-imidazol-1-yl)-propane-1-amine (**2b**)

Fig. 2.4.

$^1\text{H-NMR}$ spectrum of N,N-bis(*tert*-butoxycarbonyl)methyl)-3-(4-nitro-1H-imidazol-1-yl)-propane-1-amine (**2c**)

Fig. 2.5.

$^1\text{H-NMR}$ spectrum of N,N-bis(*tert*-butoxycarbonyl)methyl)-3-(5-nitro-1H-imidazol-1-yl)-propane-1-amine (**2d**)

Fig. 2.6.

$^1\text{H-NMR}$ spectrum of 2,2'-((3-(2-nitro-1H-imidazol-1-yl)propyl)imino)diacetic acid (**2L1**)

Fig. 2.7.

ESI-MS of 2,2'-((3-(2-nitro-1H-imidazol-1-yl)propyl)imino)diacetic acid (**2L1**)

Fig. 2.8.

¹H-NMR spectrum of 2,2'-((3-(4-nitro-1H-imidazol-1-yl)propyl)imino)diacetic acid (**2L2**)

Fig. 2.9.

ESI-MS of 2,2'-((3-(4-nitro-1H-imidazol-1-yl)propyl)imino)diacetic acid (**2L2**)

Fig. 2.10.

¹H-NMR spectrum of 2,2'-((3-(5-nitro-1H-imidazol-1-yl)propyl)imino)diacetic acid (**2L3**)

Fig. 2.11.

ESI-MS of 2,2'-((3-(5-nitro-1H-imidazol-1-yl)propyl)imino)diacetic acid (**2L3**)

Fig. 2.12.

¹H-NMR spectrum of Re(CO)₃ complex of ligand **2L1** (**2e**)

Fig. 2.13.

Synthesis of DETA derivatives of nitroimidazole (i) BOC-ON, DIEA, tetrahydrofuran, 0°C (ii) 1,3 dibromopropane, DIEA, acetonitrile, reflux (iii) 2-nitroimidazole, DIEA, acetonitrile, reflux (iv) 4-nitroimidazole, DIEA, acetonitrile, reflux (v) **2k**, DIEA, acetonitrile, reflux (vi) 6N HCl, 25°C

Fig. 2.14.

¹H-NMR spectrum of *tert*-butyl 2-((2-(*tert*-butoxycarbonyl)aminoethyl)amino)ethyl carbamate (**2f**)

Fig. 2.15.

¹H-NMR spectrum of *tert*-butyl 2-((2-(*tert*-butoxycarbonyl)aminoethyl)(3-bromopropyl)amino)ethyl carbamate (**2g**)

Fig. 2.16.

¹H-NMR spectrum of *tert*-butyl 2-((2-(*tert*-butoxycarbonyl)aminoethyl)(3-(2-nitro-1H-imidazol-1-yl)propyl)amino)ethyl carbamate (**2h**)

Fig. 2.17.

¹H-NMR spectrum of *tert*-butyl 2-((2-(*tert*-butoxycarbonyl)aminoethyl)(3-(4-nitro-1H-imidazol-1-yl)propyl)amino)ethyl carbamate (**2i**)

Fig. 2.18.

¹H-NMR spectrum of 1-(3-bromopropyl)-5-nitro-1H-imidazole (**2k**)

Fig. 2.19.

¹H-NMR spectrum of *tert*-butyl 2-((2-(*tert*-butoxycarbonyl)aminoethyl)(3-(5-nitro-1H-imidazol-1-yl)propyl)amino)ethyl carbamate (**2j**)

Fig. 2.20.

¹H-NMR spectrum of N¹-(2-aminoethyl)-N¹-(3-(2-nitro-1H-imidazol-1-yl)propyl)ethane-1,2-diamine hydrochloride (**2L4**)

Fig. 2.21.

ESI-MS of N¹-(2-aminoethyl)-N¹-(3-(2-nitro-1H-imidazol-1-yl)propyl)ethane-1,2-diamine hydrochloride (**2L4**)

Fig. 2.22.

¹H-NMR spectrum of N¹-(2-aminoethyl)-N¹-(3-(4-nitro-1H-imidazol-1-yl)propyl)ethane-1,2-diamine hydrochloride (**2L5**)

Fig. 2.23.

ESI-MS of N¹-(2-aminoethyl)-N¹-(3-(4-nitro-1H-imidazol-1-yl)propyl)ethane-1,2-diamine hydrochloride (**2L5**)

Fig. 2.24.

$^1\text{H-NMR}$ spectrum of N^1 -(2-aminoethyl)- N^1 -(3-(5-nitro-1H-imidazol-1-yl)propyl)ethane-1,2-diamine hydrochloride (**2L6**)

Fig. 2.25.

ESI-MS of N^1 -(2-aminoethyl)- N^1 -(3-(5-nitro-1H-imidazol-1-yl)propyl)ethane-1,2-diamine hydrochloride (**2L6**)

Fig. 2.26.

$^1\text{H-NMR}$ spectrum of $\text{Re}(\text{CO})_3$ complex of **2L6** (**2l**)

Fig. 2.27.

ESI-MS of $\text{Re}(\text{CO})_3$ complex of **2L6** (**2l**)

Fig. 2.28.

Synthesis of AEG derivatives of nitroimidazoles (i) *tert*-butyl bromoacetate, DIEA, acetonitrile, 0°C (ii) 1,3 dibromopropane, DIEA, acetonitrile, reflux (iii) 2-nitroimidazole, DIEA, acetonitrile, reflux (iv) 4-nitroimidazole, DIEA, acetonitrile, reflux (v) **2k**, DIEA, acetonitrile, reflux (vi) 6N HCl, 25°C

Fig. 2.29.

$^1\text{H-NMR}$ spectrum of *tert*-butyl 2-(((*tert*-butoxycarbonyl)methylamino)ethyl carbamate (**2m**)

Fig. 2.30.

$^1\text{H-NMR}$ spectrum of *tert*-butyl 2-(((*tert*-butoxycarbonyl)methyl)(3-bromopropyl)amino)ethyl carbamate (**2n**)

Fig. 2.31.

$^1\text{H-NMR}$ spectrum of *tert*-butyl 2-(((*tert*-butoxycarbonyl)methyl)(3-(2-nitro-1H-imidazol-1-yl)propyl)amino)ethyl carbamate (**2o**)

Fig. 2.32.

¹H-NMR spectrum of *tert*-butyl 2-(((*tert*-butoxycarbonyl)methyl)(3-(4-nitro-1H-imidazol-1-yl)propyl)amino)ethyl carbamate (**2p**)

Fig. 2.33.

¹H-NMR spectrum of *tert*-butyl 2-(((*tert*-butoxycarbonyl)methyl)(3-(5-nitro-1H-imidazol-1-yl)propyl)amino)ethyl carbamate (**2q**)

Fig. 2.34.

¹H-NMR spectrum of 2-(N-(2-aminoethyl)-N-(3-(2-nitro-1H-imidazol-1-yl)propyl)amino)acetic acid (**2L7**)

Fig. 2.35.

ESI-MS of 2-(N-(2-aminoethyl)-N-(3-(2-nitro-1H-imidazol-1-yl)propyl)amino)acetic acid (**2L7**)

Fig. 2.36.

¹H-NMR spectrum of 2-(N-(2-aminoethyl)-N-(3-(4-nitro-1H-imidazol-1-yl)propyl)amino)acetic acid (**2L8**)

Fig. 2.37.

ESI-MS of 2-(N-(2-aminoethyl)-N-(3-(4-nitro-1H-imidazol-1-yl)propyl)amino)acetic acid (**2L8**)

Fig. 2.38.

¹H-NMR spectrum of 2-(N-(2-aminoethyl)-N-(3-(5-nitro-1H-imidazol-1-yl)propyl)amino)acetic acid (**2L9**)

Fig. 2.39.

ESI-MS of 2-(N-(2-aminoethyl)-N-(3-(5-nitro-1H-imidazol-1-yl)propyl)amino)acetic acid (**2L9**)

Fig. 2.40.

Qualitative $^1\text{H-NMR}$ spectrum of $\text{Re}(\text{CO})_3$ complex of **2L8 (2r)**

Fig. 2.41.

ESI-MS of $\text{Re}(\text{CO})_3$ complex of **2L8 (2r)**

Fig. 2.42.

Chemical structures of various nitroimidazole ligands

Fig. 2.43.

Probable structure of $^{99\text{m}}\text{Tc}(\text{CO})_3$ complexes formed by IDA, DETA and AEG ligands

Fig. 2.44.

HPLC elution profile of (a) $[\text{}^{99\text{m}}\text{Tc}(\text{CO})_3(\text{H}_2\text{O})_3]^+$ precursor complex (b) 2-nitroimidazole-IDA- $^{99\text{m}}\text{Tc}(\text{CO})_3$ complex (c) 4-nitroimidazole-IDA- $^{99\text{m}}\text{Tc}(\text{CO})_3$ complex (d) 5-nitroimidazole-IDA- $^{99\text{m}}\text{Tc}(\text{CO})_3$ complex (e) 2-nitroimidazole-DETA- $^{99\text{m}}\text{Tc}(\text{CO})_3$ complex (f) 4-nitroimidazole-DETA- $^{99\text{m}}\text{Tc}(\text{CO})_3$ complex and (g) 5-nitroimidazole-DETA- $^{99\text{m}}\text{Tc}(\text{CO})_3$ complex

Fig. 2.45.

HPLC elution profile of (a) 2-nitroimidazole-AEG- $^{99\text{m}}\text{Tc}(\text{CO})_3$ complex (b) 4-nitroimidazole-AEG- $^{99\text{m}}\text{Tc}(\text{CO})_3$ complex and (c) 5-nitroimidazole-AEG- $^{99\text{m}}\text{Tc}(\text{CO})_3$ complex

Fig. 2.46.

HPLC elution profile of (a) 2-nitroimidazole-IDA- $\text{Re}(\text{CO})_3$ complex (b) 5-nitroimidazole-DETA- $\text{Re}(\text{CO})_3$ complex and (c) 4-nitroimidazole-AEG- $\text{Re}(\text{CO})_3$ complex

Fig. 2.47.

Structure of $\text{Re}(\text{CO})_3$ complexes of nitroimidazole ligands (a) **2L1** (b) **2L6** and (c) **2L8**

Fig. 2.48.

Activity of (a) 2-,4-,5- nitroimidazole-IDA- $^{99\text{m}}\text{Tc}(\text{CO})_3$ complexes (b) 2-,4-,5- nitroimidazole-DETA- $^{99\text{m}}\text{Tc}(\text{CO})_3$ complexes (c) 2-,4-,5- nitroimidazole-AEG- $^{99\text{m}}\text{Tc}(\text{CO})_3$

complexes and (d) [^{18}F]FMISO in tumor at different time points

Fig. 2.49.

Clearance of activity of (a) 2-,4-,5- nitroimidazole-IDA- $^{99\text{m}}\text{Tc}(\text{CO})_3$ complexes (b) 2-,4-,5- nitroimidazole-DETA- $^{99\text{m}}\text{Tc}(\text{CO})_3$ complexes, (c) 2-,4-,5- nitroimidazole-AEG- $^{99\text{m}}\text{Tc}(\text{CO})_3$ complexes and (d) [^{18}F]FMISO from blood at different time points

Fig 2.50.

Blood clearance of [^{18}F]FMISO compared to 2-nitroimidazole- $^{99\text{m}}\text{Tc}(\text{CO})_3$ complexes of IDA, DETA and AEG ligands

Fig. 2.51.

Distribution of $^{99\text{m}}\text{Tc}(\text{CO})_3$ complexes of (a) 2-nitroimidazole-IDA [**2L1**] (b) 4-nitroimidazole-IDA [**2L2**] (c) 5-nitroimidazole-IDA [**2L3**] in various organs at different time points.

Fig. 2.52.

Distribution of $^{99\text{m}}\text{Tc}(\text{CO})_3$ complexes of (a) 2-nitroimidazole-DETA [**2L4**] (b) 4-nitroimidazole-DETA [**2L5**] (c) 5-nitroimidazole-DETA [**2L6**] in various organs at different time points

Fig. 2.53.

Distribution of $^{99\text{m}}\text{Tc}(\text{CO})_3$ complexes of (a) 2-nitroimidazole-AEG [**2L7**] (b) 4-nitroimidazole-AEG [**2L8**] (c) 5-nitroimidazole-AEG [**2L9**] in various organs at different time points

Fig. 2.54.

Distribution of [^{18}F]FMISO in various organs at different time points

Fig. 3.1.

$^{99\text{m}}\text{Tc}(\text{CO})_3$ complexes of 2-, 4- and 5- nitroimidazole (a) IDA ligands (b) DETA ligands and (c) AEG ligands

Fig. 3.2.

Structure of (a) ^{99m}Tc -tetrofosmin and (b) ^{99m}Tc -sestamibi

Fig. 3.3.

Structure of (a) 2-nitroimidazole ligand with a propyl spacer and (b) 2-nitroimidazole ligand with an ether spacer

Fig. 3.4.

Synthesis of 2-(carboxymethyl(2-(2-nitroimidazolylethoxy)ethyl)amino)acetic acid (i) dibromoethyl ether, anhyd. K_2CO_3 , acetonitrile, reflux (ii) phthalimide, anhyd. K_2CO_3 , acetonitrile, reflux (iii) (1) hydrazine hydrate, ethanol, reflux (2) 2N HCl, 50°C (iv) *tert*-butyl bromoacetate, DIEA, acetonitrile, reflux (v) 6N HCl, 25°C

Fig. 3.5.

^1H -NMR spectrum of 1-(2-(2-bromoethoxy)ethyl)-2-nitro-1H-imidazole (**3a**)

Fig. 3.6.

^1H -NMR spectrum of 2-(2-(2-(2-nitro-1H-imidazol-1-yl)ethoxy)ethyl)isoindoline-1,3-dione (**3b**)

Fig. 3.7.

^1H -NMR spectrum of 1-(N,N-bis(*tert*-butoxycarbonylmethyl)-2-(2-(2-nitroimidazolyl)ethoxy)ethane (**3d**)

Fig. 3.8.

^1H -NMR spectrum of 2-(carboxymethyl(2-(2-nitroimidazolylethoxy)ethyl)amino)acetic acid (**3e**)

Fig. 3.9.

ESI-MS of 2-(carboxymethyl(2-(2-nitroimidazolylethoxy)ethyl)amine)acetic acid (**3e**)

Fig. 3.10.

^1H -NMR spectrum of $\text{Re}(\text{CO})_3$ complex of ligand **3e** (**3f**)

Fig. 3.11.

HPLC elution profile of (a) [$^{99m}\text{Tc}(\text{CO})_3(\text{H}_2\text{O})_3$] $^+$ precursor complex (b) $^{99m}\text{Tc}(\text{CO})_3$ complex **3g** and (c) $\text{Re}(\text{CO})_3$ complex **3f**

Fig. 3.12.

Structure of (a) 2-nitroimidazole- $\text{Re}(\text{CO})_3$ complex (**3f**) with an ether spacer (b) 2-nitroimidazole- $^{99m}\text{Tc}(\text{CO})_3$ complex (**3g**) with an ether spacer and (c) 2-nitroimidazole-IDA- $^{99m}\text{Tc}(\text{CO})_3$ complex (**3h**) with a propyl spacer

Fig. 3.13.

Tumor uptake observed with 2-nitroimidazole- $^{99m}\text{Tc}(\text{CO})_3$ complex with an ether spacer (**3g**) and a propyl spacer (**3h**) at different time points

Fig. 3.14.

Blood clearance observed with 2-nitroimidazole- $^{99m}\text{Tc}(\text{CO})_3$ complex with an ether spacer (**3g**) and a propyl spacer (**3h**) at different time points

Fig. 3.15.

Distribution of 2-nitroimidazole- $^{99m}\text{Tc}(\text{CO})_3$ complex (a) with an ether spacer (**3g**) and (b) with a propyl spacer (**3h**) in various organs at different time points

Fig. 3.16.

Variation in tumor to blood and tumor to muscle ratio of 2-nitroimidazole- $^{99m}\text{Tc}(\text{CO})_3$ complex with an ether spacer (**3g**) and a propyl spacer (**3h**) at different time points

Fig. 4.1.

Structure of [^{18}F]FMISO

Fig. 4.2.

Synthesis of 2-(N-carboxymethyl, N-((2-hydroxy)-3-(2-nitroimidazolyl) propyl)amino)acetic acid (i) 2,3-epoxypropyl phthalimide, ethanol, reflux (ii) (1) hydrazine hydrate, ethanol,

reflux (2) 2N HCl, 50°C (iii) *tert*-butylbromoacetate, DIEA, acetonitrile, 25°C (iv) 6N HCl, 25°C

Fig. 4.3.

¹H-NMR spectrum of 2-(2-hydroxy-3-(2-nitro-1H-imidazol-1-yl)propyl)isoindoline-1,3-dione (**4a**)

Fig. 4.4.

¹H-NMR spectrum of 1-amino-3-(2-nitro-1H-imidazol-1-yl)propan-2-ol hydrochloride (**4b**)

Fig. 4.5.

¹H-NMR spectrum of N,N-bis(*tert*-butoxycarbonylmethyl)-((2-hydroxy)-3-(2-nitroimidazolyl))propyl amine (**4c**)

Fig. 4.6.

¹H-NMR spectrum of 2-(N-carboxymethyl,N-((2-hydroxy)-3-(2-nitroimidazolyl)propyl)amino)acetic acid (**4d**)

Fig. 4.7.

Structure of (a) misonidazole (b) [¹⁸F]FMISO and (c) miso-IDA

Fig. 4.8.

HPLC elution profile of (a) [^{99m}Tc(CO)₃(H₂O)₃]⁺ precursor (b) miso-IDA-^{99m}Tc(CO)₃ complex and (c) miso-IDA-Re(CO)₃ complex

Fig. 4.9.

Structure of miso-IDA-^{99m}Tc(CO)₃ complex

Fig. 4.10.

Tumor uptake observed with miso-IDA-^{99m}Tc(CO)₃ complex and [¹⁸F]FMISO at different time points

Fig. 4.11.

Clearance of miso-IDA-^{99m}Tc(CO)₃ complex and [¹⁸F]FMISO from blood at different time points

Fig. 4.12.

Variation in tumor to blood ratio of miso-IDA-^{99m}Tc(CO)₃ complex and [¹⁸F]FMISO at different time points

Fig. 4.13.

Distribution of (a) miso-IDA-^{99m}Tc(CO)₃ complex and (b) [¹⁸F]FMISO in various organs at different time points

LIST OF TABLES

Table 1.1.

Different invasive and non-invasive techniques available for the detection of tissue hypoxia

Table 1.2.

Some of the diagnostic isotopes useful for radiopharmaceutical applications

Table 2.1.

LogP_{o/w} of different nitroimidazole-^{99m}Tc(CO)₃ complexes

Table 2.2.

TBR and TMR of various 2-, 4- and 5-nitroimidazole-^{99m}Tc(CO)₃ complexes and [¹⁸F]FMISO at different time points

CHAPTER 1
INTRODUCTION

“If we knew what it was we were doing, it would not be called research, would it?”

— Albert Einstein

1.1. Background

Currently, cancer is one of the most dreaded disease, causing about 12% of all deaths worldwide.¹ In India, while the incidence of new cases of cancer is over 8,00,000, the number of cancer-related deaths reported annually is alarmingly high figure of 5,50,000. There is a need to develop effective drugs to cure patients suffering from this disease, and relentless efforts are being made by various research groups world-wide to achieve this objective. However, clinical research of the past three decades had unambiguously demonstrated that there are certain other medically relevant issues which have a large bearing on the prognosis of the disease and efficacy of the treatment even with the best medicines available. Hypoxic (below normal level of oxygen) nature of the cancerous lesions and its associated problems is one such issue which makes the clinical management of cancer a herculean task.² Finding effective ways to counter hypoxic cancerous tissue is thus a challenging problem, and its solution will empower the oncologist to significantly improve the quality of life of cancer patients or, possibly, even cure the disease completely. This makes quantitative detection of hypoxia in cancerous lesion another significant medical problem and the need to develop precise tools for the detection of hypoxia a necessity. In this regard, nuclear medicine can play an important role through hypoxia specific imaging agents.

1.2. Hypoxia and its causes

Hypoxia is a pathological condition that arises in organs or tissue in the body due to inadequate oxygen level. Medical conditions such as cancers, cardiovascular disease, cerebrovascular disease, diabetes, infection and wound healing are few of the several causes for tissue hypoxia.^{2,3}

1.3. Problems posed by hypoxia

Among the different causes, probably, hypoxia in cancerous tissue (tumor) pose the most serious problem as it has direct implications on the prognosis and therapeutic outcome

of the disease. Hypoxia in tumor can be perfusion related (acute hypoxia) or diffusion related (chronic hypoxia).³ Tumor microvasculature often has severe functional and structural abnormalities, such as absence of blood flow regulation, lack of physiological and pharmacological receptor, tortuous shape, intermittent stasis etc. which limits efficient perfusion, and hence, adequate oxygen supply. Structural abnormalities lead to increased diffusion lengths and deteriorated diffusion geometry for oxygen delivery, causing oxygen starvation in cells beyond certain distance (>70 μm) from the nutritive blood vessels.

Evidence for the negative role of hypoxic microenvironment in the pathogenesis and progression of human cancer was first obtained in 1953, when well-oxygenated tumor cells were found to exhibit a 3-fold higher response to radiotherapy compared to anoxic cells.⁴ Later, numerous experimental and clinical investigations confirmed the negative influence of hypoxia in tumor propagation, malignant progression and resistance to radiation therapy and chemotherapy.⁵⁻¹³

Though hypoxic cells are quiescent they are potentially dangerous, if ignored, for several reasons.¹⁴ Unlike adequately well oxygenated cells, hypoxic cells are resistant to radiation therapy and chemotherapy. Irrespective of the choice of therapy, well oxygenated tumor cells are predominantly eliminated during therapy, exposing the underlying hypoxic tumor cells to higher oxygen levels and nutrients enabling them to re-grow. Secondly, cellular functions are highly oxygen-dependent and are subject to modulation according to oxygen availability. Several clinical studies have indicated extreme hypoxic environment (0.2 – 1 mm Hg) to be a potential stimulus for genetic changes in cells which may result in acquisition of drug resistance.^{2,14} Another aspect which makes hypoxic cells dangerous is their HIF (hypoxia-inducible factor) mediated adaptive response to survival under hypoxic conditions.¹⁴ The HIF-1 mediates the activation of glucose transporters and glycolytic enzymes to shift the cellular metabolism to anaerobic glycolysis. The HIF-1 also stimulates

up-regulation of angiogenic growth factors and cytokines that promotes angiogenesis leading to re-oxygenation of the hypoxic cells which is the starting point of recurrence and malignancy. These factors highlight the necessity to consider hypoxic status of cancer as an important clinical parameter before finalizing the treatment strategy for a patient. Information on hypoxic status of the disease can help physicians to isolate patients who will benefit from hypoxia directed treatment from those who will not, relieving the latter group from taking unnecessary therapeutic burden on their already deteriorated health condition. Available options for hypoxia directed treatment have been thoroughly discussed.^{15,16}

1.4. Measuring tumor hypoxia

Considering the significance of hypoxia in clinical management of cancer, precise determination of its existence, extent and spatial distribution in the cancerous lesions assumes paramount importance. Spatial distribution of hypoxic region in cancerous tissue is especially important for planning hypoxia-directed treatment using external radiation sources.^{15,16} Methods available for the detection and quantification of hypoxia in tissue can be divided into two classes, invasive or non-invasive. Techniques currently being used for the detection of hypoxia is summarized in Table 1.1.¹⁷ Few select techniques which are employed in routine clinical practice are briefly described.

1.4.1. Invasive techniques

1.4.1.1. Polarographic oxygen electrode

At present, polarographic oxygen electrode, also known as Eppendorf electrode is considered the 'gold standard' for the measurement of tissue hypoxia.⁴¹ Several studies have clearly established strong correlation between hypoxia measured using this device and poor prognosis.^{5,7,42,43} In this technique, multiple tracks in the tissue are made using this electrode, and oxygen partial pressures are recorded at different depths in each track. This information is used to construct a histogram showing the distribution of oxygen partial pressure in the

tissue under investigation. Though this electrode can directly measure oxygen partial pressure at a given depth in a tissue, nature of the technique requires that the tissue under investigation is readily accessible. These electrodes are, therefore, practically ineffective for detecting and quantifying hypoxia in deep-seated tumors. Also, due to the heterogeneous and dynamic nature of hypoxia, observed distribution of oxygen partial pressure in the tissue, which is based on a limited number of measurements, may not reflect the actual oxygenation status of the entire tissue. These factors have restricted adoption of this technique in a clinical setup to a larger extent.

Table 1.1. Different invasive and non-invasive techniques available for the detection of tissue hypoxia

Invasive techniques		
Technique name	Probe	References
Needle based sensors	Polarographic oxygen electrode	18, 19, 20
	Fluorescent oxygen sensors	21, 22
Immunohistochemical markers	Pimonidazole	23, 24
	EF5	25
	HIF-1 α	26
	CA IX	27
Noninvasive techniques		
Endogenous contrast	Near IR spectroscopy	28
	BOLD MRI	28, 29
	ESR	30
Exogenous contrast		
MRI/MRS	[¹⁹ F]hexofluorobenzene	31, 32
PET	[¹⁸ F]Fluoromisonidazole	33, 34
	[¹⁸ F]Fluoroazomycin arabinoside	35, 36
	[¹⁸ F]EF5	37
	[⁶⁴ Cu]ATSM	38, 39
SPECT	[¹²³ I]Iodoazomycin arabinoside	40

1.4.1.2. Immuno-histochemical markers

This is an indirect technique for the detection of hypoxia. It requires a monoclonal antibody developed against adduct of the metabolites of oxygen-dependent bio-reductive

marker with the cellular components. EF5 and pimonidazole (code named Ro03-8799) are two such bio-reductive markers used for the detection and quantification of hypoxia.^{23-25,45,46} The technique allows appropriate bio-reductive marker to distribute in the tissue of interest where they will undergo selective reduction in hypoxic cells resulting in the formation of adducts of their metabolites with the cellular components. Subsequently, antibodies are used to detect and estimate the amount of adduct formed in the biopsied tissue which is a measure of hypoxia. This technique is also prone to error due to heterogeneous nature of hypoxia, since biopsied tissue may not represent the actual hypoxic status of the entire tissue.

1.4.2. Non-invasive methods

Magnetic resonance imaging (MRI) and imaging using radiopharmaceuticals are the two important non-invasive modalities available for the detection and quantification of hypoxia.⁴⁷ The techniques are briefly discussed below.

1.4.2.1. MRI

MRI relies on oxygen-dependent relaxation of magnetically active nuclei (¹⁹F or ¹H) in the contrast agents such as perfluorocarbons (PFC) and hexamethyldisiloxane (HMDSO). Variation in relaxation time is used as signal for mapping oxygen partial pressure in the tissue of interest. Several studies have correlated oxygen partial pressure maps, generated using MRI, with clinically measurable parameter such as tumor volume doubling time. This information has also been utilized for selecting patients who would benefit from hypoxia-directed therapy.^{46,48-50} Though MRI with PFC's offers good spatial resolution, lack of ¹⁹F-MR capability in majority of the clinical scanners has limited its application. On the other hand, MRI with HMDSO is often associated with strong background resonance signals from the methylene groups of body fat (adipose tissue). Other disadvantages of MRI include, influence of temperature, pH, presence of other metal ions etc. on the relaxation time of the contrast agent, which makes direct correlation with oxygen partial pressure difficult.⁴⁷

1.4.2.2. Imaging using radiopharmaceuticals

Imaging using radiopharmaceuticals has emerged as an important tool for the diagnosis of cancer as well as several other pathological conditions.⁵¹⁻⁵³ A brief account on radiopharmaceuticals follows.

1.5. Radiopharmaceuticals

Radiopharmaceuticals have been defined as radioactive drugs that can be used, either in the diagnosis or monitoring of a disease or manifestation of a disease in a body, or to effect therapy of the diseased organ or tissue. Radiopharmaceutical can be simple ions like ^{131}I (^{131}I -iodide) or $^{99\text{m}}\text{TcO}_4^-$ ($^{99\text{m}}\text{Tc}$ -pertechnetate)⁵⁴⁻⁵⁶ or complex molecules like proteins, antibodies or peptides tagged with appropriate radionuclide.⁵⁷ Iodine-131, which is the most efficacious radiopharmaceutical for the treatment of thyroid cancer, is taken up in thyroid because, iodine is essential for the biosynthesis of hormones secreted by thyroid gland. Pertechnetate mimics iodide in size as well as charge and hence it has also been used to image thyroid gland.⁵⁶ Proteins and antibodies on the other hand target a specific organ or tissue by virtue of their specific biological function. Between these two classes of compounds are small molecules which may or may not have a biological function in the body. Small molecules, which by themselves do not have any biological function, still may target an organ after tagging with an appropriate metallic radionuclide. Such radiopharmaceuticals are called ‘metal essential radiopharmaceuticals’. Molecules that can target an organ or tissue due to their biological function are called ‘metal non-essential radiopharmaceuticals’.

It is not necessary that a biomolecule always possesses appropriate functional groups which could be utilized to tag a radionuclide. Hence, more recently, radiopharmaceuticals are developed by bifunctional chelator approach. A bifunctional chelating agent (BFCA), as the name implies, has two functions. It forms complex with a suitable radionuclide at one end and holds the biomolecule at the other. General representation of a radiopharmaceutical

formed by bifunctional chelator approach is shown in figure 1.1. Biologically active molecule, which is primarily responsible for the selective targeting action of the radiopharmaceutical, is connected to a chelator which binds with the radionuclide through a linker. The linker has an additional function to hold the biomolecule sufficiently away from the metal-chelate to avoid a possible steric hindrance which may compromise the selective action of the biomolecule on the target tissue in the body.

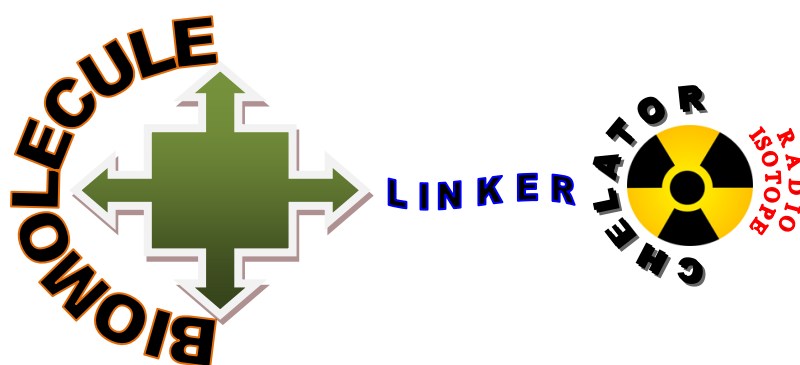


Fig. 1.1. Typical design of a radiopharmaceutical using bifunctional chelator approach

Radiopharmaceuticals can be broadly classified into diagnostic or therapeutic depending on the emission characteristics of the radioisotope. A discussion on therapeutic radiopharmaceuticals is beyond the scope of the present work.

1.6. Diagnostic radiopharmaceuticals

Medical diagnosis is the process of detecting the presence of a disease or disorder in a body and reaching a logical, and reasonable, conclusion based on which the best possible treatment strategy could be adopted. The essential difference between a diagnostic and therapeutic radiopharmaceutical is in the nature of radionuclide used. A diagnostic radionuclide should be, preferably, a pure gamma or positron emitter whereas a therapeutic radionuclide should be invariably a particulate emitter (alpha, beta, Auger electrons etc.) with or without accompanying gamma emission. Upon systemic administration of the diagnostic radiopharmaceutical, it either passes through or retained in organs/diseased tissue. A highly sophisticated medical instrument, known as gamma camera, is used to detect the gamma

photons emerging from the body, penetrating the tissue, to construct 2D images that will provide information on the functioning of an organ or the presence of cancerous lesions in the body. Single photon emission computed tomography (SPECT) cameras are used for constructing 3D images. Gamma photons with energy between 100 KeV to 250 KeV is ideal for diagnostic imaging applications using SPECT. For positron emitting radioisotopes, positron emission tomography (PET) cameras are used. PET camera employs detectors capable of detecting 512 KeV gamma photos emitted during the annihilation of positron. Bismuth germanium oxide (BGO) or LSO are examples of such detectors. Some of the widely used diagnostic radioisotopes, their production route and their decay modes are summarized in Table 1.2.⁵⁸

Table 1.2. Some of the diagnostic isotopes useful for radiopharmaceutical applications

Isotope	Production route	Half-life (h)	Decay mode
Gamma emitting radioisotopes			
⁶⁷ Ga	Cyclotron	78.26	EC (100%)
¹²³ I	Cyclotron	13.0	EC
¹³¹ I	Reactor	193.4	β^-
²⁰¹ Tl	Cyclotron	73.1	γ (16), EC (94)
^{99m} Tc	⁹⁹ Mo/ ^{99m} Tc Generator	6.0	IT (100%)
¹¹¹ In	Cyclotron	67.9	EC (100%)
Positron emitting radioisotopes			
⁶⁴ Cu	Cyclotron, ⁶⁴ Ni(p,n) ⁶⁴ Cu	12.8	β^+ (19%), EC (41%), β^- (40%)
⁶⁸ Ga	⁶⁸ Ge/ ⁶⁸ Ge Generator	1.1	β^+ (90%), EC (10%)
¹⁸ F	Cyclotron, ¹⁸ O(p,n) ¹⁸ F	1.83	β^+ (97%), EC (3%)
¹²⁴ I	Cyclotron, ¹²⁴ Te(p,n) ¹²⁴ I	100.3	β^+ (25%), EC (75%)

1.7. Essential characteristics of a diagnostic radiopharmaceutical

Though it is an immensely challenging task to develop a diagnostic radiopharmaceutical which possesses ideal characteristics for a given application, knowledge of ideal characteristics expected could serve as guidelines while developing novel diagnostic radiopharmaceuticals. Also, the guidelines would be helpful to assess the merits and demerits

of a diagnostic radiopharmaceutical.⁵⁹ Characteristics of an ideal diagnostic radiopharmaceutical are listed below.

a) ***Effective half-life***

In general, half-life is used to define the time required to reduce the initial value of a given parameter, like radioactivity, concentration of a substance in blood etc., to half its initial value. The half-life of a radioisotope ($t_{1/2}$) is defined as the time taken to reduce its activity to half the initial value. This is also called physical half-life (t_{phy}). Similarly, for radiopharmaceuticals injected into the body, a term biological half-life (t_{bio}) can be defined, which is the time to reduce its amount to half its initial value by different excretory mechanisms of the body. Thus, the activity due to the injected radiopharmaceutical decreases by two independent path ways. Combining these two independent processes, the term effective half-life (t_{eff}) can be defined, which could be calculated using the following equation.

$$t_{\text{eff}} = \frac{t_{\text{phy}} \times t_{\text{bio}}}{t_{\text{phy}} + t_{\text{bio}}}$$

In general, a radiopharmaceutical having a very short effective half-life may not be a useful diagnostic agent, since it may not spend enough time in the body to provide the required information. As a rule of thumb, a diagnostic radiopharmaceutical should have an effective half-life of ~1.5 times the duration of the diagnostic procedure. This provides a good compromise between radiation dose to the patient and the dose to be injected to obtain image of optimal quality.

b) ***High target to non-target ratio***

In nuclear medicine, target is defined as the organ or tissue or receptors expressed on the cells, which is under investigation. All other organs or tissue or receptors can be considered as non-targets. Though a radiopharmaceutical is designed to target a specific

organ, tissue or receptor, there is always a significant level of non-specific uptake in other organs and tissues, which compromises the quality of the image, and thus, the quality of the diagnostic information that could be obtained from those images. The target to non-target ratio is a measure of specificity of the diagnostic radiopharmaceutical. Higher the target to non-target ratio, more specific is the radiopharmaceutical. As a rule of thumb, this ratio should be at least 5:1 for planar (2D) images and 2:1 for SPECT (3D) images to obtain a scan which can clearly distinguish pathology from background.

c) ***Availability, cost and chemistry***

The radiopharmaceutical should be inexpensive, readily available and the chemistry involved should be simple enough for routine preparation.

1.8. Radiopharmaceuticals for the detection of tumor hypoxia

Radiopharmaceuticals for the detection of tissue hypoxia rely on the oxygen dependent chemical changes to it, which results in selective accumulation in hypoxic cells, delineating them from the oxygenated cells. Such radiopharmaceuticals can be classified into nitroimidazole-based or non-nitroimidazole-based radiopharmaceuticals. Following sequel briefly discusses these two classes of radiopharmaceuticals which have been used to detect and quantify hypoxic status of malignant tumors.

1.8.1. Non-nitroimidazole radiopharmaceuticals for the detection of hypoxia

^{64}Cu -diacetyl-bis(N^4 -methylthiosemicarbazone) (^{64}Cu -ATSM) and $^{99\text{m}}\text{Tc}$ -4,9-diaza-3,3,10,10-tetramethyldodecane-2,11-dione dioxime ($^{99\text{m}}\text{Tc}$ -HL-91) are two prominent non-nitroimidazole radiopharmaceuticals which showed considerable promise as tumor hypoxia marker in vivo. Several pre-clinical studies have validated its use for detecting hypoxia in tumors and other tissues.⁶⁰⁻⁶⁷ Though the mechanism of trapping of ^{64}Cu -ATSM in hypoxic cells is not clearly understood, a biphasic mechanism is suggested which involves initial reduction of ^{64}Cu -ATSM into a charged species. Reduction occurs irrespective of the

oxygenation status of the cell. The charge on ^{64}Cu -ATSM slows down its clearance from the cell. In normal cells, molecular oxygen re-oxidizes the charged intermediate to the parent compound, which eventually clears from the cell. In hypoxic cells however, the charged intermediate undergo further reduction resulting in irreversible trapping of ^{64}Cu .⁶⁸ Apart from oxygen concentration, reduction of ^{64}Cu -ATSM in cells depends on pH as well as nicotinamide adenine dinucleotide (NADH) concentration. Since these cell parameters vary between different tumor types, so does the hypoxia detection efficiency of ^{64}Cu -ATSM.

The $^{99\text{m}}\text{Tc}$ -HL-91 (PROGNOXTM) is another non-nitroimidazole radiopharmaceutical that showed oxygen-dependent accumulation in tissue.⁶⁹ Pre-clinical evaluation of this agent in murine and xenograft tumor models has clearly demonstrated its utility to detect hypoxia. Excellent correlation was observed between $^{99\text{m}}\text{Tc}$ -HL-91 retention and hypoxia measured with Eppendorf oxygen electrode in tumor.⁷⁰ Available evidence indicates that $^{99\text{m}}\text{Tc}$ -HL-91 complex exist in two conformations in solution, one being lipophilic and the other hydrophilic.⁶⁹ The selective uptake of this complex in hypoxic cells is assumed to be due to this peculiar characteristic of $^{99\text{m}}\text{Tc}$ -HL-91 complex.⁷¹

1.8.2. Nitroimidazole radiopharmaceuticals for the detection of hypoxia

1.8.2.1. Evolution

Evolution of nitroimidazole radiopharmaceuticals for hypoxia detection in living tissue was gradual. As early as 1960, metronidazole, a 5-nitroimidazole, and later, several other nitroimidazoles were found to have cytotoxic effects against several anaerobic bacteria and protozoa.⁷² Studies on the mechanism of action of these molecules revealed that, like molecular oxygen, they act as electron acceptors to electron transport protein present in the cell.^{73,74} The feasibility of electron transfer (reduction) depended on the potential of the redox couple formed between nitroimidazole and electron transport protein. The redox potential of such reactions was of the order of -450 mV, with respect to standard hydrogen electrode

(SHE), which occurred only in anaerobes. This explained selective toxicity of these molecules towards anaerobes. Further studies revealed that nitroimidazole reduction process was not the lethal event that killed the cell, but metabolites of nitroimidazole were responsible for the lethal effect. This finding inspired an interesting possibility of using nitroimidazoles as of hypoxic cell sensitizers.⁷⁵ Subsequently, misonidazole, code named Ro 07-0582, was developed which showed radiosensitization in all solid tumors of murine origin in which it was evaluated.

1.8.2.2. Nitroimidazole reduction process and hypoxia selectivity

Nitroimidazole reduction in hypoxic cells involves a series of one-electron reductions mediated by nitro-reductase enzymes present in the cells [Fig. 1.2].⁷⁶

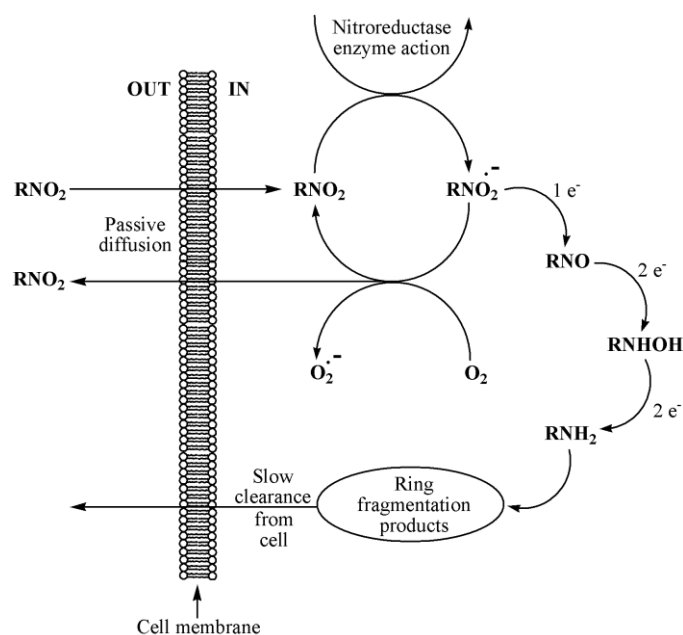


Fig. 1.2. Different steps involved in the nitroimidazole reduction process in hypoxic cell

Initial step in the nitroimidazole reduction process involves the formation of nitroimidazole radical anion, which has a very short life-time. In normoxic cells, the radical anion was quickly oxidized to its initial state by molecular oxygen, which has a more positive reduction potential (-150 mV with respect to SHE).⁷⁶ Eventually, after several such reduction-oxidation cycles, the unreduced nitroimidazole is cleared from the normoxic cells. However, in viable

hypoxic cells, where availability of molecular oxygen is limited, nitroimidazole radical anions undergo further reduction. The reduction process results in trapping of the metabolites in the cells. Thus, appropriately radiolabeled nitroimidazole could be utilized to delineate viable hypoxic cells from normoxic cells in vivo.

1.8.2.3. An overview of nitroimidazole radiopharmaceuticals

Several nitroimidazole radiopharmaceuticals with a variety of diagnostic radioisotopes has been prepared and evaluated to detect hypoxic tissues.⁷⁷⁻⁸¹ Structures of some of the prominent radiopharmaceuticals that have been evaluated clinically are shown in figure 1.3.⁸²

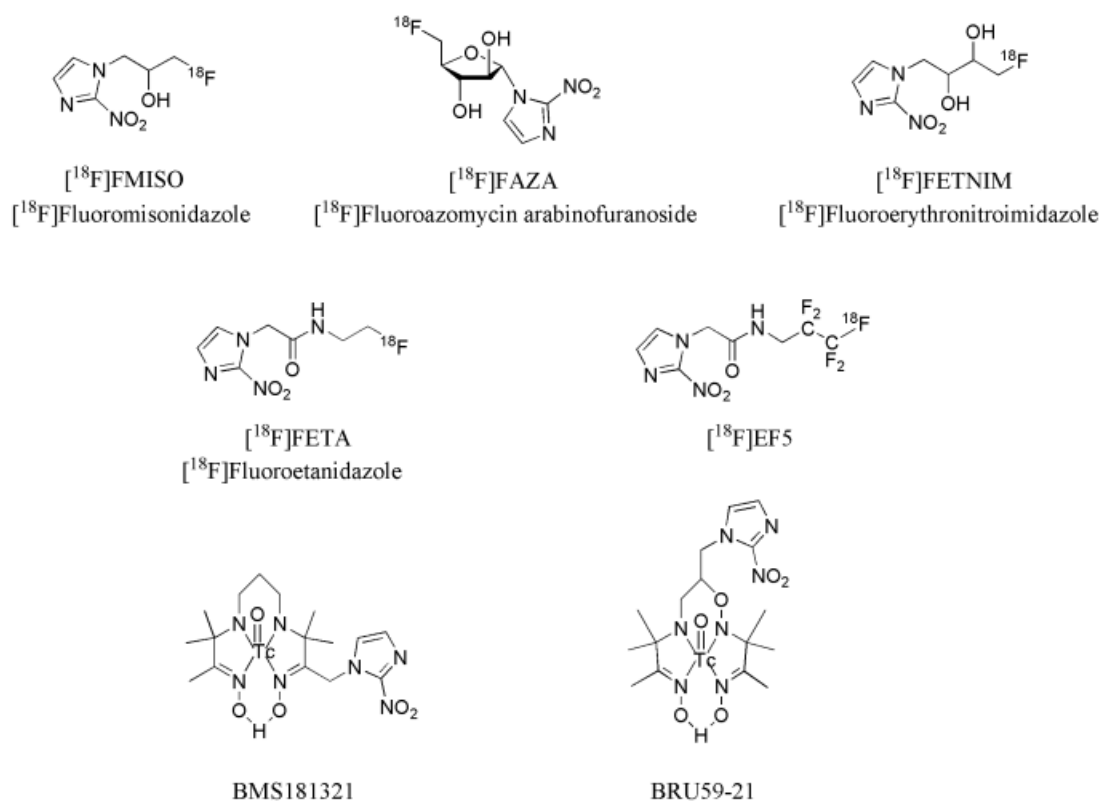


Fig. 1.3. Few clinically evaluated nitroimidazole radiopharmaceuticals for detecting hypoxia in cancerous lesions

[¹⁸F]Fluoromisonidazole ([¹⁸F]FMISO) is probably the most widely used PET radiopharmaceutical for the clinical imaging of hypoxia.⁸³ Other clinically evaluated PET-radiopharmaceuticals include [¹⁸F]FAZA ([¹⁸F]fluoroazomycin arabinofuranoside),^{84,85}

[¹⁸F]FETNIM ([¹⁸F]fluoroerythronitroimidazole),⁸⁶ [¹⁸F]FETA ([¹⁸F]fluoroetanidazole),⁸⁷ [¹⁸F]EF1⁸⁸ and [¹⁸F]EF5.⁸⁹⁻⁹²

Two important SPECT radiopharmaceuticals clinically evaluated for the detection of tissue hypoxia are BMS181321 and BRU59-21.⁹³⁻⁹⁵ Both are 2-nitroimidazole radiopharmaceuticals containing ^{99m}Tc and showed selective accumulation in hypoxic cells in several tumor models. However, very high lipophilicity of these complexes resulted in slow clearance from blood as well as other non-target organs. High background activity due to slow clearance of the BMS181321 and BRU59-21 often resulted in images with poor contrast that provided limited clinical information. There are several other SPECT radiopharmaceuticals to detect tumor hypoxia.^{96,97} However, none of them possessed the ideal or near ideal characteristics required for a hypoxia detecting radiopharmaceutical.

Though [¹⁸F]FMISO is widely used for imaging tissue hypoxia, this radiopharmaceutical also has some undesirable characteristics. [¹⁸F]FMISO, owing to its high lipophilicity, showed uptake in brain and cleared slowly through hepatobiliary route.^{98,99} Apart from these undesirable characteristics, requirement of a cyclotron for the production of ¹⁸F and specialized modules necessary for the preparation of [¹⁸F]FMISO adds to the cost of this radiopharmaceutical. Despite all these factors, [¹⁸F]FMISO continues to be the agent of choice for the detection of tissue hypoxia. This is mainly because of the absence of an alternate radiopharmaceutical which can provide equivalent or superior diagnostic information than [¹⁸F]FMISO.

1.9. Need for a SPECT radiopharmaceutical for detecting hypoxia

The number of PET scanners and cyclotrons in operation all over the world has shown a sharp increase over the past decade. However, especially in India, number of SPECT scanners still far exceeds the number of PET scanners. Also, advances being made in the SPECT hardware and image reconstruction algorithms has significantly improved the spatial

resolution of the images obtained with SPECT.¹⁰⁰ Hence, a hypoxia imaging radiopharmaceutical using a SPECT radionuclide that can provide diagnostic information equivalent to or superior than [¹⁸F]FMISO may find wider applicability. Among different SPECT isotopes, ^{99m}Tc would be the natural choice for developing SPECT radiopharmaceuticals. Because of its optimal decay characteristics, easy availability, low cost and versatile chemistry, ^{99m}Tc is called the ‘Work horse of nuclear medicine’.

1.10. Technetium-99m in nuclear medicine

Carlo Perrier and Emilio Segrè may not even have had a faintest of idea about the importance of their contribution to the field of nuclear medicine when they discovered the element Technetium (Technetium-95 and Technetium-97 isotopes).¹⁰¹ Later, Segre and Glenn T. Seaborg isolated the meta-stable isotope, ^{99m}Tc. Development of the ⁹⁹Mo/^{99m}Tc generator by Walter Tucker and Margaret Greene opened the possibility of wide applications in the field of nuclear medicine. Recent estimates show that ^{99m}Tc was used in over 30 million diagnostic nuclear medical procedures annually (6-7 million are in Europe, 15 million in North America, 6-8 million in Asia/Pacific and 0.5 million in other regions), half of which are bone scans, and the other half are roughly divided between kidney, heart and lung scans.¹⁰² Approximately 85 percent of diagnostic imaging procedures in nuclear medicine use this radionuclide which speaks volumes of its importance in the field of nuclear medicine.

It is a combination of several factors that makes ^{99m}Tc a very useful radionuclide for nuclear medicine applications.¹⁰³⁻¹⁰⁶ ^{99m}Tc decays by ‘isomeric transition’ emitting gamma photons of energy 140 KeV (abundance 89%), which is ideal for imaging applications (Fig. 1.4). It has a half-life of six hours which is long enough to examine metabolic processes, yet short enough to minimize the radiation dose to the patient. Being a transition metal, technetium show variable oxidation states (-1 to +7) making its chemistry versatile enough to incorporate into a wide variety of suitably modified biologically active molecules.

Additionally, low cost of production of ^{99}Mo and availability of $^{99\text{m}}\text{Tc}$ from $^{99}\text{Mo}/^{99\text{m}}\text{Tc}$ generator system makes this isotope invaluable in nuclear medicine.

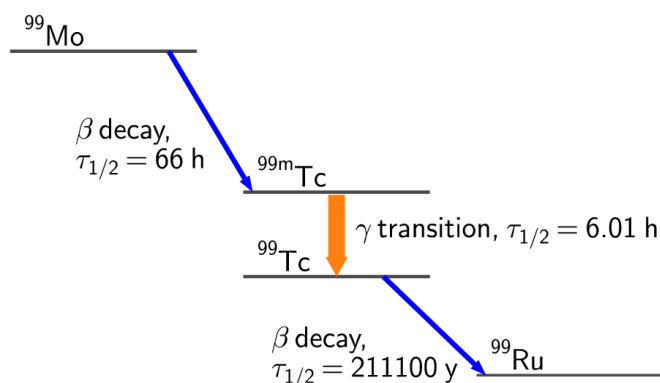


Fig. 1.4. Simplified ^{99}Mo decay scheme

1.10.1. $^{99}\text{Mo}/^{99\text{m}}\text{Tc}$ generator

Walter Tucker and Margaret Greene of Brookhaven National Laboratory developed the $^{99}\text{Mo}/^{99\text{m}}\text{Tc}$ generator system, which has in actual practice helped the end-users in radiopharmacy units in the nuclear medicine centers for easy and widespread sourcing of $^{99\text{m}}\text{Tc}$.^{95,107} A radionuclide generator is a device in which a long-lived parent and short-lived daughter exist in radioactive equilibrium, from which the daughter activity could be separated conveniently at regular intervals with a high degree of radiochemical and radionuclidic purity.^{108,109}

- **Radiochemical purity** – is defined as the percentage of total radioactivity in a sample due to the required chemical form.
- **Radionuclidic purity** – is defined as the percentage of total radioactivity in a sample due to the radionuclide of interest.

Molybdenum-99 (half-life = ~66 h), the parent isotope in $^{99}\text{Mo}/^{99\text{m}}\text{Tc}$ generator system, can be conveniently produced in a nuclear reactor, either by fission of ^{235}U or by neutron activation of ^{98}Mo .¹¹⁰ Former method uses high enriched or low enriched ^{235}U (reaction cross section = 600 barns) as target, while the latter method uses natural molybdenum (abundance

of ^{98}Mo = 24.13%, reaction cross section = 0.13 barns) as target. While fission method produces ^{99}Mo with very high specific activity ($> 10^5$ Ci/g), direct irradiation of ^{98}Mo yields low specific activity ^{99}Mo ($< 2\text{Ci/g}$).

Depending on the methodology of separation of daughter radionuclide from the parent, generators can be classified into column generators, solvent extraction generators or sublimation generators.¹¹¹ Details on the construction and operation of these generator systems are described elsewhere.^{112,113}

1.10.2. Radiolabeling with $^{99\text{m}}\text{Tc}$: Available options

Radiolabeling is the process of tagging a radionuclide to a molecule through a chemical bond. The bond can be covalent or coordinate bond. Radioactive halogens are attached to a molecule by a single covalent bond. However, transition metals form complexes through multiple coordinate bonds. The molecule with appropriate donor atom(s) which form coordinate bond with a metal is called a ligand. The number of donor atoms in a ligand is called its denticity. A ligand with one, two, three, four etc. number of donor atoms are respectively called monodentate, bidentate, tridentate, tetradentate etc. ligand. Sometimes, the biomolecule itself can act as a ligand. In cases where biomolecule does not have appropriate donor atoms, the radiolabeling is carried out by bifunctional chelator approach as described in *section 1.5*.

Technetium belongs to the group VIIB of the periodic table with electronic configuration $[\text{Kr}]4\text{d}^65\text{s}^1$ (neutral atom). Being a transition metal, it shows variable oxidation states between +7 to -1, where +7, +5, +4, +1 and 0 oxidation states are most common. Other oxidation states viz. +6, +3 and -1 has been reported, but are rare and very difficult to stabilize.¹¹⁴ The most stable oxidation state of technetium is +7, which occur in pertechnetate ($^{99\text{m}}\text{TcO}_4^-$) obtained from $^{99}\text{Mo}/^{99\text{m}}\text{Tc}$ generator. Technetium in +7 oxidation state is least reactive towards any donor atom and hence, not useful for radiopharmaceutical

applications. Thus, it has to be reduced to lower oxidation state to make it reactive towards ligands to form ^{99m}Tc -complexes useful for radiopharmaceutical applications. This is the core strategy adopted for the preparation of ^{99m}Tc -radiopharmaceuticals.

During reduction of $^{99m}\text{TcO}_4^-$ to form ^{99m}Tc -complexes, complete reduction of $^{99m}\text{TcO}_4^-$ to ^{99m}Tc -metal is rare, and happens only with certain type of ligands. Generally, one or two oxygen atoms remain associated with ^{99m}Tc in the complex. ^{99m}Tc together with such atom(s) is often called ‘technetium core’. Thus, a ^{99m}Tc -radiopharmaceutical could be thought of as formed by radiolabeling a ligand with a ^{99m}Tc -core. There are several types of ^{99m}Tc -cores available for radiolabeling, each having their own advantages. Some of the most important ^{99m}Tc -cores are ^{99m}Tc -oxo core $[\text{}^{99m}\text{TcO}]^{3+}$, ^{99m}Tc -dioxo core $[\text{}^{99m}\text{TcO}_2]^+$, ^{99m}Tc -nitrido core $[\text{}^{99m}\text{TcN}]^{2+}$, ^{99m}Tc -HYNIC core (HYNIC – hydrazine nicotinic acid) and ^{99m}Tc -tricarbonyl core $[\text{}^{99m}\text{Tc}(\text{CO})_3]^+$ core. Though this thesis concentrates on $^{99m}\text{Tc}(\text{CO})_3$ -core for radiopharmaceutical applications, the use of other ^{99m}Tc -cores are briefly mentioned.

1.10.2.1. Radiolabeling with $[\text{}^{99m}\text{TcO}]^{3+}$ and $[\text{}^{99m}\text{TcO}_2]^+$ core

The chemistry of ^{99m}Tc -oxo core has been thoroughly studied by several authors and extensive literature is available on this topic.¹¹⁵⁻¹²⁰ This is one of the earliest and most widely used ^{99m}Tc -core for radiopharmaceutical applications. Majority of the ^{99m}Tc -radiopharmaceuticals have ^{99m}Tc in +5 oxidation state either as $[\text{}^{99m}\text{Tc}(\text{V})\text{O}]^{3+}$ or $[\text{}^{99m}\text{Tc}(\text{V})\text{O}_2]^+$ [Fig. 1.5].

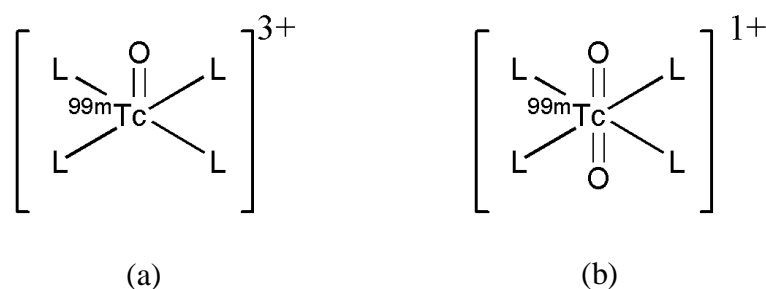


Fig. 1.5. Structure of (a) technetium oxo core $[\text{}^{99m}\text{Tc}(\text{V})\text{O}]^{3+}$ and (b) technetium dioxo core $[\text{}^{99m}\text{Tc}(\text{V})\text{O}_2]^+$. L represents the ligands

^{99m}Tc -oxo complexes are generally square pyramidal, whereas, ^{99m}Tc -dioxo complexes are octahedral. The radiolabeling procedure involves *in situ* reduction of $^{99m}\text{TcO}_4^-$ to generate technetium oxo/dioxo core, which is immediately stabilized by appropriate ligands to form the complex. Some of the common reducing agents used for the reduction of $^{99m}\text{TcO}_4^-$ in solution are stannous chloride, which is useful for reducing $^{99m}\text{TcO}_4^-$ under acidic conditions, or, sodium borohydride (NaBH_4) or sodium dithionite ($\text{Na}_2\text{S}_2\text{O}_4$), which is used under alkaline conditions.

The formation of mono-oxo or dioxo ^{99m}Tc -core in a complex depends on the nature of the ligand as well as the reducing agent. The classical approach for ^{99m}Tc -radiopharmaceutical preparation involves *in situ* reduction of $^{99m}\text{TcO}_4^-$ in presence of the ligand. In the absence of any stabilizing ligands, reduction of $^{99m}\text{TcO}_4^-$ leads to the formation of colloidal $^{99m}\text{Tc(IV)O}_2$. Hence, while reducing $^{99m}\text{TcO}_4^-$, it is very important to maintain sufficient ligand concentration in solution such that the lower oxidation state of ^{99m}Tc is stabilized as soon as it is formed.¹²¹ However, this approach has limitations particularly when the ligand is a receptor binding biomolecule such as peptide, antibody, steroid etc. Excess use of such ligands can lead to saturation of the receptor binding sites on the target tissue by the unlabeled ligand, thereby significantly reducing the binding of ^{99m}Tc -radiopharmaceutical. This can compromise the quality of diagnostic information obtained from the images. A solution to this problem eventually evolved using sodium or calcium salt of glucoheptanoic acid. This approach involves pre-formation of ^{99m}Tc -oxo core with glucoheptanoate ligand. This intermediate complex was then reacted with the actual ligand to form the required ^{99m}Tc -radiopharmaceutical. Since ^{99m}Tc core was stabilized using glucoheptanoate, amount of ligand required to prepare the complex was significantly less compared to the earlier approach. Some of the clinically used radiopharmaceuticals containing ^{99m}Tc -oxo or dioxo core are shown in Fig. 1.6.

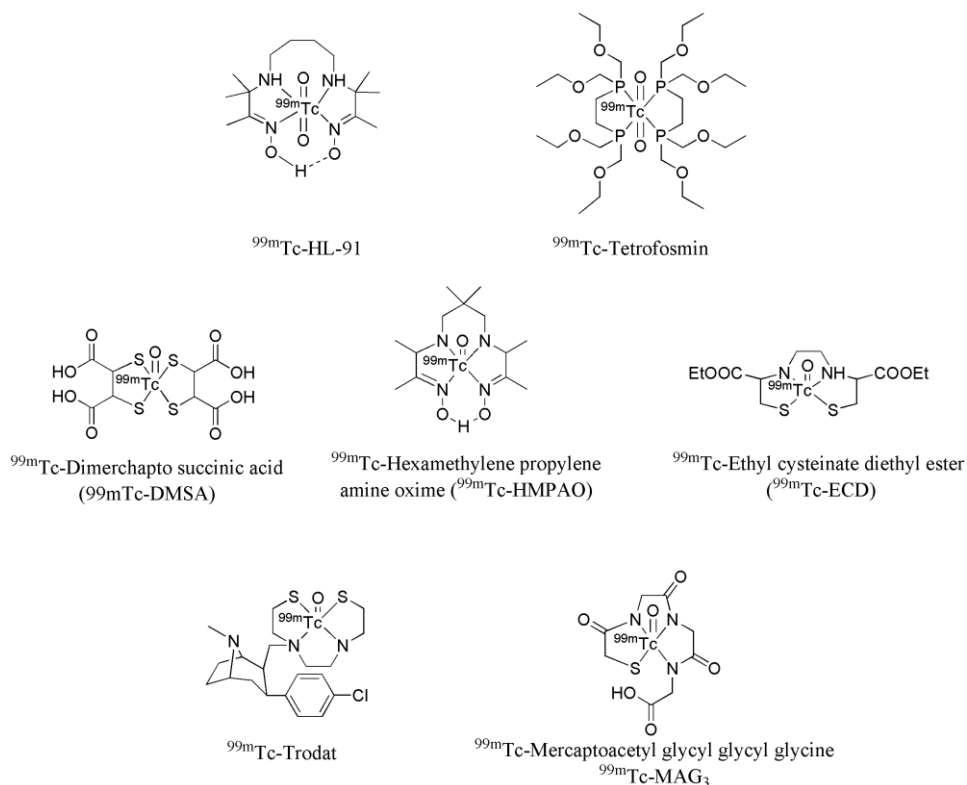


Fig. 1.6. Some clinically useful radiopharmaceuticals having ^{99m}Tc -oxo or dioxo core

The oxidation state of ^{99m}Tc in a given complex depends on the nature of the ligand. With appropriate selection of ligands, complexes of ^{99m}Tc in other oxidation state can also be prepared.^{122,114}

1.10.2.2. Radiolabeling with [^{99m}TcN]²⁺ core

Though, ^{99m}Tc -radiolabeling using glucoheptanoate could significantly reduce the amount of ligand required for the preparation of ^{99m}Tc radiopharmaceuticals, stability of the resulting ^{99m}Tc -oxo or ^{99m}Tc -dioxo complexes were still an issue. These complexes decomposed to $^{99m}\text{TcO}_4^-$ with time. Efforts to find a solution to this problem lead to several other ^{99m}Tc -cores. The [$^{99m}\text{Tc(V)N}$]²⁺ core [Fig. 1.7], originally reported by Baldas et al.,^{123,124} is one such core which is isoelectronic to [$^{99m}\text{Tc(V)O}$]³⁺. This core has recently found wide applicability in the field of radiopharmaceutical chemistry after Duatti et al. introduced a simple method for its preparation.^{125,126}

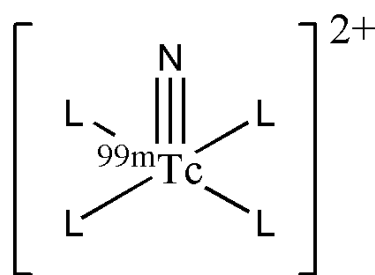


Fig. 1.7. Structure of technetium nitrido $[^{99m}\text{Tc(V)N}]^{2+}$ core

Unlike $[^{99m}\text{TcO}]^{3+}$ core, $[^{99m}\text{TcN}]^{2+}$ core is stable under redox conditions and pH variations which allowed radiolabeling of suitable molecules at lower concentrations.¹²⁷ $[^{99m}\text{TcN}]^{2+}$ core formed stable complexes with ligands containing soft donor atoms like sulphur, as in dithiocarbamates and xanthates.¹²³ With these bidentate chelates, $[^{99m}\text{TcN}]^{2+}$ precursor formed symmetric [2+2] complexes with $[^{99m}\text{TcN}]^{2+}$ moiety occupying the apical position and the other four donor atoms occupying the basal plane of a square pyramidal structure.¹²⁸⁻¹³¹ Some of the radiopharmaceuticals based on $[^{99m}\text{TcN}]^{2+}$ core that showed potential myocardial applications are shown in figure 1.8. The complex $^{99m}\text{TcN}(\text{NOEt})_2$ [NOEt = *N*-ethoxy, *N*-ethyl dithiocarbamate] is a myocardial agent which went upto phase III clinical trials.¹³²

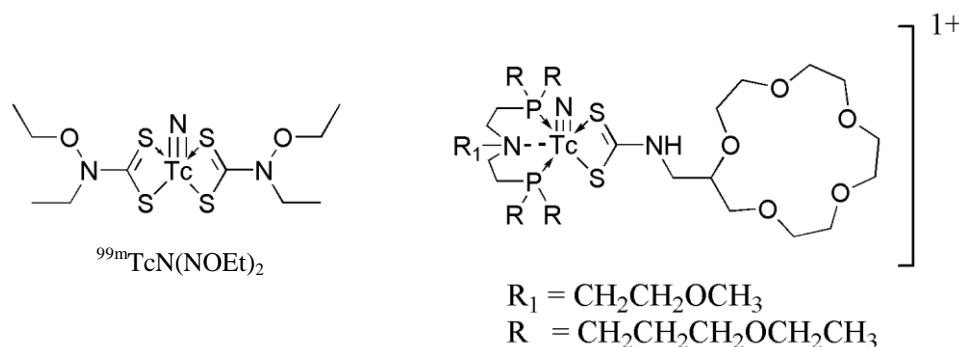


Fig. 1.8. Structure of two potential myocardial perfusion imaging agents based on $[^{99m}\text{TcN}]^{2+}$ core

Apart from symmetric [2+2] $[^{99m}\text{TcN}]^{2+}$ complexes, a large number of asymmetric [2+2] complexes have been prepared using long chain bidentate phosphorus co-ligand (PNP).¹³³⁻¹⁴⁴ A unique feature of PNP ligands is that it occupies two *cis*-positions in the basal plane of the

$[^{99m}\text{TcN}]^{+2}$ precursor complex leaving the other two *cis*-positions to be occupied by bidentate π -donor ligands having NS/OS/ SS donor atoms [Fig. 1.9].^{134,141,143} This approach is particularly useful for bulky biomolecules where a symmetric [2+2] complex would probably result in loss of biological activity due to sterically hindered ^{99m}TcN -complex. The PNP approach offers an additional option to modulate the pharmacokinetics of the complex by altering the lipophilicity of the complex through appropriate selection of pendant groups in PNP ligand.

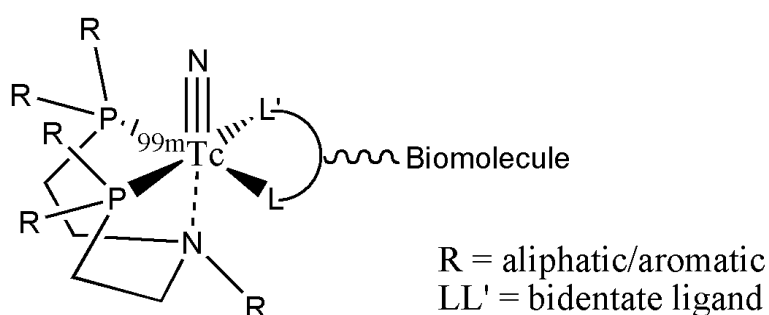


Fig. 1.9. Typical structure of radiopharmaceutical containing $^{99m}\text{TcN}(\text{PNP})$ core

1.10.2.3. Radiolabeling with ^{99m}Tc -HYNIC core

Hydrazino nicotinic acid [HYNIC] is another BFCA generally used for radiolabeling peptides, antibodies and antibody fragments with ^{99m}Tc . In ^{99m}Tc -HYNIC core, ^{99m}Tc exist in +5 oxidation state and it is coordinated to the HYNIC moiety through hydrazine nitrogen. Since HYNIC generally act as a monodentate chelator, co-ligands are required to fill the other vacancies of ^{99m}Tc . Most common co-ligands for ^{99m}Tc -HYNIC systems are tricine and ethylenediaminediacetic acid (EDDA) [Fig. 1.10(a)]. Structural modifications to co-ligands or changing the co-ligand as a whole can modulate the hydrophilicity/lipophilicity of the complex to obtain a desirable in vivo pharmacokinetics. Recently, it has been reported that use of water soluble phosphine ligands like trisodium triphenylphosphine-3,3',3''-trisulfonate (TPPTS) ligands along with tricine can also be used to prepare ^{99m}Tc -HYNIC complexes with high specific activity and stability [Fig. 1.10(b)].¹⁴⁵⁻¹⁶⁶

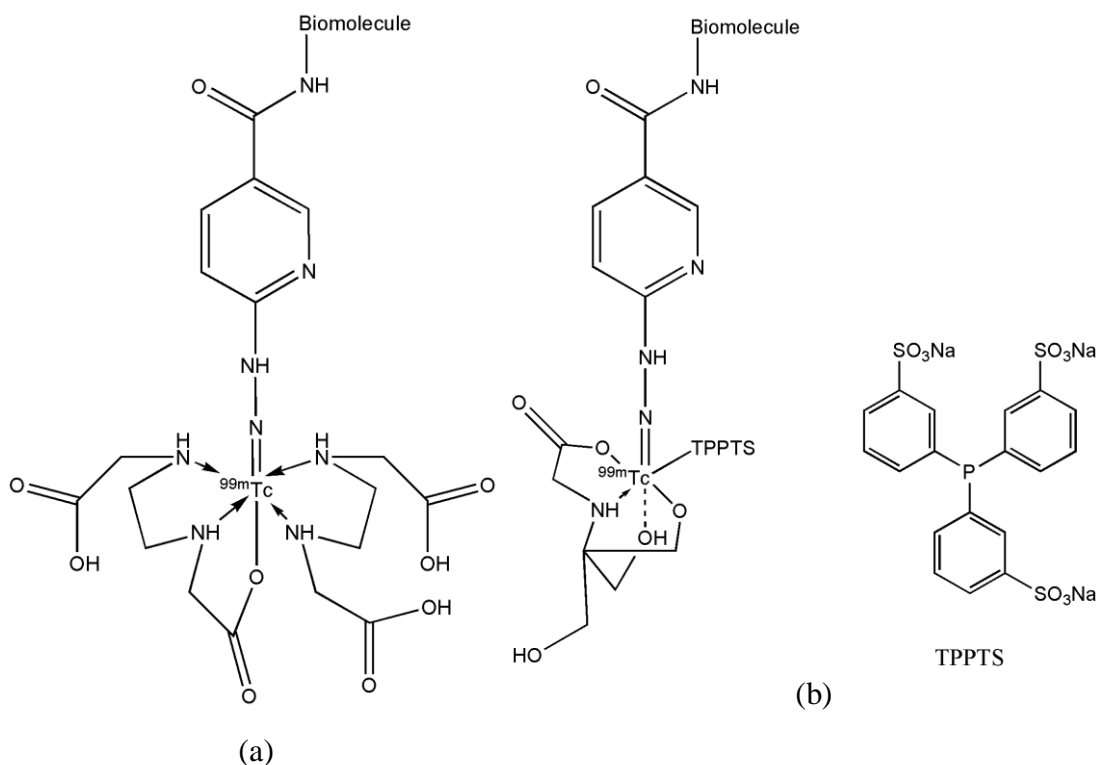


Fig. 1.10. Typical structure ^{99m}Tc -HYNIC-biomolecule complex using (a) EDDA/tricine as co-ligand and (b) TPPTS/tricine co-ligand

1.10.2.4. Radiolabeling with $^{99m}\text{Tc}(\text{CO})_3$ core

The $[\text{}^{99m}\text{Tc}(\text{CO})_3(\text{H}_2\text{O})_3]^+$ precursor complex introduced by Alberto et al. is a significant addition to the options available for radiolabeling biomolecules and other small molecules with ^{99m}Tc .¹⁶⁷ In $[\text{}^{99m}\text{Tc}(\text{CO})_3(\text{H}_2\text{O})_3]^+$ precursor complex, ^{99m}Tc exists in +1 oxidation state. Despite low oxidation state of the metal, the stability of $^{99m}\text{Tc}(\text{CO})_3$ core is not compromised due to π -back bonding from the filled d-orbital of the metal to the empty anti-bonding orbital of CO ligand. The three CO ligands in $^{99m}\text{Tc}(\text{CO})_3$ core could be seen similar to O and N atoms in $[\text{}^{99m}\text{TcO}]^{+3}$ and $[\text{}^{99m}\text{TcN}]^{+2}$, respectively, and they occupy the three facial positions of a regular octahedron. The other three positions are occupied by substitution labile water molecules [Fig. 1.11 (a)], which could be replaced with suitable ligands to form the $^{99m}\text{Tc}(\text{CO})_3$ complexes [Fig. 1.11 (b)].

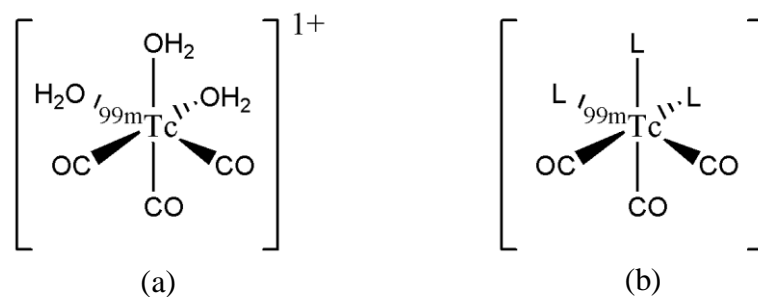


Fig. 1.11. Typical structure of (a) $[^{99m}\text{Tc}(\text{CO})_3(\text{H}_2\text{O})_3]^+$ precursor complex and (b) a complex formed with ligand **L**

The utility of organometallic complexes, including metal-tricarbonyl complexes, in medicine was recognized in early nineties.^{168,169} However, preparation of such complexes often involved harsh conditions, which are not conducive for radiopharmaceutical applications. Alberto et al. developed a novel protocol for the preparation of $[^{99m}\text{Tc}(\text{CO})_3(\text{H}_2\text{O})_3]^+$ precursor complex, from $\text{Na}^{99m}\text{TcO}_4$ in saline using CO gas, which provided impetus for its application in radiopharmaceuticals.¹⁶⁷ Since CO gas was involved, even this procedure was not entirely suitable for radiopharmaceutical applications, especially in hospitals. An elegant solution to this problem came from the same group in the form of potassium boranocarbonate ($\text{K}_2[\text{H}_3\text{BCO}_2]$) which was an in situ source of CO gas.¹⁷⁰ This compound decomposed upon heating releasing CO gas. Though boranocarbonates were initially reported by Malone and Parry in 1967, its synthesis involved tedious procedures. Alberto et al. introduced a more viable method which can be used for the large scale preparation of this compound. This allowed manufacture of lyophilized kits for the preparation of $[^{99m}\text{Tc}(\text{CO})_3(\text{H}_2\text{O})_3]^+$ precursor complex, at the same time avoided the use of CO gas. A photograph of lyophilized kit vial used for the preparation of $[^{99m}\text{Tc}(\text{CO})_3(\text{H}_2\text{O})_3]^+$ precursor complex is shown in figure 1.12. The three substitution labile water molecules in $[^{99m}\text{Tc}(\text{CO})_3(\text{H}_2\text{O})_3]^+$ precursor complex allowed radiolabeling with ligands having appropriate donor atoms such as N, O, P, S etc. The ligands can be mono-, bi-, tridentate or a suitable combination of such ligand systems.¹⁷¹⁻¹⁸⁵ Cyclopentadienyl ligands also formed very stable complexes with $^{99m}\text{Tc}(\text{CO})_3$

core.¹⁸⁶⁻¹⁸⁹ However, difficulty in the preparation of cyclopentadienyl ligands limited exploration of their utility in the field of radiopharmaceuticals, at least till now.



Fig. 1.12. Lyophilized kit vial for the preparation of $[\text{}^{99\text{m}}\text{Tc}(\text{CO})_3(\text{H}_2\text{O})_3]^+$ precursor complex

For radiolabeling with $^{99\text{m}}\text{Tc}(\text{CO})_3$ core, the biomolecule is synthetically modified to incorporate appropriate ligands and subsequently reacted with $[\text{}^{99\text{m}}\text{Tc}(\text{CO})_3(\text{H}_2\text{O})_3]^+$ precursor complex. Complexes of the type shown in figure 1.13(a) are generally preferred for small molecules. Figure 1.13(b) shows the (2+1) approach where a bidentate-monodentate ligand combination is used for radiolabeling with $^{99\text{m}}\text{Tc}(\text{CO})_3$ core. Here, the biomolecule is modified into a monodentate or bidentate ligand and the co-ligand is selected accordingly. The third approach is most common where the biomolecule of interest is modified to possess a tridentate ligand [Fig.1.13(c)]. Radiolabeling could be performed at very low ligand concentration but heating may be required in order to achieve quantitative labeling at μM concentrations. Practically tridentate ligands are found to be most versatile and equally useful to small as well as large biomolecules except proteins, antibodies or antibody fragments. Since quantitative radiolabeling using $[\text{}^{99\text{m}}\text{Tc}(\text{CO})_3(\text{H}_2\text{O})_3]^+$ precursor complex require heating, its applications to complex biomolecules is currently limited. Figure 1.13(d) shows the typical structure of cyclopentadienyl- $^{99\text{m}}\text{Tc}(\text{CO})_3$ complex.

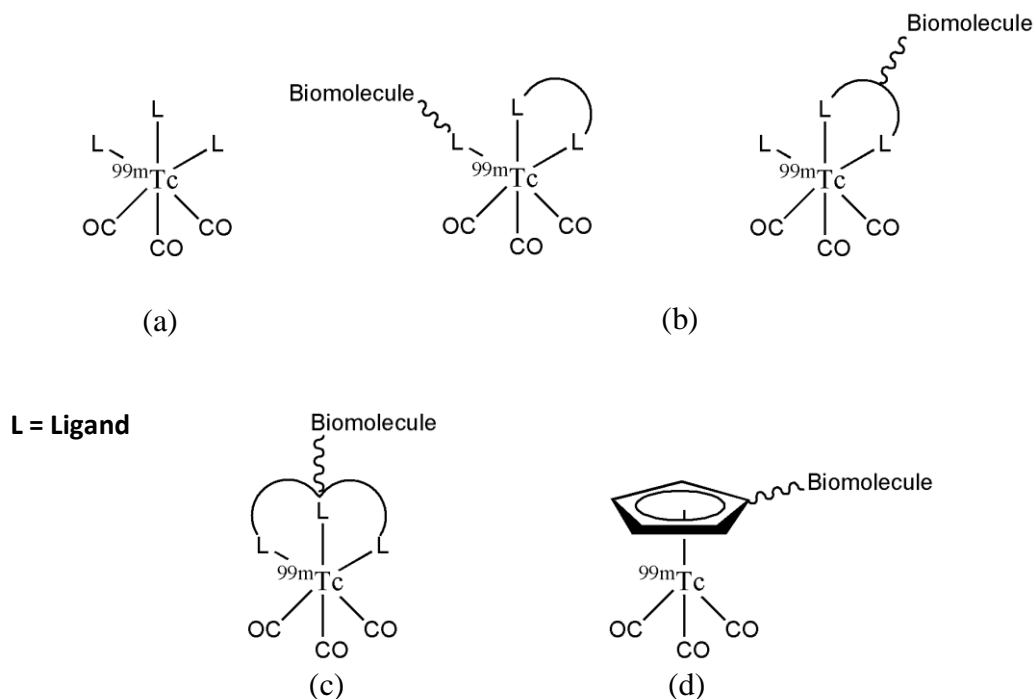


Fig. 1.13. Different approaches of radiolabeling with $^{99m}\text{Tc}(\text{CO})_3$ core

1.11. Quality control of radiopharmaceuticals

Quality control of radiopharmaceutical is essential before it can be administered in a biological system. Typical parameters in the quality control of a radiopharmaceutical are radiochemical purity, pH, appearance etc. Radiochemical purity is assessed by HPLC. The details on the HPLC procedure are briefly mentioned in subsequent sections. The pH of the radiopharmaceutical preparation is determined by pH paper. Generally, pH of the preparation is maintained between 7 and 8 for in vivo applications, and this rule was strictly followed in the present thesis. The radiopharmaceutical preparation is visually inspected for the presence of any particulate matter. The preparation should be clear.

1.12. Evaluation of radiopharmaceuticals

Preliminary testing of new radiopharmaceuticals is initially carried out in appropriate animal models to understand its pharmacokinetics in biological system. The results obtained serves as input for further modifications of the radiopharmaceutical to alter its pharmacokinetics to suit the requirement. A new radiopharmaceutical may go through such

cycles several times before a decision could be made whether it is worth evaluating in higher forms of animals like dogs, pigs, monkeys etc., culminating in human clinical trials. For tumor targeting radiopharmaceuticals, animals bearing appropriate tumor models are used for preliminary evaluation. For testing hypoxia detecting radiopharmaceuticals, a hypoxic tumor model is necessary. A brief description on the hypoxic tumor model used in the present thesis is provided in *Section 1.14.7*.

1.13. Brief overview of present thesis

As mentioned in the previous sections, hypoxia is an important parameter to consider in the clinical management of cancer. Though, [^{18}F]FMISO is currently being used for detection and quantification of hypoxia, considering the economic and logistic aspects, a $^{99\text{m}}\text{Tc}$ -radiopharmaceutical may find wider applicability. Development of a $^{99\text{m}}\text{Tc}$ -radiopharmaceutical for this purpose requires a clear understanding of the influence of various molecular parameters which decides its overall efficacy in a biological system. This thesis attempts to understand this core issue rather than to develop an ideal hypoxia detecting agent. However, information obtained during the work has been utilized to improve the pharmacokinetics of some of the $^{99\text{m}}\text{Tc}$ -radiopharmaceuticals reported in this thesis.

Present chapter is an introduction to some of the basic concepts such as hypoxia, their significance in cancer management, different way of detecting and estimating hypoxia etc. This chapter also provides an overview of various radiopharmaceuticals evaluated for the detection of hypoxia and emphasizes the need for a $^{99\text{m}}\text{Tc}$ -radiopharmaceutical.

Chapter 2 of this thesis in an attempt to understand the effect of SERP, lipophilicity and charge on nitroimidazole- $^{99\text{m}}\text{Tc}(\text{CO})_3$ complexes on their pharmacokinetics. This chapter describes the logic of envisaging nine nitroimidazole ligands, their synthesis, radiolabeling with $^{99\text{m}}\text{Tc}(\text{CO})_3$ core, characterization and subsequent biological evaluation in murine tumor model. The biodistribution results obtained with the different nitroimidazole- $^{99\text{m}}\text{Tc}(\text{CO})_3$

complexes are compared with that of [^{18}F]FMISO in the same animal mode and carefully analyzed to correlate the influence of various molecular properties on their overall efficacy to detect hypoxic cells.

Chapter 3 of this thesis describes the structural modification of 2-nitroimidazole- $^{99\text{m}}\text{Tc}(\text{CO})_3$ complex to alter its pharmacokinetics in a desirable manner. The modified nitroimidazole complex was evaluated in tumor bearing animal model and the results are thoroughly discussed.

Chapter 4 describes an attempt to prepare and evaluate a $^{99\text{m}}\text{Tc}$ -analogue of misonidazole. This chapter discusses the synthesis of a misonidazole-IDA derivative and its radiolabeling with $^{99\text{m}}\text{Tc}(\text{CO})_3$ core. Iminodiacetic acid was chosen because it clears relatively slower from blood, compared to the DETA and AEG derivatives evaluated in Chapter 2, which is essential for the radiotracer to distribute in tumor. This complex was also evaluated in fibrosarcoma tumor bearing animal model and the results obtained are compared with that of [^{18}F]FMISO.

Following sections provides the details on materials, synthetic and characterization methods, procedures involved in biological evaluations etc. which are common to different chapters of present thesis.

1.14. Common materials and methods

Solvents and some of the common chemicals which are used for the synthesis of various compounds described in different chapters of this thesis are mentioned here. Other chemicals which are specific are mentioned in respective chapters. Similarly, techniques used for the characterization of different compounds, quality control of the prepared complexes, protocols followed while carrying out in vivo evaluations etc. which are common throughout the thesis are also briefly described below.

1.14.1. Solvents and chemicals

Solvents such as acetonitrile and diethylether were purchased from s.d. fine chemicals, India. Chloroform, ethylacetate, anhydrous sodium sulphate and sodium hydroxide pellets were purchased from Thomas Baker, India. Anhydrous tetrahydrofuran (THF), anhydrous ethanol, anhydrous methanol, *tert*-butyl bromoacetate and 2-nitroimidazole were purchased from Aldrich, USA. Anhydrous potassium carbonate, triethylamine and diisopropylethylamine (DIEA) are purchased from Fluka, Germany. Silica gel plates (silica gel 60 F₂₅₄) used for TLC, silica gel (60-120 mesh) for column chromatography and supra pure hydrochloric acid were obtained from Merck, India. Sodium pertechnetate was eluted using normal saline from a ⁹⁹Mo/^{99m}Tc column generator. The [^{99m}Tc(CO)₃(H₂O)₃]⁺ core was prepared using Isolink[®] carbonyl kit vial obtained as a gift from Mallinckrodt Medical B. V.

1.14.2. Characterization of the ligands and intermediate compounds

Most of the synthesized compounds were characterized by IR, ¹H-NMR and low resolution mass spectroscopy. Couples of compounds, however, were characterized by IR only. IR spectra were recorded on a JASCO FT/IR-420 spectrophotometer, Japan. IR spectra of oily samples were recorded neat by forming a thin film on NaCl plate, whereas the IR spectra of solid samples were recorded forming a pellet in KBr. ¹H-NMR of the compounds were recorded, either on a 300/400 MHz Varian VXR 300S spectrophotometer, USA or 300 MHz Bruker AvanceII spectrophotometer, Germany, dissolving the sample in appropriate deuteriated solvent containing tetramethylsilane (TMS) as the internal standard. For compounds whose field induction decay files (.fid) could be obtained, the ¹H-NMR spectra were plotted using ACD/NMR Processor Academic Edition (Release:12, Product version:12.01, Build:39104 18 Mar 2010), which is available online. Other spectra were scanned and reported. Mass spectrum of the target compounds were recorded on a Varian 500MS Ion trap mass spectrometer, USA.

1.14.3. Preparation of [^{99m}Tc(CO)₃(H₂O)₃]⁺ precursor complex

The [^{99m}Tc(CO)₃(H₂O)₃]⁺ precursor complex was prepared by adding 1 mL of freshly eluted Na^{99m}TcO₄ from ⁹⁹Mo/^{99m}Tc alumina column generator to Isolink[®] kit vial and heating at 95°C for 20 min. After cooling and re-equilibrating to atmospheric pressure, the pH of the reaction mixture was adjusted to 7 using 1:3 mixture of 0.5 M phosphate buffer (pH 7.4):1 N HCl.

1.14.4. Characterization of [^{99m}Tc(CO)₃(H₂O)₃]⁺ precursor complex and various ^{99m}Tc(CO)₃/Re(CO)₃ complexes

Various nitroimidazole-^{99m}Tc(CO)₃ complexes prepared in the present work were characterized by JASCO PU 2080 Plus dual pump HPLC system, Japan, with JASCO 2075 Plus tunable absorption detector and Gina Star radiometric detector system, using a C18 reversed phase HiQ Sil (5 μm, 4 x 250 mm) column. About 15 μL of the test solution (~0.37 MBq) was injected into the column. Aqueous 0.05M triethylammonium phosphate (TEAP) buffer, pH = 2.5 (Solvent A) and methanol (Solvent B) were used as the mobile phase. The elution started with 100% A from 0 to 6 min. At 6 min the eluent switched to 75% A and 25% B and at 9 min to 66% A and 34% B followed by a linear gradient 66% A/34% B to 100% B from 9 to 20 min. Up to 30 min the eluent remained at 100% B before switching back to the initial condition. The flow rate was maintained at 1 mL/min. For ^{99m}Tc(CO)₃ complexes, elution was monitored by observing the radioactivity profile. Percentage complexation was determined by peak area measurements from the elution profile using the following formula.

$$\% \text{ complexation} = (\text{PA}_{\text{complex}} / \text{PA}_{\text{total}}) * 100$$

Where, PA_{complex} = Peak area corresponding to the complex and PA_{total} = Peak area corresponding to all the peaks in the elution profile.

For $\text{Re}(\text{CO})_3$ -complexes, elution was monitored by observing the UV profile. The UV profile of the $\text{Re}(\text{CO})_3$ -complexes prepared in macroscopic scale were matched with the corresponding radioactivity profile of $^{99\text{m}}\text{Tc}(\text{CO})_3$ -complexes prepared at no-carrier-added (nca) level to establish their structural similarity. Subsequently, the mode of coordination of the ligand with the metal core was established by ^1H -NMR spectroscopy of the $\text{Re}(\text{CO})_3$ -complex in appropriate deuterated solvent.

1.14.5. Determination of partition coefficient ($\text{LogP}_{\text{o/w}}$)

Partition coefficient of the prepared $^{99\text{m}}\text{Tc}(\text{CO})_3$ -complexes were determined following a reported procedure.¹⁹⁰ About 100 μL of the labeled compound was mixed with 0.9 mL of double distilled water (DDW) and 1 mL of octanol on a vortex mixer for 3 min. The mixture was then centrifuged at 3500g for 5 min to effect clear separation of the two layers. About 0.8 mL of the octanol layer was withdrawn into another test tube and equal volume of fresh DDW was added. The mixture was vortexed and then centrifuged as described above. Equal aliquots in triplicate were withdrawn from n-octanol and aqueous layer and radioactivity associated with each layer was determined in a NaI(Tl) counter. The partition coefficients were calculated using the following equation.

$$\text{LogP}_{\text{o/w}} = \text{LogP}[(\text{counts in n-octanol layer})/(\text{counts in aqueous layer})]$$

1.14.6. Serum stability studies

The stability of the prepared $^{99\text{m}}\text{Tc}(\text{CO})_3$ -complexes in human serum was determined following a reported procedure. About 50 μL of the labeled compound was added to 0.5 mL of human serum and this mixture was incubated at 37°C . Equal aliquots (100 μL) were drawn at 1 h, 2 h and 3 h and an equal volume of ethanol was added to precipitate the serum proteins. The mixtures were centrifuged and the supernatants were analyzed by HPLC to assess the stability of the complex in serum.

1.14.7. Biological evaluation

1.14.7.1. Tumor model

When a radiopharmaceutical is evaluated in murine tumor model, the question whether the results could be extrapolated to human tumors assumes significance. Adam et al. had precisely worked on this problem and compared the hypoxic status of several human and mice tumors.¹⁹¹ The study clearly demonstrated that mice tumors are more hypoxic than most human tumors and could be good hypoxia models. In the present study, a fibrosarcoma tumor model (HSDM1C1) of murine origin was used. However, very limited reports are available in the literature where this tumor model is used for hypoxia. Majority of literature report on hypoxia uses tumors developed using KHT cells, CHO cells etc.⁸³⁻⁹⁵ Therefore, a direct comparison of the results obtained with various nitroimidazole complexes from the present study, with the existing literature reports is not appropriate. Hence, the author evaluated [¹⁸F]FMISO, presently the radiopharmaceutical of choice for the detection and estimation of tumor hypoxia, in fibrosarcoma tumor model such that the results can be compared with other nitroimidazole complexes.

1.14.7.2. Biodistribution studies

Swiss mice were used for in vivo distribution study of the labeled complex. Tumor models were developed by subcutaneous administration of murine fibrosarcoma cell line (~10⁶ cells/animal) on the dorsal region of the mice. The tumors were allowed to grow till they reached a size of approximately 1 cm in diameter and then the animals were used for biodistribution study. The radioactive preparation [~100 μCi (3.7 MBq) per animal] was injected intravenously into the tumor bearing mice via the tail vein. Individual sets of animals (n=3) were utilized for studying the biodistribution at different time points (30 min, 60 min, and 180 min). At the end of various time periods, animals in respective sets were immediately sacrificed and the relevant organs excised for measurement of retained activity.

The activity associated with each organ was then measured in a flat-bed type NaI(Tl) counter with suitable energy window for ^{99m}Tc . All procedures performed herein were in strict compliance with the national laws of governing the conduct of animal experiments.

1.14.8. Statistical analysis

Whereever applicable, statistical analysis of relevant data was performed by one-way analysis of variance (ANOVA). Confidence level of 95% ($p < 0.05$) was taken for statistical significance.

CHAPTER 2

ANALYSIS OF THE EFFECT OF DIFFERENT PROPERTIES OF NITROIMIDAZOLE-^{99m}Tc(CO)₃ COMPLEXES ON THEIR IN VIVO UPTAKE AND RETENTION IN HYPOXIC TUMOR

Although we often hear that data speak for themselves, their voices can be soft and sly.

— Frederick Mostelle, An eminent statistician of the 20th century

2.1. Introduction

One of the possible reasons for the unsuccessful attempts to develop a hypoxia imaging radiopharmaceutical superior to [¹⁸F]FMISO is the unclear understanding on the optimal combination of physico-chemical properties of the radiotracer. This is especially true for SPECT-based radiopharmaceuticals containing metallic radionuclides of transition group such as ^{99m}Tc, which may form charged complexes. A charge on the complex can alter its pharmacokinetics compared to the neutral compounds, thus leading to additional complexity. However, this apparent ‘complication’ may as well be considered as a tool to fine-tune the pharmacokinetics of the complex in a desirable manner.

The effect of lipophilicity on the *in vitro* distribution behavior of complexes has been reported.¹⁹² A potential problem with such studies is the possibility of overlooking the interdependence between the various factors that decides the overall efficacy of a radiotracer *in vivo*. However, literature report which collectively deals with the effect of different properties, that decides the overall efficacy and clinical utility of a radiopharmaceutical for detecting and quantifying tissue hypoxia, is lacking.

For the nitroimidazole radiopharmaceuticals, properties like SERP, lipophilicity and charge are the main factors that decide their pharmacokinetics. This chapter focuses on a comprehensive evaluation of the influence of such factors on the overall efficacy of nitroimidazole radiopharmaceuticals to detect tumor hypoxia. To achieve this objective, three series of 2-, 4- and 5- nitroimidazole ligands having tridentate ligands, viz. iminodiacetic acid (IDA), diethylenetriamine (DETA) and aminoethyl glycine (AEG), were envisaged and synthesized. These ligands upon radiolabeling with [^{99m}Tc(CO)₃(H₂O)₃]⁺ precursor, formed complexes with different overall charge, SERP and lipophilicity. Biological evaluation of these complexes were carried out in fibrosarcoma tumor bearing animal model and the results obtained were carefully analyzed to understand the influence of these properties on the

overall pharmacokinetics of the radiotracer in vivo. [^{18}F]FMISO was also evaluated in the same animal model, as a reference standard, and the results are compared with other nitroimidazole- $^{99\text{m}}\text{Tc}(\text{CO})_3$ complexes.

2.2. Materials and methods

3-Bromopropylamine hydrobromide, 1,3-dibromopropane, 4-nitroimidazole, 2-(*tert*-butoxycarbonyloxyimino)-2-phenylacetonitrile (BOC-ON), diethylenetriamine, N-Boc-ethylenediamine were purchased from Sigma-Aldrich, USA. Other common chemicals used and methods followed in the present chapter are mentioned in Chapter 1, *Section 1.14*.

2.3. Synthesis

2.3.1. Synthesis of IDA derivatives of 2-, 4- and 5-nitroimidazole

The synthesis of IDA derivatives of 2-, 4- and 5- nitroimidazole are shown in figure 2.1. The target compounds (**2L1-2L3**) are shown in boxes.

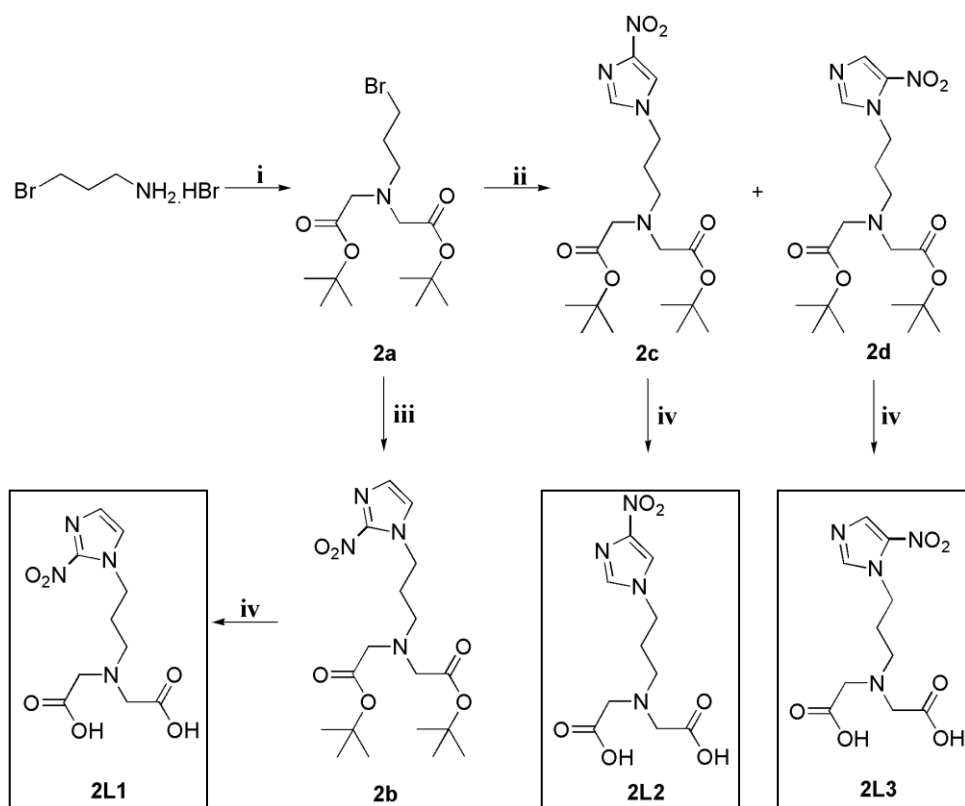


Fig. 2.1. Synthesis of IDA derivatives of nitroimidazole (i) *tert*-butyl bromoacetate, DIEA, acetonitrile, 25°C (ii) 4-nitroimidazole, anhyd. K_2CO_3 , acetonitrile, reflux (iii) 2-nitroimidazole, anhyd. K_2CO_3 , acetonitrile, reflux (iv) 6N HCl, 25°C

2.3.1.1. Synthesis of *N,N*-bis(*tert*-butoxycarbonyl)methyl)-3-bromopropylamine (**2a**)

To 3-bromopropylamine hydrobromide (0.5 g, 2.3 mmol) in acetonitrile (15 mL), DIEA (1.04 g, 8.05 mmol) and *tert*-butylbromoacetate (0.94 g, 4.8 mmol) were added and the reaction mixture stirred at room temperature till completion of reaction (*cf.* TLC). The solvent was removed in vacuo and the residue was worked-up as described in *Section 2.3.4*. Compound **2a** was purified by silica gel column chromatography eluting with chloroform (0.84 g, 82%). R_f (Ethyl acetate) = 0.83. IR (neat, cm^{-1}): 2980 (m); 2939 (m); 1741 (vs); 1444 (m); 1371 (m); 1252 (s); 1190 (vs); 1144 (w); 1030 (s); 993 (w); 918 (w); 864 (w); 731 (w); 649 (w); 565 (w). $^1\text{H-NMR}$ (CDCl_3 , δ ppm): 1.46 (s, 18H, $-\text{N}(\text{CH}_2\text{CO}_2\text{C}(\text{CH}_3)_3)_2$); 2.03 (quintet, 2H, $J = 5.3$ Hz, $\text{BrCH}_2\text{CH}_2\text{CH}_2\text{N-}$); 2.90 (t, 2H, $J = 5.3$ Hz, $\text{BrCH}_2\text{CH}_2\text{CH}_2\text{N-}$); 3.47 (s, 4H, $-\text{N}(\text{CH}_2\text{CO}_2\text{C}(\text{CH}_3)_3)_2$); 3.5 (t, 2H, $J = 5.3$ Hz, $\text{BrCH}_2\text{CH}_2\text{CH}_2\text{N-}$) [Fig. 2.2]. MS(ESI) m/z : 364.4 (M-H) $^-$.

2.3.1.2. Synthesis of *N,N*-bis(*tert*-butoxycarbonyl)methyl)-3-(2-nitro-1*H*-imidazol-1-yl)propane-1-amine (**2b**)

To 2-nitroimidazole (0.17 g, 1.5 mmol) in acetonitrile (15 mL), crushed K_2CO_3 (0.41 g, 3 mmol) was added and the suspension stirred for 15 min. To this suspension, compound **2a** (0.52 g, 1.36 mmol) was added and the mixture refluxed till completion of the reaction (*cf.* TLC). The solvent was removed in vacuo and further work-up was carried out following the general procedure described in *Section 2.3.4*. Compound **2b** was obtained by silica gel chromatography using chloroform/ethyl acetate (80:20 v/v) mixture as the eluent (0.51 g, 94 %). R_f (Ethyl acetate) = 0.7. IR (neat, cm^{-1}): 3124 (m); 2977 (m); 2931 (m); 1737 (vs); 1543 (s); 1491 (m); 1336 (m); 1222 (m); 1147 (vs); 1077 (m); 982 (m); 938 (w); 850 (m); 823 (m); 754 (m); 658 (m). $^1\text{H-NMR}$ (CDCl_3 , δ ppm): 1.47 (s, 18H, $-\text{N}(\text{CH}_2\text{CO}_2\text{C}(\text{CH}_3)_3)_2$); 1.98 (quintet, 2H, $J = 6.0$ Hz, 2-nitroimidazole- $\text{CH}_2\text{CH}_2\text{CH}_2\text{N-}$); 2.73 (t, 2H, $J = 6.0$ Hz, 2-nitroimidazole- $\text{CH}_2\text{CH}_2\text{CH}_2\text{N-}$); 3.39 (s, 4H, $-\text{N}(\text{CH}_2\text{CO}_2\text{C}(\text{CH}_3)_3)_2$); 4.60 (t, 2H, $J = 6.0$ Hz,

2-nitroimidazole-CH₂CH₂CH₂N-); 7.12 (s, 1H, 2-nitroimidazole C5-H); 7.35 (s, 1H, 2-nitroimidazole C4-H) [Fig. 2.3]. MS(ESI⁺) m/z: 399.4 (M+H)⁺.

2.3.1.3. *Synthesis of N,N-bis((tert-butoxycarbonyl)methyl)-3-(4-nitro-1H-imidazol-1-yl)-propane-1-amine (2c) and N,N-bis((tert-butoxycarbonyl)methyl)-3-(5-nitro-1H-imidazol-1-yl)-propane-1-amine (2d)*

To 4-nitroimidazole (0.22 g, 1.93 mmol) in acetonitrile (15 mL), crushed K₂CO₃ (0.53 g, 3.86 mmol) was added and the suspension stirred for 15 min. To this suspension, compound **2a** (0.60 g, 1.6 mmol) was added and the mixture refluxed till completion of the reaction (*cf.* TLC). Thereafter, solvent was removed in vacuo and further work-up was carried out following the general procedure described in *Section 2.3.4*. The 4- and 5-nitroimidazole *tert*-butyl ester derivatives were separated by silica gel chromatography using diethyl ether as the eluent. The 4-nitroimidazole-*tert*-butylester derivative (**2c**) was obtained in an overall yield of 65 % (0.42 g) and the 5-nitroimidazole-*tert*-butylester derivative (**2d**) was obtained in 15 % (0.10 g) overall yield.

Compound **2c**: R_f (Diethyl ether) = 0.52. IR (neat, cm⁻¹): 3134 (m); 2980 (m); 2929 (m); 1734 (vs); 1540 (s); 1500 (m); 1337 (m); 1225 (m); 1150 (vs); 1071 (m); 988 (m); 940 (w); 854 (m); 823 (m); 761 (m); 659 (m). ¹H-NMR (CDCl₃, δ ppm): 1.46 (s, 18H, -N(CH₂CO₂C(CH₃)₃)₂); 1.92 (quintet, 2H, *J* = 6.0 Hz, 4-nitroimidazole-CH₂CH₂CH₂N-); 2.71 (t, 2H, *J* = 6.0 Hz, 4-nitroimidazole-CH₂CH₂CH₂N-); 3.36 (s, 4H, -N(CH₂CO₂C(CH₃)₃)₂); 4.28 (t, 2H, *J* = 6.0 Hz, 4-nitroimidazole-CH₂CH₂CH₂N-); 7.56 (s, 1H, 4-nitroimidazole C2-H); 7.88 (s, 1H, 4-nitroimidazole C5-H) [Fig. 2.4]. MS (ESI⁺) m/z: 399.4 (M+H)⁺.

Compound **2d**: R_f (Diethyl ether) = 0.72. IR (neat, cm⁻¹): 3130 (m); 2980 (m); 2931 (m); 1733 (vs); 1540 (s); 1497 (m); 1336 (m); 1222 (m); 1147 (vs); 1070 (m); 987 (m); 938 (w); 854 (m); 823 (m); 760 (m); 658 (m). ¹H-NMR (CDCl₃, δ ppm): 1.46 (s, 18H, -N(CH₂CO₂C(CH₃)₃)₂); 1.93 (quintet, 2H, *J* = 6.0 Hz, 5-nitroimidazole-CH₂CH₂CH₂N-); 2.71

(t, 2H, $J = 6.0$ Hz, 5-nitroimidazole-CH₂CH₂CH₂N-); 3.37 (s, 4H, -N(CH₂CO₂C(CH₃)₃)₂); 4.57 (t, 2H, $J = 6.0$ Hz, 5-nitroimidazole-CH₂CH₂CH₂N-); 7.82 (s, 1H, 5-nitroimidazole C2-H); 8.0 (s, 1H, 5-nitroimidazole C4-H) [Fig. 2.5]. MS(ESI⁺) m/z : 399.3 (M+H)⁺.

2.3.1.4. Synthesis of ligands **2L1** – **2L3**

Compounds **2b**, **2c** and **2d** (0.25 mmol) were hydrolyzed following the general procedure described in Section 2.3.5 to obtain the target ligands **2L1** (96%), **2L2** (90%) and **2L3** (97%), respectively, as the hydrochloride salt.

2,2'-((3-(2-nitro-1H-imidazol-1-yl)propyl)imino)diacetic acid (2L1):

IR (KBr, cm⁻¹) 3136 (m); 2970 (m); 2847 (m); 1760 (vs); 1724 (s); 1559 (m); 1499 (m); 1392 (m); 1350 (m); 1230 (m); 1198 (m); 1138 (s); 1006 (w); 860 (m); 827 (m); 751 (w); 653 (m).

¹H-NMR (D₂O, δ ppm) 2.23 (quintet, 2H, $J = 8.1$ Hz, 2-nitroimidazole-CH₂CH₂CH₂N-); 3.32 (m, 2H, 2-nitroimidazole-CH₂CH₂CH₂N-); 3.88 (s, 4H, -N(CH₂CO₂H)₂); 4.21 (m, 2H, 2-nitroimidazole-CH₂CH₂CH₂N-); 7.35 (s, 1H, 2-nitroimidazole C5-H); 7.45 (s, 1H, 2-nitroimidazole C4-H) [Fig. 2.6]. MS(ESI⁻) m/z : 285.0 (M-H)⁻ [Fig. 2.7].

2,2'-((3-(4-nitro-1H-imidazol-1-yl)propyl)imino)diacetic acid (2L2):

IR (KBr, cm⁻¹) 3132 (m); 2975 (m); 2847 (m); 1761 (vs); 1727 (s); 1559 (m); 1498 (m); 1394 (m); 1350 (m); 1231 (m); 1182 (m); 1140 (s); 1015 (w); 861 (m); 829 (m); 758 (w); 656 (m).

¹H-NMR (D₂O, δ ppm) 2.23 (quintet, 2H, $J = 7.5$ Hz, 4-nitroimidazole-CH₂CH₂CH₂N-); 3.27 (m, 2H, 4-nitroimidazole-CH₂CH₂CH₂N-); 3.96 (s, 4H, -N(CH₂CO₂H)₂); 4.14 (t, 2H, $J = 7.5$ Hz, 4-nitroimidazole-CH₂CH₂CH₂N-); 7.65 (s, 1H, 4-nitroimidazole C2-H); 8.10 (s, 1H, 4-nitroimidazole C5-H) [Fig. 2.8]. MS(ESI⁻) m/z : 286.6 (M-H)⁻ [Fig. 2.9].

2,2'-((3-(5-nitro-1H-imidazol-1-yl)propyl)imino)diacetic acid (2L3):

IR (KBr, cm⁻¹) 3130 (m); 2974 (m); 2847 (m); 1763 (vs); 1724 (s); 1559 (m); 1499 (m); 1392 (m); 1350 (m); 1230 (m); 1180 (m); 1140 (s); 1014 (w); 861 (m); 827 (m); 758 (w); 654 (m).

¹H-NMR (D₂O, δ ppm) 2.27 (quintet, 2H, $J = 7.5$ Hz, 5-nitroimidazole-CH₂CH₂CH₂N-); 3.42

(m, 2H, 5-nitroimidazole-CH₂CH₂CH₂N-); 4.04 (s, 4H, -N(CH₂CO₂H)₂); 4.52 (m, 2H, 5-nitroimidazole-CH₂CH₂CH₂N-); 8.26 (s, 1H, 5-nitroimidazole C2-H); 8.46 (s, 1H, nitroimidazole C4-H) [Fig. 2.10]. MS(ESI) m/z: 285.0 (M-H)⁻ [Fig. 2.11].

2.3.1.5. Preparation of Re(CO)₃ complex of ligand **2L1** (**2e**)

The compound bis(tetraethylammonium)-*fac*-tribromotricarbonylrhenate was prepared following a procedure reported by Alberto et al.¹⁹³ The rhenium analogue of 2-nitroimidazole-IDA-[^{99m}Tc(CO)₃] was prepared by reacting sodium salt of 2-nitroimidazole-IDA derivative (0.12 g, 0.41 mmol) with bis(tetraethylammonium)-*fac*-tribromotricarbonylrhenate (0.33 g, 0.45 mmol) in water (5 mL). The reaction mixture was refluxed for 12 h and then cooled to room temperature. The precipitate formed was removed by filtration and the filtrate upon evaporation gave the target compound **2e** as tetraethylammonium salt (0.12 g, 52%). IR (KBr, cm⁻¹) 3130 (m); 2984 (m); 2950 (m); 2692 (w); 2016 (vs); 1878 (vs); 1646 (s); 1491 (w); 1395 (m); 1337 (m); 1288 (w); 1183 (w); 1133 (w). ¹H-NMR (D₂O, δ ppm) 1.15 (m, 24H, [N(CH₂CH₃)₄]₂); 2.20 (quintet, 2H, *J* = 8.3 Hz, 2-nitroimidazole-CH₂CH₂CH₂N-); 3.14 (q, 16H, *J* = 7.4 Hz, [N(CH₂CH₃)₄]₂); 3.39 (m, 2H, 2-nitroimidazole-CH₂CH₂CH₂N-); 3.54 (d, 2H, *J* = 16.3 Hz, -NCH_AH_BCO-); 3.76 (d, 2H, *J* = 16.3 Hz, -NCH_AH_BCO-); 4.13 (t, 2H, *J* = 7.4 Hz, 2-nitroimidazole-CH₂CH₂CH₂N-); 7.23 (s, 1H, 2-nitroimidazole C5-H); 7.41 (s, 1H, 2-nitroimidazole C4-H) [Fig. 2.12].

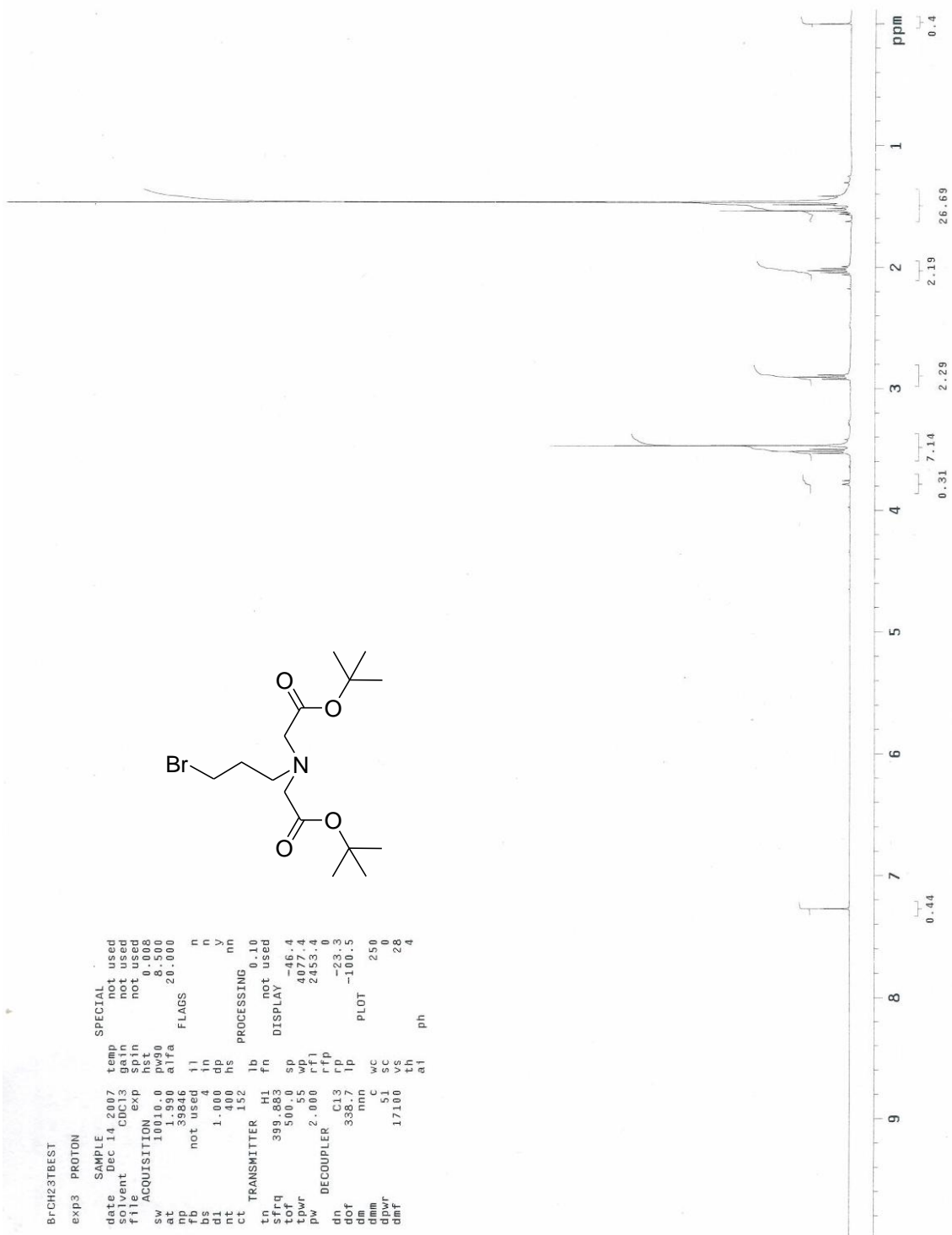


Fig. 2.2. ¹H-NMR spectrum of N,N-bis((tert-butoxycarbonyl)methyl)-3-bromopropyl amine (2a)

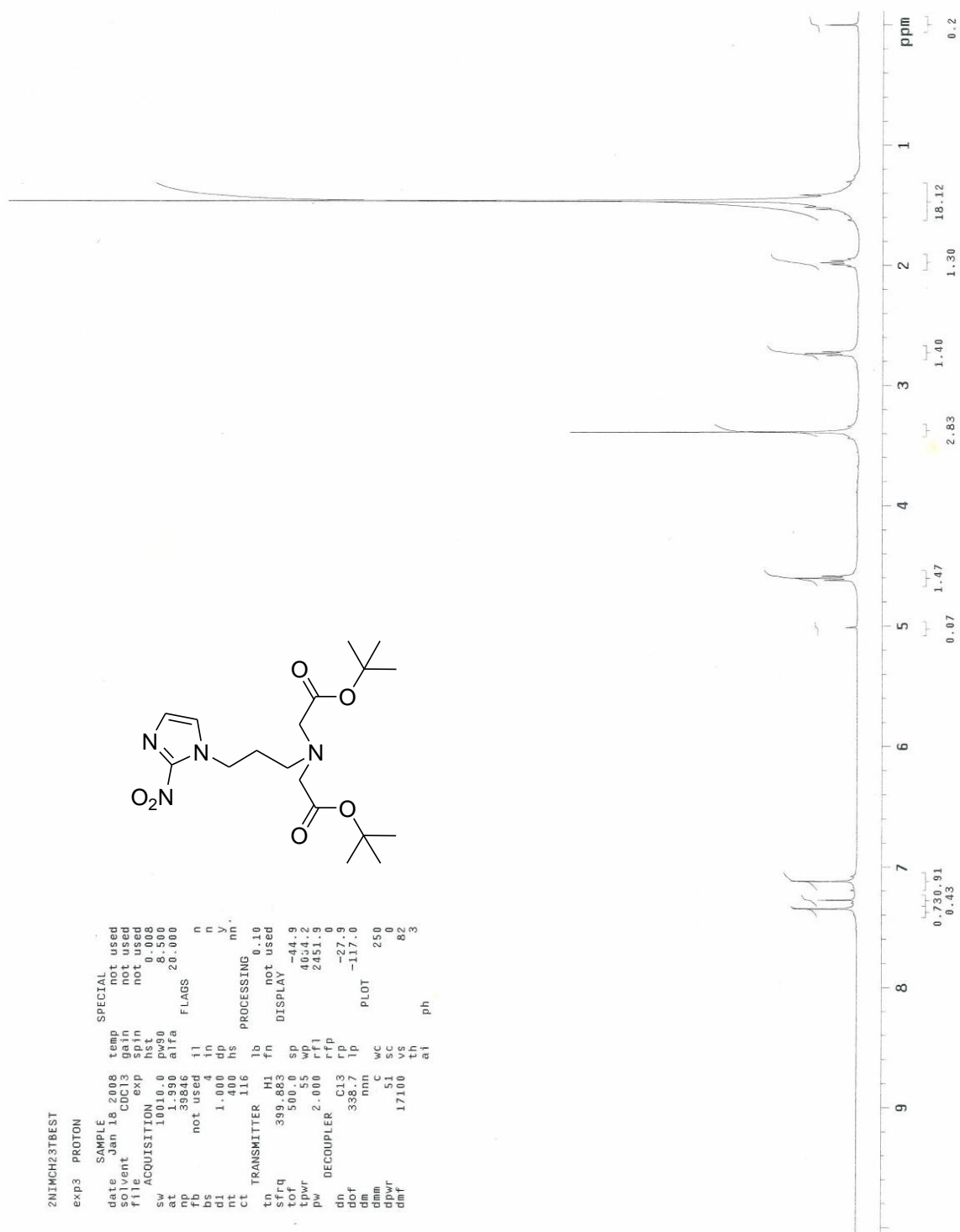


Fig. 2.3. ^1H -NMR spectrum of *N,N*-bis(*tert*-butoxycarbonyl)methyl)-3-(2-nitro-1*H*-imidazol-1-yl)propane-1-amine (**2b**)

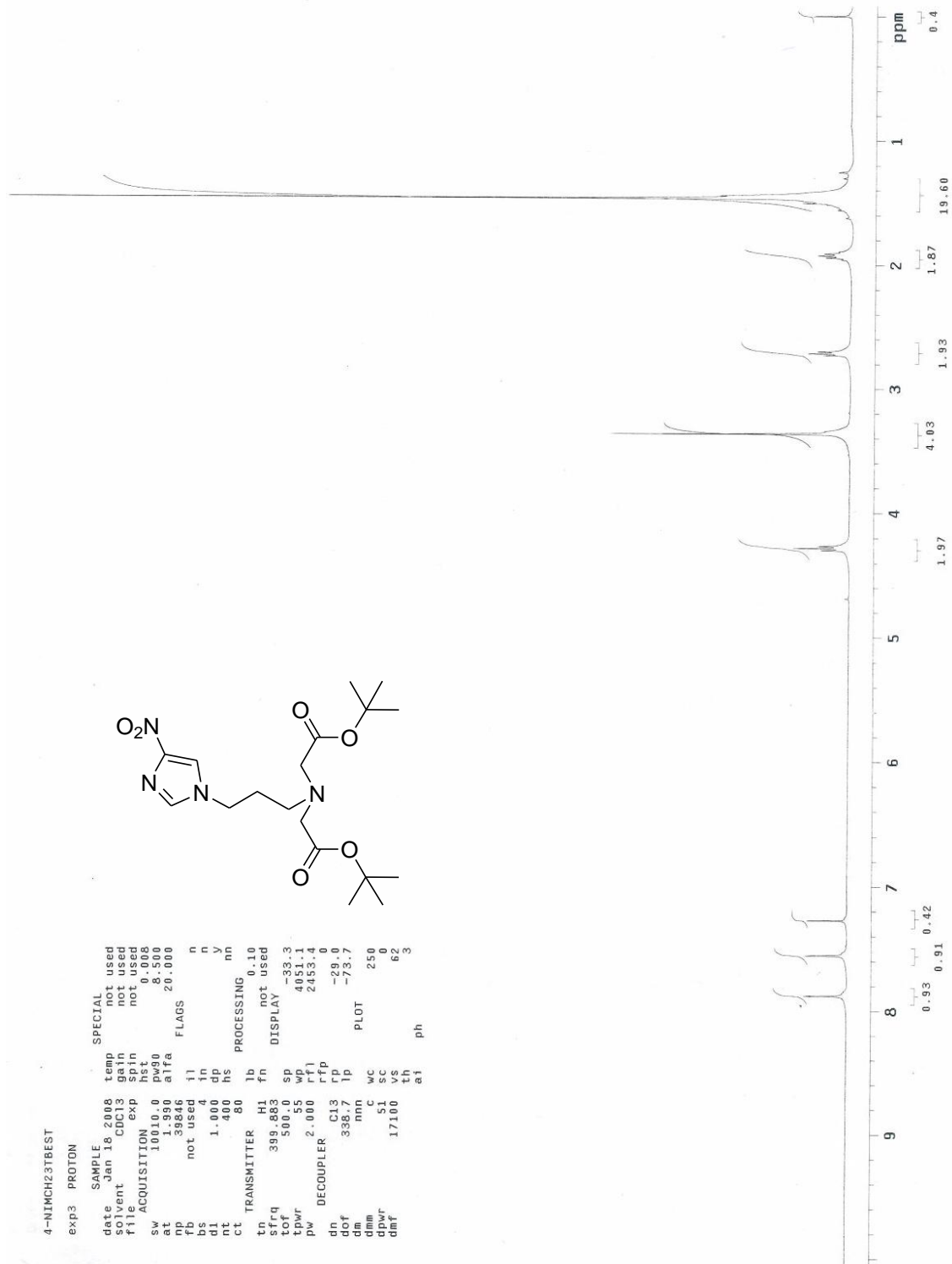


Fig. 2.4. $^1\text{H-NMR}$ spectrum of *N,N*-bis(*tert*-butoxycarbonyl)methyl)-3-(4-nitro-1*H*-imidazol-1-yl)propane-1-amine (**2c**)

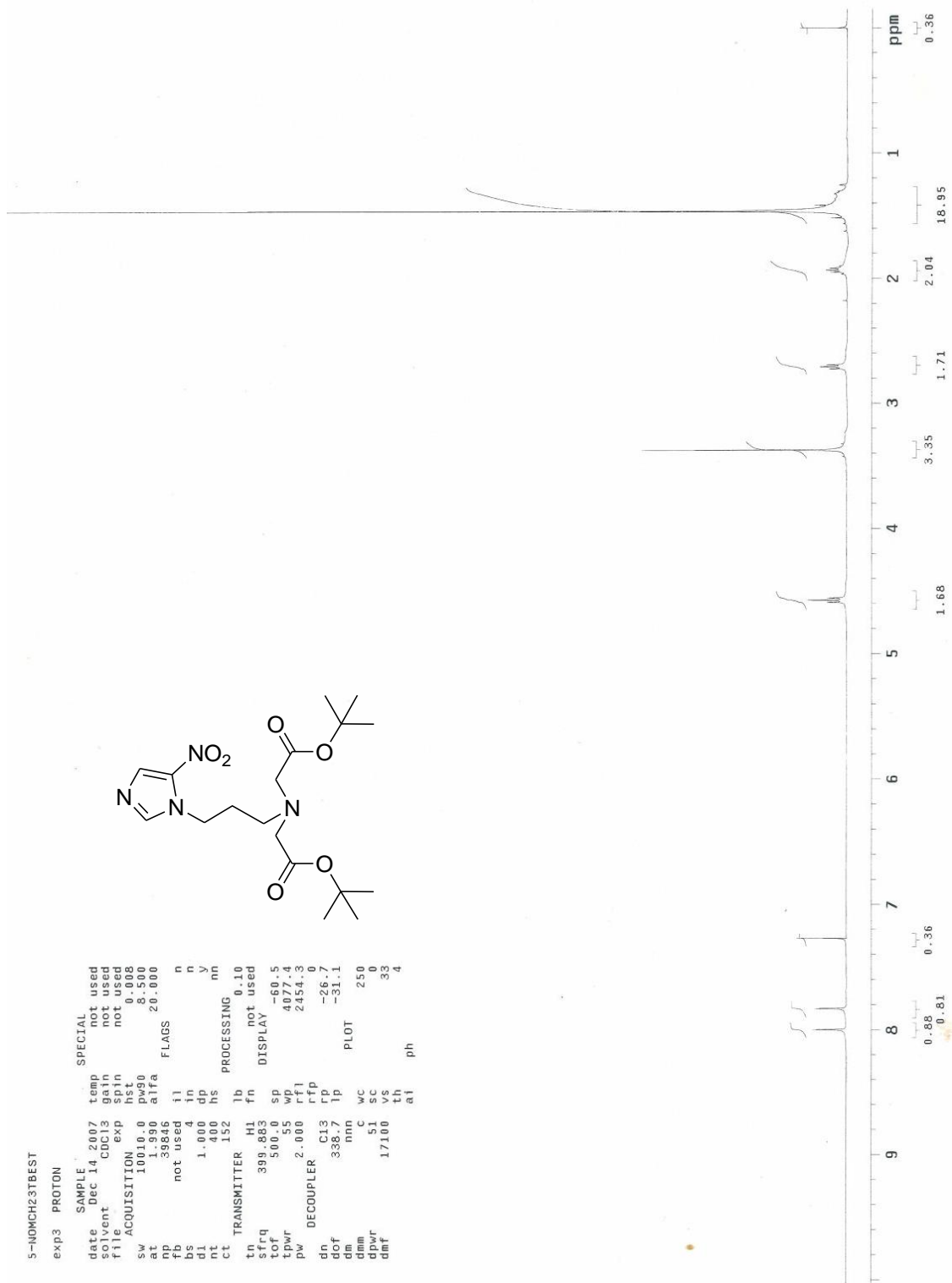


Fig. 2.5. $^1\text{H-NMR}$ spectrum of *N,N*-bis(*tert*-butoxycarbonyl)methyl)-3-(5-nitro-1*H*-imidazol-1-yl)propane-1-amine (**2d**)

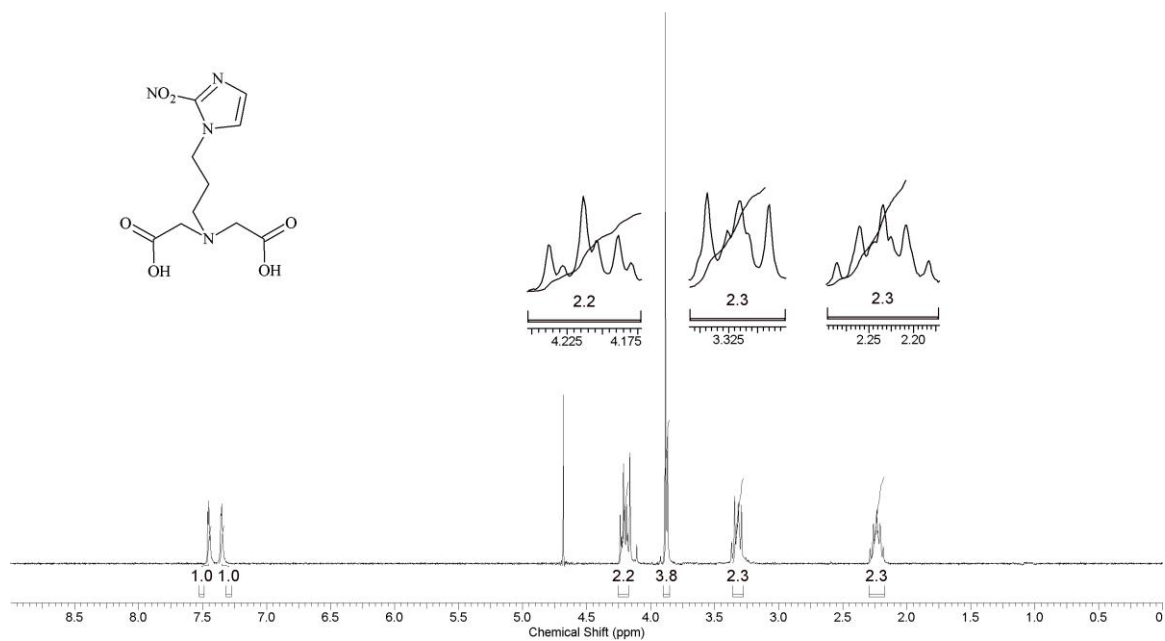


Fig. 2.6. ¹H-NMR spectrum of 2,2'-((3-(2-nitro-1H-imidazol-1-yl)propyl)imino)diacetic acid (**2L1**)

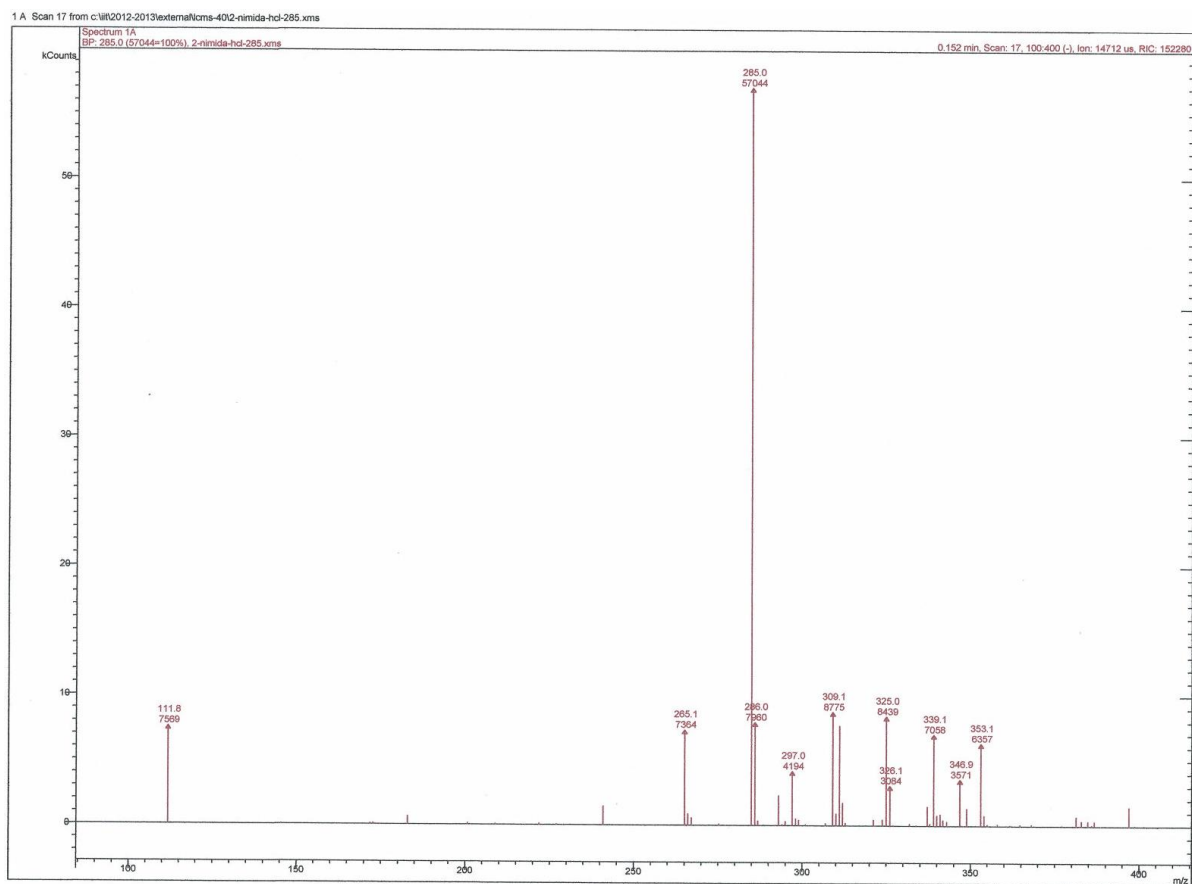


Fig. 2.7. ESI-MS of 2,2'-((3-(2-nitro-1H-imidazol-1-yl)propyl)imino)diacetic acid (**2L1**)

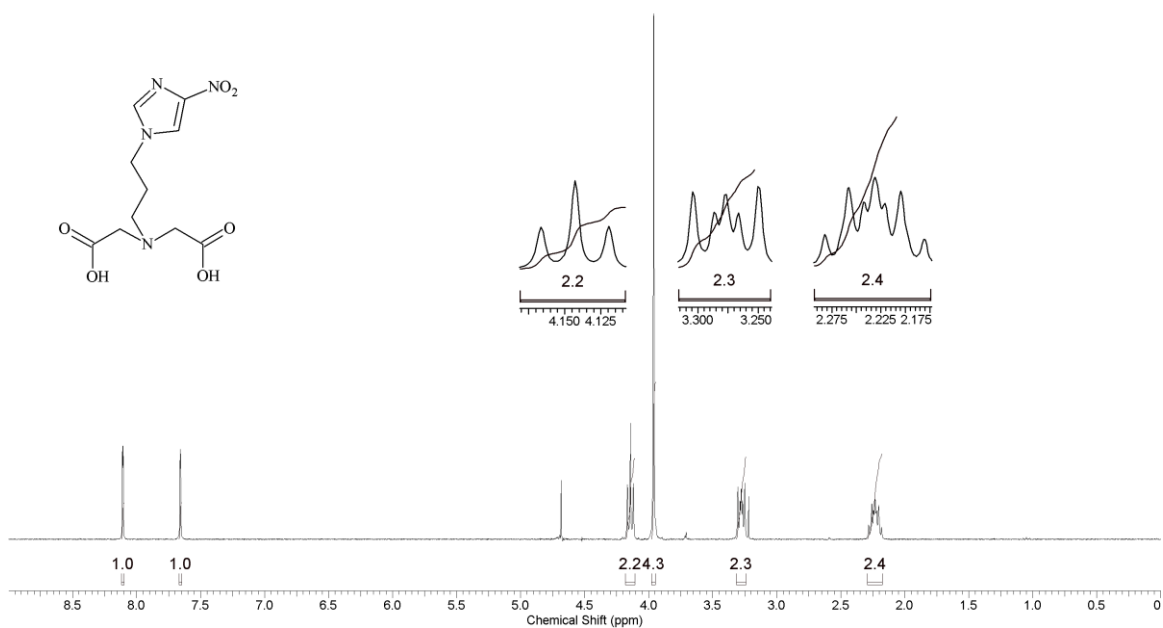


Fig. 2.8. ¹H-NMR spectrum of 2,2'-((3-(4-nitro-1H-imidazol-1-yl)propyl)imino) diacetic acid (**2L2**)

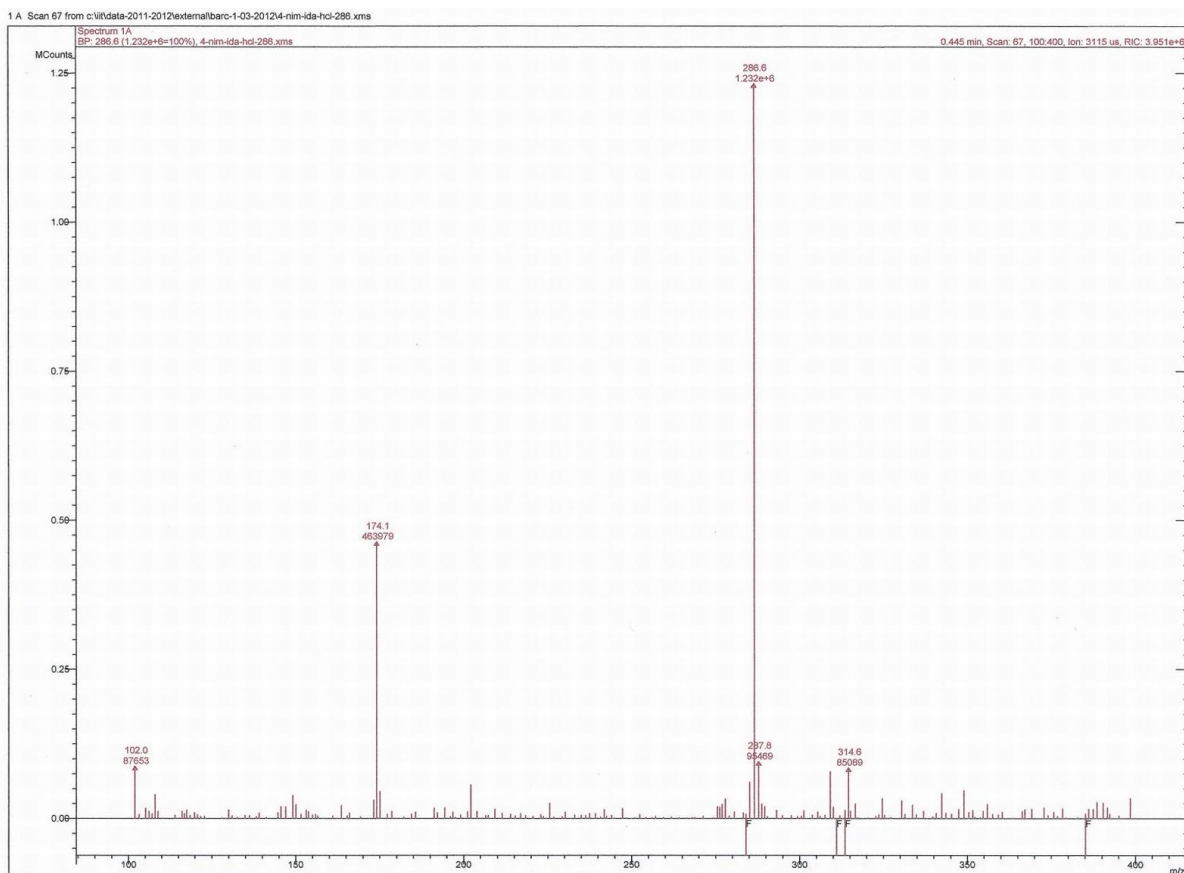


Fig. 2.9. ESI-MS of 2,2'-((3-(4-nitro-1H-imidazol-1-yl)propyl)imino) diacetic acid (**2L2**)

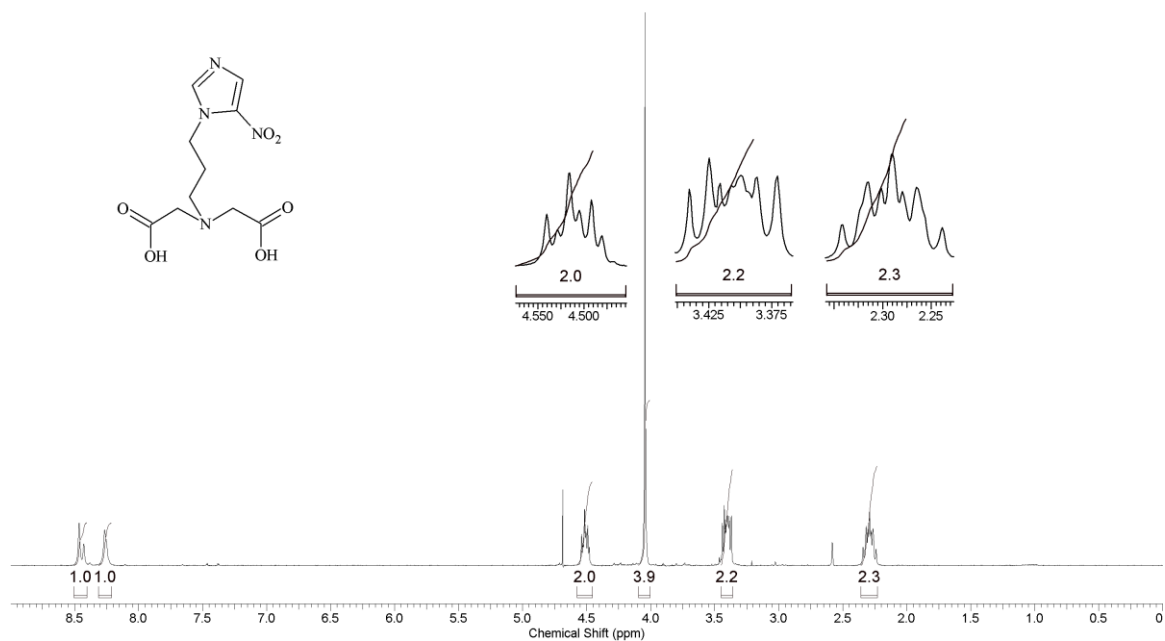


Fig. 2.10. ¹H-NMR spectrum of 2,2'-((3-(5-nitro-1H-imidazol-1-yl)propyl)imino)diacetic acid (**2L3**)

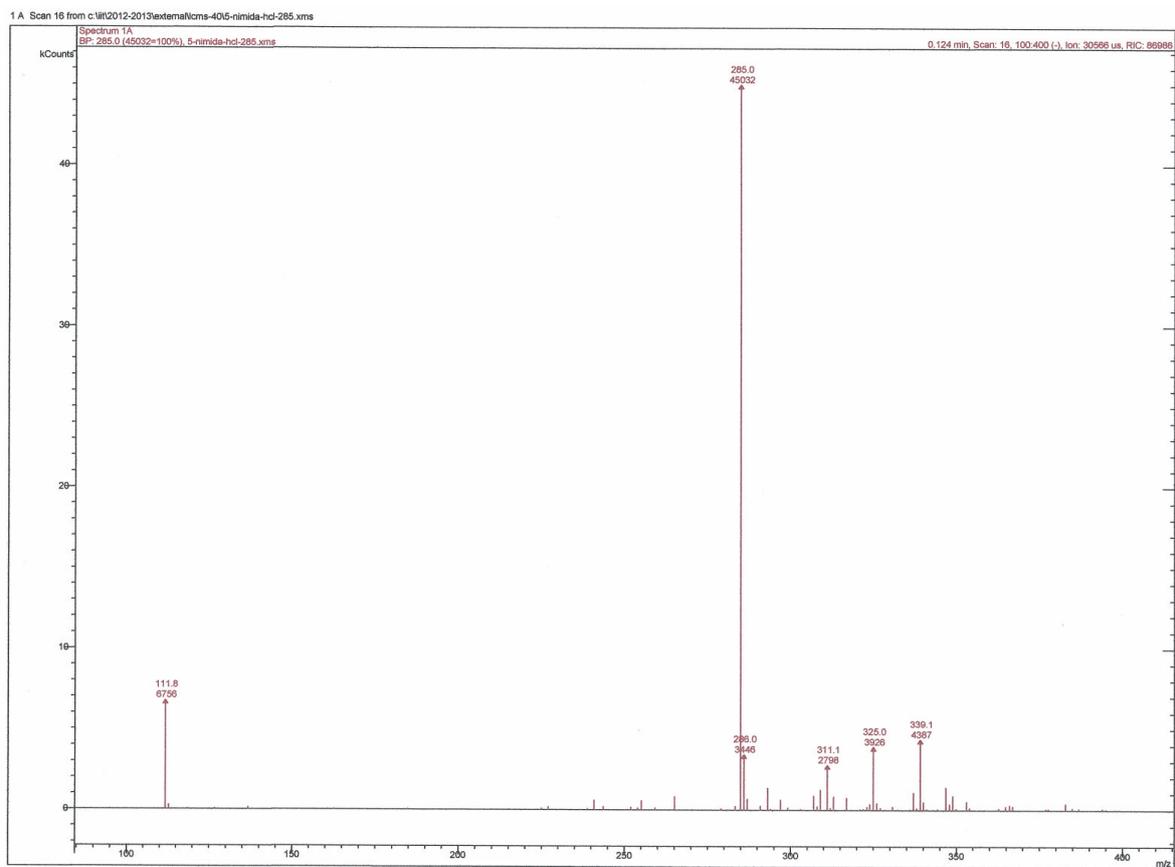


Fig. 2.11. ESI-MS of 2,2'-((3-(5-nitro-1H-imidazol-1-yl)propyl)imino)diacetic acid (**2L3**)

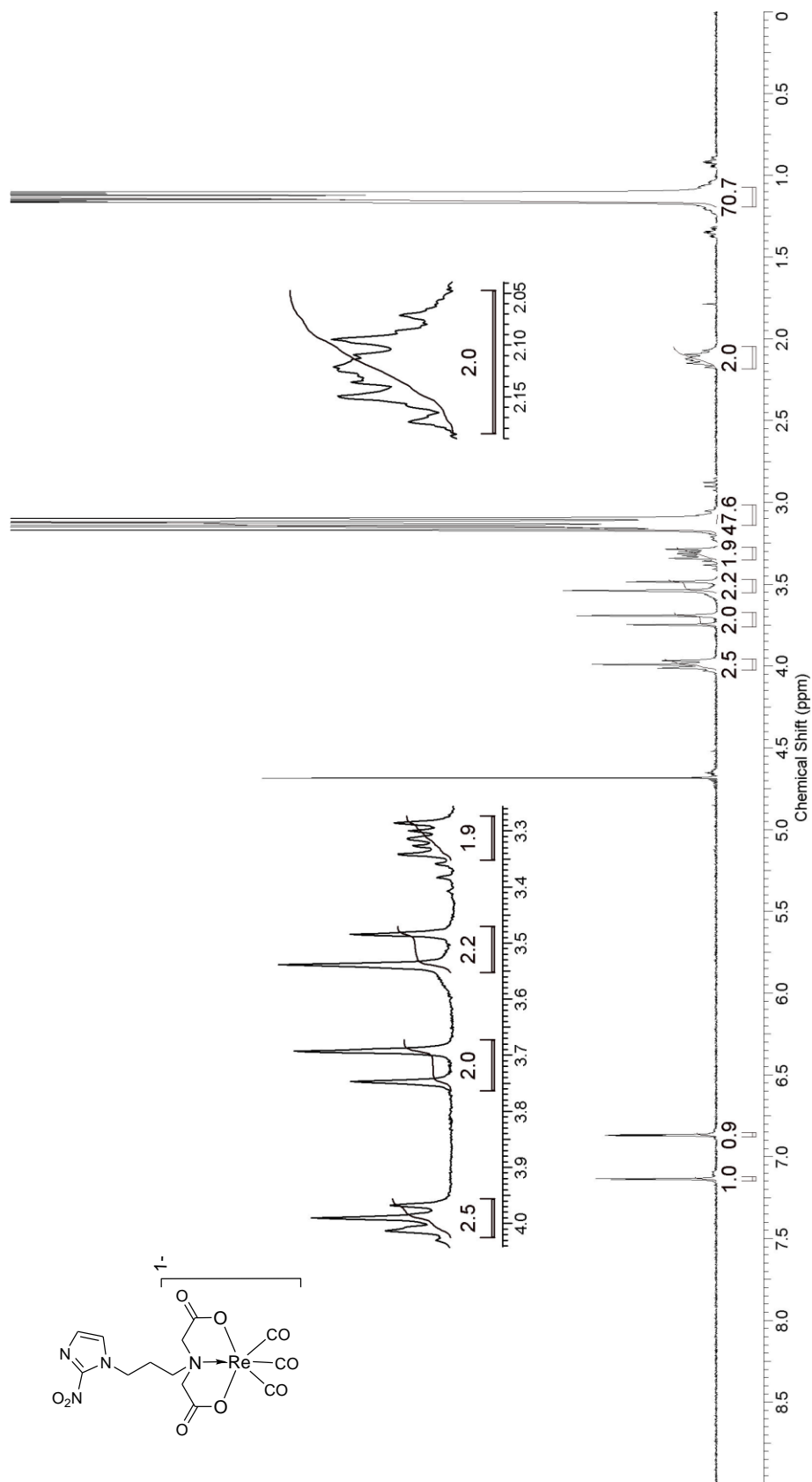


Fig. 2.12. $^1\text{H-NMR}$ spectrum of $\text{Re}(\text{CO})_3$ complex of ligand **2L1** (**2e**)

2.3.2. Synthesis of DETA derivatives of 2-, 4- and 5-nitroimidazole

The synthesis of IDA derivatives of 2-, 4- and 5- nitroimidazole are shown in figure 2.13. The target compounds (**2L4-2L6**) are shown in boxes.

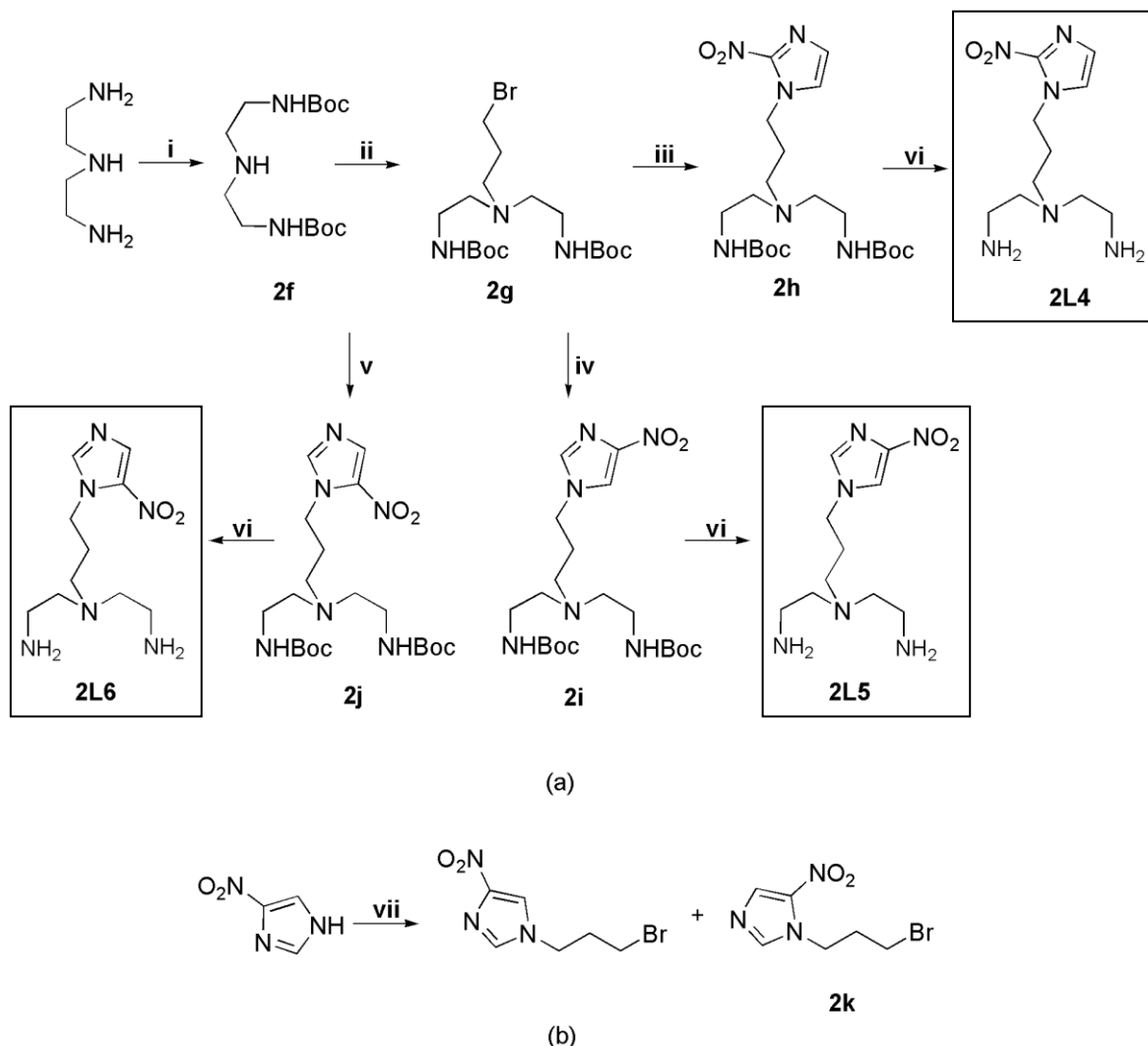


Fig. 2.13. Synthesis of DETA derivatives of nitroimidazole (i) BOC-ON, DIEA, tetrahydrofuran, 0°C (ii) 1,3 dibromopropane, DIEA, acetonitrile, reflux (iii) 2-nitroimidazole, DIEA, acetonitrile, reflux (iv) 4-nitroimidazole, DIEA, acetonitrile, reflux (v) **2k**, DIEA, acetonitrile, reflux (vi) 6N HCl, 25°C

2.3.2.1. Synthesis of tert-butyl 2-(2-(tert-butoxycarbonyl)aminoethyl)aminoethyl carbamate

(**2f**)

Selective protection of primary amine groups of diethylenetriamine was carried out using BOC-ON.¹⁹⁴ Diethylenetriamine (0.95 g, 9.2 mmol) in dry tetrahydrofuran (20 mL) was cooled to 0°C in an ice bath. BOC-ON dissolved in dry tetrahydrofuran (10 mL) was

added dropwise to this solution over a period of 3 h with continuous stirring. On completion of the addition, the reaction mixture was brought to room temperature and the stirring was continued for another 24 h. The solvent was removed using rotary evaporator. The pale yellow residue was dissolved in chloroform (100 mL) and washed with 10% NaOH (50 mL portions) till organic layer turned colorless. The organic layer was washed with brine (50 mL) and dried over anhydrous sodium sulphate. The solvent was removed in vacuo and the residue was purified by silica gel column chromatography eluting with ethyl acetate (2.34 g, 84%). R_f (Methanol) = 0.70. IR (neat, cm^{-1}): 3342(w); 2976 (m); 2932(w); 2854(w); 2816(w); 1695(s); 1528(m); 1455(w); 1391(w); 1366(m); 1774(m); 1750(m); 1172(s); 781(w). $^1\text{H-NMR}$ (CDCl_3 , δ ppm): 1.41 (s, 18H, $((\text{CH}_3)_3\text{CO}(\text{CO})\text{NHCH}_2\text{CH}_2)_2\text{NH}$); 2.71 (t, 4H, $J = 5.9$ Hz, $((\text{CH}_3)_3\text{CO}(\text{CO})\text{NHCH}_2\text{CH}_2)_2\text{NH}$); 3.19 (m, 4H, $((\text{CH}_3)_3\text{CO}(\text{CO})\text{NHCH}_2\text{CH}_2)_2\text{NH}$) [Fig. 2.14]. MS(ESI^+): 304.4 ($\text{M}+\text{H}$) $^+$.

2.3.2.2. Synthesis of tert-butyl 2-((2-(tert-butoxycarbonyl)aminoethyl)(3-bromopropyl)amino)ethyl carbamate (2g)

To compound **2f** (0.55 g, 1.8 mmol) in acetonitrile (5 mL), DIEA (0.35 g, 2.7 mmol) and 1,3-dibromopropane (3.6 g, 18 mmol) were added and the mixture was refluxed for 24 h with continuous stirring. The solvent was removed in vacuo and further work-up was carried out following the general procedure described in *Section 2.3.4*. Pure compound **2g** was obtained by silica gel column chromatography eluting with diethyl ether (0.35 g, 45%). R_f (Diethyl ether) = 0.66. IR (neat, cm^{-1}): 3345(w); 2975 (m); 2926(w); 2850(w); 2814(w); 1694(s); 1517(m); 1455(w); 1391(w); 1365(m); 1774(m); 1749(m); 1171(s); 783(w). $^1\text{H-NMR}$ (CDCl_3 , δ ppm): 1.45 (s, 18H, $((\text{CH}_3)_3\text{CO}(\text{CO})\text{NHCH}_2\text{CH}_2)_2\text{N-}$); 1.98 (quintet, 2H, $J = 6.9$ Hz, $\text{BrCH}_2\text{CH}_2\text{CH}_2\text{N-}$); 2.56 (t, 4H, $J = 5.4$ Hz, $((\text{CH}_3)_3\text{CO}(\text{CO})\text{NHCH}_2\text{CH}_2)_2\text{N-}$); 2.62 (t, 2H, $J = 6.9$ Hz, $\text{BrCH}_2\text{CH}_2\text{CH}_2\text{N-}$); 3.19 (m, 4H, $((\text{CH}_3)_3\text{CO}(\text{CO})\text{NHCH}_2\text{CH}_2)_2\text{N-}$); 3.47 (t, 2H, $J = 6.9$ Hz, $\text{BrCH}_2\text{CH}_2\text{CH}_2\text{N-}$) [Fig. 2.15]. MS(ESI^+): 426.4 ($\text{M}+\text{H}$) $^+$.

2.3.2.3. Synthesis of tert-butyl 2-((2-(tert-butoxycarbonyl)aminoethyl)(3-(2-nitro-1H-imidazol-1-yl)propyl)amino)ethyl carbamate (2h)

To compound **2g** (0.1 g, 0.24 mmol) in acetonitrile (5 mL), DIEA (0.07 g, 0.54 mmol) and 2-nitroimidazole (0.04 g, 0.36 mmol) were added and the reaction mixture was refluxed for 12 h with continuous stirring. The solvent was removed in vacuo and further work-up was carried out following the general procedure described in Section 2.3.4. Pure compound **2h** was obtained by silica gel column chromatography eluting with ethyl acetate (0.1 g, 87 %). R_f (Ethyl acetate) = 0.56. IR (neat, cm^{-1}): 3345 (m); 3115(w); 2972 (m); 2931 (m); 2853(w); 2818(w); 1699 (s); 1530 (s); 1471 (m); 1369 (m); 1251 (m); 1173 (s); 1122(m); 1062 (w); 972 (m); 917 (w); 859 (w); 825 (w); 745 (w); 656 (w). $^1\text{H-NMR}$ (CDCl_3 , δ ppm): 1.43 (s, 18H, $((\text{CH}_3)_3\text{CO}(\text{CO})\text{NHCH}_2\text{CH}_2)_2\text{N-}$); 2.05 (quintet, 2H, $J = 7.5$ Hz, 2-nitroimidazole- $\text{CH}_2\text{CH}_2\text{CH}_2\text{N-}$); 2.55 (m, 6H, $((\text{CH}_3)_3\text{CO}(\text{CO})\text{NHCH}_2\text{CH}_2)_2\text{NCH}_2\text{-}$); 3.20 (m, 4H, $((\text{CH}_3)_3\text{CO}(\text{CO})\text{NHCH}_2\text{CH}_2)_2\text{N-}$); 4.46 (t, 2H, $J = 7.5$ Hz, 2-nitroimidazole- $\text{CH}_2\text{CH}_2\text{CH}_2\text{N-}$); 7.14 (s, 1H, 2-nitroimidazole-C5-H); 7.20 (s, 1H, 2-nitroimidazole-C4-H) [Fig. 2.16]. MS(ESI $^+$): 457.4 (M+H) $^+$.

2.3.2.4. Synthesis of tert-butyl 2-((2-(tert-butoxycarbonyl)aminoethyl)(3-(4-nitro-1H-imidazol-1-yl)propyl)amino)ethyl carbamate (2i)

To compound **2g** (0.1 g, 0.24 mmol) in acetonitrile (5 mL), DIEA (0.07 g, 0.54 mmol) and 4-nitroimidazole (0.04 g, 0.36 mmol) were added and the reaction mixture refluxed for 12 h with continuous stirring. Thereafter, the solvent was removed in vacuo and further work-up was carried out following the general procedure mentioned in Section 2.3.4. Pure compound **2i** was obtained by silica gel column chromatography eluting with ethyl acetate (0.09 g, 79 %). R_f (Ethyl acetate) = 0.41. IR (neat, cm^{-1}): 3342 (m); 3111(w); 2976 (m); 2930 (m); 2853(w); 2819(w); 1695 (s); 1529 (s); 1475 (m); 1368 (m); 1250 (m); 1170 (s); 1121(m); 1065 (w); 972 (m); 917 (w); 858 (w); 827 (w); 744 (w); 654 (w). $^1\text{H-NMR}$

(CDCl₃, δ ppm): 1.44 (s, 18H, ((CH₃)₃CO(CO)NHCH₂CH₂)₂N-); 1.99 (quintet, 2H, *J* = 7.1 Hz, 4-nitroimidazole-CH₂CH₂CH₂N-); 2.57 (m, 6H, ((CH₃)₃CO(CO)NHCH₂CH₂)₂NCH₂-); 3.20 (m, 4H, ((CH₃)₃CO(CO)NHCH₂CH₂)₂N-); 4.12 (t, 2H, *J* = 7.1 Hz, 4-nitroimidazole-CH₂CH₂CH₂N-); 7.52 (s, 1H, 4-nitroimidazole-C2-H); 7.86 (s, 1H, 4-nitroimidazole-C5-H) [Fig. 2.17]. MS(ESI⁺): 457.4 (M+H)⁺.

2.3.2.5. Synthesis of tert-butyl 2-((2-(tert-butoxycarbonyl)aminoethyl)(3-(5-nitro-1H-imidazol-1-yl)propyl)amino)ethyl carbamate (2j)

Synthesis of compound **2j** involved two steps.

a) Synthesis of 1-(3-bromopropyl)-5-nitro-1H-imidazole (2k)

To 4-nitroimidazole (1 g, 9 mmol) in acetonitrile (50 mL), DIEA (1.75 g, 14 mmol) and 1, 3-dibromopropane (9 g, 45 mmol) were added and the reaction mixture stirred at room temperature for 48 h. The reaction mixture was filtered and the filtrate was evaporated to dryness using rotary evaporator. Further work-up was carried out following the general procedure described in Section 2.3.4. Pure compound **2k** was obtained by silica gel column chromatography eluting with diethyl ether (0.23 g, 11%). R_f (Diethyl ether) = 0.47. IR (neat, cm⁻¹): 3114 (w); 2969 (w); 2923 (w); 1529 (s); 1371 (vs); 1121 (vs); 741 (s); 650(w). ¹H-NMR (CDCl₃, δ ppm): 2.39 (quintet, 2H, *J* = 6.3 Hz, 5-nitroimidazole-CH₂CH₂CH₂Br); 3.36 (t, 2H, *J* = 6.3 Hz, 5-nitroimidazole-CH₂CH₂CH₂Br); 4.59 (t, 2H, *J* = 6.3 Hz, 5-nitroimidazole-CH₂CH₂CH₂Br); 7.74 (s, 1H, 5-nitroimidazole-C2-H); 8.03 (s, 1H, 5-nitroimidazole-C4-H) [Fig. 2.18]. MS(ESI⁺) m/z: 233.8 (M+H)⁺.

b) Synthesis of tert-butyl 2-((2-(tert-butoxycarbonyl)aminoethyl)(3-(5-nitro-1H-imidazol-1-yl)propyl)amino)ethyl carbamate (2j)

To compound **2k** (0.07 g, 0.31 mmol) in acetonitrile (5 mL), DIEA (0.06 g, 0.47 mmol) and compound **2f** (0.15 g, 0.47 mmol) were added and the reaction mixture refluxed for 12 h with continuous stirring. The solvent was removed in vacuo and further work-up

was carried out following the general procedure described in *Section 2.3.4*. Pure compound **2j** was obtained by silica gel column chromatography eluting with ethyl acetate. (0.09 g, 66%). R_f (Ethyl acetate) = 0.53. IR (neat, cm^{-1}): 3342 (m); 3111(w); 2976 (m); 2930 (m); 2853(w); 2819(w); 1695 (s); 1529 (s); 1475 (m); 1368 (m); 1250 (m); 1170 (s); 1121(m); 1065 (w); 972 (m); 917 (w); 858 (w); 827 (w); 744 (w); 654 (w). $^1\text{H-NMR}$ (CDCl_3 , δ ppm): 1.44 (s, 18H, $((\text{CH}_3)_3\text{CO}(\text{CO})\text{NHCH}_2\text{CH}_2)_2\text{N-}$); 1.96 (quintet, 2H, $J = 7.1$ Hz, 5-nitroimidazole- $\text{CH}_2\text{CH}_2\text{CH}_2\text{N-}$); 2.55 (m, 6H, $((\text{CH}_3)_3\text{CO}(\text{CO})\text{NHCH}_2\text{CH}_2)_2\text{NCH}_2\text{CH}_2\text{CH}_2\text{-}$); 3.20 (m, 4H, $((\text{CH}_3)_3\text{CO}(\text{CO})\text{NHCH}_2\text{CH}_2)_2\text{N-}$); 4.41 (t, 2H, $J = 7.1$ Hz, 5-nitroimidazole- $\text{CH}_2\text{CH}_2\text{CH}_2\text{N-}$); 7.68 (s, 1H, 5-nitroimidazole-C2-H); 8.01 (s, 1H, 5-nitroimidazole-C4-H) [Fig. 2.19]. MS (ESI^+): 457.4 ($\text{M}+\text{H}$) $^+$.

2.3.2.6. Synthesis of ligands **2L4** – **2L6**

Compounds **2h**, **2i** and **2j** (0.25 mmol) were hydrolyzed following the general procedure described in *Section 2.3.5* to obtain the target ligands **2L4** (86%), **2L5** (91%) and **2L6** (89%), respectively, as the hydrochloride salt.

N 1 -(2-aminoethyl)-*N* 1 -(3-(2-nitro-1H-imidazol-1-yl)propyl)ethane-1,2-diamine hydrochloride (**2L4**):

IR (neat, cm^{-1}): 3433 (s); 3114 (w); 3013 (w); 2921 (w); 2863 (w); 1624 (m); 1531 (m); 1480 (m); 1375 (m); 1301 (w); 1268 (w); 1236 (w); 1129 (w); 1022 (w); 835 (w); 773 (w); 732 (w). $^1\text{H-NMR}$ (D_2O , δ ppm): 2.13 (quintet, 2H, $J = 7.2$ Hz, 2-nitroimidazole- $\text{CH}_2\text{CH}_2\text{CH}_2\text{N-}$); 2.85 (t, 2H, $J = 7.2$ Hz, 2-nitroimidazole- $\text{CH}_2\text{CH}_2\text{CH}_2\text{N-}$); 2.98 (t, 4H, $J = 6.6$ Hz, $(\text{NH}_2\text{CH}_2\text{CH}_2)_2\text{N-}$); 3.18 (t, 4H, $J = 6.6$ Hz, $(\text{NH}_2\text{CH}_2\text{CH}_2)_2\text{N-}$); 4.50 (t, 2H, $J = 7.2$ Hz, 2-nitroimidazole- $\text{CH}_2\text{CH}_2\text{CH}_2\text{N-}$); 7.18 (s, 1H, 2-nitroimidazole-C5-H); 7.48 (s, 1H, 2-nitroimidazole-C4-H) [Fig. 2.20]. MS(ESI^+): 257.8 ($\text{M}+\text{H}$) $^+$ [Fig. 2.21].

N 1 -(2-aminoethyl)-*N* 1 -(3-(4-nitro-1H-imidazol-1-yl)propyl)ethane-1,2-diamine hydrochloride (**2L5**):

IR (neat, cm^{-1}): 3438 (s); 3112 (w); 3009 (w); 2922 (w); 2861 (w); 1626 (m); 1530 (m); 1479 (m); 1378 (m); 1303 (w); 1267 (w); 1239 (w); 1123 (w); 1021 (w); 833 (w); 777 (w); 729 (w). $^1\text{H-NMR}$ (D_2O , δ ppm): 2.02 (quintet, 2H, $J = 7.2$ Hz, 4-nitroimidazole- $\text{CH}_2\text{CH}_2\text{CH}_2\text{N-}$); 2.66 (m, 2H, 4-nitroimidazole- $\text{CH}_2\text{CH}_2\text{CH}_2\text{N-}$); 2.84 (m, 4H, $(\text{NH}_2\text{CH}_2\text{CH}_2)_2\text{N-}$); 3.03 (m, 4H, $(\text{NH}_2\text{CH}_2\text{CH}_2)_2\text{N-}$); 4.08 (t, 2H, $J = 7.2$ Hz, 4-nitroimidazole- $\text{CH}_2\text{CH}_2\text{CH}_2\text{N-}$); 7.67 (s, 1H, 4-nitroimidazole-C2-H); 8.13 (s, 1H, 4-nitroimidazole-C5-H) [Fig. 2.22]. MS(ESI⁺): 257.3 (M+H)⁺ [Fig. 2.23].

*N*¹-(2-aminoethyl)-*N*¹-(3-(5-nitro-1H-imidazol-1-yl)propyl)ethane-1,2-diamine hydrochloride (**2L6**):

IR (neat, cm^{-1}): 3432 (s); 3110 (w); 3013 (w); 2922 (w); 2863 (w); 1625 (m); 1530 (m); 1475 (m); 1379 (m); 1301 (w); 1265 (w); 1238 (w); 1125 (w); 1017 (w); 831 (w); 771 (w); 734 (w). $^1\text{H-NMR}$ (D_2O , δ ppm): 2.22 (quintet, 2H, $J = 7.2$ Hz, 5-nitroimidazole- $\text{CH}_2\text{CH}_2\text{CH}_2\text{N-}$); 3.06 (t, 2H, $J = 7.2$ Hz, 5-nitroimidazole- $\text{CH}_2\text{CH}_2\text{CH}_2\text{N-}$); 3.18 (m, 4H, $(\text{NH}_2\text{CH}_2\text{CH}_2)_2\text{N-}$); 3.28 (m, 4H, $(\text{NH}_2\text{CH}_2\text{CH}_2)_2\text{N-}$); 4.54 (t, 2H, $J = 7.2$ Hz, 5-nitroimidazole- $\text{CH}_2\text{CH}_2\text{CH}_2\text{N-}$); 8.27 (s, 1H, 5-nitroimidazole-C2-H); 8.31 (s, 1H, 5-nitroimidazole-C4-H) [Fig. 2.24]. MS(ESI⁺): 257.4 (M+H)⁺ [Fig. 2.25].

2.3.2.7. Preparation of $\text{Re}(\text{CO})_3$ complex of **2L6** (**2I**)

Compound **2L6** (0.08 g, 0.2 mmol) was dissolved in water (5 mL) and the pH of the solution was adjusted to 6 with 0.1 N NaOH. To this solution bis(tetraethylammonium)-*fac*-tribromotricarbonylrhenate (0.15 g, 0.2 mmol), prepared following a reported procedure¹⁹³ was added and the mixture was heated at 50°C for 12 h. The precipitate formed was removed by filtration and the filtrate upon evaporation gave the target compound **2I** (0.04 g, 32%). IR (KBr, cm^{-1}): 3130 (m); 2984 (m); 2950 (m); 2692 (w); 2016 (vs); 1878 (vs); 1646 (s); 1491 (w); 1395 (m); 1337 (m); 1288 (w); 1183 (w); 1133 (w). $^1\text{H-NMR}$ (D_2O , δ ppm): 2.39 (quintet, 2H, $J = 7.9$ Hz, 5-nitroimidazole- $\text{CH}_2\text{CH}_2\text{CH}_2\text{N-}$); 2.89 and 3.00 (m, 4H,

(H₂NCH₂CH₂)₂NCH₂CH₂CH₂-); 3.15 (m, ((H₂NCH₂CH₂)₂NCH₂CH₂CH₂-); 3.44 and 3.90 (m, 4H, (H₂NCH₂CH₂)₂NCH₂CH₂CH₂N-); 4.45 (t, 2H, *J* = 7.9 Hz, 5-nitroimidazole-CH₂CH₂CH₂N-); 7.99 (s, 1H, 5-nitroimidazole-C2-H); 8.11 (s, 1H, 5-nitroimidazole-C4-H) [Fig. 2.26]. MS(ESI⁺): 528.2 (M+H)⁺ [Fig. 2.27].

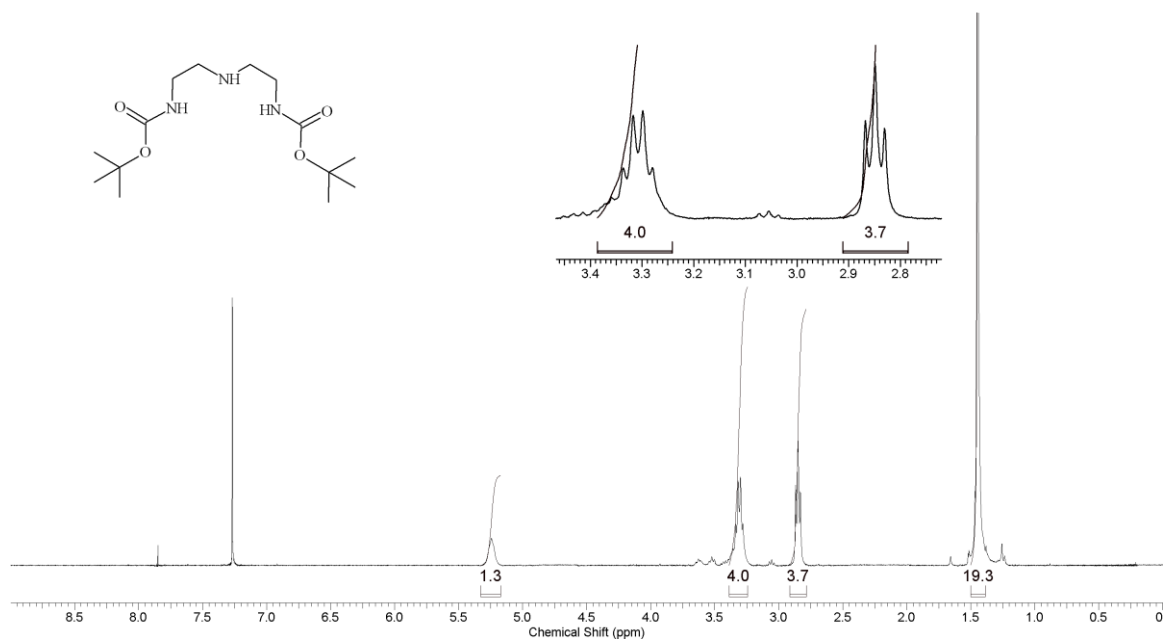


Fig. 2.14. ¹H-NMR spectrum of *tert*-butyl 2-((2-(*tert*-butoxycarbonyl)amino)ethyl)amino)ethyl carbamate (**2f**)

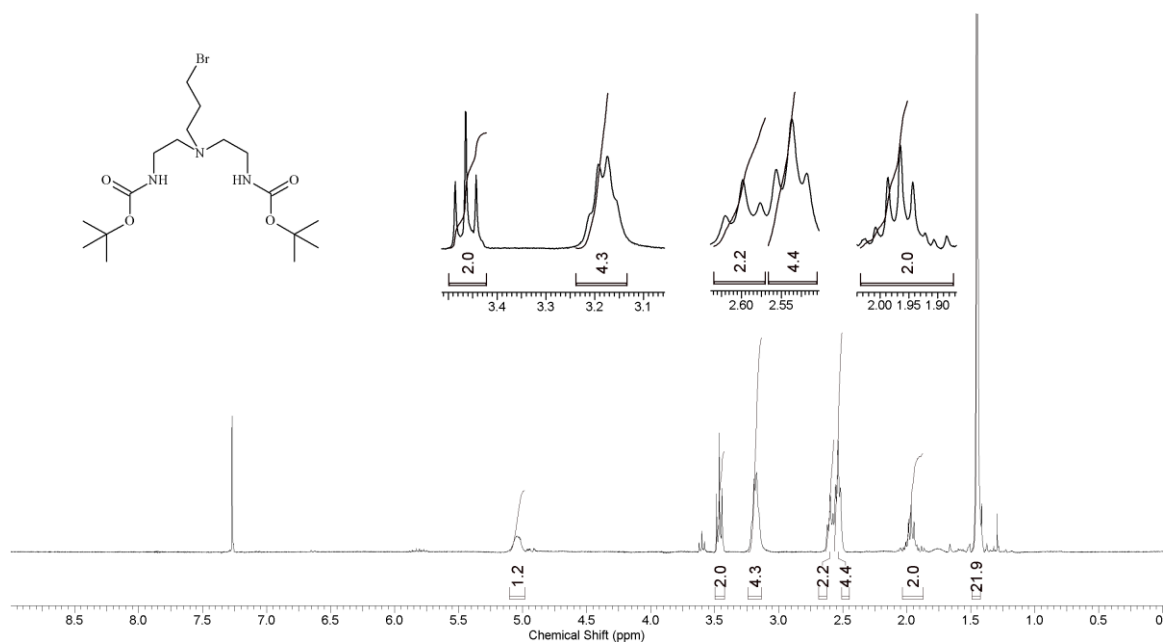


Fig. 2.15. ¹H-NMR spectrum of *tert*-butyl 2-((2-(*tert*-butoxycarbonyl)amino)ethyl)(3-bromopropyl)amino)ethyl carbamate (**2g**)

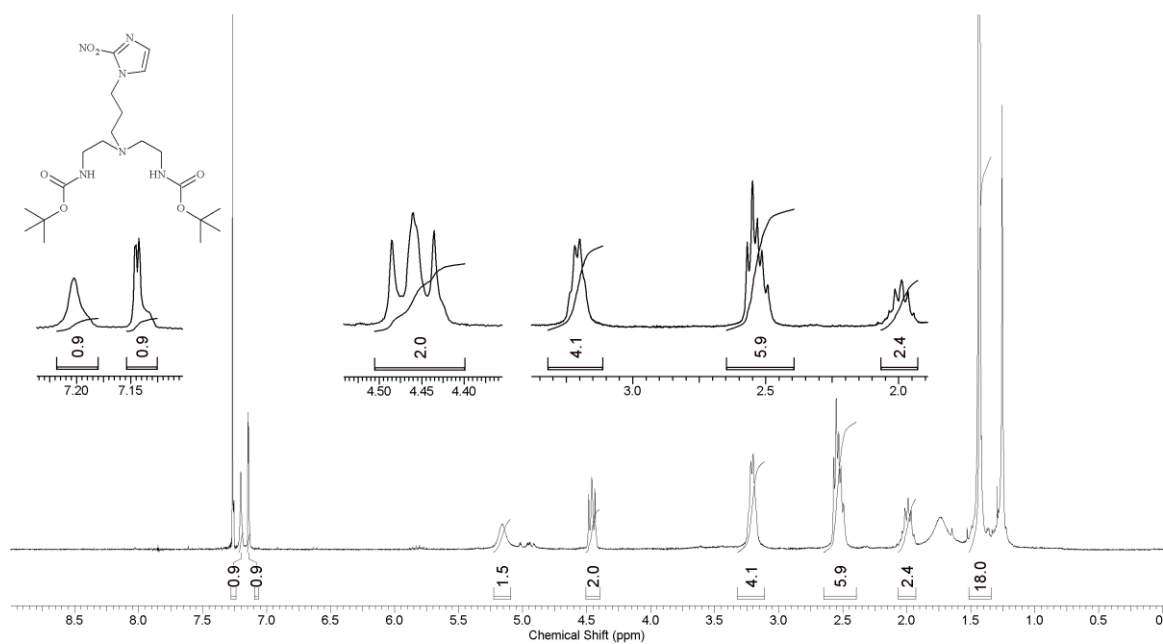


Fig. 2.16. ¹H-NMR spectrum of *tert*-butyl 2-((2-(*tert*-butoxycarbonyl)aminoethyl)(3-(2-nitro-1H-imidazol-1-yl)propyl)amino)ethyl carbamate (**2h**)

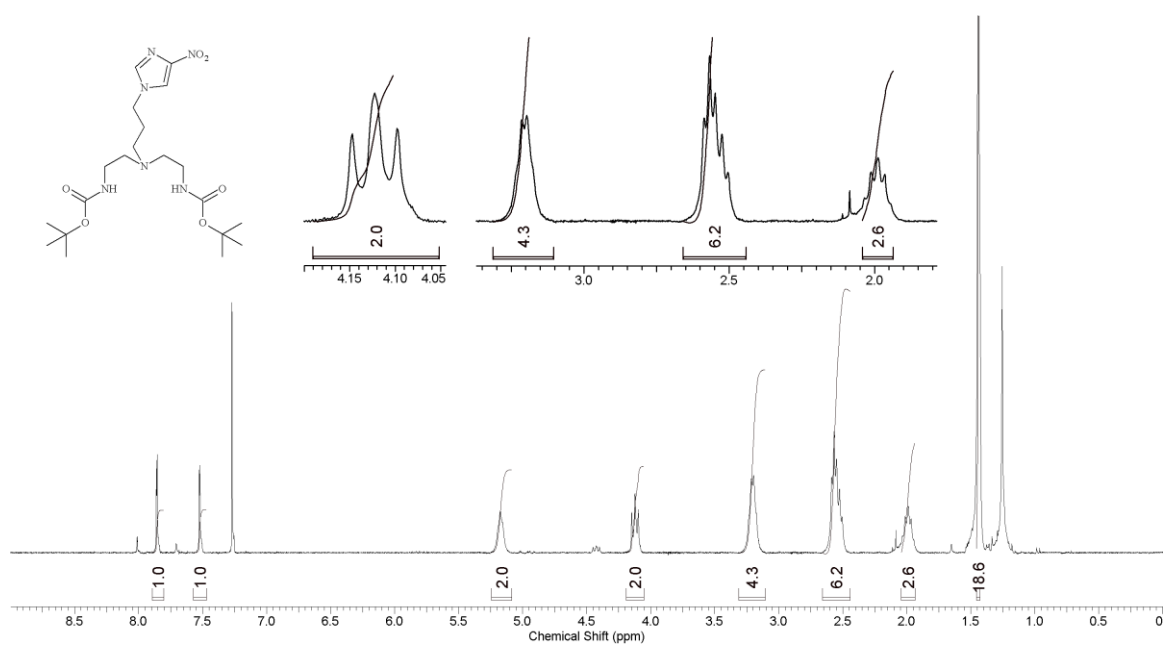


Fig. 2.17. ¹H-NMR spectrum of *tert*-butyl 2-((2-(*tert*-butoxycarbonyl)aminoethyl)(3-(4-nitro-1H-imidazol-1-yl)propyl)amino)ethyl carbamate (**2i**)



Current Data Parameters
NAME lllu proton
EXPNO 51
PROCNO 1

F2 - Acquisition Parameters

Date_ 20080616
Time_ 17.14
INSTRUM spect
PROBHD 5 mm BBO BB-1H
PULPROG zg30
TD 32768
SOLVENT CDCl3
NS 27
DS 0
SWH 4807.692 Hz
FIDRES 0.146719 Hz
AQ 3.4079220 sec
RG 228
DW 104.000 usec
DE 6.00 usec
TE 291.4 K
D1 1.00000000 sec
TDO 1

==== CHANNEL f1 =====
NUC1 1H
P1 11.00 usec
PL1 0.00 dB
SFO1 300.1318008 MHz

F2 - Processing parameters
SI 16384
SF 300.1300000 MHz
WDW EM
SSB 0
LB 0.00 Hz
GB 0
PC 1.00

5N1MCH23Br

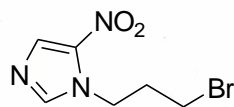
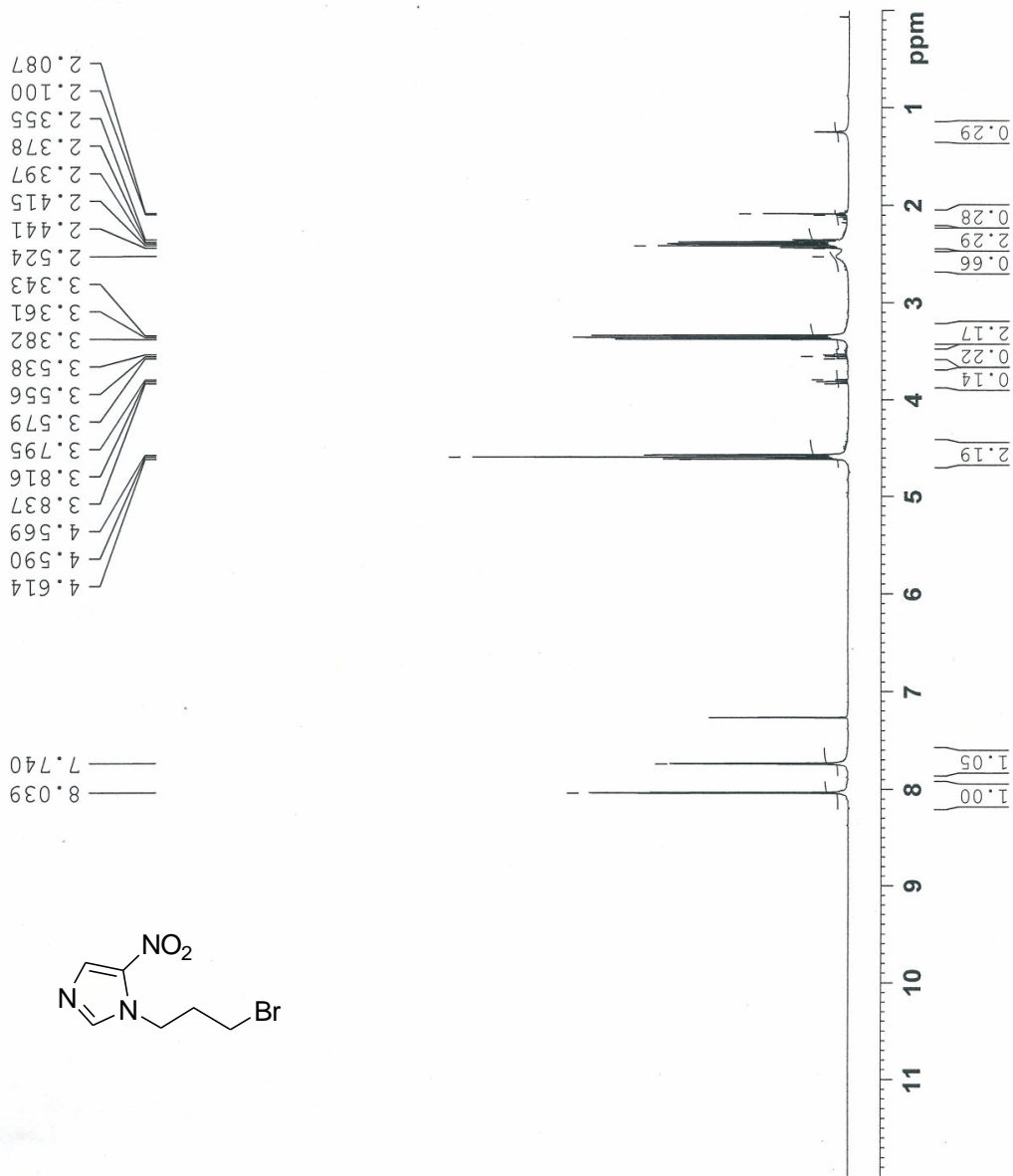
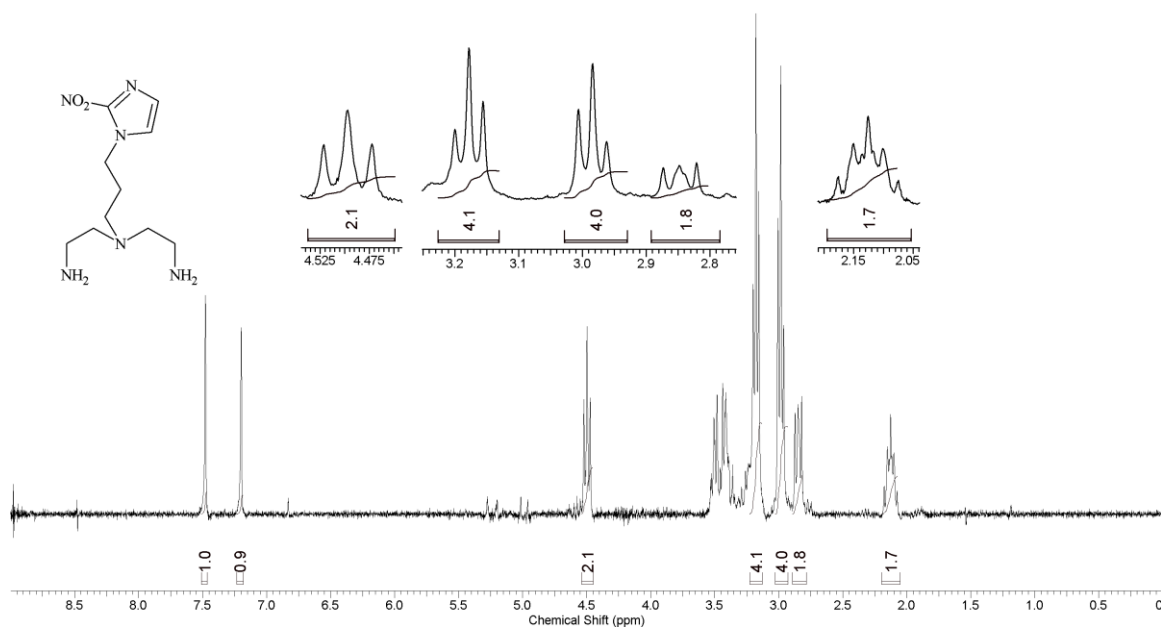
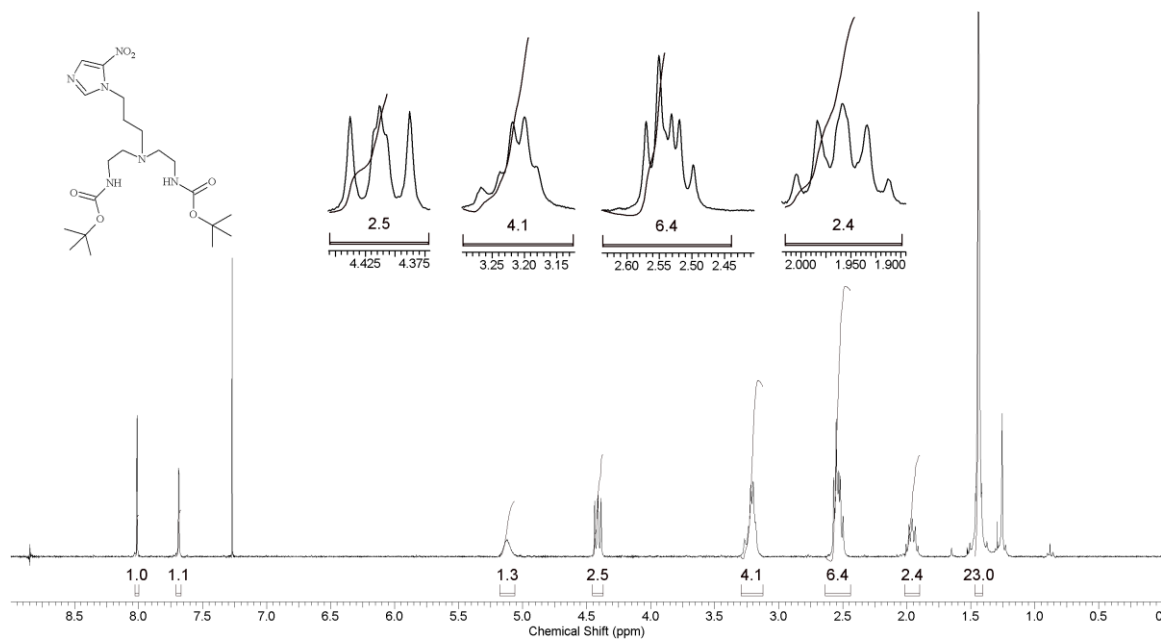


Fig. 2.18. ¹H-NMR spectrum of 1-(3-bromopropyl)-5-nitro-1H-imidazole (2k)



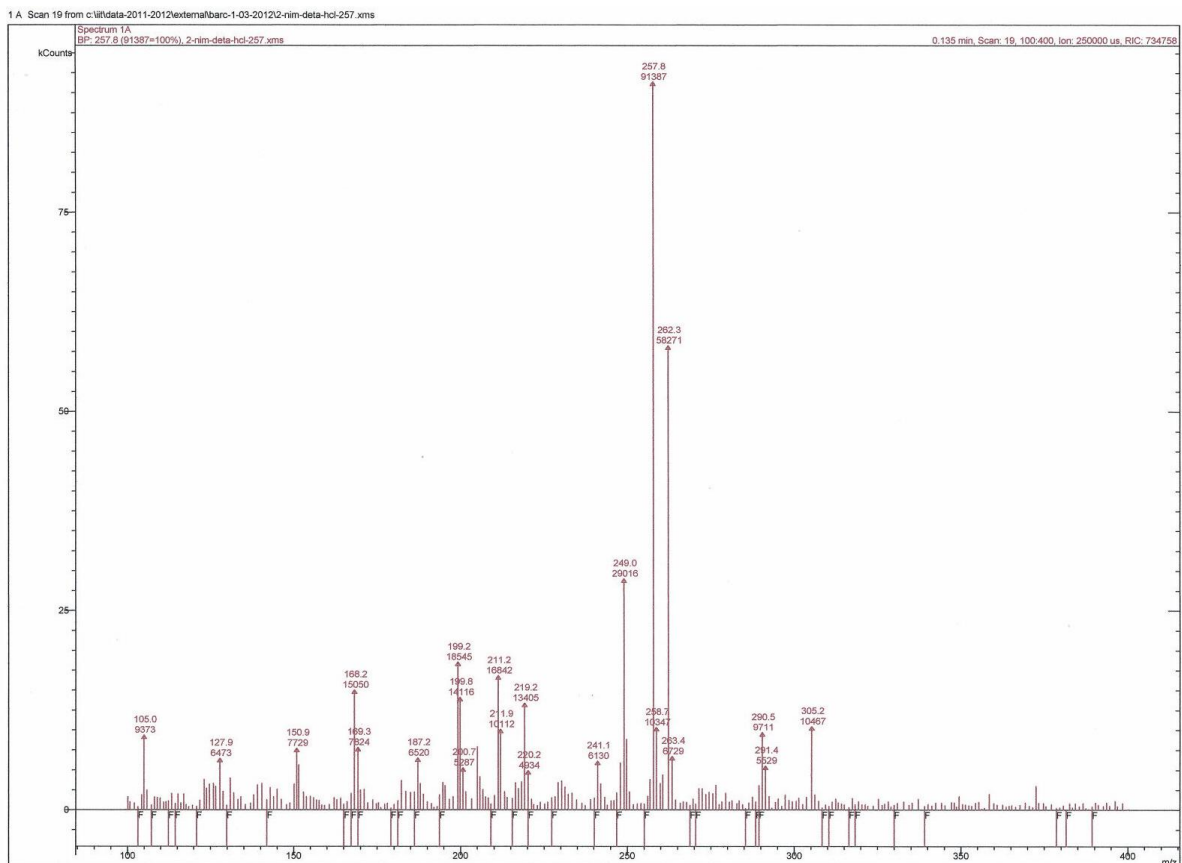


Fig. 2.21. ESI-MS of N^1 -(2-aminoethyl)- N^1 -(3-(2-nitro-1H-imidazol-1-yl)propyl)ethane-1,2-diamine hydrochloride (**2L4**)

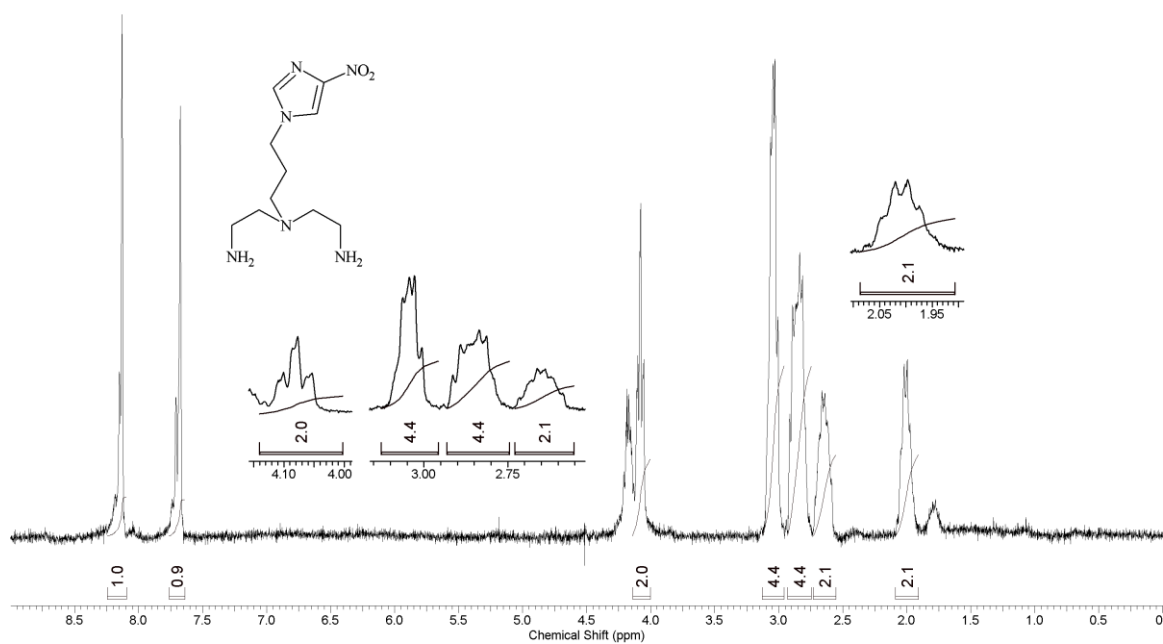


Fig. 2.22. $^1\text{H-NMR}$ spectrum of N^1 -(2-aminoethyl)- N^1 -(3-(4-nitro-1H-imidazol-1-yl)propyl)ethane-1,2-diamine hydrochloride (**2L5**)

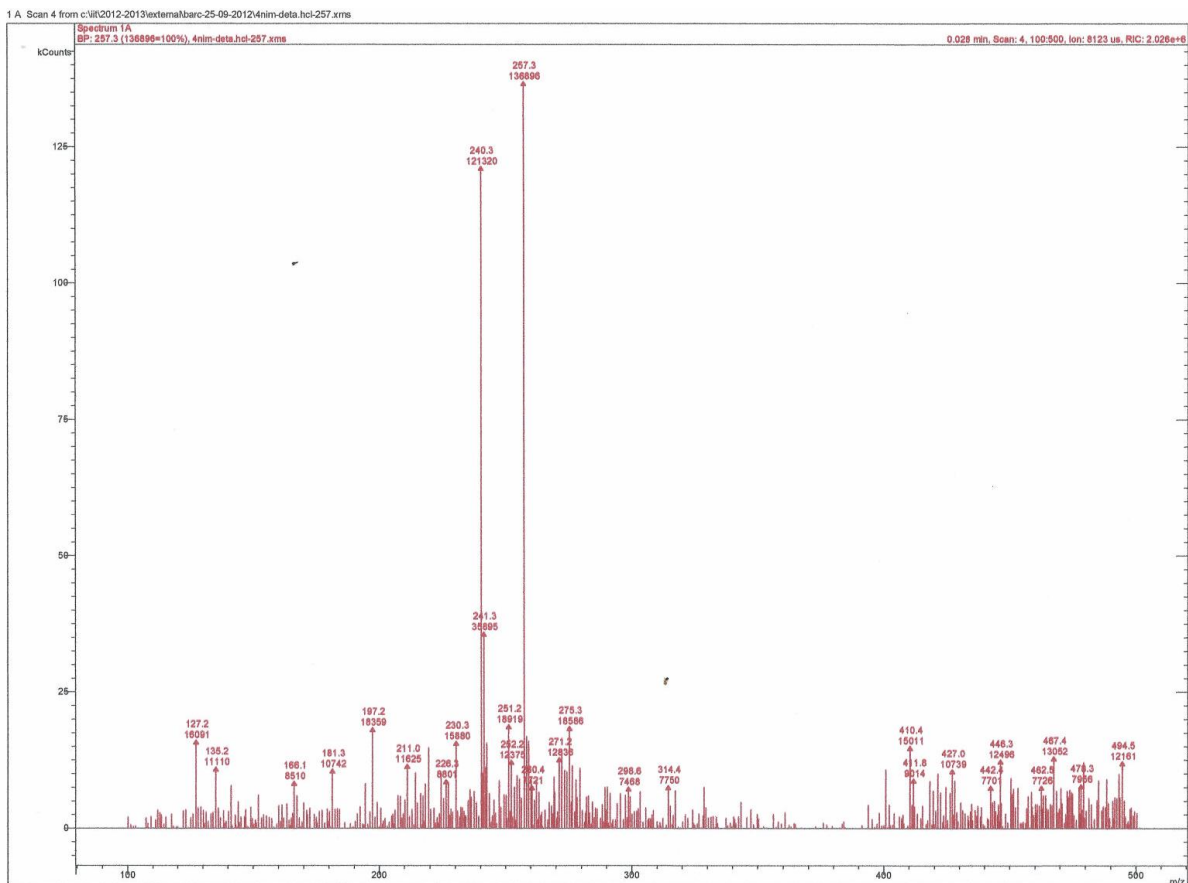


Fig. 2.23. ESI-MS of N^1 -(2-aminoethyl)- N^1 -(3-(4-nitro-1H-imidazol-1-yl)propyl) ethane-1,2-diamine hydrochloride (**2L5**)

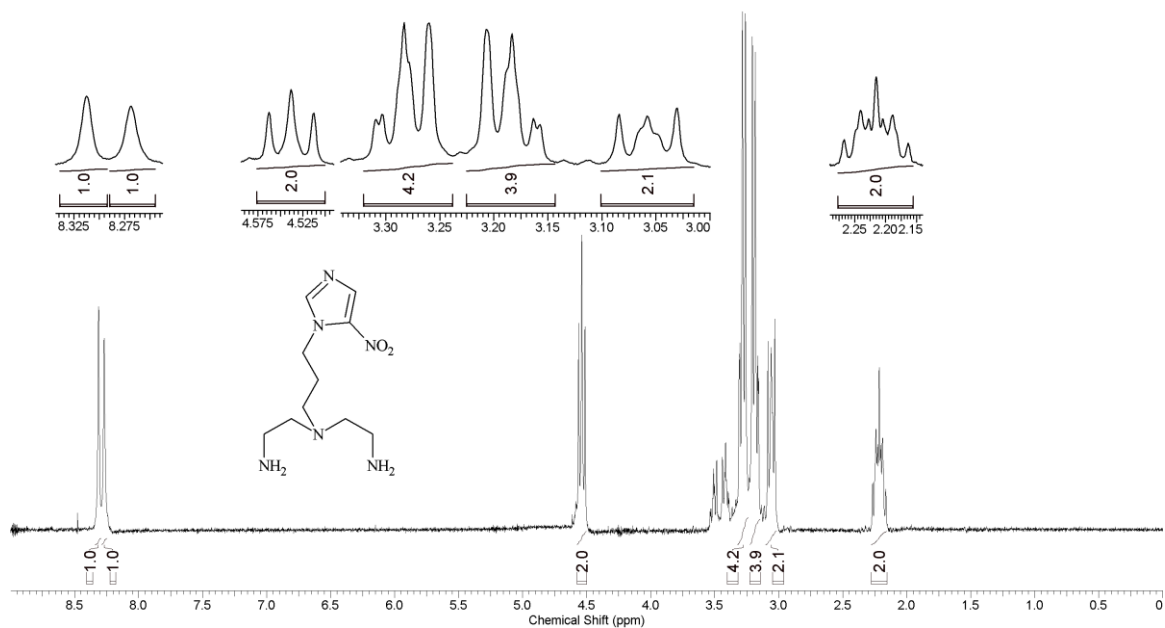


Fig. 2.24. $^1\text{H-NMR}$ spectrum of N^1 -(2-aminoethyl)- N^1 -(3-(5-nitro-1H-imidazol-1-yl)propyl)ethane-1,2-diamine hydrochloride (**2L6**)

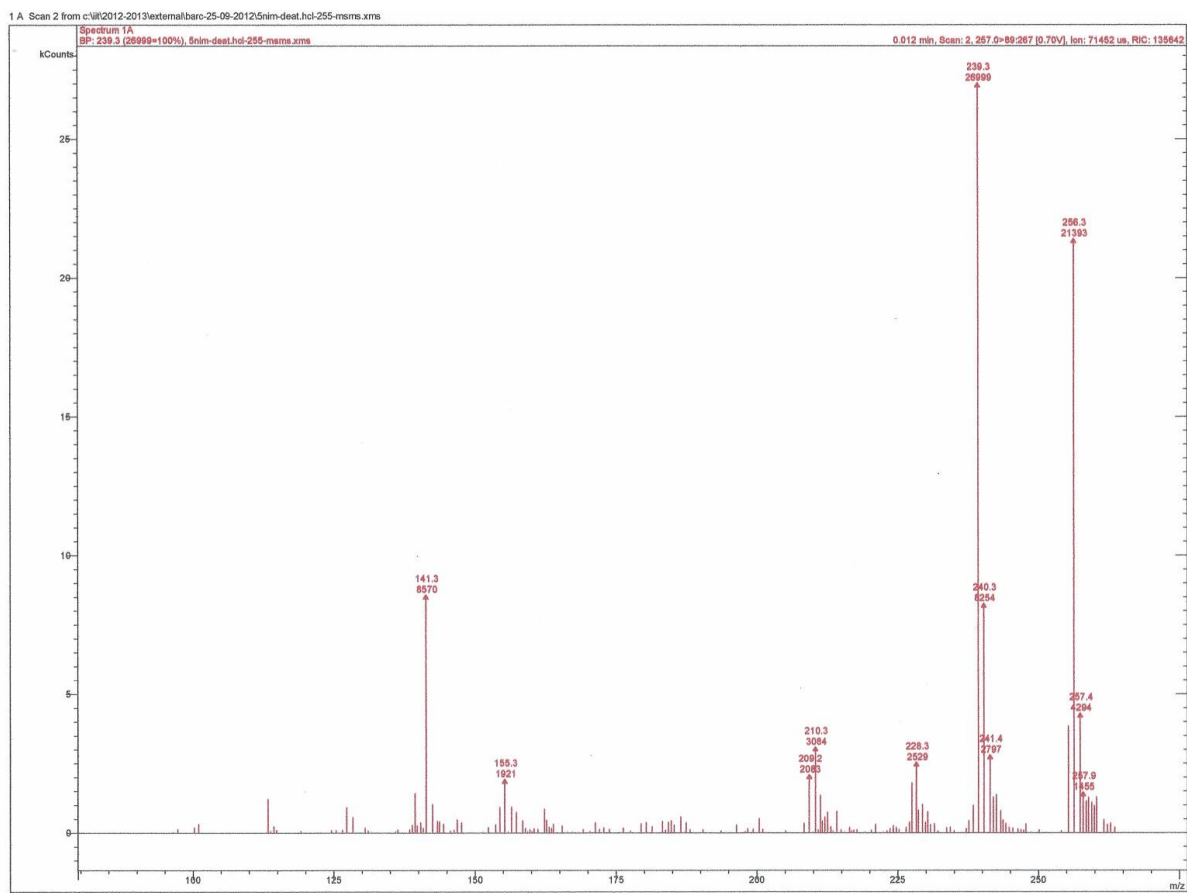


Fig. 2.25. ESI-MS of N^1 -(2-aminoethyl)- N^1 -(3-(5-nitro-1H-imidazol-1-yl)propyl)ethane-1,2-diamine hydrochloride (**2L6**)

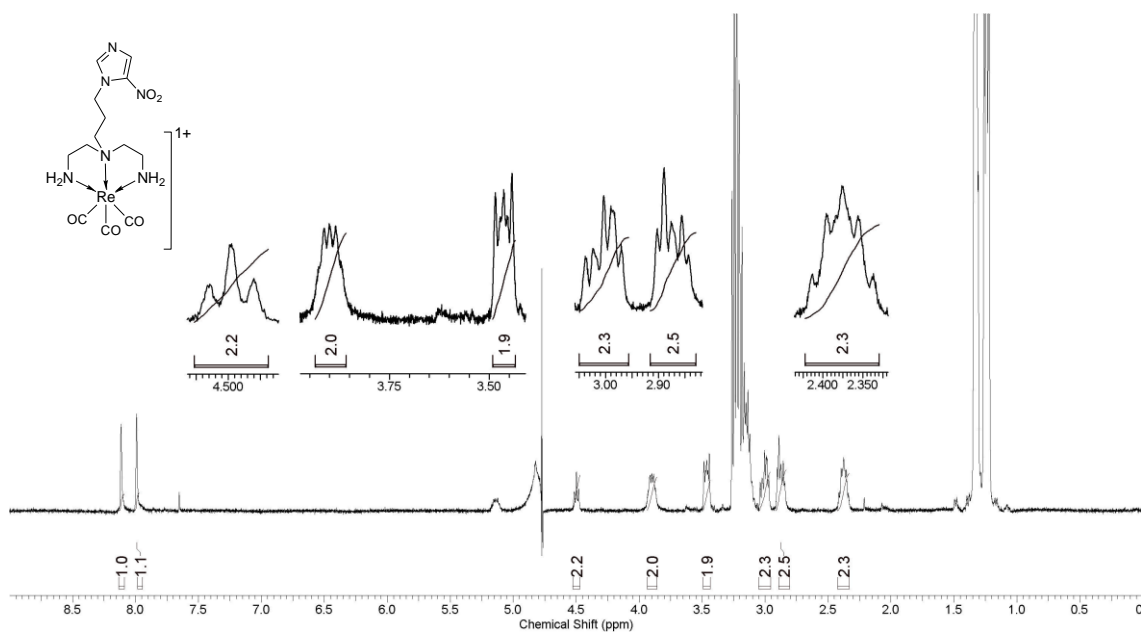


Fig. 2.26. $^1\text{H-NMR}$ spectrum of $\text{Re}(\text{CO})_3$ complex of **2L6** (**2I**)

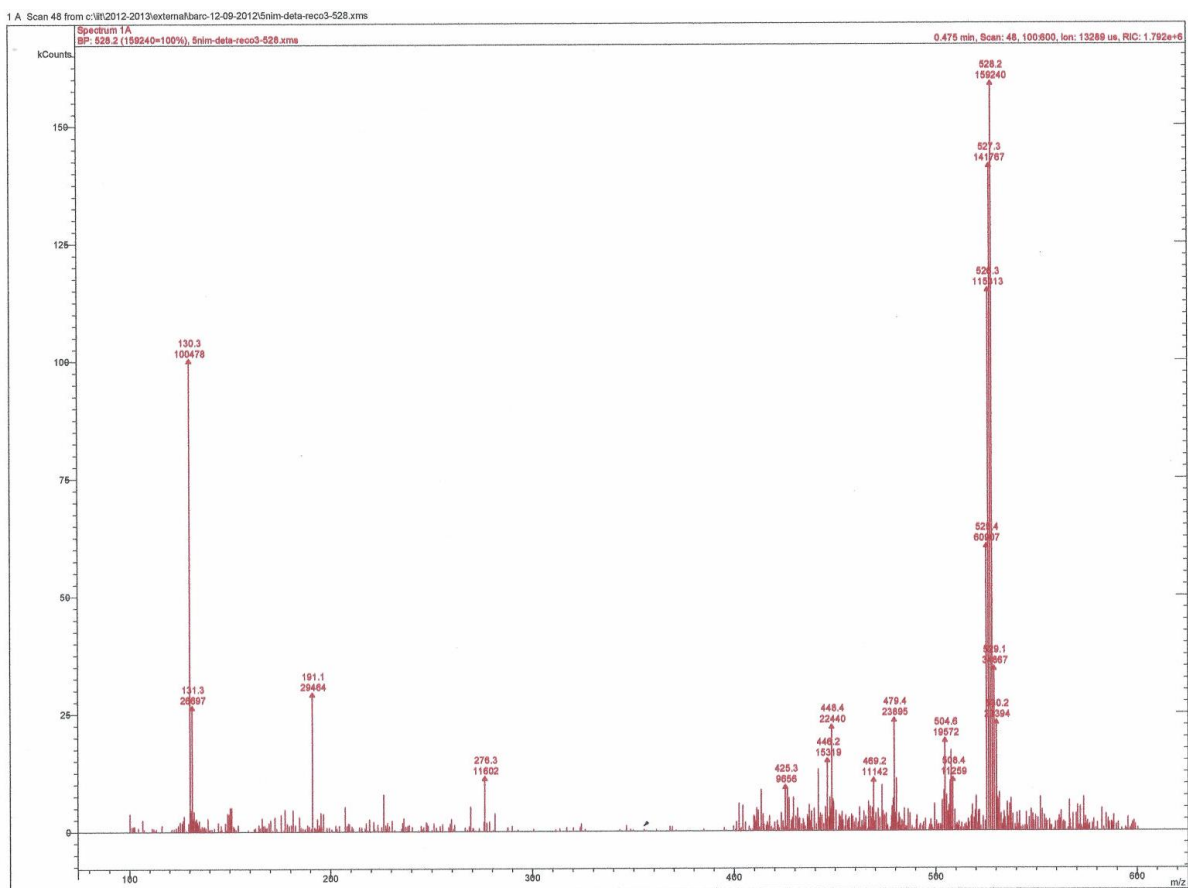


Fig. 2.27. ESI-MS of $\text{Re}(\text{CO})_3$ complex of **2L6 (2I)**

2.3.3. Synthesis of AEG derivatives of 2-, 4- and 5-nitroimidazole

The synthesis of AEG derivatives of 2-, 4- and 5- nitroimidazole are shown in figure 2.28. The target compounds (**2L7-2L9**) are shown in boxes.

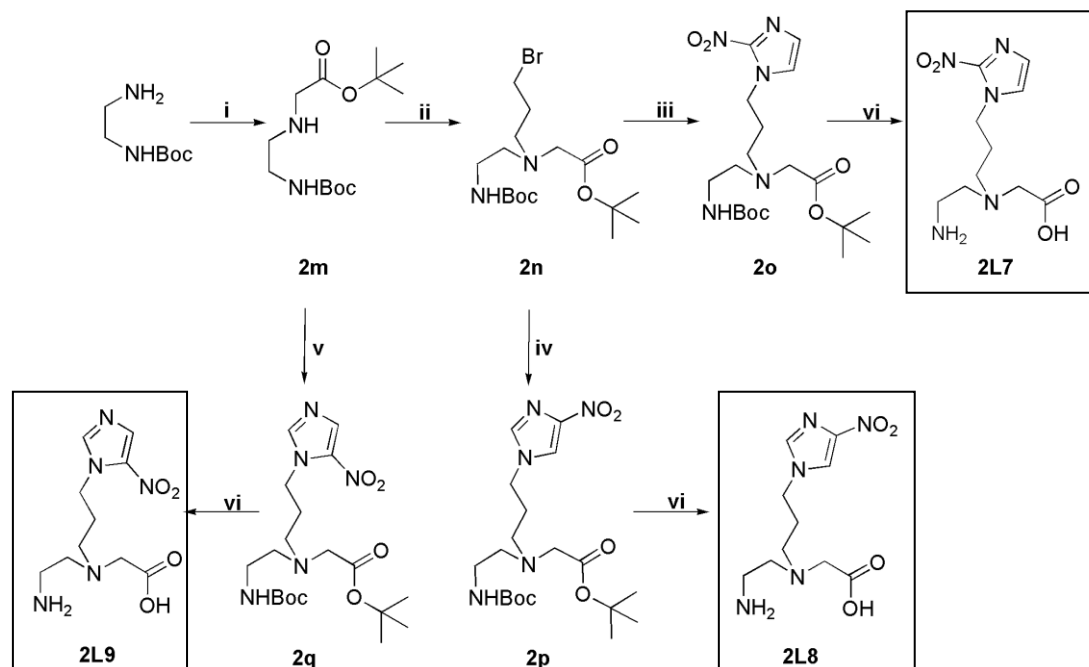


Fig. 2.28. Synthesis of AEG derivatives of nitroimidazoles (i) *tert*-butyl bromoacetate, DIEA, acetonitrile, 0°C (ii) 1,3 dibromopropane, DIEA, acetonitrile, reflux (iii) 2-nitroimidazole, DIEA, acetonitrile, reflux (iv) 4-nitroimidazole, DIEA, acetonitrile, reflux (v) **2k**, DIEA, acetonitrile, reflux (vi) 6N HCl, 25°C

2.3.3.1. Synthesis of *tert*-butyl 2-((*tert*-butoxycarbonyl)methylamino)ethyl carbamate (**2m**)

To an ice cooled solution of N-Boc-ethylenediamine (1 g, 6.28 mmol) and DIEA (0.65 g, 5.04 mmol) in acetonitrile (10 mL) *tert*-butyl bromoacetate (0.98 g, 5.04 mmol) was added drop-wise over a period of 3 h with vigorous stirring. After the addition was complete, the reaction mixture was brought to room temperature and the stirring continued for another 12 h. The solvent was removed in vacuo and further work-up was carried out following the general procedure described in *Section 2.3.4*. Compound **2m** was obtained by silica gel column chromatography eluting with ethyl acetate (0.99 g, 72%). R_f (Ethyl acetate) = 0.5. IR (neat, cm^{-1}): 3343 (w); 2977 (m); 2931(w); 1730 (s); 1714 (s); 1517 (w); 1454 (w); 1392 (w); 1366 (m); 1248 (m); 1158 (s); 1045 (w); 847 (w); 780 (w). $^1\text{H-NMR}$ (CDCl_3 , δ ppm): 1.47 (s,

18H, $(\text{CH}_3)_3\text{CO}(\text{CO})\text{CH}_2\text{NHCH}_2\text{CH}_2\text{NH}(\text{CO})\text{OC}(\text{CH}_3)_3$; 2.75 (t, 2H, $J = 5.7$ Hz, $(\text{CH}_3)_3\text{CO}(\text{CO})\text{CH}_2\text{NHCH}_2\text{CH}_2\text{NH}(\text{CO})\text{OC}(\text{CH}_3)_3$); 3.23 (m, 2H, $(\text{CH}_3)_3\text{CO}(\text{CO})\text{CH}_2\text{NHCH}_2\text{CH}_2\text{NH}(\text{CO})\text{OC}(\text{CH}_3)_3$); 3.31 (s, 2H, $(\text{CH}_3)_3\text{CO}(\text{CO})\text{CH}_2\text{NHCH}_2\text{CH}_2\text{NH}(\text{CO})\text{OC}(\text{CH}_3)_3$) [Fig. 2.29]. MS(ESI⁺): 275.4 (M+H)⁺.

2.3.3.2. Synthesis of tert-butyl 2-(((tert-butoxycarbonyl)methyl)(3-bromopropyl)amino)ethyl carbamate (**2n**)

To compound **2m** (0.68 g, 2.46 mmol) in acetonitrile (5 mL), DIEA (0.35 g, 2.7 mmol) and 1,3-dibromopropane (4.97 g, 24.6 mmol) were added and the mixture refluxed for 24 h with continuous stirring. The solvent was removed in vacuo and the residue was worked-up following the general procedure described in Section 2.3.4. Compound **2n** was obtained by silica gel column chromatography eluting with chloroform (0.70 g, 72%). R_f (Chloroform) = 0.55. IR (neat, cm^{-1}): 3345(w); 2975 (m); 2926(w); 2850(w); 2814(w); 1694(s); 1517(m); 1455(w); 1391(w); 1365(m); 1774(m); 1749(m); 1171(s); 783(w). ¹H-NMR (CDCl_3 , δ ppm): 1.46 (s, 18H, $(\text{CH}_3)_3\text{CO}(\text{CO})\text{CH}_2\text{N}(-)\text{CH}_2\text{CH}_2\text{NH}(\text{CO})\text{OC}(\text{CH}_3)_3$); 1.99 (quintet, 2H, $J = 6.6$ Hz, $\text{BrCH}_2\text{CH}_2\text{CH}_2\text{N}(-)$); 2.72 (t, 2H, $J = 5.9$ Hz, $(-\text{CO})\text{CH}_2\text{N}(-)\text{CH}_2\text{CH}_2\text{NH}(-)$); 2.75 (t, 2H, $J = 6.6$ Hz, $\text{BrCH}_2\text{CH}_2\text{CH}_2\text{N}(-)$); 3.18 (m, 2H, $(-\text{CO})\text{CH}_2\text{N}(-)\text{CH}_2\text{CH}_2\text{NH}(-)$); 3.22 (s, 2H, $(-\text{CO})\text{CH}_2\text{N}(-)\text{CH}_2\text{CH}_2\text{NH}(-)$); 3.48 (t, 2H, $J = 6.6$ Hz, $\text{BrCH}_2\text{CH}_2\text{CH}_2\text{N}(-)$) [Fig. 2.30]. MS(ESI⁺): 395.4 (M+H)⁺.

2.3.3.3. Synthesis of tert-butyl 2-(((tert-butoxycarbonyl)methyl)(3-(2-nitro-1H-imidazol-1-yl)propyl)amino)ethyl carbamate (**2o**)

To compound **2n** (0.42 g, 1.06 mmol) in acetonitrile (5 mL), DIEA (0.23 g, 1.75 mmol) and 2-nitroimidazole (0.13 g, 1.1 mmol) were added and the reaction mixture refluxed for 12 h with continuous stirring. The solvent was removed in vacuo and further work-up was carried out following the general procedure described in Section 2.3.4. Compound **2o** was obtained by silica gel column chromatography eluting with ethyl acetate (0.40 g, 89%).

R_f (Ethyl acetate) = 0.8. IR (neat, cm^{-1}): 3413 (w); 3116 (w); 2976 (m); 2928 (m); 2855 (w); 1714 (s); 1538 (m); 1487 (m); 1455 (w); 1365 (s); 1250 (w); 1159 (s); 1074 (w); 835 (w); 784 (w). $^1\text{H-NMR}$ (CDCl_3 , δ ppm): 1.45 (s, 9H, $(\text{CH}_3)_3\text{CO}(\text{CO})\text{CH}_2\text{N}(-)\text{CH}_2\text{CH}_2\text{NH}(\text{CO})\text{OC}(\text{CH}_3)_3$); 1.48 (s, 9H, $(\text{CH}_3)_3\text{CO}(\text{CO})\text{CH}_2\text{N}(-)\text{CH}_2\text{CH}_2\text{NH}(\text{CO})\text{OC}(\text{CH}_3)_3$); 1.98 (quintet, 2H, $J = 6.6$ Hz, 2-nitroimidazole- $\text{CH}_2\text{CH}_2\text{CH}_2\text{N}(-)$); 2.63 (t, 2H, $J = 6.3$ Hz, $-(\text{CO})\text{CH}_2\text{N}(-)\text{CH}_2\text{CH}_2\text{NH}-$); 2.75 (t, 2H, $J = 6.6$ Hz, 2-nitroimidazole- $\text{CH}_2\text{CH}_2\text{CH}_2\text{N}(-)$); 3.22 (m, 4H, $-(\text{CO})\text{CH}_2\text{N}(-)\text{CH}_2\text{CH}_2\text{NH}-$); 4.54 (t, 2H, $J = 6.6$ Hz, 2-nitroimidazole- $\text{CH}_2\text{CH}_2\text{CH}_2\text{N}(-)$); 7.12 (s, 1H, 2-nitroimidazole-C5-H); 7.27 (s, 1H, 2-nitroimidazole-C4-H) [Fig. 2.31]. MS(ESI^+): 450.4 ($\text{M}+\text{Na}$) $^+$.

2.3.3.4. Synthesis of tert-butyl 2-(((tert-butoxycarbonyl)methyl)(3-(4-nitro-1H-imidazol-1-yl)propyl)amino)ethyl carbamate (2p)

To compound **2n** (0.15 g, 0.38 mmol) in acetonitrile (5 mL), DIEA (0.06 g, 0.46 mmol) and 4-nitroimidazole (0.05 g, 0.42 mmol) were added and the reaction mixture refluxed for 12 h with continuous stirring. After the solvent was removed in vacuo, further work-up was carried out following the general procedure mentioned in Section 2.3.4. Compound **2p** was obtained by silica gel column chromatography eluting with diethyl ether (0.12 g, 72%). R_f (Diethyl ether) = 0.3. IR (neat, cm^{-1}): 3404 (w); 3127 (w); 2976 (w); 2919 (w); 2849 (w); 1731 (w); 1698 (s); 1541 (m); 1513 (w); 1455 (w); 1366 (w); 1337 (w); 1287 (w); 1247 (w); 1156 (s); 975 (w); 854 (w). $^1\text{H-NMR}$ (CDCl_3 , δ ppm): 1.41 (s, 9H, $(\text{CH}_3)_3\text{CO}(\text{CO})\text{CH}_2\text{N}(-)\text{CH}_2\text{CH}_2\text{NH}(\text{CO})\text{OC}(\text{CH}_3)_3$); 1.43 (s, 9H, $(\text{CH}_3)_3\text{CO}(\text{CO})\text{CH}_2\text{N}(-)\text{CH}_2\text{CH}_2\text{NH}(\text{CO})\text{OC}(\text{CH}_3)_3$); 1.98 (quintet, 2H, $J = 6.6$ Hz, 4-nitroimidazole- $\text{CH}_2\text{CH}_2\text{CH}_2\text{N}(-)$); 2.65 (m, 4H, $-\text{CH}_2\text{CH}_2\text{CH}_2\text{N}(-)\text{CH}_2\text{CH}_2\text{NH}-$); 3.15 (m, 4H, $-(\text{CO})\text{CH}_2\text{N}(-)\text{CH}_2\text{CH}_2\text{NH}-$); 4.19 (t, 2H, $J = 6.6$ Hz, 4-nitroimidazole- $\text{CH}_2\text{CH}_2\text{CH}_2\text{N}(-)$); 7.50 (s, 1H, 4-nitroimidazole-C2-H); 7.84 (s, 1H, 4-nitroimidazole-C5-H) [Fig. 2.32]. MS(ESI^+): 450.4 ($\text{M}+\text{Na}$) $^+$.

2.3.3.5. Synthesis of tert-butyl 2-(((tert-butoxycarbonyl)methyl)(3-(5-nitro-1H-imidazol-1-yl)propyl)amino)ethyl carbamate (2q)

To compound **2k** (0.07 g, 0.31 mmol) in acetonitrile (5 mL), DIEA (0.6 g, 0.47 mmol) and compound **2m** (0.13 g, 0.47 mmol) were added and the reaction mixture refluxed for 12 h with continuous stirring. The solvent was removed in vacuo and further work-up was carried out following the general procedure mentioned in *Section 2.3.4*. Compound **2q** was obtained by silica gel column chromatography eluting with diethyl ether (0.09 g, 70%). R_f (Diethyl ether) = 0.55. IR (neat, cm^{-1}): 3402 (w); 3109 (w); 2976 (m); 2930 (w); 2860 (w); 1713 (s); 1529 (m); 1474 (m); 1368 (s); 1248 (m); 1157 (s); 1145 (w); 854 (w); 826 (w); 744 (w). $^1\text{H-NMR}$ (CDCl_3 , δ ppm): 1.45 (s, 9H, $(\text{CH}_3)_3\text{CO}(\text{CO})\text{CH}_2\text{N}(-)\text{CH}_2\text{CH}_2\text{NH}(\text{CO})\text{OC}(\text{CH}_3)_3$); 1.48 (s, 9H, $(\text{CH}_3)_3\text{CO}(\text{CO})\text{CH}_2\text{N}(-)\text{CH}_2\text{CH}_2\text{NH}(\text{CO})\text{OC}(\text{CH}_3)_3$); 1.94 (quintet, 2H, $J = 6.4$ Hz, 5-nitroimidazole- $\text{CH}_2\text{CH}_2\text{CH}_2\text{N}(-)$); 2.61 (t, 2H, $J = 6.4$ Hz, 5-nitroimidazole- $\text{CH}_2\text{CH}_2\text{CH}_2\text{N}(-)$); 2.68 (t, 2H, $J = 6.2$ Hz, $-\text{CH}_2\text{N}(-)\text{CH}_2\text{CH}_2\text{NH}(-)$); 3.21 (m, 4H, $-\text{CH}_2\text{N}(-)\text{CH}_2\text{CH}_2\text{NH}(-)$); 4.50 (t, 2H, $J = 6.4$ Hz, 5-nitroimidazole- $\text{CH}_2\text{CH}_2\text{CH}_2\text{N}(-)$); 7.72 (s, 1H, 5-nitroimidazole-C2-H); 8.01 (s, 1H, 5-nitroimidazole-C4-H) [Fig. 2.33]. MS(ESI $^+$): 450.5 (M+Na) $^+$.

2.3.3.6. Synthesis of ligands 2L7 – 2L9

Compounds **2o**, **2p** and **2q** (0.25 mmol) were hydrolyzed following the general procedure described in *Section 2.3.5* to obtain the target ligands **2L7** (90%), **2L8** (84%) and **2L9** (90%), respectively, as the hydrochloride salt.

2-(N-(2-aminoethyl)-N-(3-(2-nitro-1H-imidazol-1-yl)propyl)amino) acetic acid (2L7):

IR (KBr, cm^{-1}): 3430 (m); 3206 (m); 3130 (w); 2990 (w); 2928 (w); 2679 (w); 2596 (w); 1688 (s); 1504 (w); 1487 (m); 1468 (w); 1357 (s); 1163 (m); 963 (m); 834 (m); 753 (w). $^1\text{H-NMR}$ (D_2O , δ ppm): 2.27 (quintet, 2H, $J = 7.9$ Hz, 2-nitroimidazole- $\text{CH}_2\text{CH}_2\text{CH}_2\text{N}(-)$); 3.37 (m, 4H, 2-nitroimidazole- $\text{CH}_2\text{CH}_2\text{CH}_2\text{N}(-)(\text{CH}_2\text{CH}_2-)$); 3.49 (m, 2H, 2-nitroimidazole-

CH₂CH₂CH₂N(-)(CH₂CH₂NH₂)); 3.84 (s, 2H, 2-nitroimidazole-CH₂CH₂CH₂N(-)CH₂COOH); 4.45 (t, 2H, *J* = 7.9 Hz, 2-nitroimidazole-CH₂CH₂CH₂N(-)CH₂COOH); 7.09 (s, 1H, 2-nitroimidazole-C5-H); 7.37 (s, 1H, 2-nitroimidazole-C4-H) [Fig. 2.34]. MS(ESI⁺): 271.3 (M)⁺ [Fig. 2.35].

2-(N-(2-aminoethyl)-N-(3-(4-nitro-1H-imidazol-1-yl)propyl)amino) acetic acid (2L8):

IR (KBr, cm⁻¹): 3432 (m); 3200 (m); 3131 (w); 2994 (w); 2924 (w); 2675 (w); 2596 (w); 1689 (s); 1506 (w); 1484 (m); 1470 (w); 1358 (s); 1165 (m); 964 (m); 837 (m); 755 (w). ¹H-NMR (D₂O, δ ppm): 2.39 (quintet, 2H, *J* = 4.8 Hz, 4-nitroimidazole-CH₂CH₂CH₂N-); 3.40 (m, 4H, 4-nitroimidazole-CH₂CH₂CH₂N(-)(CH₂CH₂NH₂)); 3.62 (t, 2H, *J* = 7.5 Hz, -CH₂CH₂CH₂N(-)(CH₂CH₂NH₂)); 4.03 (s, 2H, -CH₂CH₂CH₂N(-)CH₂COOH); 4.27 (t, 2H, *J* = 4.8 Hz, 4-nitroimidazole-CH₂CH₂CH₂N-); 7.79 (s, 1H, 4-nitroimidazole-C2-H); 8.24 (s, 1H, 4-nitroimidazole-C5-H) [Fig. 2.36]. MS(ESI⁺) *m/z*: 271.4 (M)⁺ [Fig. 2.37].

2-(N-(2-aminoethyl)-N-(3-(5-nitro-1H-imidazol-1-yl)propyl)amino) acetic acid (2L9):

Compound **2q** (0.05 g, 0.15 mmol) was hydrolyzed as per the general procedure described in *Section 2.3.5* to obtain compound **2L9** as the hydrochloride salt. The hydrochloride salt was further purified by recrystallization from methanol/ether (0.05 g, 90%). IR (KBr, cm⁻¹): 3435 (m); 3201 (m); 3133 (w); 2991 (w); 2931 (w); 2675 (w); 2599 (w); 1689 (s); 1500 (w); 1489 (m); 1465 (w); 1360 (s); 1164 (m); 961 (m); 835 (m); 756 (w). ¹H-NMR (D₂O, δ ppm): 2.41 (quintet, 2H, *J* = 4.8 Hz, 5-nitroimidazole-CH₂CH₂CH₂N-); 3.42 (m, 4H, 5-nitroimidazole-CH₂CH₂CH₂N(-)(CH₂CH₂NH₂)); 3.60 (m, 2H, -CH₂CH₂CH₂N(-)(CH₂CH₂NH₂)); 4.10 (s, 2H, -CH₂CH₂CH₂N(-)CH₂COOH); 4.45 (t, 2H, *J* = 4.8 Hz, 5-nitroimidazole-CH₂CH₂CH₂N-); 8.28 (s, 1H, 5-nitroimidazole-C2-H); 8.35 (s, 1H, 5-nitroimidazole-C4-H) [Fig. 2.38]. MS(ESI⁺): 271.4 (M)⁺ [Fig. 2.39].

2.3.3.7. Preparation of $Re(CO)_3$ complex of **2L8** (**2r**)

Complex **2r** was prepared following the same procedure described for the preparation of complex **2l** (Section 2.3.2.9), from compound **2L8** (0.07 g, 0.18 mmol) and bis(tetraethylammonium)-*fac*-tribromotricarbonylrhenate (0.14 g, 0.18 mmol) in water (5 mL, pH = 6). Overall yield obtained is 38% (0.04 g). IR (KBr, cm^{-1}): 3132 (m); 2984 (m); 2953 (m); 2695 (w); 2017 (vs); 1878 (vs); 1646 (s); 1492 (w); 1395 (m); 1339 (m); 1287 (w); 1182 (w); 1133 (w). 1H -NMR (D_2O , δ ppm): 1.97 (quintet, 2H, $J = 7.62$ Hz, 4-nitroimidazole- $CH_2CH_2CH_2N-$); 2.40 (t, 2H, 7.62, 4-nitroimidazole- $CH_2CH_2CH_2N(-)(CH_2CH_2NH_2)$); 2.63 and 3.25 (m, $-CH_2CH_2CH_2N(-)(CH_2CH_2NH_2)$); 3.85 (m, 2H, $-CH_2CH_2CH_2N(-)CH_2COOH$); 4.06 (t, 2H, 4-nitroimidazole- $CH_2CH_2CH_2N-$); 7.65 (s, 1H, 4-nitroimidazole-C2-H); 8.11 (s, 1H, 4-nitroimidazole-C5-H) [Fig. 2.40]. MS(ESI $^+$): 566.2 (M+H) $^+$ [Fig. 2.41].

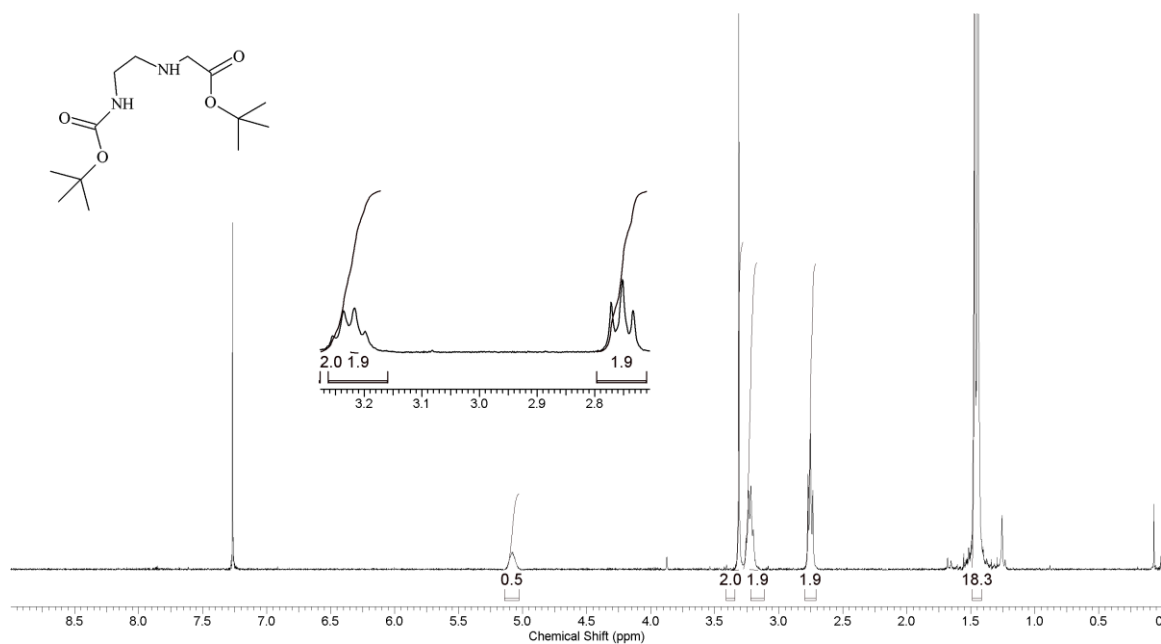


Fig. 2.29. 1H -NMR spectrum of *tert*-butyl 2-((*tert*-butoxycarbonyl)methylamino)ethyl carbamate (**2m**)

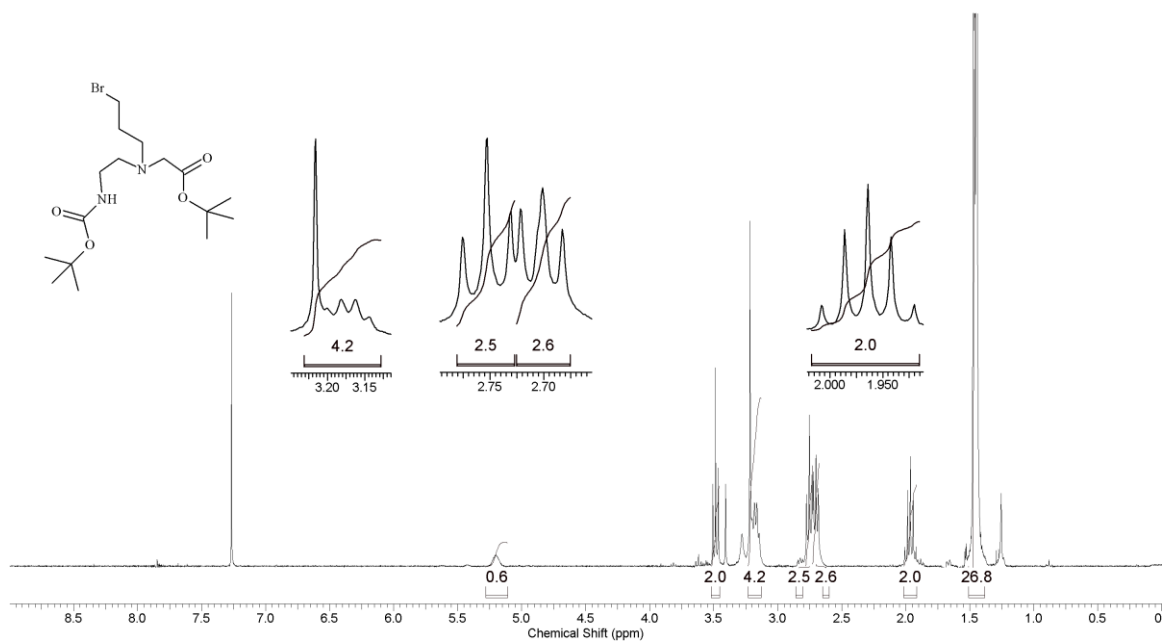


Fig. 2.30. ¹H-NMR spectrum of *tert*-butyl 2-(((*tert*-butoxycarbonyl)methyl)(3-bromopropyl)amino)ethyl carbamate (**2n**)

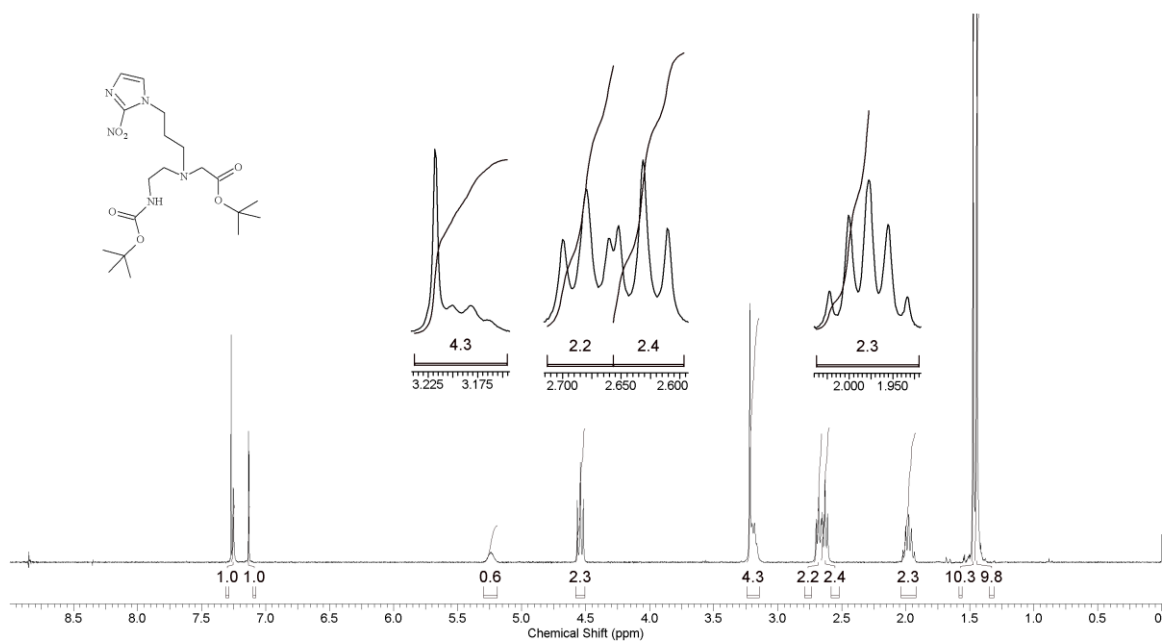


Fig. 2.31. ¹H-NMR spectrum of *tert*-butyl 2-(((*tert*-butoxycarbonyl)methyl)(3-(2-nitro-1H-imidazol-1-yl)propyl)amino)ethyl carbamate (**2o**)

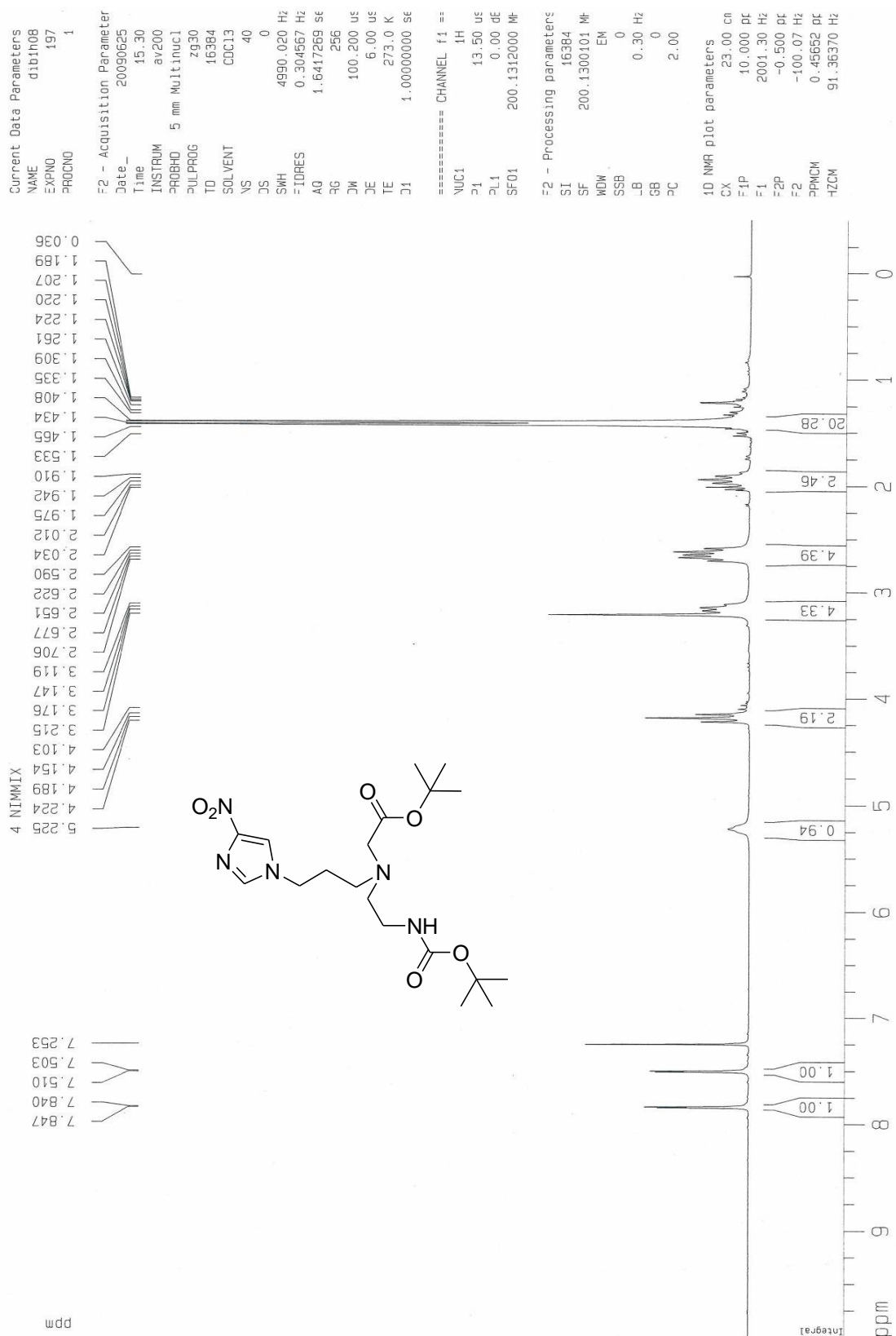


Fig. 2.32. $^1\text{H-NMR}$ spectrum of *tert*-butyl 2-(((*tert*-butoxycarbonyl)methyl)(3-(4-nitro-1H-imidazol-1-yl)propyl)amino)ethyl carbamate (**2p**)

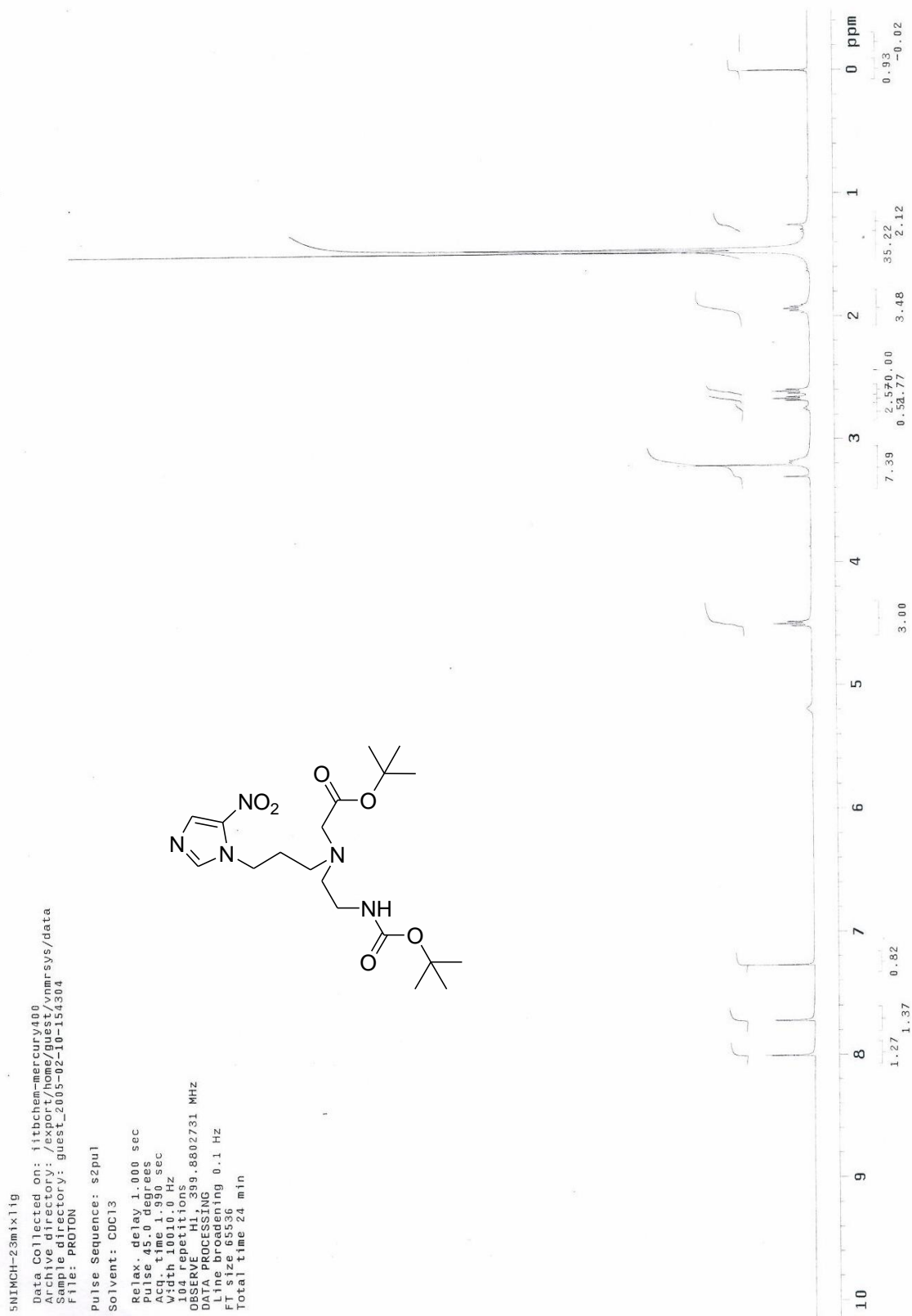


Fig. 2.33. $^1\text{H-NMR}$ spectrum of *tert*-butyl 2-(((*tert*-butoxycarbonyl)methyl)(3-(5-nitro-1H-imidazol-1-yl)propyl)amino)ethyl carbamate (**2q**)

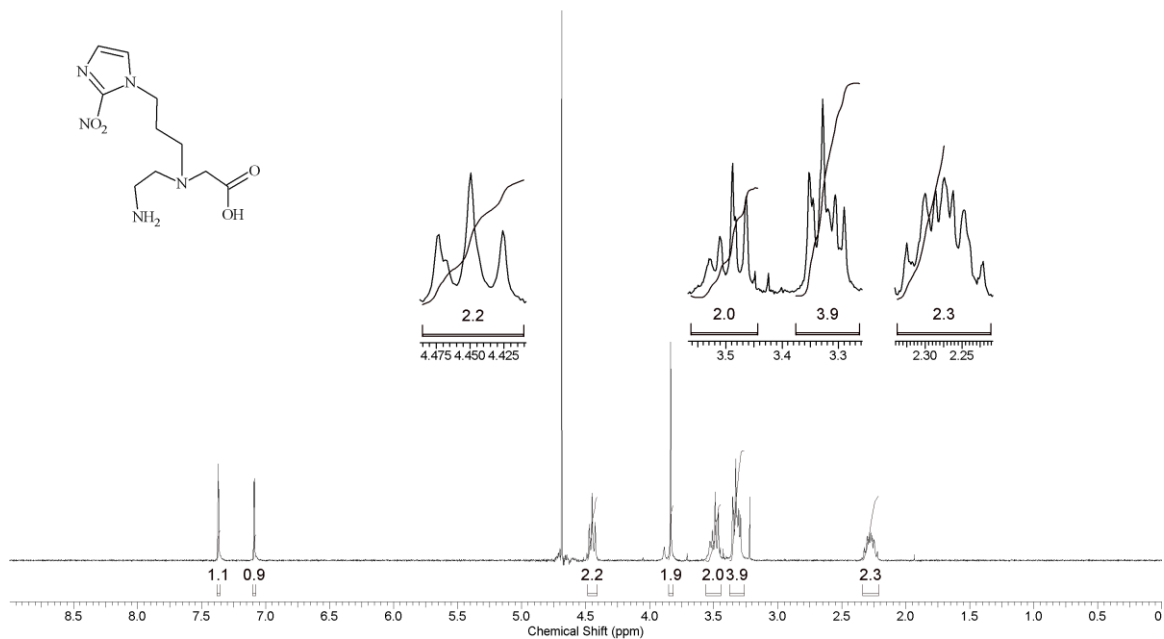


Fig. 2.34. ¹H-NMR spectrum of 2-(N-(2-aminoethyl)-N-(3-(2-nitro-1H-imidazol-1-yl)propyl)amino)acetic acid (**2L7**)

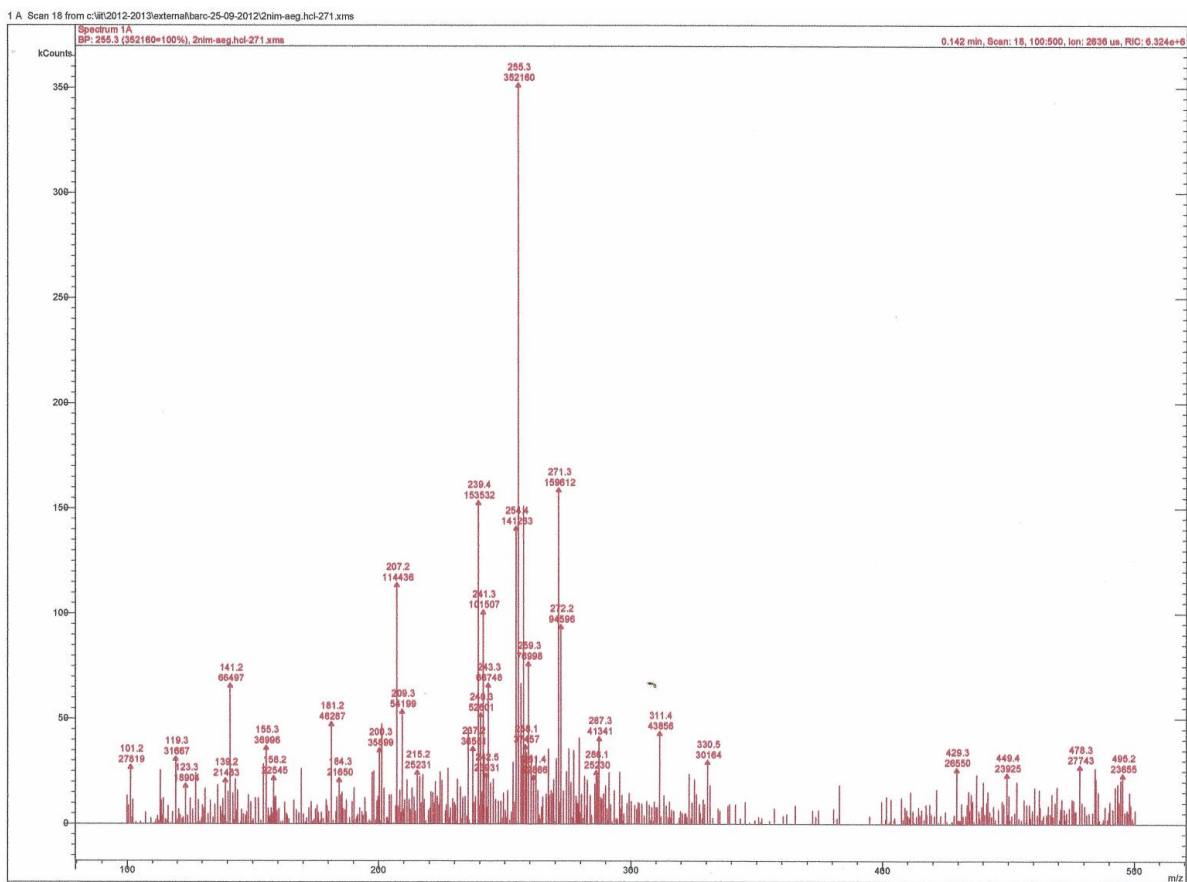


Fig. 2.35. ESI-MS of 2-(N-(2-aminoethyl)-N-(3-(2-nitro-1H-imidazol-1-yl)propyl)amino)acetic acid (**2L7**)

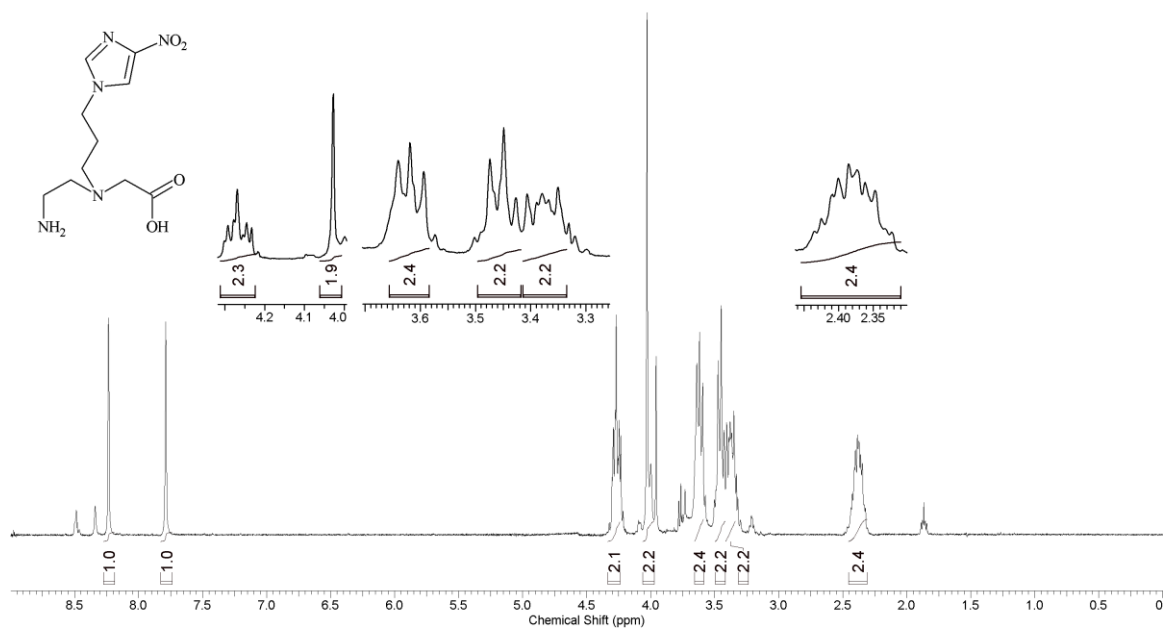


Fig. 2.36. $^1\text{H-NMR}$ spectrum of 2-(N-(2-aminoethyl)-N-(3-(4-nitro-1H-imidazol-1-yl)propyl)amino)acetic acid (**2L8**)

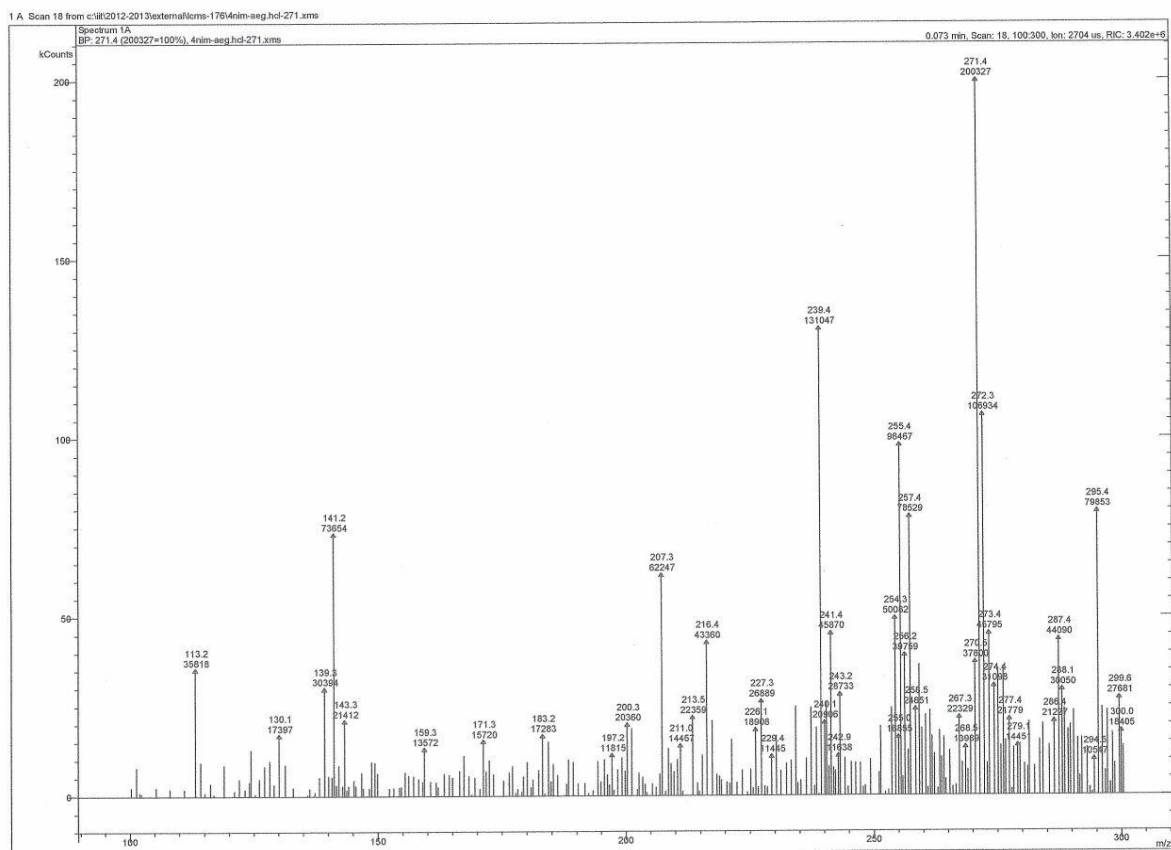


Fig. 2.37. ESI-MS of 2-(N-(2-aminoethyl)-N-(3-(4-nitro-1H-imidazol-1-yl)propyl)amino)acetic acid (**2L8**)

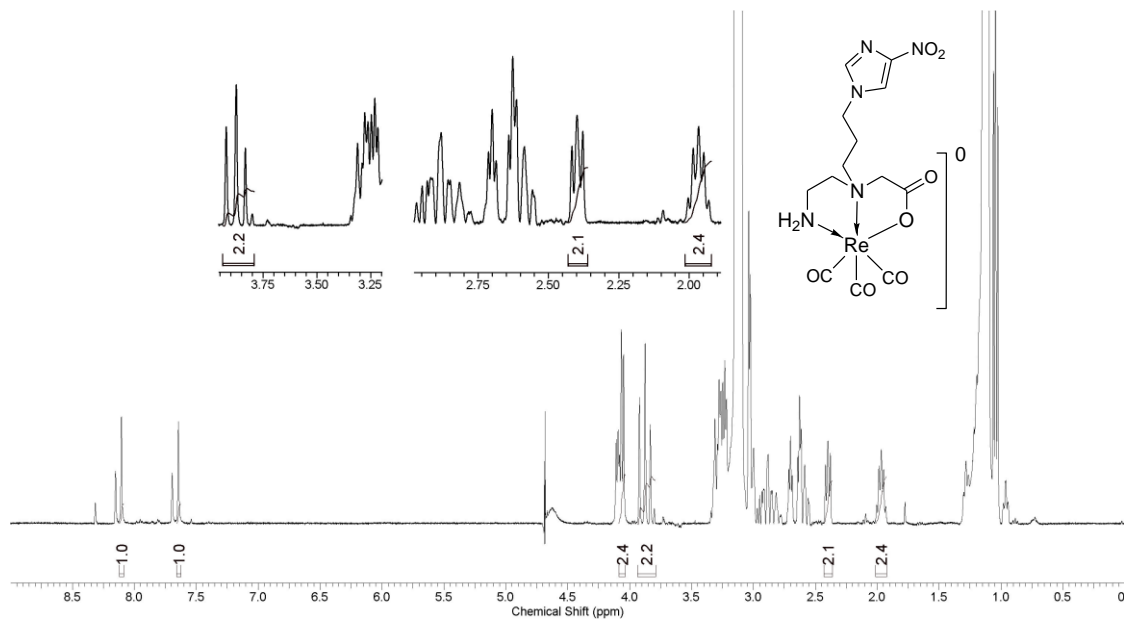


Fig. 2.40. Qualitative $^1\text{H-NMR}$ spectrum of $\text{Re}(\text{CO})_3$ complex of **2L8** (**2r**)

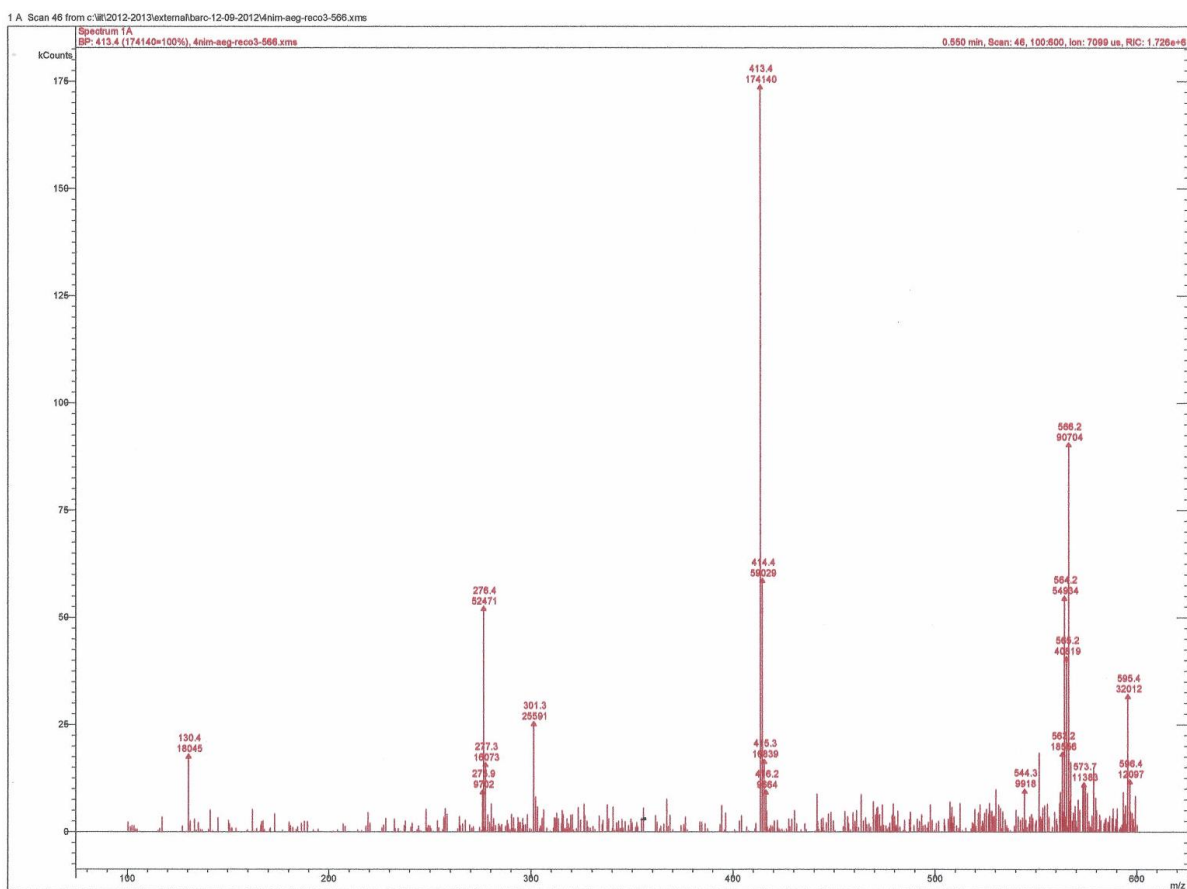


Fig. 2.41. ESI-MS of $\text{Re}(\text{CO})_3$ complex of **2L8** (**2r**)

2.3.4. General work-up procedure for compounds 2a-2d, 2g-2k and 2m-2q

The residue obtained after the removal of the solvent of reaction was dissolved in chloroform (30 mL) and washed with water (15 mL x 3) followed by brine (30 mL). The organic phase was dried over anhydrous sodium sulphate, concentrated and purified by silica gel column chromatography using appropriate solvent.

2.3.5. General procedure for the hydrolysis of Boc- and tert-butyl ester groups in compounds 2b – 2d, 2h – 2j and 2o – 2q

The respective compound was dissolved in minimum volume of methanol and added to 6N HCl (5 mL). The reaction mixture was stirred at room temperature for 12 h. The solvent was removed using a rotary evaporator at 40°C to yield the corresponding hydrochloride salt.

2.4. Radiolabeling

2.4.1. General procedure for the preparation of $^{99m}\text{Tc}(\text{CO})_3$ complexes of ligands 2L1-2L9

About 100 μL of $[\text{}^{99m}\text{Tc}(\text{CO})_3(\text{H}_2\text{O})_3]^+$ precursor, prepared following the procedure described in Chapter 1, *Section 1.14.3*, was added to 900 μL of 10^{-3} M solution of the respective ligand in phosphate buffer (pH 7.4) and incubated for 45 min at 70°C in a water bath. The reaction mixture was then cooled to room temperature and characterized by HPLC.

2.5. Quality control

The HPLC analysis, determination of partition coefficient and in vitro serum stability of different $^{99m}\text{Tc}(\text{CO})_3$ complexes prepared are carried out following the general protocol described in Chapter 1, *Sections 1.14.4, 1.14.5 and 1.14.6* respectively.

2.6. Biological evaluation

Development of the tumor model and the procedures followed for carrying out biological evaluation of different nitroimidazole- $^{99m}\text{Tc}(\text{CO})_3$ complexes are described in Chapter 1, *Sections 1.14.7*.

2.7. Results and discussion

2.7.1. Synthesis

For studying the effect of physicochemical properties of nitroimidazole radiopharmaceuticals on their pharmacokinetics, a series of nitroimidazole ligands were synthesized. The structure of nitroimidazole ligands (**2L1** – **2L9**) are shown in figure 2.42.

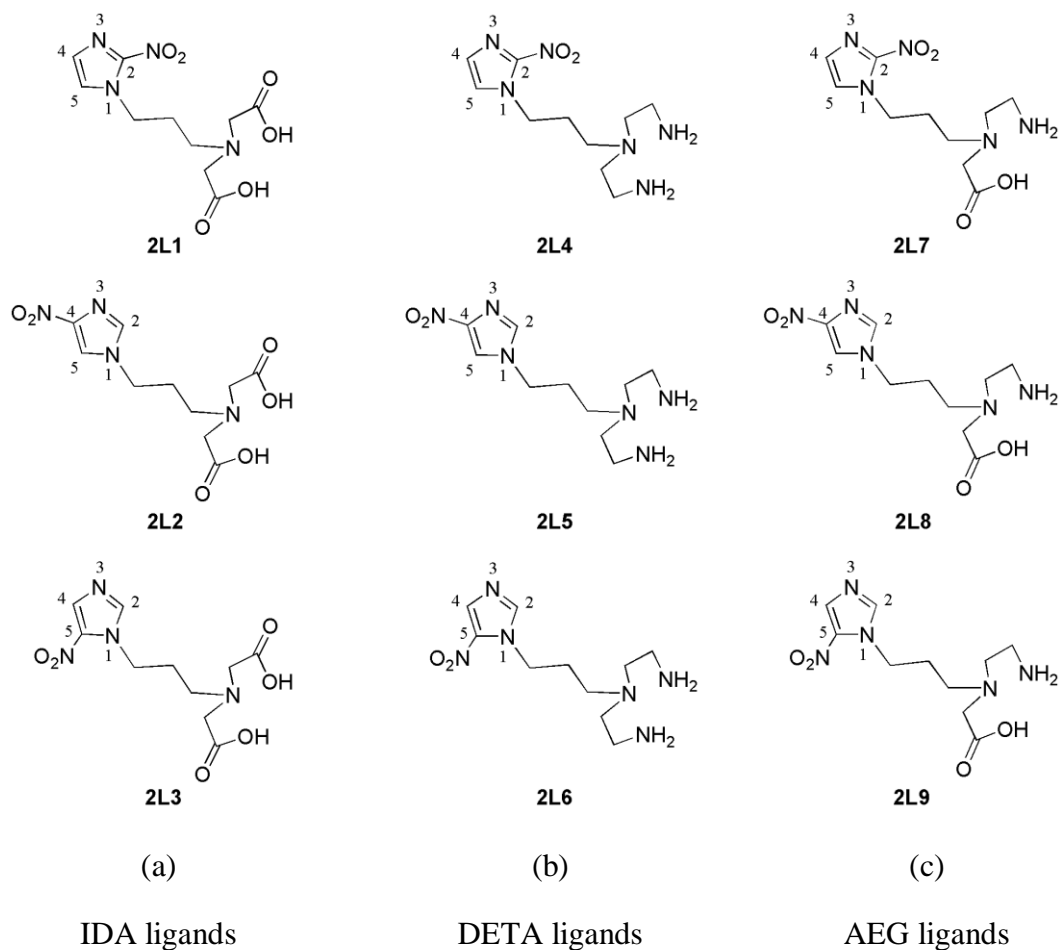


Fig. 2.42. Chemical structures of various nitroimidazole ligands

The SERP of a nitroimidazole depends on the position of the nitro-group as well as the nature and position of other groups in the imidazole ring. The ligands synthesized for the present study had one of the three tridentate ligands, viz. IDA, DETA or AEG, connected to the nitroimidazole moiety at one of the imidazole N-atom through a propyl spacer (Fig. 2.42).

Adams et al. had observed that groups that are separated by two or more bonds from the nitroimidazole ring had minimal effect on its SERP.¹⁹⁵ Hence, it was assumed that variation in SERP's due to this synthetic modification will be insignificant for different 2-nitroimidazole (**2L1**, **2L4**, **2L7**), 4-nitroimidazole (**2L2**, **2L5**, **2L8**), and 5-nitroimidazole (**2L3**, **2L6**, **2L9**) derivatives, and the trend observed in the SERP's of unsubstituted 2-, 4- and 5-nitroimidazole (-418 mV, -527 mV, -450 mV with respect to standard hydrogen electrode, respectively) will also be valid with their respective derivatives.¹⁹⁶ Therefore, with this set of nine ligands, corresponding $^{99m}\text{Tc}(\text{CO})_3$ complexes with different SERP could be prepared.

It has been reported that IDA-ligands upon radiolabeling with $[\text{}^{99m}\text{Tc}(\text{CO})_3(\text{H}_2\text{O})_3]^+$ precursor form complexes with overall charge of -1.¹⁹⁵ Similarly, DETA ligands formed complexes with overall charge of +1¹⁹⁸ and nitroimidazole-AEG ligands formed neutral complexes (Fig. 2.43). Hence, using the ligands **2L1-2L9**, complexes with different overall charge could be prepared.

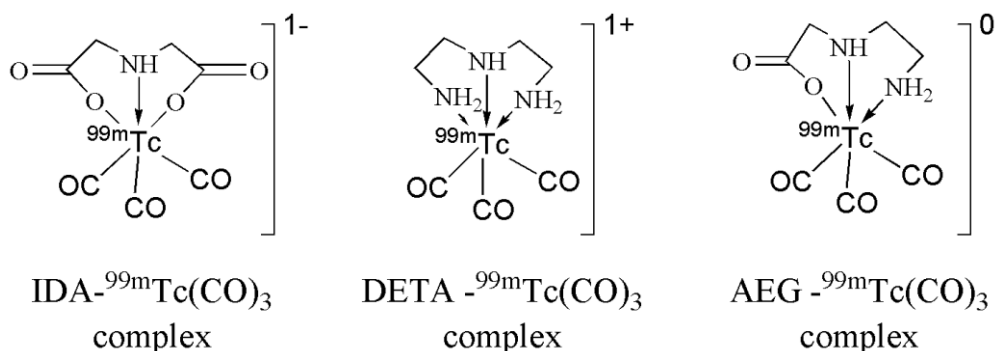


Fig. 2.43. Probable structure of $^{99m}\text{Tc}(\text{CO})_3$ complexes formed by IDA, DETA and AEG ligands

Due to the structural diversity of these complexes, their lipophilicity values will be different. Thus, nine different nitroimidazole- $^{99m}\text{Tc}(\text{CO})_3$ complexes with different SERP's, charges and lipophilicities could be prepared using the ligands **2L1-2L9**.

The ligands were synthesized via bifunctional chelator approach (Fig. 2.1). The BFCA **2a** [N,N-bis((*tert*-butoxycarbonyl)methyl)-3-bromopropylamine], was synthesized from 3-bromopropylamine hydrobromide and *tert*-butyl bromoacetate. Subsequently, the

BFCA was conjugated to the 2-nitroimidazole to obtain the corresponding *tert*-butyl ester derivative (**2b**). However, 5-nitroimidazole derivative could not be prepared by a similar reaction, since 5-nitroimidazole is not available commercially. Due to its instability in solution, emerging from higher acidity of its -NH- proton, 5-nitroimidazole tautomerizes to more stable 4-nitroimidazole. Earlier, Rao et al. reported the formation of 5-nitroimidazole derivative during base mediated N-alkylation of 4-nitroimidazole.¹⁹⁹ Following similar strategy, base-catalyzed N-alkylation of 4-nitroimidazole with BFCA **2a** was carried out, and it was found that *tert*-butyl esters of both 5-nitroimidazole (**2d**) and 4-nitroimidazole (**2c**) were formed.²⁰⁰ However, the yield (~15%) of 5-nitroimidazole derivative **2d** was much less than that of 4-nitroimidazole derivative **2c** (~65%). The two derivatives were separated by column chromatography. The *tert*-butyl esters of 2-, 4- and 5-nitroimidazoles (**2a-2c**) were then hydrolyzed to obtain the target ligands **2L1-2L3**.

The synthesis of nitroimidazole-DETA ligands (**2L4-2L6**) was carried out following a strategy similar to that for IDA ligands (Fig. 2.13). Compounds **2h** and **2i** were synthesized by coupling 2- and 4-nitroimidazole, respectively, to BFCA **2g**. In this case also, the formation of 5-nitroimidazole derivative was observed. However, the yield of isomeric 5-nitroimidazole derivative **2j** was too low to be of any practical utility. Therefore, compound **2j** was synthesized by an alternate route from compound **2k** and **2f** under basic condition [Fig. 2.13(b)]. Compound **2k** could be obtained from 4-nitroimidazole and 1,3-dibromopropane under basic condition. Compounds **2h-2j** are subsequently hydrolyzed to yield nitroimidazole-DETA ligands **2L4-2L6**.

The AEG derivatives of 2-, 4- and 5-nitroimidazole (**2L7-2L9**) were also synthesized by BFCA approach (Fig. 2.28). It is pertinent to note that 5-nitroimidazole isomer, **2q**, was formed in better yield (~10% overall) than compound **2j** (~4% overall) in the reaction between 4-nitroimidazole and compound **2n**. Purified compounds, **2o-2q**, upon acidic

hydrolysis gave the target ligands **2L7-2L9**, respectively, as hydrochloride salts. All compounds were characterized by IR, ¹H-NMR as well as low resolution mass spectrometer. The ¹H-NMR and mass spectra of the compounds were consistent with the expectations.

2.7.2. Radiolabeling, quality control and characterization

Nitroimidazole ligands (**2L1-2L9**) were radiolabeled with [^{99m}Tc(CO)₃(H₂O)₃]⁺ precursor to obtain corresponding ^{99m}Tc(CO)₃ complexes. As mentioned in Chapter 1, *Section 1.10.2.4*, [^{99m}Tc(CO)₃(H₂O)₃]⁺ precursor complex could be prepared in two ways. The classical method involves the use of carbon monoxide gas as the CO source. The modified method uses potassium boranocarbonate as a source for CO gas. In the present thesis, [^{99m}Tc(CO)₃(H₂O)₃]⁺ precursor complex was prepared using lyophilized kits, following the procedure briefly mentioned in Chapter 1, *Section 1.14.3*. General procedure for the preparation of nitroimidazole-^{99m}Tc(CO)₃ complexes is mentioned in *Section 2.2.3.1*. All the complexes were characterized by HPLC. The HPLC elution profile of [^{99m}Tc(CO)₃(H₂O)₃]⁺ core, nitroimidazole-IDA-^{99m}Tc(CO)₃ complexes and nitroimidazole-DETA-^{99m}Tc(CO)₃ complexes are shown in figure 2.44. The HPLC elution profile of nitroimidazole-AEG-^{99m}Tc(CO)₃ complexes are shown in figure 2.45. The octanol/water partition coefficients (LogP_{o/w}) of the complexes, determined following reported protocol,¹⁹⁰ are summarized in Table 2.1. The serum stability studies of the prepared complexes did not showed any sign of decomposition during the period of study.

Table 2.1. LogP_{o/w} of different nitroimidazole-^{99m}Tc(CO)₃ complexes

	IDA- ^{99m} Tc(CO) ₃ complex	DETA- ^{99m} Tc(CO) ₃ complex	AEG- ^{99m} Tc(CO) ₃ complex
2-nitroimidazole	0.48	0.28	0.06
4-nitroimidazole	0.43	0.17	-0.43
5-nitroimidazole	0.39	0.15	-0.53

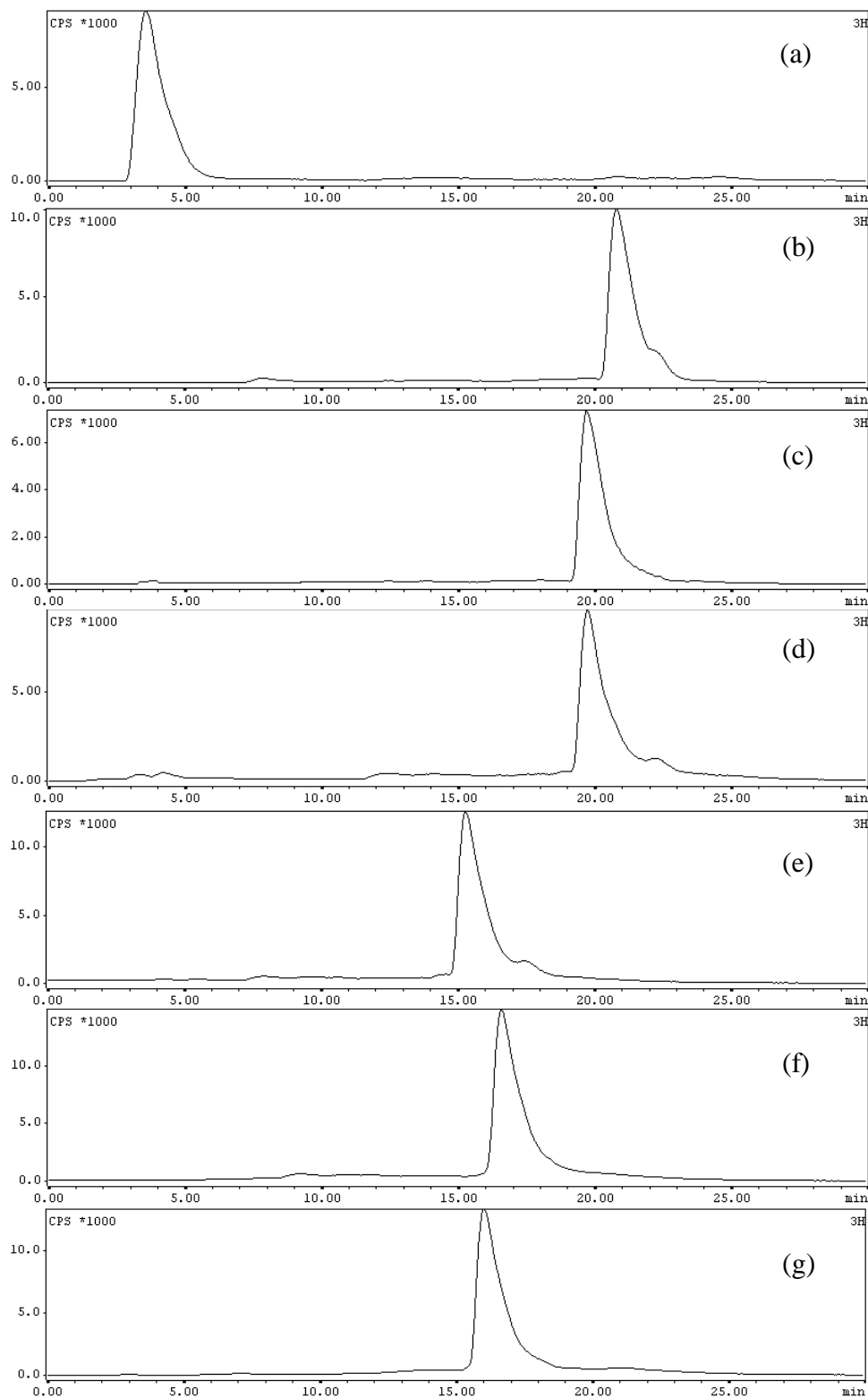


Fig. 2.44. HPLC elution profile of (a) $[^{99m}\text{Tc}(\text{CO})_3(\text{H}_2\text{O})_3]^+$ precursor complex (b) 2-nitroimidazole-IDA- $^{99m}\text{Tc}(\text{CO})_3$ complex (c) 4-nitroimidazole-IDA- $^{99m}\text{Tc}(\text{CO})_3$ complex (d) 5-nitroimidazole-IDA- $^{99m}\text{Tc}(\text{CO})_3$ complex (e) 2-nitroimidazole-DETA- $^{99m}\text{Tc}(\text{CO})_3$ complex (f) 4-nitroimidazole-DETA- $^{99m}\text{Tc}(\text{CO})_3$ complex and (g) 5-nitroimidazole-DETA- $^{99m}\text{Tc}(\text{CO})_3$ complex

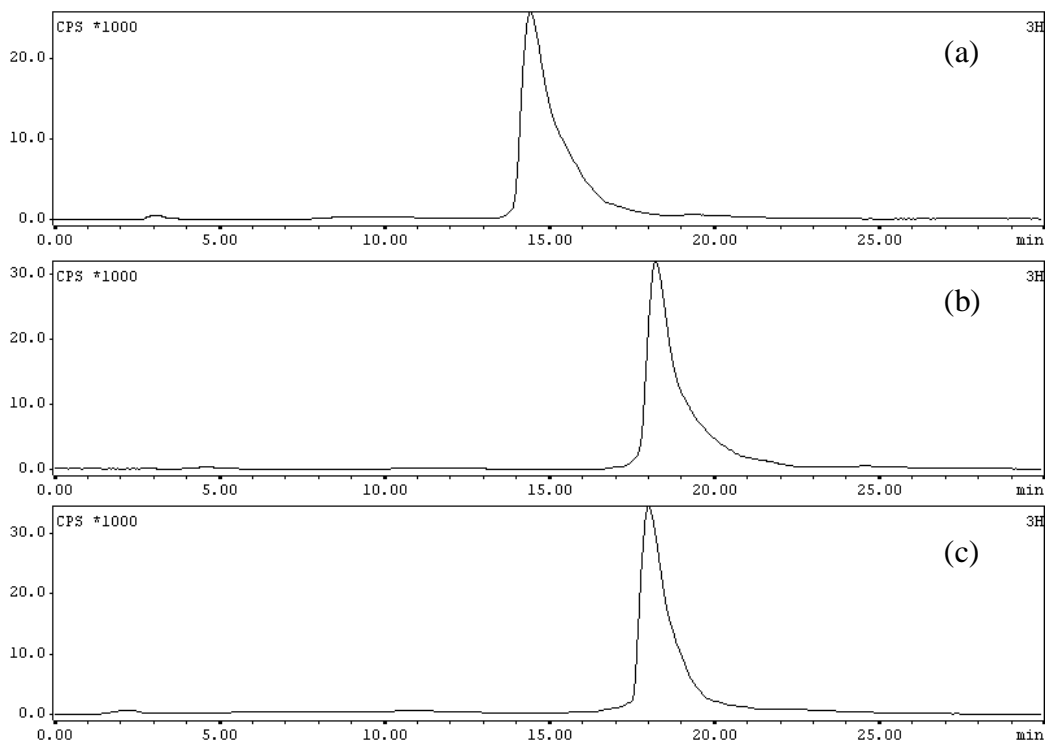


Fig. 2.45. HPLC elution profile of (a) 2-nitroimidazole-AEG- $^{99m}\text{Tc}(\text{CO})_3$ complex (b) 4-nitroimidazole-AEG- $^{99m}\text{Tc}(\text{CO})_3$ complex and (c) 5-nitroimidazole-AEG- $^{99m}\text{Tc}(\text{CO})_3$ complex

To elucidate the mode of binding of nitroimidazole ligand with the $^{99m}\text{Tc}(\text{CO})_3$ core, corresponding $\text{Re}(\text{CO})_3$ complexes of ligands **2L1**, **2L6** and **2L8** were prepared. The procedure followed for the preparation of $\text{Re}(\text{CO})_3$ complexes is described in experimental section. It could be observed that elution profiles of $\text{Re}(\text{CO})_3$ complexes, **2L1**, **2L6** and **2L8**, matched with their $^{99m}\text{Tc}(\text{CO})_3$ counterparts, prepared at nca level (Fig. 2.46), which indicated the formation of similar type of complexes, both at the nca level as well as macroscopic level. Observation of $(\text{M}+\text{H})^+$ ion peak at m/z 528.2, and $(\text{M}+\text{H})^+$ ion peak at m/z 566.2, provided additional evidence for the formation of 5-nitroimidazole-DETA- $\text{Re}(\text{CO})_3$ and 4-nitroimidazole-AEG- $\text{Re}(\text{CO})_3$ complexes, respectively. The ^1H -NMR spectrum of $\text{Re}(\text{CO})_3$ complex of **2L1** (Fig. 2.12) showed two AB quartets, centered at 3.54 δ ppm and 3.78 δ ppm respectively, corresponding to the $-\text{N}(\text{CH}_\text{A}\text{CH}_\text{B}\text{CO})_2$ proton, which otherwise appeared as a singlet at 3.88 δ ppm in ligand **2L1** (Fig. 2.6). This change in the ^1H -NMR pattern is consistent with tridentate coordination of the IDA ligand to the metal core.²⁰¹

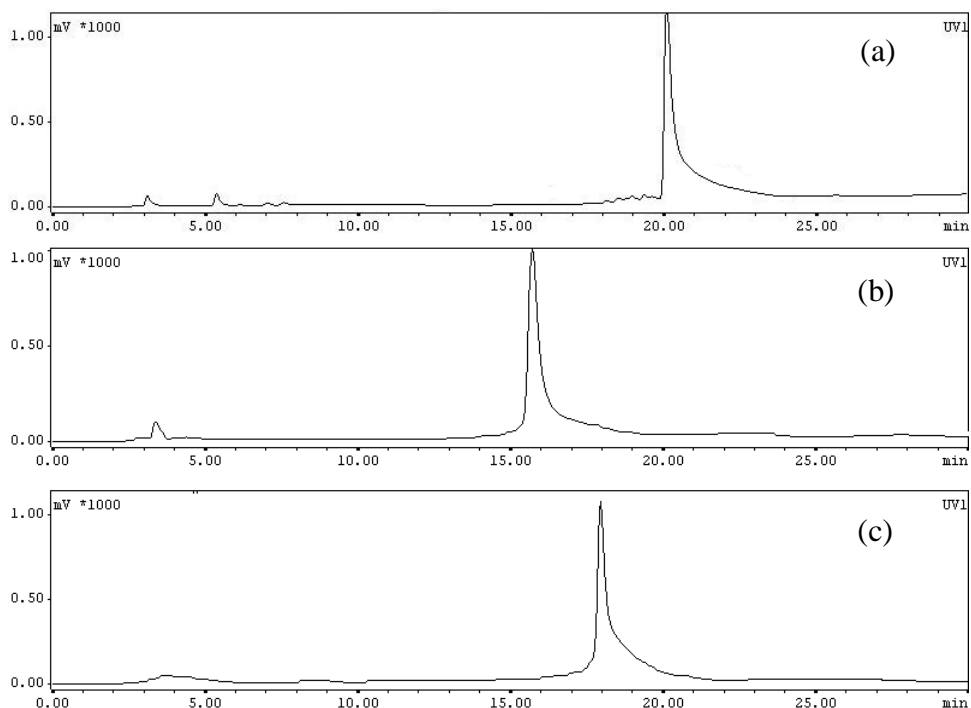


Fig. 2.46. HPLC elution profile of (a) 2-nitroimidazole-IDA-Re(CO)₃ complex (b) 5-nitroimidazole-DETA-Re(CO)₃ complex and (c) 4-nitroimidazole-AEG-Re(CO)₃ complex

The ¹H-NMR spectrum of 5-nitroimidazole-DETA-Re(CO)₃ complex (**2l**) also showed a complex splitting pattern, typical of AB spin systems, corresponding to the eight methylene protons of the diethylenetriamine moiety, which indicated tridentate coordination between the three nitrogen atoms of diethylenetriamine ligand and Re(CO)₃ metal core [Fig. 2.26].²⁰² The eight methylene protons appeared as multiplets in four groups centered at 2.87 δ ppm, 3.00 δ ppm, 3.47 δ ppm and 3.90 δ ppm each integrating to 2 protons. Similar, complicated, splitting pattern, which could be observed in the ¹H-NMR spectrum of 4-nitroimidazole-AEG-Re(CO)₃ complex (**2r**) [Fig. 2.40], together with the disappearance of singlet at 4.03 δ ppm, corresponding to the two methylene protons of acetic acid moiety in the uncomplexed ligand (Fig. 2.36), indicated tridentate coordination between aminoethyl glycine and Re(CO)₃ core.²⁰² The sample used for recording the spectrum, however, contained significant amount of tetraethylammonium bromide, because of which the splitting pattern of four ethylene protons is not clearly evident. The spectrum is, hence, a qualitative one. Considering the

spectroscopic evidences, the proposed structure of $\text{Re}(\text{CO})_3$ complexes of ligands **2L1**, **2L6** and **2L8** is as in figure 2.47. Since the HPLC chromatograms of the $\text{Re}(\text{CO})_3$ complexes of ligands **2L1**, **2L6** and **2L8** matched with corresponding $^{99\text{m}}\text{Tc}(\text{CO})_3$ complexes prepared at the nca level, tridentate coordination similar to $\text{Re}(\text{CO})_3$ complexes could be assumed between the nitroimidazole ligands and the $^{99\text{m}}\text{Tc}(\text{CO})_3$ core.

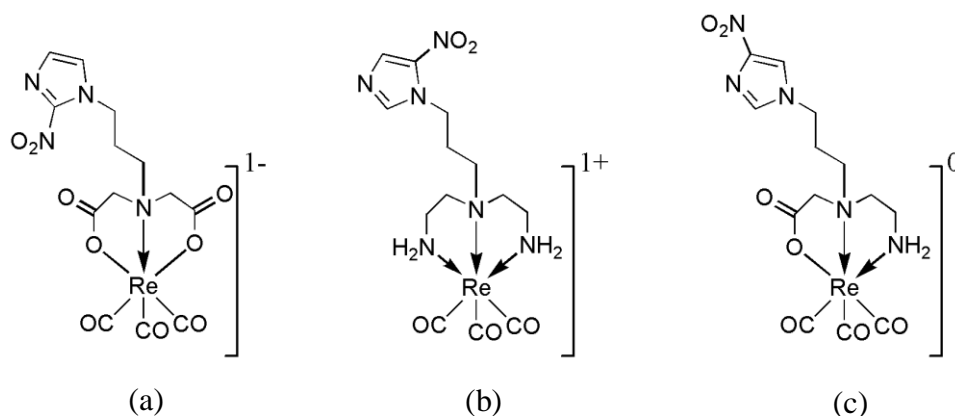


Fig. 2.47. Structure of $\text{Re}(\text{CO})_3$ complexes of (a) **2L1** (b) **2L6** and (c) **2L8**

2.7.3. Biological evaluation

All the $^{99\text{m}}\text{Tc}(\text{CO})_3$ complexes as well as $[^{18}\text{F}]\text{FMISO}$ was evaluated in fibrosarcoma tumor bearing Swiss mice following the general protocol mentioned in Chapter 1, *Section 1.14.7.2*. The activity in tumor shown by different nitroimidazole- $^{99\text{m}}\text{Tc}(\text{CO})_3$ complexes and $[^{18}\text{F}]\text{FMISO}$ are shown in Figure 2.48. At 30 min p.i., small differences were observed in tumor uptake among different nitroimidazole-IDA- $^{99\text{m}}\text{Tc}(\text{CO})_3$ complexes [0.97(0.06), 0.56(0.17), 0.45(0.09) %ID/g for 2-, 4- and 5-nitroimidazole derivatives, respectively] and nitroimidazole-AEG- $^{99\text{m}}\text{Tc}(\text{CO})_3$ complexes [1.33(0.28), 1(0.11), 0.91(0.03) %ID/g for 2-, 4- and 5-nitroimidazole derivatives, respectively]. However, these differences were not significant ($p > 0.05$) for the 4- and 5-nitroimidazole complexes of either groups. Among the three DETA- $^{99\text{m}}\text{Tc}(\text{CO})_3$ complexes, no significant differences were observed in tumor uptake at 30 min p.i. [1.05 (0.25), 1.1 (0.07) and 1.07 (0.09) %ID/g for 2-, 4- and 5-nitroimidazole derivatives, respectively]. At the same reference time, $[^{18}\text{F}]\text{FMISO}$ showed

significantly higher uptake in tumor [4.65 (0.86) %ID/g] than any of the nitroimidazole-^{99m}Tc(CO)₃ complexes evaluated in the present study.

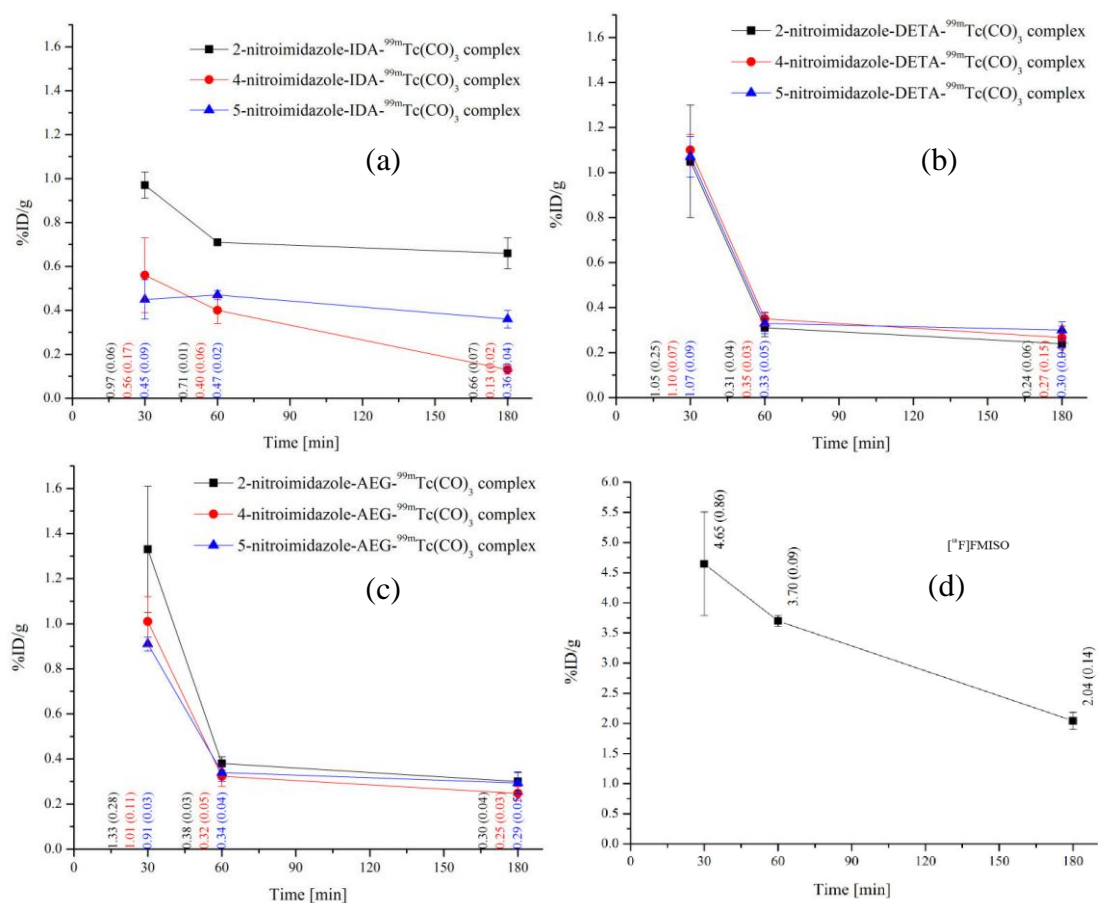


Fig. 2.48. Activity of (a) 2-, 4-, 5- nitroimidazole-IDA-^{99m}Tc(CO)₃ complexes (b) 2-, 4-, 5- nitroimidazole-DETA-^{99m}Tc(CO)₃ complexes (c) 2-, 4-, 5- nitroimidazole-AEG-^{99m}Tc(CO)₃ complexes and (d) [¹⁸F]FMISO in tumor at different time points

These observations could not be explained considering the SERP of nitroimidazole complexes alone. Also, Zhang et al. had studied a number of 2-nitroimidazole ^{99m}Tc complexes with P values ranging from 0.0002 to 5 (LogP ranging from -3.7 to 0.70) and they have observed that variation in aerobic cell accumulation of the radiotracer in vitro is within a very narrow range.¹⁹² Since lipophilicity values of different nitroimidazole-^{99m}Tc(CO)₃ complexes being evaluated are within the range from -3.7 to 0.70, the observed variation in tumor uptake may not be due to the lipophilicity. However, a possible explanation could be obtained considering the blood clearance pattern of respective radiotracers [Fig. 2.49].

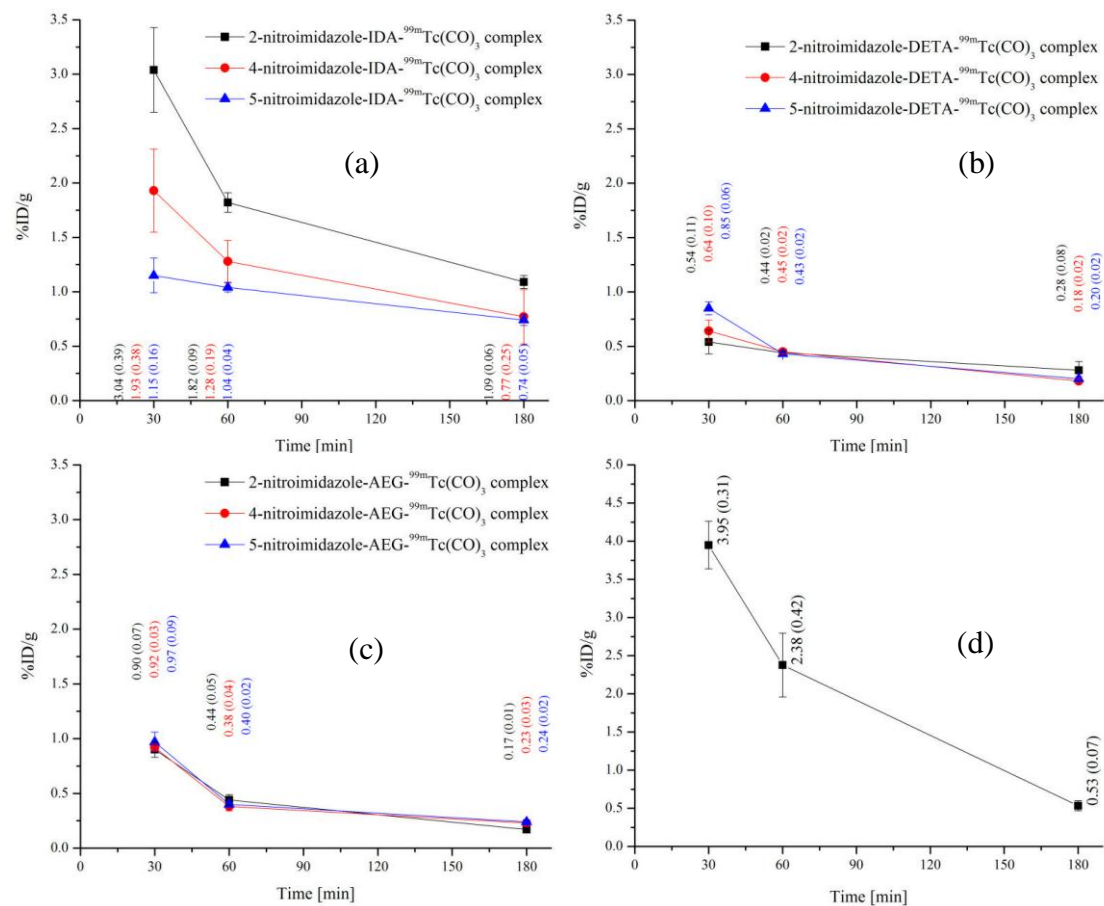


Fig. 2.49. Clearance of activity of (a) 2-, 4-, 5- nitroimidazole-IDA- $^{99m}\text{Tc}(\text{CO})_3$ complexes (b) 2-, 4-, 5- nitroimidazole-DETA- $^{99m}\text{Tc}(\text{CO})_3$ complexes, (c) 2-, 4-, 5- nitroimidazole-AEG- $^{99m}\text{Tc}(\text{CO})_3$ complexes and (d) [^{18}F]FMISO from blood at different time points

A radiotracer that clears slowly from blood enables it to distribute better in tumor, by passive diffusion, along the concentration gradient established between blood and the intracellular environment of the tumor. The rate of diffusion depends on the lipophilicity of the radiotracer, where a more lipophilic tracer diffuses faster than a less lipophilic one. Considering the deteriorated vasculature that could be expected in a tumor, the radiotracer may have to traverse a longer diffusion path from the blood vessels to distribute across the entire tumor mass. This requires the concentration gradient of the radiotracer between blood and intra-tumoral environment to hold for sufficient period of time to facilitate efficient and complete distribution of the radiotracer in the tumor. Fast clearance of activity from the blood can lead to early reversal of concentration gradient which may affect the distribution of the

radiotracer in the tumor mass. Reversal of the concentration gradient of the radiotracer between blood and intra-tumoral environment can also initiate the clearance of unreduced radiotracer from the tumor, thereby significantly decreasing the tumor residence time of the radiotracer. The observed tumor uptake of different radiotracers at 30 min p.i. may be the resultant of these two effects happening in varying proportions. At 30 min p.i., about 4% ID/g of [^{18}F]FMISO activity was observed in blood, whereas, only about 1% or less blood activity was observed for nitroimidazole-DETA as well as nitroimidazole-AEG $^{99\text{m}}\text{Tc}(\text{CO})_3$ complexes which implies that concentration gradient of [^{18}F]FMISO between blood and intra-tumoral environment is higher and holding for a longer time than that of other nitroimidazole-DETA and nitroimidazole-AEG $^{99\text{m}}\text{Tc}(\text{CO})_3$ complexes. Consequently, [^{18}F]FMISO showed higher tumor uptake compared to the latter group of complexes.

The three nitroimidazole-IDA- $^{99\text{m}}\text{Tc}(\text{CO})_3$ complexes cleared more slowly than DETA and AEG- $^{99\text{m}}\text{Tc}(\text{CO})_3$ complexes. Accordingly, they showed relatively higher tumor uptake than DETA and AEG- $^{99\text{m}}\text{Tc}(\text{CO})_3$ complexes, but lower than [^{18}F]FMISO. It is pertinent to note that, while tumor uptake (%ID/g) observed with [^{18}F]FMISO as well as different DETA and AEG- $^{99\text{m}}\text{Tc}(\text{CO})_3$ complexes at 30 min p.i. were similar or slightly higher than their respective activity in blood (expressed in %ID/g), the tumor uptake observed with nitroimidazole-IDA $^{99\text{m}}\text{Tc}(\text{CO})_3$ complexes were lower, despite having higher lipophilicity and blood activity than DETA and AEG $^{99\text{m}}\text{Tc}(\text{CO})_3$ complexes. Pauletti et al. had reported similar observations where tripeptides with comparable sizes diffused across the cell membrane in a charge-dependent manner, the order of diffusion rates being negative < positive \leq neutral.²⁰³ Possibly the negative charge on the compound hinders its smooth diffusion across the negatively charged cell membrane.

At 60 min p.i., [^{18}F]FMISO as well as other nitroimidazole- $^{99\text{m}}\text{Tc}(\text{CO})_3$ complexes, except 5-nitroimidazole-IDA- $^{99\text{m}}\text{Tc}(\text{CO})_3$ complex, showed a reduction in tumor activity

observed at 30 min p.i. The decrease was shallow for [^{18}F]FMISO and three nitroimidazole-IDA- $^{99\text{m}}\text{Tc}(\text{CO})_3$ complexes, whereas for DETA and AEG- $^{99\text{m}}\text{Tc}(\text{CO})_3$ complexes the decrease was sharp [Fig. 2.48]. The activity of different nitroimidazole radiotracers accumulated in tumor at 60 min p.i. cleared slowly, indicating that it could be associated with the radiotracer reduced and trapped in hypoxic tumor cells. The possibility that observed activity in tumor is due to the non-specific binding of the radiotracer could be ruled out considering the steadily decreasing radioactivity level in muscles with time. This is also evident from the increase in tumor to muscle ratio (TMR) of all nitroimidazole radiotracers with time. The decrease in tumor activity between 30 and 60 min p.i. observed for different radiotracers could be attributed to the clearance of unbound nitroimidazole radiotracer from the tumor. The difference in the tumor activity at 60 min p.i. showed by different nitroimidazole- $^{99\text{m}}\text{Tc}(\text{CO})_3$ complexes and [^{18}F]FMISO could be explained considering respective SERP and residence time in tumor.

Different processes involved in the reduction of nitroimidazole in hypoxic cells in already discussed in Chapter 1, *Section 1.8.2.2*. The ease of nitroimidazole radical anion formation in the cell depends on the SERP of the nitroimidazole, wherein a nitroimidazole with more positive SERP form radical anions more readily than the nitroimidazole with lower SERP. However, owing to small levels of molecular oxygen present in viable hypoxic cells, the nitroimidazole radiotracer may have to undergo several futile reduction-oxidation cycles, between the radical anion of the complex and the parent complex, before it undergoes further reduction and trapping. Hence, it could be presumed that even nitroimidazoles with highly favorable SERP need to spend adequate time in hypoxic cells before reduction takes place. Therefore, fast clearance of nitroimidazole radiotracer from blood could significantly reduce its tumor residence time, and hence, its reduction in hypoxic cells despite having favorable SERP. This may be the reason for the lower tumor retention showed by different

nitroimidazole-DETA and nitroimidazole-AEG $^{99m}\text{Tc}(\text{CO})_3$ complexes, especially the 2-nitroimidazole complexes with relatively favorable SERP. While the difference in tumor retention showed by 2-, 4- and 5-nitroimidazole AEG- $^{99m}\text{Tc}(\text{CO})_3$ complexes at 60 min p.i. were found to be significant ($p < 0.05$), that showed by respective nitroimidazole-DETA- $^{99m}\text{Tc}(\text{CO})_3$ complexes were insignificant. The tumor activity observed with [^{18}F]FMISO and the three nitroimidazole-IDA- $^{99m}\text{Tc}(\text{CO})_3$ complexes at 60 min p.i. could be correlated to their respective tumor residence time and SERP. [^{18}F]FMISO, that had higher tumor residence time and a more favorable SERP (-389 mV), showed highest retention in tumor, followed by 2-, 5- and 4-nitroimidazole IDA- $^{99m}\text{Tc}(\text{CO})_3$ complexes, respectively. The exact cause for slow blood clearance of nitroimidazole-IDA- $^{99m}\text{Tc}(\text{CO})_3$ complexes is not clear. However, it has been reported that molecules with overall negative charge showed relatively higher binding to serum compared to positively charged and neutral molecules. Also, molecules with higher lipophilicity are known to show higher serum binding.^{204, 205}

Retrospectively, evidence for the negative influence of fast blood clearance of nitroimidazole radiotracers on tumor uptake as well as retention could be obtained from literature. BMS181321 and BRU59-21 are two 2-nitroimidazole-based ^{99m}Tc -complexes which showed oxygen-dependent accumulation in hypoxic cells, *in vitro* as well as *in vivo*.⁹⁴⁻
⁹⁵ Though a direct comparison between different nitroimidazole- $^{99m}\text{Tc}(\text{CO})_3$ complexes evaluated in the present work, BMS181321 and BRU59-21 would be inappropriate due to the difference in tumor models used, the trends in their distribution may be analyzed. Upon intravenous administration of BMS181321 in mice bearing KHT tumor, tumor uptake of 1.91 ± 0.29 %ID/g was observed at 10 min p.i., which then decreased to 0.73 ± 0.22 at 1 h p.i. and 0.53 ± 0.26 at 4 h p.i. BMS181321 is a highly lipophilic complex ($\text{LogP}_{o/w} = \sim 40$) and cleared slowly from blood (~ 5 %ID/g at 10 min p.i. and ~ 2 %ID/g at 4 h p.i.). BRU59-21 ($\text{LogP}_{o/w} = \sim 11$) was a similar 2-nitroimidazole complex designed to overcome the problems associated

with the higher lipophilicity of BMS181321. This complex, which was also evaluated in mice bearing KTH tumor, showed very fast clearance from blood (1.56 ± 0.43 %ID/g at 10 min p.i., 0.53 ± 0.05 %ID/g at 1 h p.i. and 0.40 ± 0.08 %ID/g at 4 h p.i.) which had a significant effect on the activity retained in tumor (0.73 ± 0.22 %ID/g at 10 min p.i., 0.37 ± 0.04 %ID/g at 1 h p.i. and 0.31 ± 0.18 %ID/g at 4 h p.i. Similarly, [^{18}F]FAZA which clears relatively faster from blood showed lower uptake in tumor than [^{18}F]FMISO in Walker 256 rat carcinosarcoma tumor bearing animal model.³⁵

Although the tumor activity observed at 60 min p.i. for different nitroimidazole radiotracers cleared slowly, the rate of clearance was highest for [^{18}F]FMISO (~44 % ID/g cleared at 180 min p.i.) compared to other nitroimidazole- $^{99\text{m}}\text{Tc}(\text{CO})_3$ complexes (~8-20 %ID/g cleared at 180 min p.i.). [^{18}F]FAZA has also been reported with rate of clearance similar to [^{18}F]FMISO between 60 and 180 min (~53 % ID/g cleared).³⁵ There is still some ambiguity on the fate of reduction products of nitroimidazoles in hypoxic cells. Though nitroimidazole adducts such as misonidazole-glutathione and metronidazole-DNA are reported,^{206,207} a more widely accepted view is the formation of less permeable reduction products that clears slowly from hypoxic cells rather than the formation of covalently bound macro-molecular adducts.⁷⁶ Present study suggests that the reduction products of nitroimidazole- $^{99\text{m}}\text{Tc}(\text{CO})_3$ complexes are less permeable than the reduction products of [^{18}F]FMISO, which is indicated by their slower rate of clearance from the tumor. This could be an advantage, since the imaging can be delayed to obtain a better target to background ratio. Though slow blood clearance increases the tumor residence time of the radiotracer, thereby increasing the reduction of nitroimidazole radiotracer in hypoxic tumor cells, a reduced rate of clearance may result in poor target to background ratio. The tumor to blood ratio [TBR] and tumor to muscle ratio [TMR] obtained with different nitroimidazole- $^{99\text{m}}\text{Tc}(\text{CO})_3$ complexes and [^{18}F]FMISO at different time points is shown in Table 2.2.

Table 2.2. TBR and TMR of various 2-, 4- and 5-nitroimidazole-^{99m}Tc(CO)₃ complexes and [¹⁸F]FMISO at different time points

		Tumor to blood ratio/ <i>Tumor to muscle</i>		
		30 min	60 min	180 min
IDA- ^{99m} Tc(CO) ₃ complex	2-nitroimidazole	0.32 (0.04)	0.39 (0.01)	0.61 (0.09)
		<i>1.76 (0.27)</i>	<i>2.40 (0.19)</i>	<i>3.68 (0.23)</i>
	4-nitroimidazole	0.29 (0.03)	0.31 (0.05)	0.18 (0.04)
		<i>1.01 (0.09)</i>	<i>0.92 (0.02)</i>	<i>0.24 (0.05)</i>
	5-nitroimidazole	0.40 (0.11)	0.45 (0.04)	0.49 (0.09)
		<i>Very high</i>	<i>Very high</i>	<i>Very high</i>
DETA- ^{99m} Tc(CO) ₃ complex	2-nitroimidazole	1.94 (0.09)	0.71 (0.08)	0.84 (0.05)
		<i>3.32 (0.34)</i>	<i>2.41 (0.06)</i>	<i>1.82 (0.19)</i>
	4-nitroimidazole	1.72 (0.17)	0.78 (0.06)	1.51 (0.27)
		<i>6.86 (0.18)</i>	<i>4.09 (0.18)</i>	<i>5.33 (1.03)</i>
	5-nitroimidazole	1.26 (0.15)	0.78 (0.13)	1.48 (0.15)
		<i>9.73 (0.13)</i>	<i>4.97 (0.72)</i>	<i>6.07 (0.59)</i>
AEG- ^{99m} Tc(CO) ₃ complex	2-nitroimidazole	1.49 (0.41)	0.86 (0.04)	1.78 (0.34)
		<i>6.20 (1.13)</i>	<i>3.34 (0.17)</i>	<i>3.05 (0.71)</i>
	4-nitroimidazole	1.09 (0.13)	0.86 (0.15)	1.06 (0.14)
		<i>1.98 (0.24)</i>	<i>1.10 (0.20)</i>	<i>2.00 (0.15)</i>
	5-nitroimidazole	0.95 (0.08)	0.85 (0.12)	1.26 (0.35)
		<i>1.56 (0.12)</i>	<i>1.42 (0.17)</i>	<i>2.68 (1.02)</i>
Standard agent	[¹⁸ F]Fluoromisonidazole	1.17 (0.18)	1.58 (0.25)	3.85 (0.23)
		<i>1.17 (0.25)</i>	<i>1.40 (0.34)</i>	<i>4.84 (0.90)</i>

For nitroimidazole-IDA-^{99m}Tc(CO)₃ complexes, presence of significant blood activity even at 3 h p.i. resulted in poor TBR. On the other hand, nitroimidazole-DETA-^{99m}Tc(CO)₃ and nitroimidazole-AEG-^{99m}Tc(CO)₃ complexes cleared very fast from blood resulting in low uptake in tumor, but better TBR (between 1 to 1.9) and TMR [between 1.9 to 5.9]. It is interesting to note at this juncture, that blood clearance of [¹⁸F]FMISO was gradual, approximately following a path between the two extremes, the slow blood clearance of

nitroimidazole-IDA- $^{99m}\text{Tc}(\text{CO})_3$ complexes on one side and fast blood clearances on the other hand, shown by nitroimidazole-DETA and nitroimidazole-AEG $^{99m}\text{Tc}(\text{CO})_3$ complexes [Fig. 2.50]. While initial high blood activity of [^{18}F]FMISO facilitated hypoxia specific reduction, by providing sufficient residence time for [^{18}F]FMISO in tumor, subsequent clearance from blood resulted in better TBR and TMR compared to the different nitroimidazole- $^{99m}\text{Tc}(\text{CO})_3$ complexes. The distribution of $^{99m}\text{Tc}(\text{CO})_3$ complexes of different nitroimidazole-IDA derivatives (**2L1-2L3**) and nitroimidazole-DETA derivatives (**2L4-2L6**) in various organs and tissues at different time points are shown in figure 2.51 and figure 2.52. Similarly, distribution observed with different nitroimidazole-AEG- $^{99m}\text{Tc}(\text{CO})_3$ complexes (**2L7-2L9**) and [^{18}F]FMISO in various organs and tissues at different time points are shown in figure 2.53 and figure 2.54.

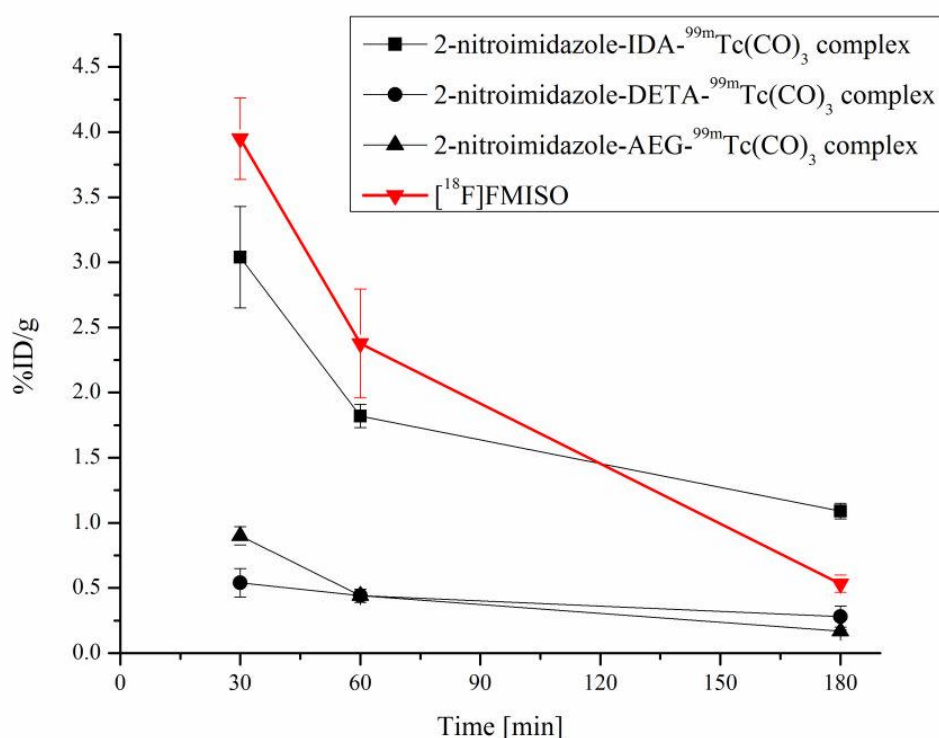


Fig 2.50. Blood clearance of [^{18}F]FMISO in comparison to 2-nitroimidazole- $^{99m}\text{Tc}(\text{CO})_3$ complexes of IDA, DETA and AEG ligands

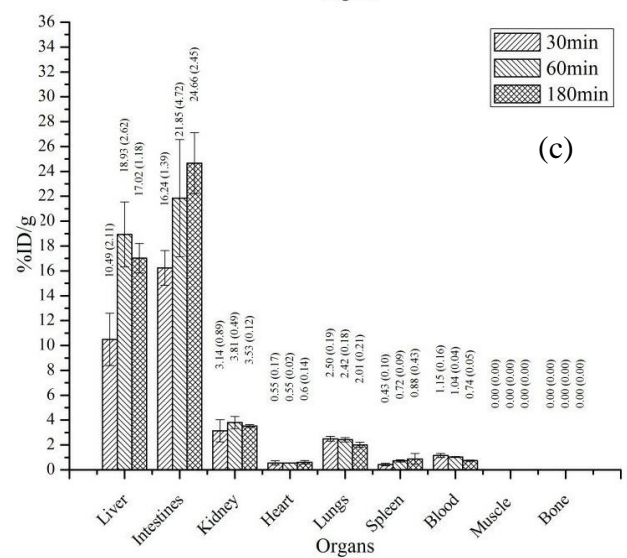
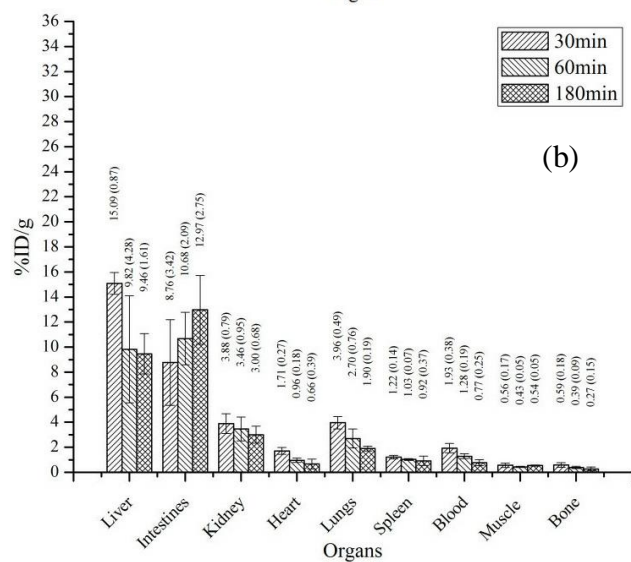
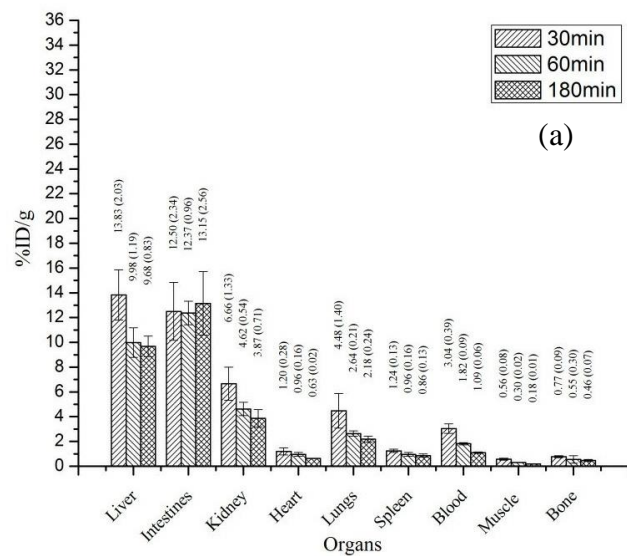


Fig. 2.51. Distribution of $^{99m}\text{Tc}(\text{CO})_3$ complexes of (a) 2-nitroimidazole-IDA [2L1] (b) 4-nitroimidazole-IDA [2L2] (c) 5-nitroimidazole-IDA [2L3] in various organs at different time points.

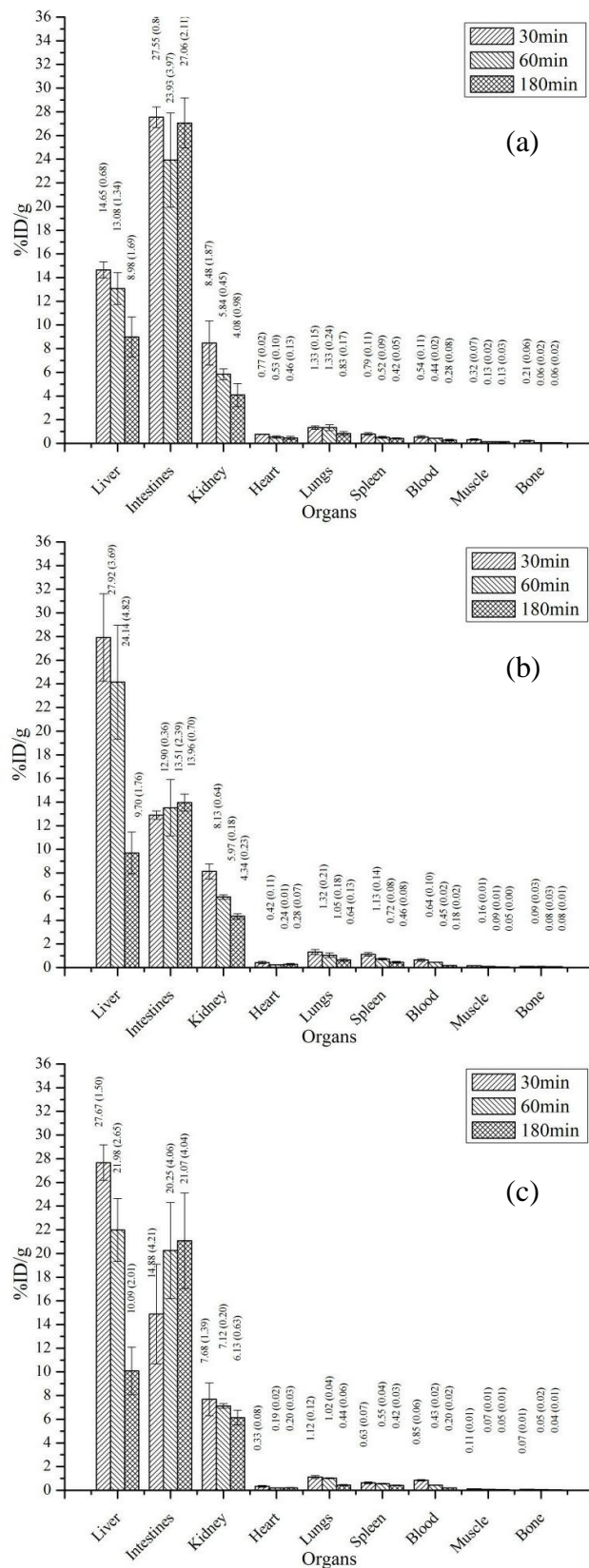


Fig. 2.52. Distribution of $^{99m}\text{Tc}(\text{CO})_3$ complexes of (a) 2-nitroimidazole-DETA [2L4] (b) 4-nitroimidazole-DETA [2L5] (c) 5-nitroimidazole-DETA [2L6] in various organs at different time points

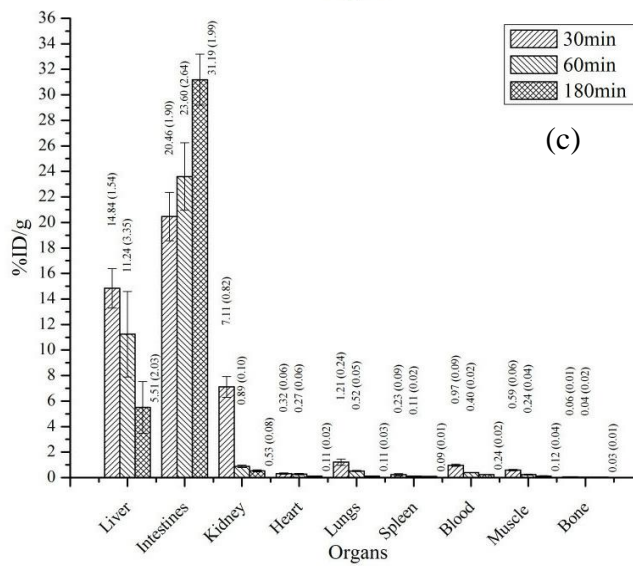
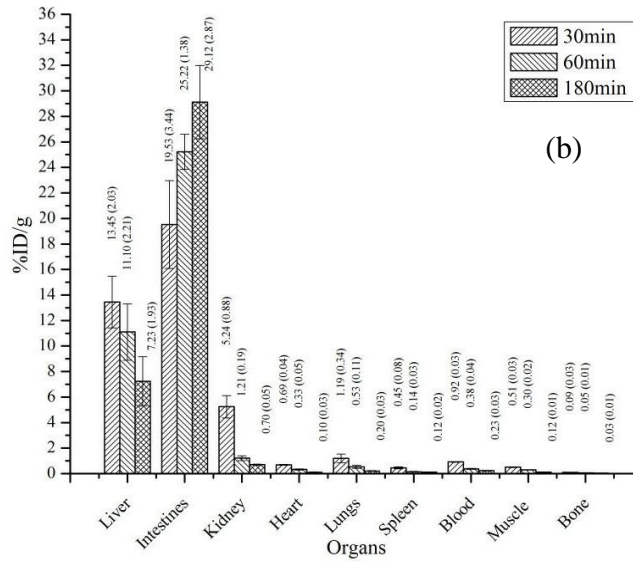
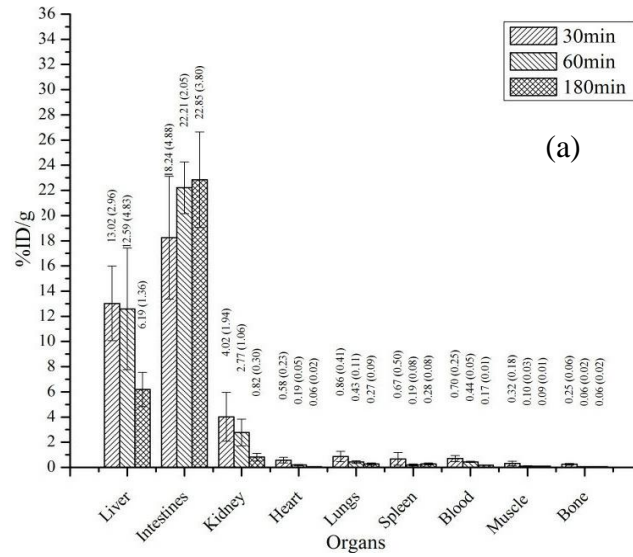


Fig. 2.53. Distribution of $^{99m}\text{Tc}(\text{CO})_3$ complexes of (a) 2-nitroimidazole-AEG [2L7] (b) 4-nitroimidazole-AEG [2L8] (c) 5-nitroimidazole-AEG [2L9] in various organs at different time points

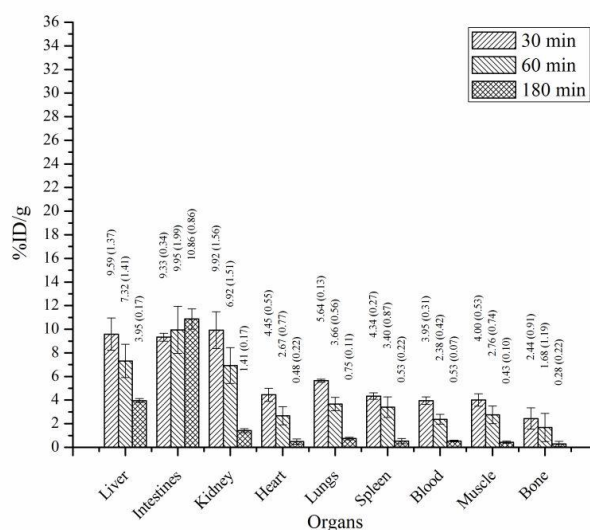


Fig. 2.54. Distribution of [^{18}F]FMISO in various organs at different time points

For all the nitroimidazole radiotracers evaluated in the present study, major clearance of activity from the body of the tumor bearing animal was through the hepatobiliary route. The nitroimidazole-DETA- $^{99\text{m}}\text{Tc}(\text{CO})_3$ as well as nitroimidazole-AEG- $^{99\text{m}}\text{Tc}(\text{CO})_3$ complex cleared faster from other vital organs compared to the nitroimidazole-IDA- $^{99\text{m}}\text{Tc}(\text{CO})_3$ complexes and [^{18}F]FMISO.

Analyses of the results suggest that SERP and optimal blood clearance of the nitroimidazole radiotracer are the two important factors to consider while developing new nitroimidazole radiopharmaceutical for targeting hypoxia. Though the role of SERP of nitroimidazole on its efficacy to target hypoxic cells was known, the significance of tumor residence time of the radiotracer is probably less noticed. Faster clearance of the radiotracer from blood was generally associated with lower tumor retention and improved TBR and TMR.^{94,95,35} However, low retention in tumor may result in some of the clinically significant hypoxic regions going undetected. Hence, improving TBR and TMR by designing molecules that clear faster from blood should not be the only criteria while developing new nitroimidazole radiopharmaceuticals for detecting hypoxia.

The $^{99m}\text{Tc}(\text{CO})_3$ chemistry provides a tool for the fine tuning of blood clearance of nitroimidazole radiotracers. It could be noted that the tridentate ligands used for coordinating the $^{99m}\text{Tc}(\text{CO})_3$ core had a significant effect on the blood clearance of the resultant nitroimidazole complexes. While the nitroimidazole-IDA- $^{99m}\text{Tc}(\text{CO})_3$ complexes showed slow blood clearance, the nitroimidazole-DETA and nitroimidazole-AEG $^{99m}\text{Tc}(\text{CO})_3$ complexes cleared very fast from blood. By incorporating appropriate hydrophilic groups it may be possible to adequately improve the blood clearance of nitroimidazole-IDA- $^{99m}\text{Tc}(\text{CO})_3$ complexes to obtain better TBR without significantly affecting the tumor uptake. Similarly, by sufficiently increasing the lipophilicity, fast clearance of nitroimidazole-DETA and nitroimidazole-AEG $^{99m}\text{Tc}(\text{CO})_3$ complexes could be slowed down to improve tumor uptake while retaining favorable TBR and TMR. However, it is difficult to predict the rate of blood clearance that would provide optimum tumor residence time for a given nitroimidazole radiotracer to undergo adequate reduction in tumor that will enable unambiguous detection of all clinically relevant hypoxic regions at the same time resulting in acceptable values of TBR and TMR. Hence, a number of structural modifications, to alter the blood clearance of the radiotracer in the required direction, and testing may be required to develop a clinically useful ^{99m}Tc -radiopharmaceutical equivalent to [^{18}F]FMISO, for imaging hypoxia.

2.7.4. Conclusions

The present study suggests that tumor residence time and SERP of the radiotracer are the two critical factors that decide its efficacy to target hypoxic cells in vivo. Probably the key to the development of a successful nitroimidazole based radiopharmaceutical for the detection of hypoxia is to optimize the tumor residence time which depends on the combined effect of lipophilicity and overall charge of the radiotracer. Though [^{18}F]FMISO was found to be superior to different nitroimidazole- $^{99m}\text{Tc}(\text{CO})_3$ complexes evaluated in the present study, information obtained from the analyses of the results could help in designing a better ^{99m}Tc -

radiopharmaceutical for targeting tumor hypoxia. A nitroimidazole with SERP closer to [^{18}F]FMISO would be better suited for targeting hypoxia as it would require lesser time to undergo reduction in hypoxic cells. This would allow further structural modifications to the radiotracer, if necessary, to affect faster clearance in order to achieve better TBR and TMR. A significant advantage observed with nitroimidazole- $^{99\text{m}}\text{Tc}(\text{CO})_3$ complexes, at least in the tumor model used in the present study, was their slower clearance from tumor compared to [^{18}F]FMISO. This aspect combined with the relatively longer half-life of $^{99\text{m}}\text{Tc}$, in comparison to ^{18}F , opens the possibility of delaying the imaging to obtain better contrast between background and hypoxic regions in the tumor. If a nitroimidazole- $^{99\text{m}}\text{Tc}(\text{CO})_3$ complex could be developed, that significantly accumulates as well as detects all clinically relevant hypoxic regions in a tumor, the option of using corresponding $^{186/188}\text{Re}(\text{CO})_3$ analogue as a radiotherapeutic agent to deliver therapeutic dose directly to the hypoxic tumor tissues could also be explored.

CHAPTER 3

MODIFIED 2-NITROIMIDAZOLE-^{99m}Tc(CO)₃ COMPLEX WITH IMPROVED PHARMACOKINETICS FOR TARGETING TUMOR HYPOXIA

No matter what...there is always scope for improvement.

— Myself

3.1. Introduction

In Chapter 2, nine nitroimidazole- $^{99\text{m}}\text{Tc}(\text{CO})_3$ complexes were evaluated in animals bearing fibrosarcoma tumor, to understand the influence of molecular properties, on in vivo efficacy to detect hypoxic cells. In general, the 2-, 4- and 5- nitroimidazole-IDA- $^{99\text{m}}\text{Tc}(\text{CO})_3$ complexes [Fig. 3.1(a)], by virtue of their slow blood clearance, showed relatively better tumor uptake and retention compared to 2-, 4- and 5- nitroimidazole-DETA- $^{99\text{m}}\text{Tc}(\text{CO})_3$ complexes [Fig. 3.1(b)] as well as 2-, 4- and 5- nitroimidazole-AEG- $^{99\text{m}}\text{Tc}(\text{CO})_3$ complexes [Fig. 3.1(c)].

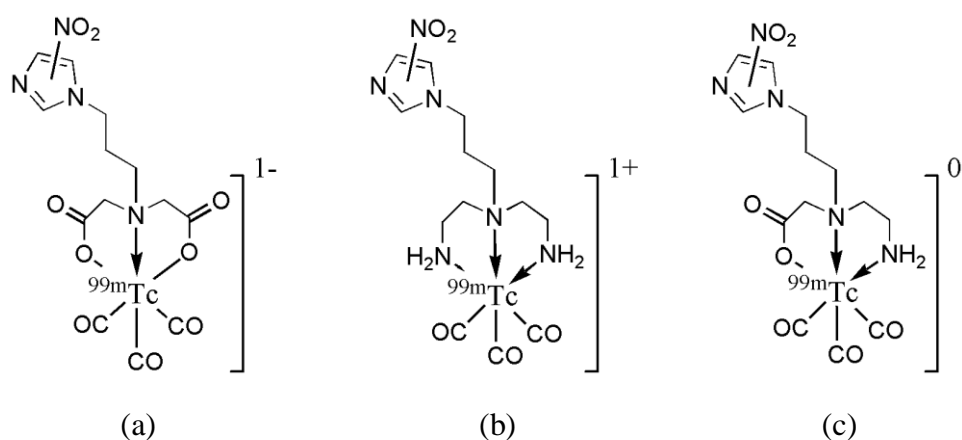


Fig. 3.1. $^{99\text{m}}\text{Tc}(\text{CO})_3$ complexes of 2-, 4- and 5- nitroimidazole (a) IDA ligands (b) DETA ligands and (c) AEG ligands

Among 2-, 4- and 5- nitroimidazole-IDA- $^{99\text{m}}\text{Tc}(\text{CO})_3$ complexes, the 2-nitroimidazole complex showed highest tumor uptake and retention. However, clearance of 2-nitroimidazole complex from the liver was an undesirable feature, as it can limit its utility to image tumors in abdominal region.

Structural modification of the radiotracer to increase hydrophilicity, which would reduce liver uptake, could be a possible solution. However, lipophilicity is essential for efficient distribution of the radiotracer in tumor, and hence decreasing this parameter may compromise its uptake, distribution and retention in tumor. Another possible solution to this problem is to incorporate appropriate functional group, for example ether group, in the radiotracer that can accelerate its liver clearance. This strategy has been utilized in the

development of ^{99m}Tc -sestamibi, ^{99m}Tc -tetrofosmin^{208,209} and several other myocardial perfusion imaging agents [Fig. 3.2].²¹⁰

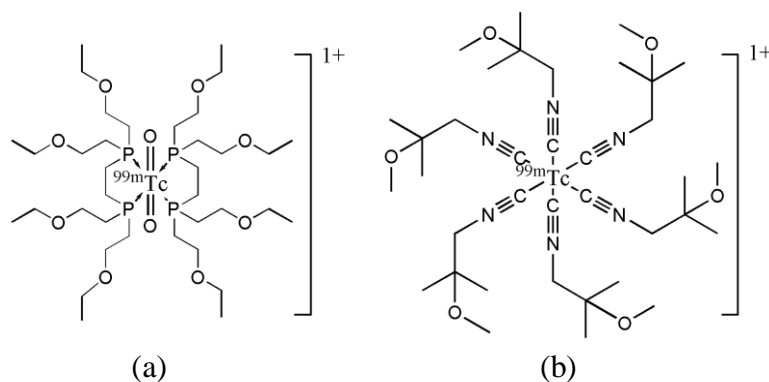


Fig. 3.2. Structure of (a) ^{99m}Tc -tetrofosmin and (b) ^{99m}Tc -sestamibi

Working on similar lines, the 2-nitroimidazole-IDA- $^{99m}\text{Tc}(\text{CO})_3$ complex, that has showed the best uptake and retention in tumor among different nitroimidazole complexes evaluated, was synthetically modified to incorporate an ether linkage [Fig. 3.3(b)] instead of a propyl linker in the original molecule [Fig. 3.1(a)]. This chapter describes the synthesis of the modified 2-nitroimidazole ligand, its radiolabeling using $[^{99m}\text{Tc}(\text{CO})_3(\text{H}_2\text{O})_3]^+$ precursor complex, characterization and evaluation in fibrosarcoma tumor bearing Swiss mice. The results obtained are discussed.

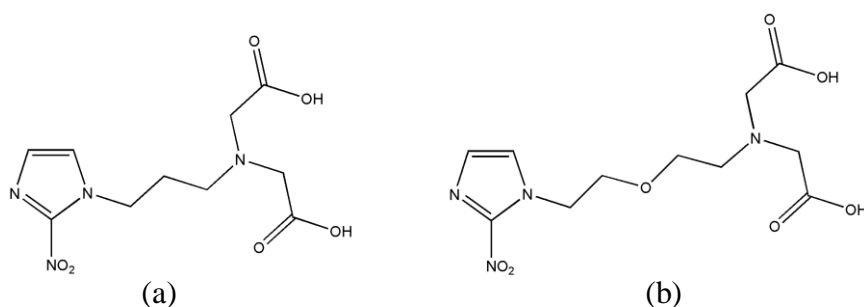


Fig. 3.3. Structure of (a) 2-nitroimidazole ligand with a propyl spacer and (b) 2-nitroimidazole ligand with an ether spacer

3.2. Materials and methods

Dibromoethyl ether was purchased from Aldrich, USA. Phthalimide was purchased from Fluka, Germany. Other common chemicals used and methods followed in the present chapter are mentioned in Chapter 1, *Section 1.14.1*.

3.3. Synthesis

The scheme followed for the synthesis of modified 2-nitroimidazole-IDA ligand is shown in figure 3.4. The target compound (**3e**) is shown in box.

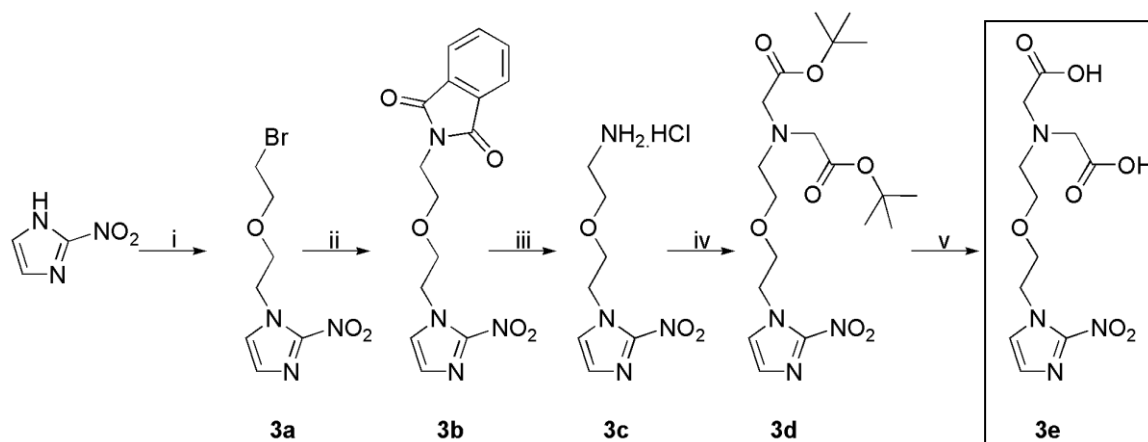


Fig. 3.4. Synthesis of 2-(carboxymethyl(2-(2-nitroimidazolylethoxy)ethyl)amino)acetic acid (i) dibromoethyl ether, anhyd. K_2CO_3 , acetonitrile, reflux (ii) phthalimide, anhyd. K_2CO_3 , acetonitrile, reflux (iii) (1) hydrazine hydrate, ethanol, reflux (2) 2N HCl, 50°C (iv) *tert*-butyl bromoacetate, DIEA, acetonitrile, reflux (v) 6N HCl, 25°C

3.3.1. Synthesis of 1-(2-(2-bromoethoxy)ethyl)-2-nitro-1H-imidazole (**3a**)

To 2-nitroimidazole (0.20 g, 1.77 mmol) in acetonitrile (10 mL), crushed potassium carbonate (0.25 g, 1.77 mmol) and dibromoethyl ether (2 g, 8.85 mmole) was added and the reaction mixture was refluxed for 12 h. Upon completion of the reaction (*cf.* TLC), the solvent was removed in vacuo. The residue obtained was dissolved in water (30 mL) and extracted with chloroform (15 mL x 3). The combined organic layer was washed with brine, dried and the solvent was evaporated to obtain the crude product as thick oil. Compound **3a** was obtained (0.40 g, 87 %) by silica gel column chromatography using diethyl ether as eluent. R_f (Diethyl ether) = 0.4. IR (neat, cm^{-1}): 3139(m); 3118(m); 2963(m); 2920(m); 2872(m); 1537(s); 1485(s); 1438(w); 1360(s); 1286(s); 1219(w); 1184(w); 1162(s); 1119(s); 1019(w); 997(w); 943(w); 916(m); 889(w); 835(s); 781(s); 665(w); 649(m); 630(w). 1H -NMR ($CDCl_3$, δ ppm): 3.40 (t, 2H, $J = 6.0$ Hz, 2-nitroimidazole- $CH_2CH_2OCH_2CH_2Br$); 3.74 (t, 2H, $J = 6.0$ Hz, 2-nitroimidazole- $CH_2CH_2OCH_2CH_2Br$); 3.86 (t, 2H, $J = 4.5$ Hz, 2-

nitroimidazole-(CH₂CH₂OCH₂CH₂Br); 4.63 (t, 2H, *J* = 4.5 Hz, 2-nitroimidazole-CH₂CH₂OCH₂CH₂Br); 7.13 (s, 1H, 2-nitroimidazole-C5-H); 7.24 (s, 1H, 2-nitroimidazole-C4-H). [Fig. 3.5]. MS(ESI⁺): 263.8 (M+H)⁺.

3.3.2. Synthesis of 2-(2-(2-(2-nitro-1H-imidazol-1-yl)ethoxy)ethyl)isoindoline-1,3-dione (**3b**)

To compound **3a** (0.20 g, 0.76 mmol) in acetonitrile (10 mL), crushed potassium carbonate (0.25 g, 1.77 mmol) and phthalimide (0.13 g, 0.91 mmol) was added and the mixture refluxed for 48 h. Thereafter, the solvent was removed in vacuo and the residue obtained was dissolved in 0.1 N NaOH (20 mL). The basic aqueous layer was extracted with chloroform (15 mL x 3). The combined organic layer was washed with brine, dried and concentrated in vacuo to obtain the crude product. Compound **3b** was obtained by silica gel column chromatography using diethyl ether as eluent (0.15 g, 60 %). R_f (Diethyl ether) = 0.3. IR (neat, cm⁻¹): 3117(w); 2922(m); 2870(m); 1771(m); 1710(s); 1536(s); 1485(s); 1359(s); 1286(m); 1160(m); 1117(m); 1025(w); 916(w); 834(m); 782(w); 721(m); 648(w). ¹H-NMR (CDCl₃, δ ppm): 3.67 (t, 2H, *J* = 5.3 Hz, 2-nitroimidazole-CH₂CH₂OCH₂CH₂-phthalimide); 3.80 (t, 2H, *J* = 4.8 Hz, 2-nitroimidazole-CH₂CH₂OCH₂CH₂-phthalimide); 3.87 (t, 2H, *J* = 5.3 Hz, 2-nitroimidazole-CH₂CH₂OCH₂CH₂-phthalimide); 4.55 (t, 2H, *J* = 4.8 Hz, 2-nitroimidazole-CH₂CH₂OCH₂CH₂-phthalimide); 6.84 (s, 1H, 2-nitroimidazole-C5-H); 7.08 (s, 1H, 2-nitroimidazole-C4-H), 7.73- 7.84 (m, 4H, *J* = 2.8 Hz, -CH₂CH₂OCH₂CH₂-phthalimide-H) [Fig. 3.6]. MS(ESI⁺): 331.2 (M+H)⁺.

3.3.3. Synthesis of 1-(2-(2-aminoethoxy)ethyl)-2-nitro-1H-imidazole (**3c**)

To compound **3b** (0.15 g, 0.45 mmol) in ethanol (10 mL), hydrazine hydrate (0.15 g, 4.5 mmol) was added and the reaction mixture refluxed overnight. A white precipitate formed was filtered, washed with cold ethanol (2 mL) and dried. The precipitate was subsequently heated with 2N HCl (5 mL) at 50°C for 2 h and the residue obtained was filtered off. Filtrate on evaporation gave amine **3c** as the hydrochloride salt, which was further purified by

recrystallization from ethanol/ether mixture (0.07 g, 79 %). IR (KBr, cm^{-1}): 3369(w); 3144(w); 3117(w); 2921(s); 2852(m); 1509(w); 1474(s); 1437(w); 1392(m); 1362(m); 1278(m); 1125(s); 912(w); 745(m); 667(m); 628(w). MS(ESI⁺): 201.1 (M+H)⁺.

3.3.4. Synthesis of 1-(*N,N*-bis(*tert*-butoxycarbonylmethyl)-2-(2-(2-nitroimidazolyl)ethoxy)ethane (**3d**)

To compound **3c** (0.07 g, 0.36 mmol) in acetonitrile (5 mL), DIEA (0.16 g, 1.26 mmol) was added and the solution was stirred for 5 minutes. To this solution *tert*-butyl bromoacetate (0.18 g, 0.9 mmol) was added and the reaction mixture was refluxed for 12 h. Upon completion of the reaction (*cf.* TLC), solvent was removed in vacuo. The residue obtained was dissolved in water (15 mL) and extracted with chloroform (10 mL x 3). The chloroform layers were combined, washed with brine and dried over anhydrous sodium sulphate. The crude product after the removal of chloroform was purified by silica gel column chromatography using diethyl ether to obtain compound **3d** (0.09 g, 57 %). R_f (Diethyl ether) = 0.6. IR (Neat, cm^{-1}): 3116(w); 2976(m); 2928(m); 2870(m); 1732(s); 1651(w); 1539(w); 1474(s); 1435(w); 1392(w); 1366(s); 1278(m); 1255(w); 1220(m); 1147(s); 1123(s); 974(w); 913(w); 835(w); 743(m); 666(m); 623(w). ¹H-NMR (CDCl₃, δ ppm): 1.45 (s, 18H, -CH₂CH₂OCH₂CH₂N(CH₂CO₂C(CH₃)₃)₂); 2.92 (t, 2H, J = 5.5 Hz, 2-nitroimidazole-CH₂CH₂OCH₂CH₂N-); 3.48 (s, 4H, 2-nitroimidazole-CH₂CH₂OCH₂CH₂N(CH₂CO₂C(CH₃)₃)₂); 3.58 (t, 2H, J = 5.5 Hz, 2-nitroimidazole-CH₂CH₂OCH₂CH₂N-); 3.69 (t, 2H, J = 5.3 Hz, 2-nitroimidazole-CH₂CH₂OCH₂CH₂N-); 4.09 (t, 2H, J = 5.3 Hz, 2-nitroimidazole-CH₂CH₂OCH₂CH₂N-); 6.93 (s, 1H, 2-nitroimidazole-C5-H); 7.05 (s, 1H, 2-nitroimidazole-C4-H). [Fig. 3.7]. MS(ESI⁺): 429.3 (M+H)⁺.

3.3.5. Synthesis of 2-(carboxymethyl(2-(2-nitroimidazolylethoxy)ethyl)amino)acetic acid (**3e**)

Compound **3d** (0.05 g, 0.12 mmol) was dissolved in 6N HCl (5 mL) and the mixture

was stirred at room temperature for 12 h. Upon removal of the solvent, target compound **3e** was obtained which was further purified by recrystallization from ethanol/ether mixture (0.03 g, 92 %). $^1\text{H-NMR}$ (D_2O , δ ppm): 3.78 (m, 6H, 2-nitroimidazole- $\text{CH}_2\text{CH}_2\text{OCH}_2\text{CH}_2\text{N}(\text{CH}_2\text{CO}_2\text{H})_2$); 3.97 (s, 4H, 2-nitroimidazole- $\text{CH}_2\text{CH}_2\text{OCH}_2\text{CH}_2\text{N}(\text{CH}_2\text{CO}_2\text{H})_2$); 4.59 (m, 2H, 2-nitroimidazole- $\text{CH}_2\text{CH}_2\text{OCH}_2\text{CH}_2\text{N}$ -); 7.09 (s, 1H, 2-nitroimidazole-C5-H); 7.4 (s, 1H, 2-nitroimidazole-C4-H) [Fig. 3.8]. MS(ESI) m/z : 315.1 (M-H)⁻ [Fig. 3.9].

3.3.6. Synthesis of $\text{Re}(\text{CO})_3$ complex of ligand **3e** (**3f**)

Compound **3e** (0.02 g, 0.06 mmol) was dissolved in water (5 mL) and the pH was adjusted to 8 using 0.1N NaOH. To this solution bis(tetraethylammonium)-*fac*-tribromotricarbonylrhenate (0.05 g, 0.06 mmol), prepared following a procedure reported earlier,¹⁹³ was added and the reaction mixture was heated at 50°C for 12 h. The reaction mixture was cooled and the precipitate formed was removed by filtration. The filtrate upon evaporation gave the target complex **3f**. The complex was used as such for further characterization. IR (KBr, cm^{-1}) 3130 (m); 2984 (m); 2950 (m); 2692 (w); 2016 (vs); 1878 (vs); 1646 (s); 1491 (w); 1395 (m); 1337 (m); 1288 (w); 1183 (w); 1133 (w). $^1\text{H-NMR}$ (D_2O , δ ppm) 1.16 (t, 12H, $-\text{N}(\text{CH}_2\text{CH}_3)_4^+$); 3.15 (q, 8H, $-\text{N}(\text{CH}_2\text{CH}_3)_4^+$); 3.43-3.48 (m, 4H, $[-\text{CH}_2\text{CH}_2\text{OCH}_2\text{CH}_2\text{N}(\text{CH}_A\text{H}_B\text{CO}_2)_2\text{Re}(\text{CO})_3]$); 3.73-3.85 (m, 6H, $[-\text{CH}_2\text{CH}_2\text{OCH}_2\text{CH}_2\text{N}(\text{CH}_A\text{H}_B\text{CO}_2)_2\text{Re}(\text{CO})_3]$); 4.62 (t, 2H, 2-nitroimidazole- $\text{CH}_2\text{CH}_2\text{OCH}_2\text{CH}_2\text{N}$ -); 7.08 (s, 1H, 2-nitroimidazole-C5-H); 7.39 (s, 1H, 2-nitroimidazole-C4-H) [Fig. 3.10].



Current Data Parameters
 NAME prasadh
 EXPNO 1013
 PROCNO 1

F2 - Acquisition Parameters
 Date_ 20100209
 Time 12.56
 INSTRUM spect
 PROBHD 5 mm BBO BB-1H
 PULPROG zg30
 TD 32768
 SOLVENT CDCl3
 NS 32
 DS 0
 SWH 4807.692 H
 FIDRES 0.146719 H
 AQ 3.4079220 s
 RG 161
 DW 104.000 u
 DE 6.00 u
 TE 293.3 K
 D1 1.00000000 s
 TDO 1

==== CHANNEL f1 =====
 NUC1 1H
 P1 11.00 u
 PL1 0.00 dB
 SF01 300.1320008 MHz

F2 - Processing parameters:
 SI 16384
 SF 300.1300033 MHz
 WDW EM
 SSB 0
 LB 1.00 Hz
 GB 0
 PC 1.00

RPhD 1H NMR in CDCl3

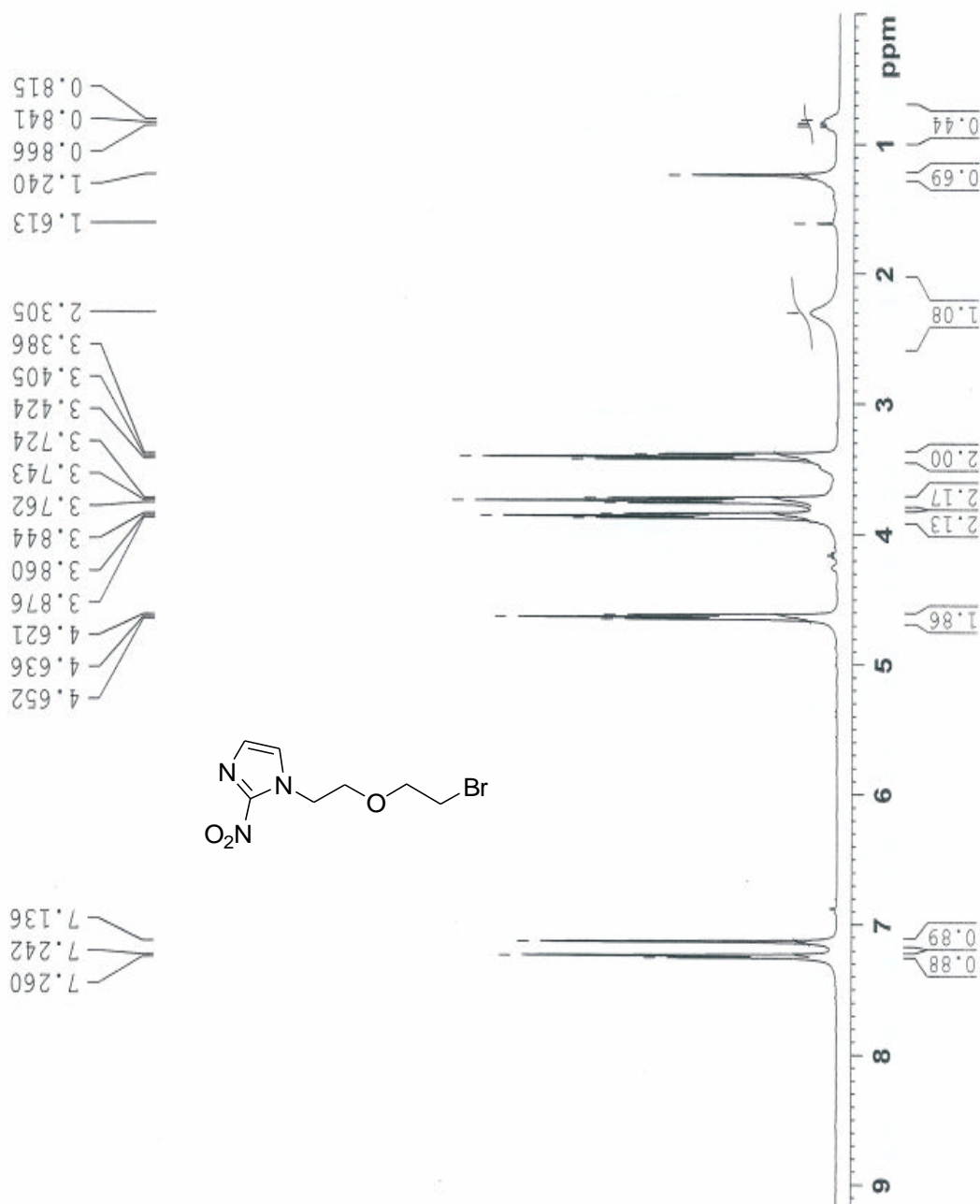


Fig. 3.5. ¹H-NMR spectrum of 1-(2-(2-bromoethoxy)ethyl)-2-nitro-1H-imidazole (3a)

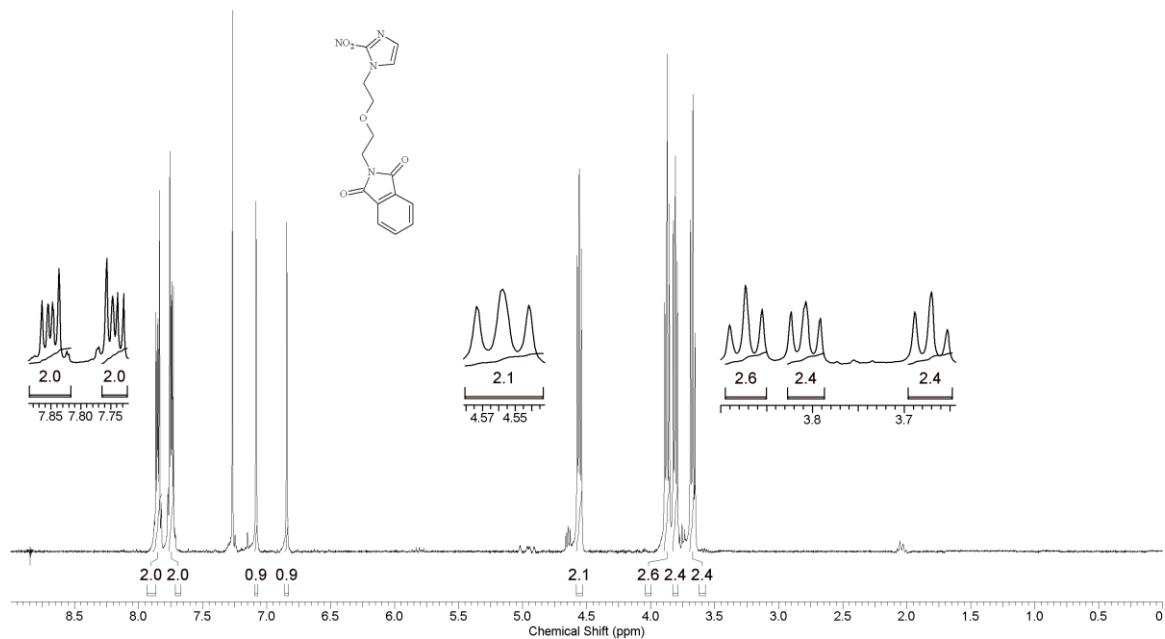


Fig. 3.6. ¹H-NMR spectrum of 2-(2-(2-(2-nitro-1H-imidazol-1-yl)ethoxy)ethyl) isoindoline-1,3-dione (**3b**)

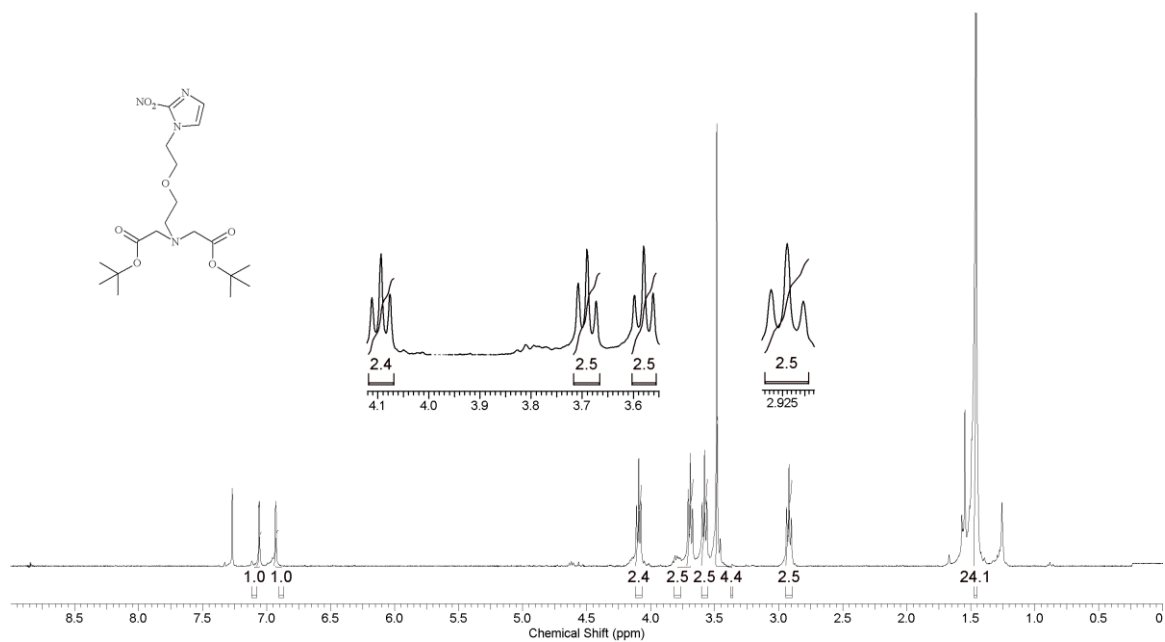


Fig. 3.7. ¹H-NMR spectrum of 1-(N,N-bis(*tert*-butoxycarbonylmethyl)-2-(2-(2-nitroimidazolyl)ethoxy)ethane (**3d**)

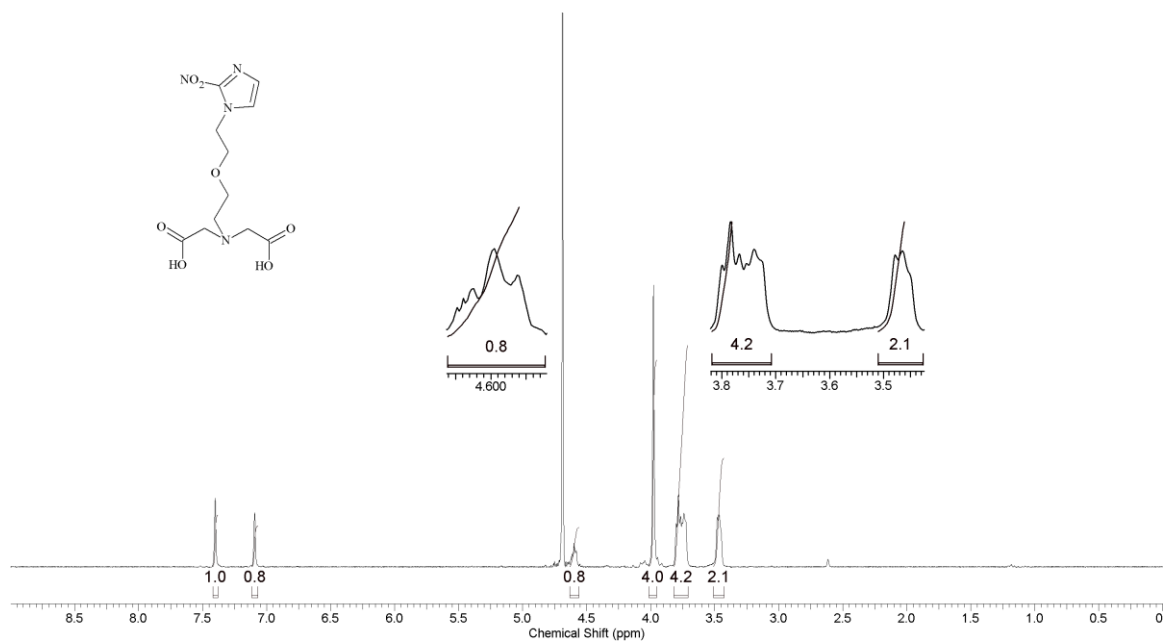


Fig. 3.8. ¹H-NMR spectrum of 2-(carboxymethyl(2-(2-nitroimidazolethoxy)ethyl)amino)acetic acid (**3e**)

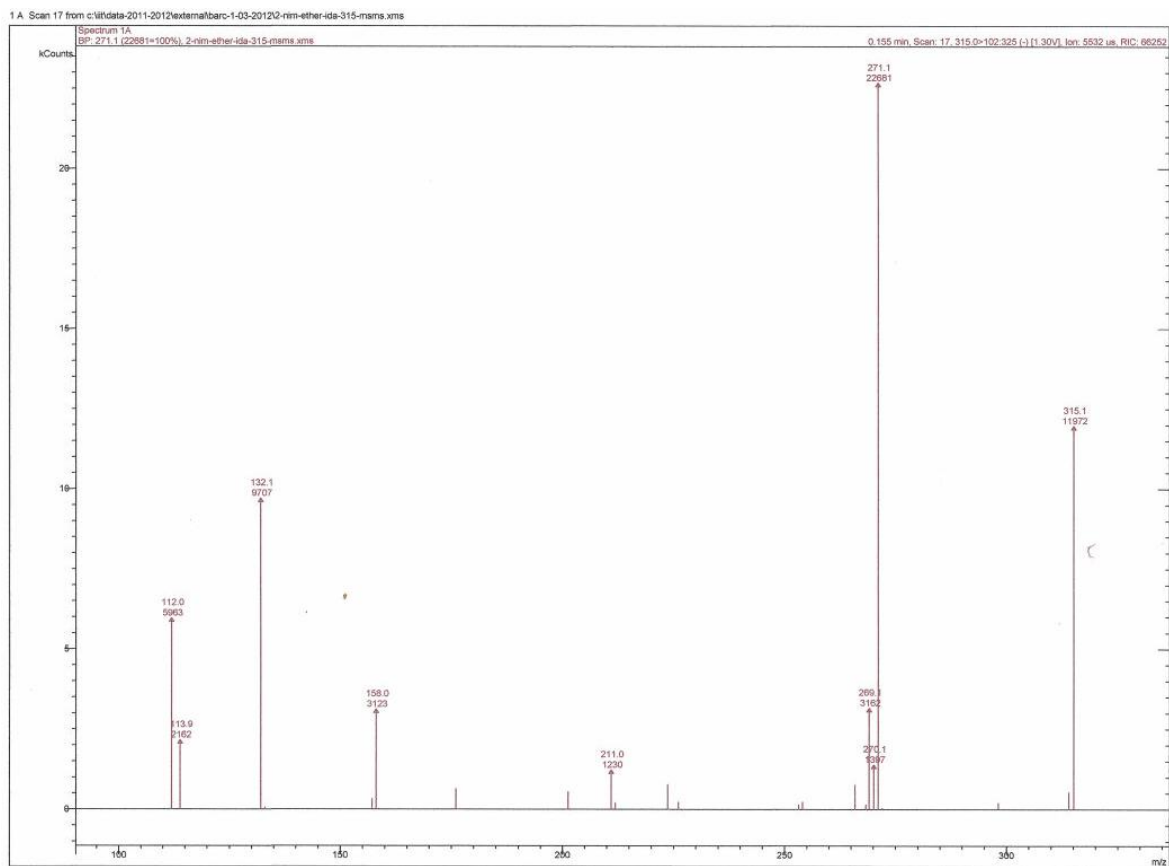


Fig. 3.9. ESI-MS of 2-(carboxymethyl(2-(2-nitroimidazolethoxy)ethyl)amine)acetic acid (**3e**)

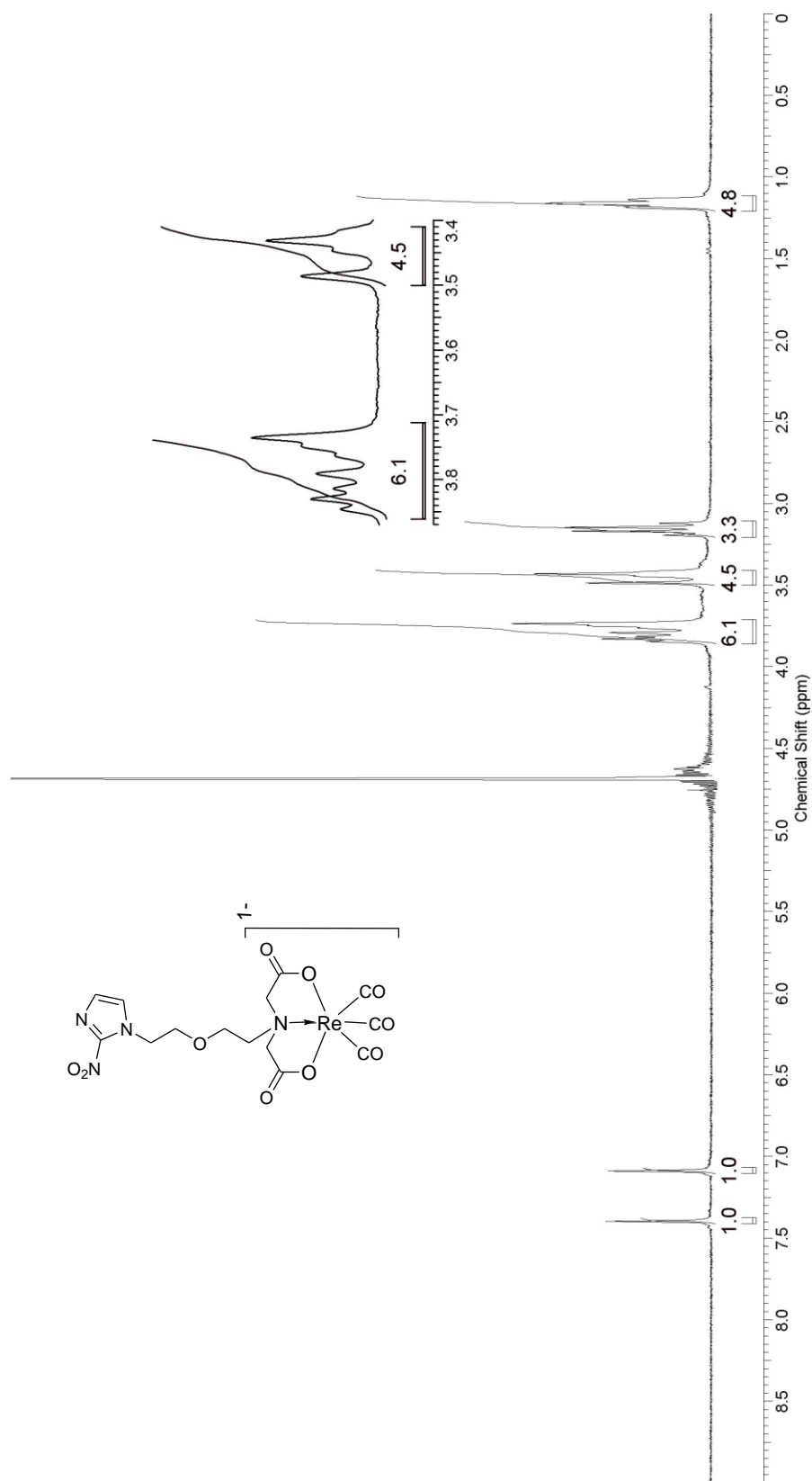


Fig. 3.10. $^1\text{H-NMR}$ spectrum of $\text{Re}(\text{CO})_3$ complex of ligand **3e** (**3f**)

3.4. Results and discussion

3.4.1. Synthesis

The synthesis of modified 2-nitroimidazole ligand with an ether linkage involved 5 steps (Fig. 3.4). 2-nitroimidazole with an ether linker, **3a**, was synthesized in the first step. The terminal halide in **3a** was then converted to corresponding amine hydrochloride (**3c**) via Gabriel synthesis through the intermediate compound **3b**, which was subsequently converted to di-*tert*-butyl ester derivative **3d**. Compound **3d** upon acidic hydrolysis using 6N HCl yielded the target ligand **3e** as the hydrochloride salt. All the compounds except **3c** were characterized by IR, ¹H-NMR and low resolution ESI-MS. Compound **3c** was characterized by IR and low resolution ESI-MS only. The ¹H-NMR spectra of the compounds were consistent with the expected structure. The mass spectrum of target compound **3e** recorded in negative mode showed a peak at *m/z* 315.1 corresponding to (M-H)⁻ ion. An additional peak at *m/z* 271.1 corresponded to the loss of CO₂ from the (M-H)⁻ ion.

3.4.2. Radiolabeling, quality control and characterization

Compound **3e** was radiolabeled using [^{99m}Tc(CO)₃(H₂O)₃]⁺ precursor complex. The precursor was prepared using Isolink[®] carbonyl kit vial following the procedure described in Chapter 1, *Section 1.14.3*. The protocol for the preparation of ^{99m}Tc(CO)₃ complex is similar to the one described in Chapter 2, *Section 2.4.1*. The [^{99m}Tc(CO)₃(H₂O)₃]⁺ precursor complex as well as modified 2-nitroimidazole-IDA-^{99m}Tc(CO)₃ complex was characterized by HPLC. The HPLC elution profile of [^{99m}Tc(CO)₃(H₂O)₃]⁺ precursor complex and modified 2-nitroimidazole-^{99m}Tc(CO)₃ complex are shown in figure 3.11(a) and (b), respectively. While [^{99m}Tc(CO)₃(H₂O)₃]⁺ precursor complex eluted at 3.7 min, modified 2-nitroimidazole complex eluted as a single sharp peak at 19.3 min. To elucidate the mode of binding of ligand **3e** to the ^{99m}Tc(CO)₃ metal core, corresponding Re(CO)₃-analogue (**3f**) was synthesized. Figure 3.11(c) shows the HPLC elution profile of **3f**, which matched with the

modified 2-nitroimidazole-IDA- $^{99m}\text{Tc}(\text{CO})_3$ complex (**3g**) prepared at nca level. This indicated the formation of similar complexes at nca level as well as at macroscopic level.

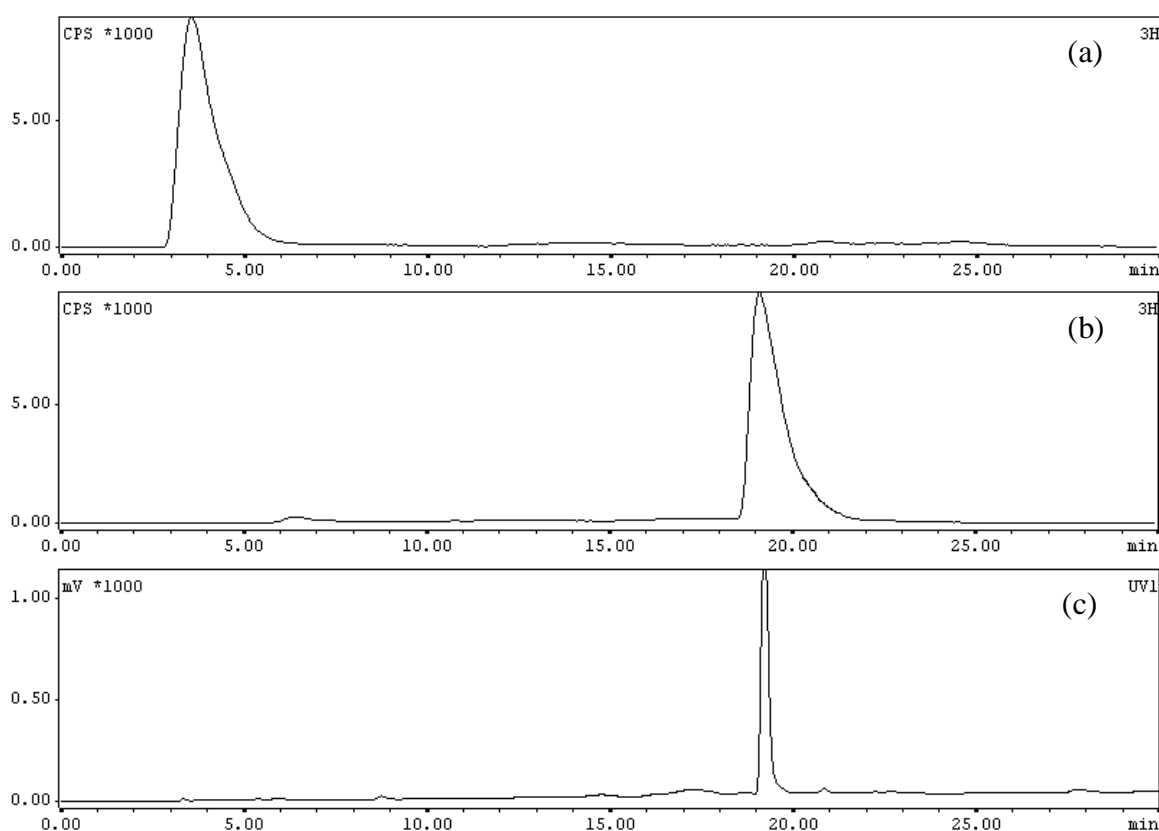


Fig. 3.11. HPLC elution profile of (a) $[\text{}^{99m}\text{Tc}(\text{CO})_3(\text{H}_2\text{O})_3]^+$ precursor complex (b) $^{99m}\text{Tc}(\text{CO})_3$ complex **3g** and (c) $\text{Re}(\text{CO})_3$ complex **3f**

A noticeable feature in the $^1\text{H-NMR}$ of **3f** (Fig. 3.10) is the absence of singlet peak at 3.98 δ ppm, which represented the four methylene protons of iminodiacetic acid group in **3e** (Fig. 3.8). This was similar to the $^1\text{H-NMR}$ spectrum (Fig. 2.12) of 2-nitroimidazole-IDA- $\text{Re}(\text{CO})_3$ complex (**2e**) described in Chapter 2. The tridentate coordination of iminodiacetic acid group with $\text{Re}(\text{CO})_3$ moiety resulted in the transformation of singlet, representing four methylene proton, into two doublets, representing the AB spin system formed due to the restricted rotation of methylene group upon coordination. Though the double-doublet pattern could not be clearly observed due to the overlapping peaks, the absence of singlet peak is an indirect indication of tridentate coordination in complex **3f**.²⁰¹ Proposed structure of $^{99m}\text{Tc}(\text{CO})_3$ complex **3g** and $\text{Re}(\text{CO})_3$ complex **3f** is shown in figure 3.12(a) and (b), respectively. The

structure of 2-nitroimidazole-IDA- $^{99\text{m}}\text{Tc}(\text{CO})_3$ complex with propyl spacer (**3h**) is also shown in figure 3.12 (c).

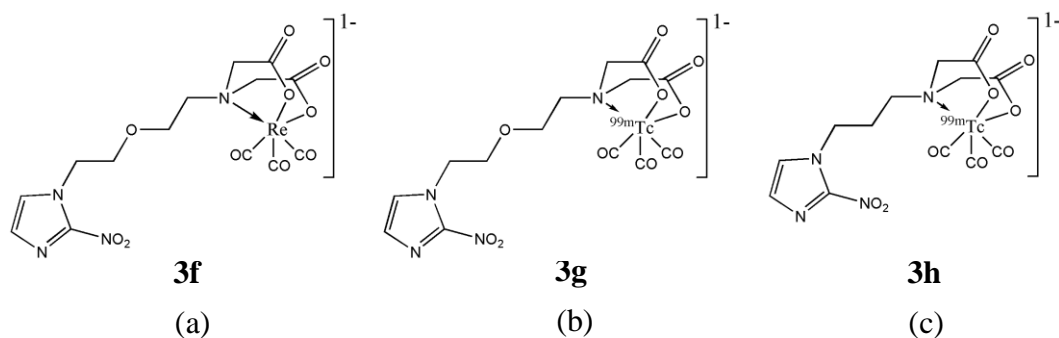


Fig. 3.12. Structure of (a) 2-nitroimidazole-Re(CO)₃ complex (**3f**) with an ether spacer (b) 2-nitroimidazole- $^{99\text{m}}\text{Tc}(\text{CO})_3$ complex (**3g**) with an ether spacer and (c) 2-nitroimidazole-IDA- $^{99\text{m}}\text{Tc}(\text{CO})_3$ complex (**3h**) with a propyl spacer

The $\text{LogP}_{\text{o/w}}$ of complex **3g**, determined following a reported procedure¹⁹⁰ discussed in Chapter 1, was found to be 0.55, which was higher than that of 2-nitroimidazole-IDA- $^{99\text{m}}\text{Tc}(\text{CO})_3$ complex **3h** ($\text{LogP}_{\text{o/w}} = 0.48$). This is expected, since the modified 2-nitroimidazole complex **3g** has a longer spacer than in original complex **3h**. The stability of complex **3g** in serum was assessed, following the protocol described in Chapter 1, *Section 1.14.6*, and it did not show any signs of decomposition during the period of study (3 h).

3.4.3. Biological studies

The purpose of introducing a structural modification in 2-nitroimidazole-IDA ligand [Fig. 3.3(a)] was to obtain a 2-nitroimidazole- $^{99\text{m}}\text{Tc}(\text{CO})_3$ complex better liver clearance without compromising its ability to target hypoxic tumor cells. The tumor uptake obtained with complex **3g** at various time points is shown in figure 3.13. For comparison, the result obtained with original complex **3h** having propyl spacer is also shown in the same figure. It could be observed that complex **3g** showed relatively higher uptake and retention in tumor than the complex **3h** at every time point studied. Tumor activity of complex **3g** apparently cleared in a biphasic manner. In the initial phase, about 17% of tumor activity observed at 30 min p.i. [1.19 (0.08) %ID/g] was cleared at 60 min p.i. [0.99 (0.09) %ID/g]. This was

followed by slower second phase where, only 16% of the tumor activity observed at 60 min p.i. was cleared in next two hours [0.84 (0.05) %ID/g at 3 h p.i.]. The relatively quick initial phase may be attributed to the clearance of unbound radiotracer from the tumor, while the second phase may be the slow clearance of activity associated with the radiotracer reduced and trapped in the hypoxic cells.

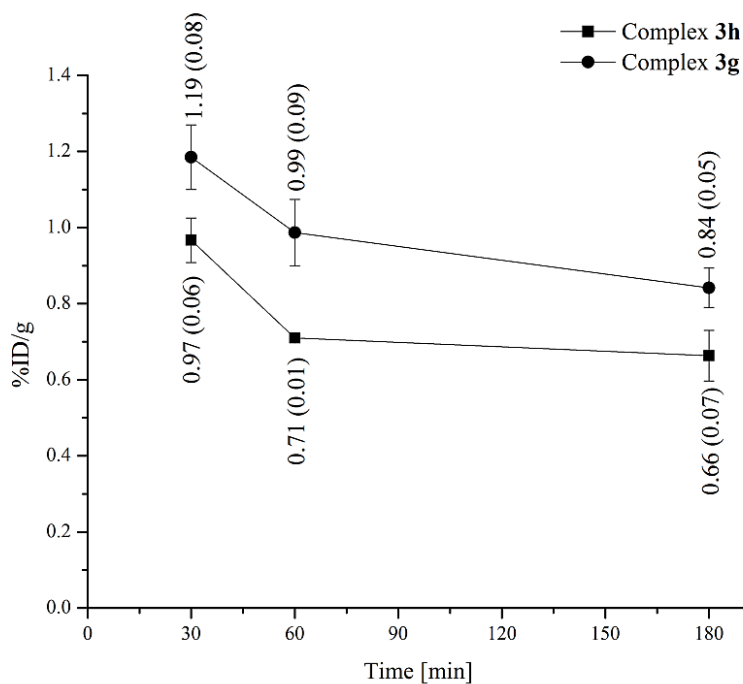


Fig. 3.13. Tumor uptake observed with 2-nitroimidazole-^{99m}Tc(CO)₃ complex with an ether spacer (**3g**) and with a propyl spacer (**3h**) at different time points

The possibility that tumor activity observed after 60 min p.i. was due to non specific accumulation, and not due to the reduction of the radiotracer, is ruled out considering the steadily falling activity levels in muscles.

It is clear from Chapter 2 that the efficiency of reduction of nitroimidazole complex in hypoxic cells depends on SERP as well as its residence time in hypoxic tumor cells. Since both complexes contain 2-nitroimidazole, their SERP values could be assumed to be similar. Hence, between these two nitroimidazole radiotracers, one with a higher residence time in tumor is expected to show higher reduction and trapping. Residence time of radiotracer in

tumor depends on its clearance from blood. From Chapter 2, it could be observed that slow clearance of radiotracer from blood help in maintaining concentration gradient between blood and intra-tumoral environment for a longer time, which results in higher tumor residence time of the radiotracer. In the present case, blood clearance of complex **3g** is slower than that of complex **3h** [Fig. 3.14]. Therefore, complex **3g** is expected to have a longer tumor residence time and hence, higher tumor retention than complex **3h**.

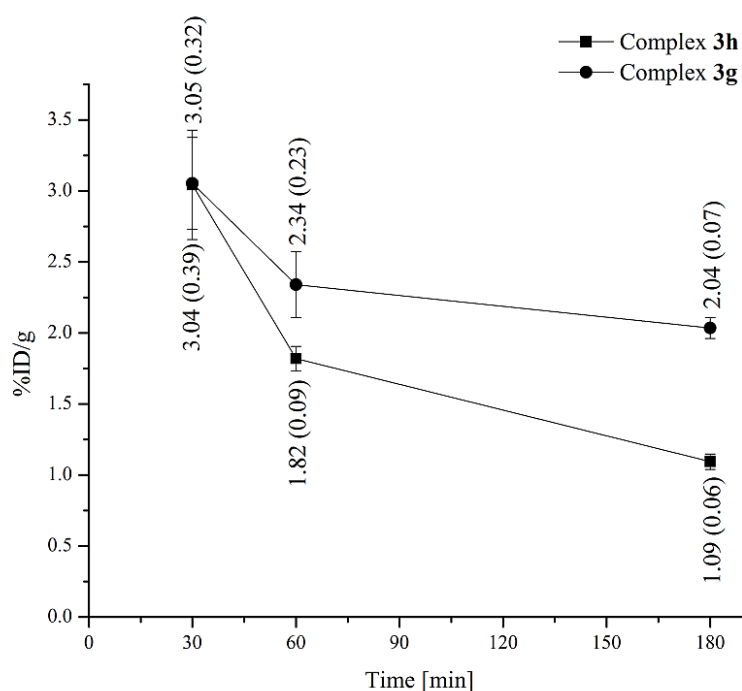


Fig. 3.14. Blood clearance observed with 2-nitroimidazole-^{99m}Tc(CO)₃ complex with an ether spacer (**3g**) and with a propyl spacer (**3h**) at different time points

The uptake and clearance of activity observed with complexes **3g** and **3h** from other organs, expressed as %ID/organ, is shown in figure 3.15(a) and (b), respectively. It could be noted that, as early as 30 min p.i., complex **3g** showed significantly lower liver activity and higher intestinal activity compared to that of complex **3h**. This is an indication of faster clearance of the radiotracer from liver, which could be attributed to the ether group incorporated in complex **3g**. Complex **3g** showed a decrease in liver activity at 60 min p.i. and then,

increased slightly at 180 min p.i. The decrease at 60 min p.i. could be due to the clearance of activity initially accumulated in liver. Subsequent increase in liver activity could be attributed to accumulation of activity from other organs, blood and muscle into liver at a faster than the rate of clearance from the liver.

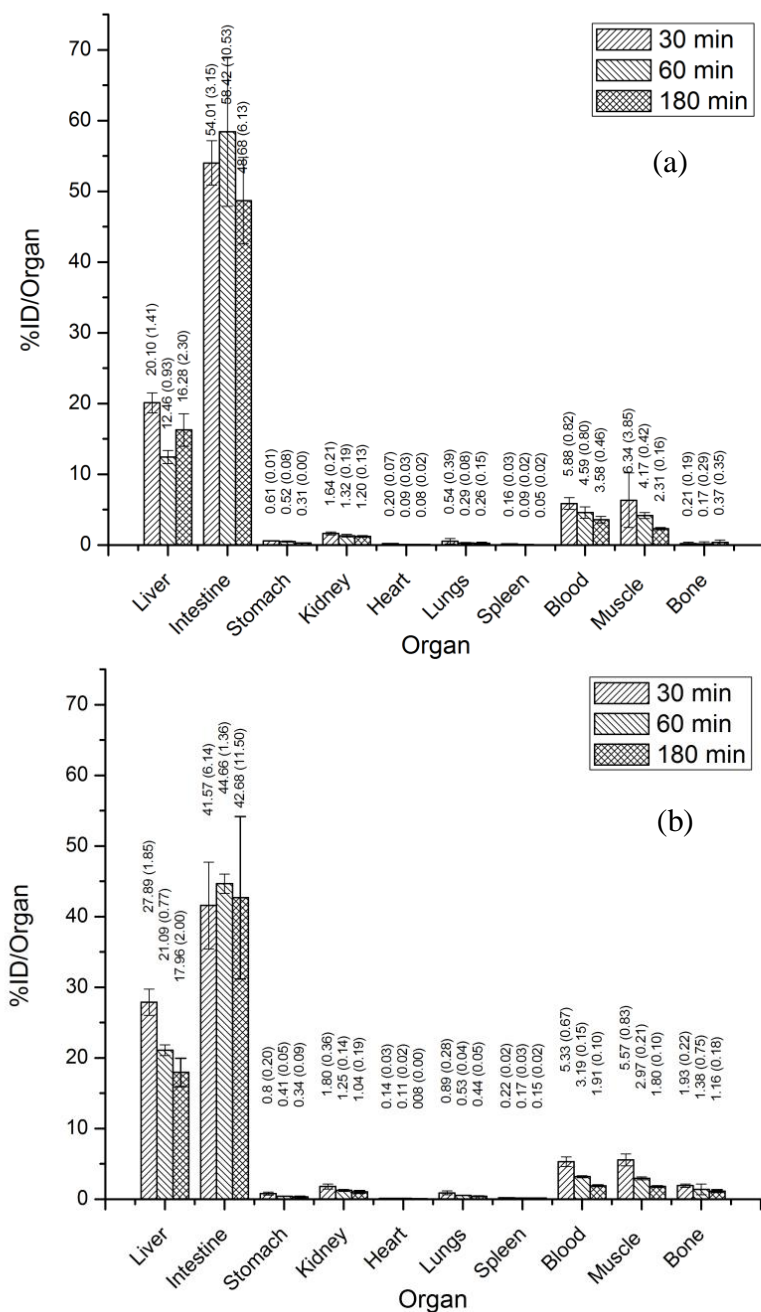


Fig. 3.15. Distribution of 2-nitroimidazole-^{99m}Tc(CO)₃ complex (a) with an ether spacer (**3g**) and (b) with a propyl spacer (**3h**) in various organs at different time points

Figure 3.16 shows the variation in tumor to blood ratio (TBR) and tumor to muscle ratio (TMR) obtained with complex **3g** and **3h** at different time points. TBR as well as TMR of complex **3h** significantly ($p < 0.05$) improved with time. For complex **3g**, the TMR increased with time and attained a maximum value of 3.66 (0.47) at 3 h p.i. which is acceptable for imaging. However, the TBR of **3g** showed only a marginal increase which was statistically insignificant ($p > 0.05$). Maximum value of TBR attained by **3g** was 0.41 (0.04) which was too low to be acceptable for imaging applications. In general, incorporation of ether group was not found to improve the TBR and TMR of complex **3g** as compared to **3h**.

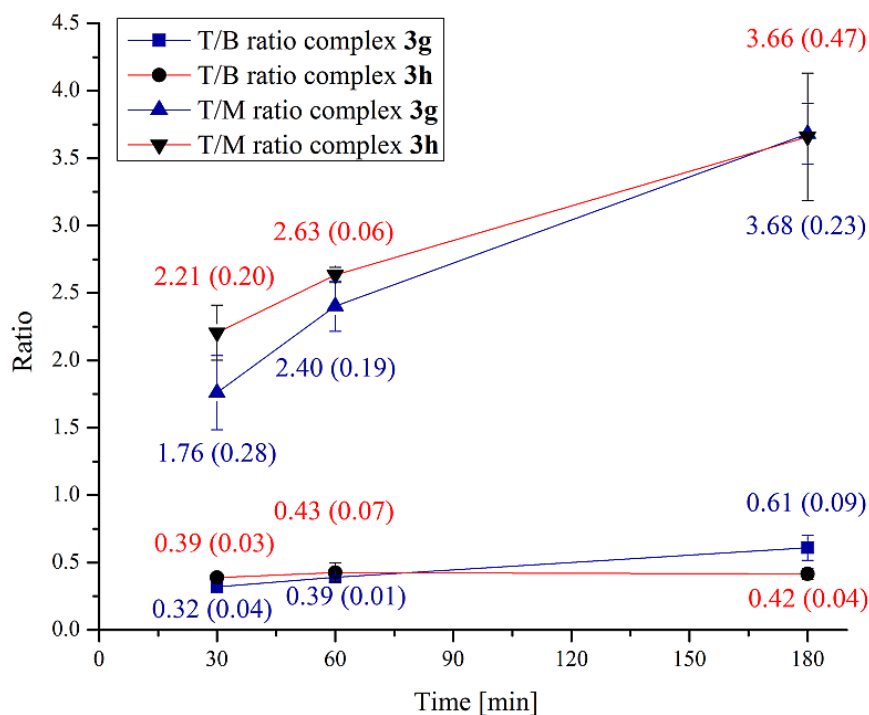


Fig. 3.16. Variation in tumor to blood and tumor to muscle ratio of 2-nitroimidazole-^{99m}Tc(CO)₃ complex with an ether spacer (**3g**) and with a propyl spacer (**3h**) at different time points

3.5. Conclusions

The present study showed that incorporation of an ether group improved the clearance of 2-nitroimidazole complex from liver, without compromising its tumor uptake and retention. However, higher lipophilicity of the complex resulted in slow clearance from

blood, resulting in lower TBR which was not acceptable for hypoxia imaging applications. Additionally, slow clearance of complex **3g** from blood resulted in the presence of liver activity even at 180 min p.i., which may impose limitation for imaging tumors in abdominal region. Though it is evident that presence of ether functionality in the complex improved its liver clearance, a single ether group may be insufficient to achieve the desired level of clearance. Incorporation of multiple ether groups, by modifying the molecule with a di- or tri-ethylene glycol spacer, could possibly help to bring down liver clearance to a desirable level without compromising the tumor uptake. Such a modification could also be expected to accelerate clearance of activity from blood improving the TBR.

CHAPTER 4

PREPARATION OF $^{99m}\text{Tc}(\text{CO})_3$ -ANALOGUE OF [^{18}F]FLUOROMISONIDAZOLE

I'm supposed to be a scientific person but I use intuition more than logic in making basic decisions.

— Seymour R. Cray, Founder Cray Research Laboratory

4.1. Introduction

[¹⁸F]Fluoromisonidazole ([¹⁸F]FMISO) [Fig. 4.1], a 2-nitroimidazole based radiotracer, has been the most widely used radiopharmaceutical for clinical imaging of hypoxia.⁸³ Though, several other ¹⁸F-labeled nitroimidazole agents, including [¹⁸F]FETA,⁸⁷ [¹⁸F]EF1,⁸⁸ [¹⁸F]EF5⁸⁹⁻⁹² and [¹⁸F]FAZA^{35,36,211} mentioned in Chapter 1, are developed and evaluated in human patients, [¹⁸F]FMISO continues to be the most widely used agent for clinical imaging of tissue hypoxia.

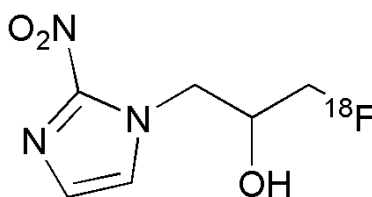


Fig. 4.1. Structure of [¹⁸F]FMISO

[¹⁸F]FMISO allows unambiguous determination of clinically significant regional oxygenation in cancerous lesions²¹² which could be utilized to isolate only those patients who will benefit by hypoxia directed treatment. However, [¹⁸F]FMISO has several inherent drawbacks which include considerable non-specific uptake^{83,213,214} in brain and slow clearance from the body through hepatobiliary route. High background activity due to slow clearance of the radiotracer compromises the contrast, and hence, the diagnostic information obtained from the images. Delaying the image acquisition to improve the contrast is difficult due to the short half-life of ¹⁸F. Other issues include the requirement of a cyclotron for the production of ¹⁸F and specialized modules for the preparation of [¹⁸F]FMISO which adds to the cost of radiopharmaceutical. Also, unlike ^{99m}Tc-radiopharmaceuticals, preparation of PET radiopharmaceuticals often involves multiple steps, involving specially designed synthesis modules, which consumes time. Hence, the radiopharmacist needs to start the radiopharmaceutical preparation with higher levels of ¹⁸F-activity to compensate for the decay losses during preparation.

An advantage of PET over SPECT imaging modality is the superior spatial resolution of the former, which is critical in planning hypoxia directed external beam radiation therapy.²¹⁵ However, advances being made in the SPECT hardware and image reconstruction algorithms have significantly improved the spatial resolution of the images obtainable with SPECT.²¹⁶ In near future, it may be possible to utilize SPECT images for hypoxia directed radiation treatment, which is presently being carried out using PET. Considering the drawbacks of [¹⁸F]FMISO and bright prospects in SPECT technology, a ^{99m}Tc-radiopharmaceutical which can provide diagnostic information equivalent or superior to [¹⁸F]FMISO may find wider applicability.

[¹⁸F]FMISO being a clinically established agent for the detection of tissue hypoxia, a logical starting point in search of a ^{99m}Tc-agent for this purpose would be to prepare and evaluate a ^{99m}Tc-analogue of misonidazole. However, unlike labeling with radiohalogens, radiolabeling with ^{99m}Tc requires appropriate modification of the molecule with a chelator to coordinate ^{99m}Tc. Synthetic modification to incorporate a suitable ligand system in misonidazole would certainly alter the in vivo pharmacokinetics of misonidazole-^{99m}Tc complex. However, this could be an advantage as well, since it provides a way to modulate the pharmacokinetics in a favorable manner by appropriate choice of the ligand systems. But, it is difficult to predict the most suitable modification that will result in ideal in vivo characteristics necessary for a hypoxia detecting radiopharmaceutical.

In the present work, an IDA analogue of misonidazole, miso-IDA, was synthesized. Miso-IDA ligand was subsequently radiolabeled using [^{99m}Tc(CO)₃(H₂O)₃]⁺ precursor to obtain corresponding ^{99m}Tc(CO)₃ complex. The Re(CO)₃ complex of miso-IDA was also prepared at macroscopic level. Misonidazole-IDA-^{99m}Tc(CO)₃ complex was subsequently evaluated in Swiss mice bearing fibrosarcoma tumor. The results obtained were compared with [¹⁸F]FMISO evaluated in the same animal model (described in Chapter 2).

4.2. Materials and methods

2,3-Epoxypropyl phthalimide was purchased from Aldrich, USA. Hydrazine hydrate was purchased from Reidel-de Haen, Germany. Other common chemicals used and methods followed are mentioned in Chapter 1, *Section 1.14.1*.

4.3. Synthesis

Synthesis of miso-IDA derivative is schematically shown in figure 4.2. The target ligand **4d** is shown in a box.

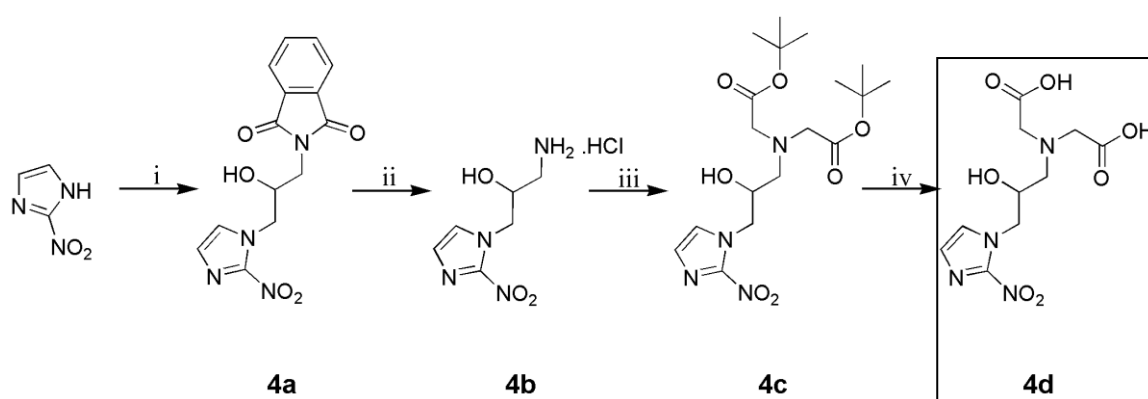


Fig. 4.2. Synthesis of 2-(N-carboxymethyl, N-((2-hydroxy)-3-(2-nitroimidazolyl) propyl)amino)acetic acid (i) 2,3-epoxypropyl phthalimide, ethanol, reflux (ii) (1) hydrazine hydrate, ethanol, reflux (2) 2N HCl, 50°C (iii) *tert*-butylbromoacetate, DIEA, acetonitrile, 25°C (iv) 6N HCl, 25°C

4.3.1. Synthesis of 2-(2-hydroxy-3-(2-nitro-1H-imidazol-1-yl)propyl)isoindoline-1,3-dione (**4a**)

To 2-nitroimidazole (0.5 g, 4.43 mmol) in absolute ethanol (20 mL), 2,3-epoxypropyl phthalimide (1 g, 4.87 mmol) was added and the reaction mixture refluxed. Upon completion of the reaction (*cf.*TLF), the off-white precipitate formed was filtered. The precipitate was washed with cold absolute ethanol (5 mL), followed by water (5mL) and then dried. Compound **4a** thus obtained (0.81 g, 58%) was pure for all practical purposes and used as such for further reaction. R_f (Ethyl acetate) = 0.66. IR (neat, cm^{-1}): 3354(w); 3128(w); 3063(w); 2937(w); 1708(vs); 1540(m); 1467(m); 1395(m); 1363(m); 722(m). $^1\text{H-NMR}$ (DMSO- D_6 , δ ppm): 3.62 (m, 2H, phthalimide- $\text{CH}_2\text{CH}(\text{OH})\text{CH}_2$ -); 4.08 (m, 1H, phthalimide-

CH₂CH(OH)CH₂-); 4.32 and 4.63 (m, 2H, CH₂CH(OH)CH₂-(2-nitroimidazole)); 5.54 (d, 1H, CH₂CH(OH)CH₂-(2-nitroimidazole)); 7.15 (s, 1H, 2-nitroimidazole-C5-H); 7.68 (s, 1H, 2-nitroimidazole-C4-H); 7.85 (m, 4H, phthalimide) [Fig. 4.3]. MS(ESI⁺) m/z: 316.2 (M+H)⁺.

4.3.2. Synthesis of 1-amino-3-(2-nitro-1H-imidazol-1-yl)propan-2-ol hydrochloride (**4b**)

To compound **4a** (0.20 g, 0.63 mmol) in absolute ethanol (10 mL), hydrazine hydrate (0.32 g, 6.3 mmol) was added and the reaction mixture refluxed for 12 h. Upon completion of the reaction (*cf.* TLC), reaction solvent and excess of hydrazine hydrate was removed in vacuo. The precipitate thus obtained was washed with absolute ethanol (2 × 2 mL), and subsequently heated with 2N HCl (10 mL) at 50°C for 2 h. The precipitate obtained was filtered and filtrate upon evaporation gave compound **4b** as the hydrochloride salt. The salt was further purified by recrystallization from methanol/ether (0.12 g, 86%). IR (KBr, cm⁻¹): 3377(m); 3293(m); 3126(w); 3106(w); 2993(m); 1538(m); 1492(m); 1352(m); 1278(m); 838(m). ¹H-NMR (D₂O, δ ppm): 2.97 and 3.23 (m, 2H, H₂NCH₂CH(OH)CH₂-); 4.25 (m, 3H, H₂NCH₂CH(OH)CH₂-); 4.69 (s, 1H, CH₂CH(OH)CH₂-(2-nitroimidazole)); 7.12 (s, 1H, 2-nitroimidazole-C5-H); 7.38 (s, 1H, 2-nitroimidazole-C4-H) [Fig. 4.4]. MS(ESI⁺) m/z: 188.3 (M+H)⁺.

4.3.3. Synthesis of *N,N*-bis(*tert*-butoxycarbonylmethyl)-((2-hydroxy)-3-(2-nitroimidazolyl)) propyl amine (**4c**)

To a solution of compound **4b** (0.10 g, 0.45 mmol) and DIEA (0.29 g, 2.25 mmol) in acetonitrile (10 mL), *tert*-butylbromoacetate (0.19 g, 0.99 mmol) was added drop-wise with vigorous stirring. The stirring was continued at room temperature till the reaction is completed (*cf.* TLC). Thereafter, the solvent was removed in vacuo and the residue obtained was dissolved in water (15 mL). The aqueous solution was extracted with chloroform (3 × 10 mL). The chloroform extracts were combined and washed with brine, dried and concentrated. Compound **4c** was obtained by silica gel column chromatography eluting with ether (0.14 g,

75%). R_f (Ethyl acetate) = 0.63. IR (neat, cm^{-1}): 3421(w); 3119(w); 2977(m); 2925(w); 1731(vs); 1540(m); 1467(m); 1366(m); 1224(m); 1150(vs); 836(m). $^1\text{H-NMR}$ (CDCl_3 , δ ppm): 1.46 (s, 18H, $-\text{N}(\text{CH}_2\text{CO}_2\text{C}(\text{CH}_3)_3)_2$); 2.38 and 3.15 (m, 2H, $-\text{CH}_2\text{CH}(\text{OH})\text{CH}_2\text{N}(\text{CH}_2\text{CO}_2\text{C}(\text{CH}_3)_3)_2$); 3.43 (m, 4H, $-\text{CH}_2\text{CH}(\text{OH})\text{CH}_2\text{N}(\text{CH}_2\text{CO}_2\text{C}(\text{CH}_3)_3)_2$); 3.93 (m, 1H, $-\text{CH}_2\text{CH}(\text{OH})\text{CH}_2\text{N}(\text{CH}_2\text{CO}_2\text{C}(\text{CH}_3)_3)_2$); 4.22 and 4.65 (m, 2H, $-\text{CH}_2\text{CH}(\text{OH})\text{CH}_2\text{N}(\text{CH}_2\text{CO}_2\text{C}(\text{CH}_3)_3)_2$); 7.13 (s, 1H, 2-nitroimidazole-C5-H); 7.34 (s, 1H, 2-nitroimidazole-C4-H) [Fig. 4.5]. MS(ESI^+) m/z : 415.4 ($\text{M}+\text{H}$) $^+$.

4.3.4. Synthesis of 2-(*N*-carboxymethyl, *N*-((2-hydroxy)-3-(2-nitroimidazolyl)propyl)amino) acetic acid (**4d**)

Compound **4c** (0.10 g, 0.24 mmol) was dissolved in 6N HCl (5 mL) and stirred at room temperature for 12 h. Upon removal of the solvent, compound **4d** could be obtained as the hydrochloride salt. The salt was further purified by recrystallization from methanol/ether (0.08 g, 95%). IR (neat, cm^{-1}): 3353(vb); 3142(w); 2977(w); 2959(w); 2845(w); 1731(s); 1557(m); 1486(m); 1369(m); 1225(m); 1095(m). $^1\text{H-NMR}$ (D_2O , δ ppm): 3.38 and 3.59 (m, 2H, $-\text{CH}_2\text{CH}(\text{OH})\text{CH}_2\text{N}(\text{CH}_2\text{CO}_2\text{H})_2$); 4.07 (s, 4H, $-\text{CH}_2\text{CH}(\text{OH})\text{CH}_2\text{N}(\text{CH}_2\text{CO}_2\text{H})_2$); 4.18 and 4.21 (m, 2H, $-\text{CH}_2\text{CH}(\text{OH})\text{CH}_2\text{N}(\text{CH}_2\text{CO}_2\text{H})_2$); 4.45 (m, 1H, $-\text{CH}_2\text{CH}(\text{OH})\text{CH}_2\text{N}(\text{CH}_2\text{CO}_2\text{H})_2$); 7.42 (s, 1H, 2-nitroimidazole-C5-H); 7.50 (s, 1H, 2-nitroimidazole-C4-H) [Fig. 4.6]. MS (ESI) m/z : 301.1 ($\text{M}-\text{H}$) $^-$.

4.3.5. Preparation of $\text{Re}(\text{CO})_3$ complex of compound **4d** (**4e**)

Compound **4d** (20 mg, 0.07 mmol) was dissolved in water (5 mL) and the pH of the solution was adjusted to 8. To this solution 1.1 equivalent of bis(tetraethylammonium)-*fac*-tribromotricarbonylrhenate (59 mg, 0.08 mmol), prepared following a procedure reported by Alberto et al.,¹⁹³ was added and mixture heated at 50°C for 12 h. The reaction mixture was cooled and the precipitate formed was filtered. The filtrate upon evaporation gave complex **4e** as

tetraethylammonium salt (32 mg, 56%). IR (KBr, cm^{-1}) 3423 (w); 3332 (w); 3129 (w); 2960 (w); 2919 (w); 2023 (s); 1885 (vs); 1675 (vs); 1543 (m); 1483 (m); 1356 (vs); 1284 (m); 1168 (m).

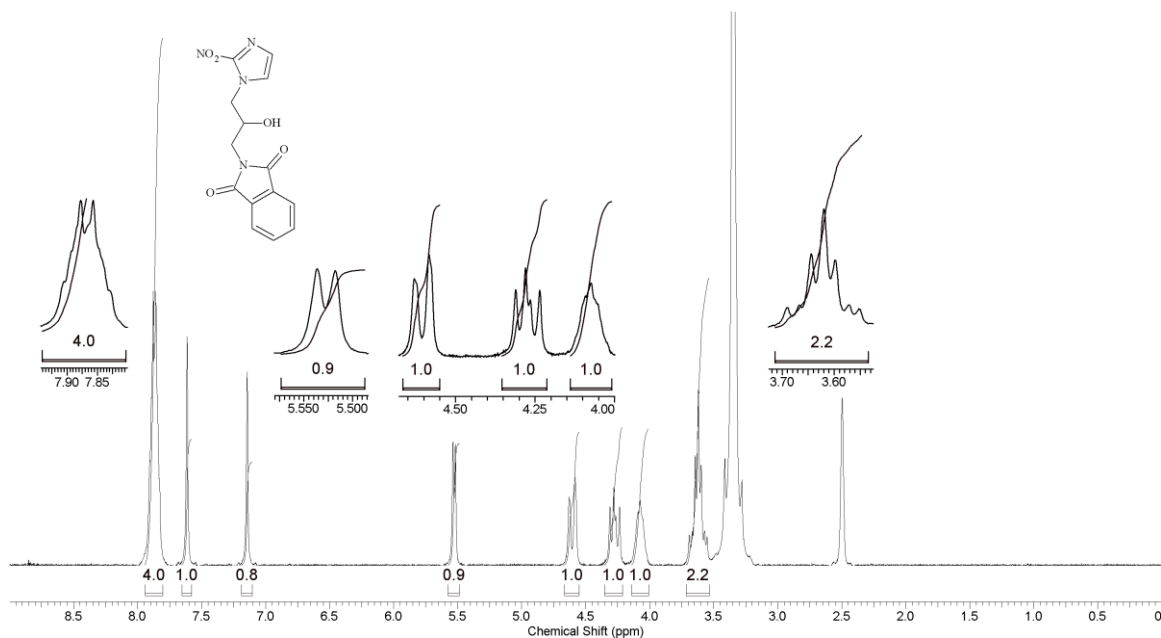


Fig. 4.3. $^1\text{H-NMR}$ spectrum of 2-(2-hydroxy-3-(2-nitro-1H-imidazol-1-yl)propyl) isoindoline-1,3-dione (**4a**)

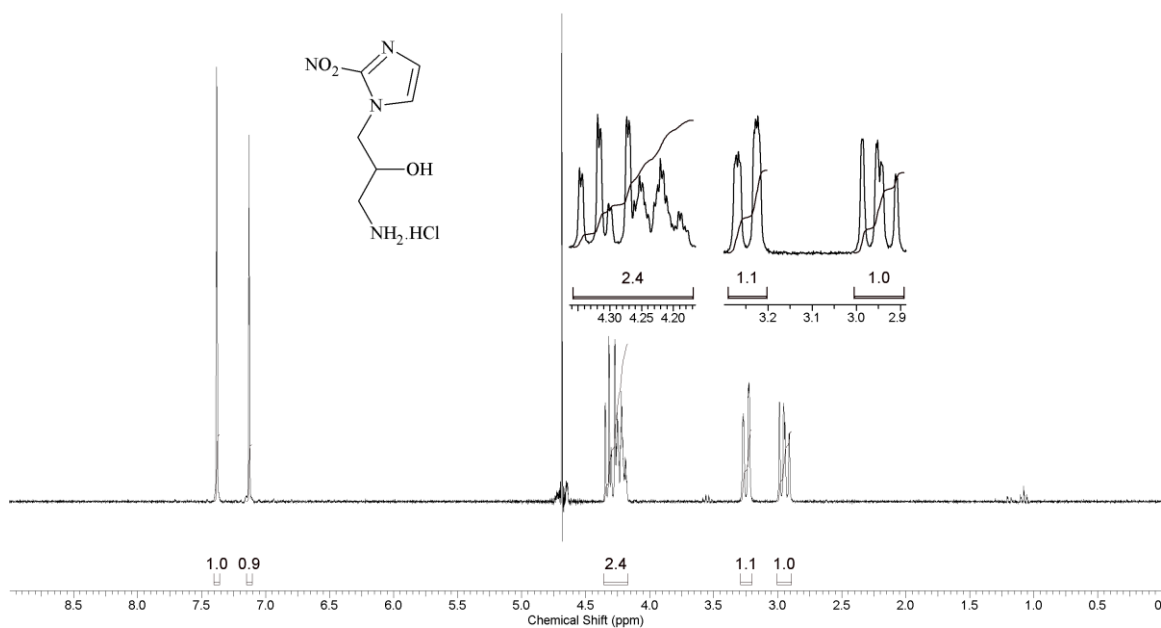
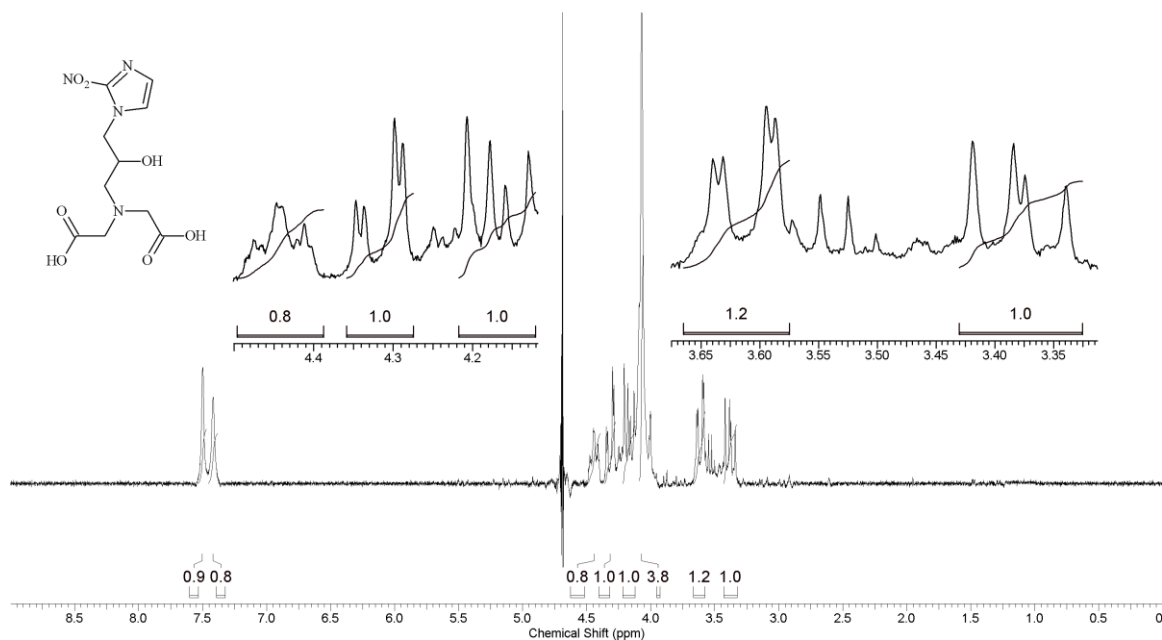
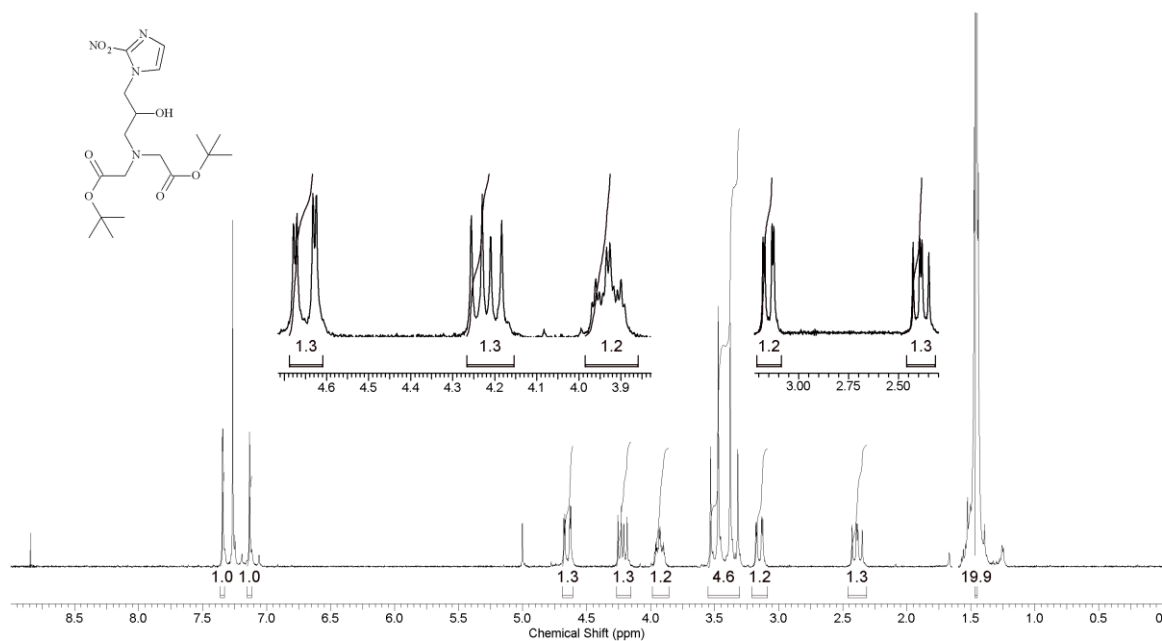


Fig. 4.4. $^1\text{H-NMR}$ spectrum of 1-amino-3-(2-nitro-1H-imidazol-1-yl)propan-2-ol hydrochloride (**4b**)



4.4. Results and discussion

4.4.1. Synthesis

[^{18}F]FMISO being a clinically used radiopharmaceutical for the detection of tissue hypoxia, a $^{99\text{m}}\text{Tc}$ -labeled misonidazole analogue would be the best possible candidate to start the exploration for a $^{99\text{m}}\text{Tc}$ -radiopharmaceutical for the same purpose. With this objective in mind an IDA derivative of misonidazole (miso-IDA) was envisaged and synthesized [Fig. 4.7(c)]. Misonidazole [Fig. 4.7(a)] as well as [^{18}F]FMISO [Fig. 4.7(b)] were found to have the same SERP of -389 mV with respect to SHE.²¹² Moreover, Adams et al.¹⁹⁵ demonstrated that structural modifications carried out two bonds away from the nitroimidazole moiety does not alter the SERP significantly. Therefore, it could be expected that SERP of misonidazole-IDA will be closer to the value of -389 mV.

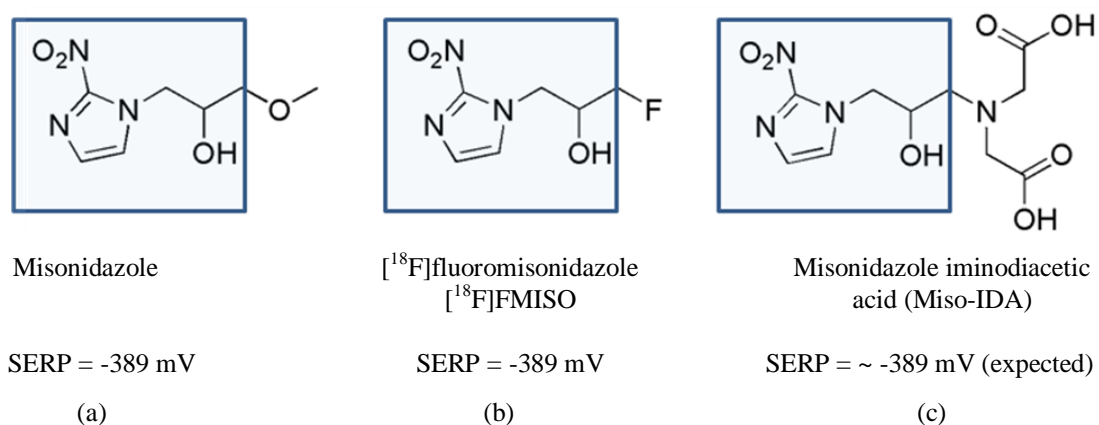


Fig. 4.7. Structure of (a) misonidazole (b) [^{18}F]FMISO and (c) miso-IDA

The synthesis of miso-IDA was carried out in a four step synthetic strategy described in the experimental section of the present chapter. 2-Nitroimidazole was coupled with 2,3-epoxypropyl phthalimide to obtain compound **4a**, which upon hydrazinolysis resulted in the amine derivative **4b**. The amine derivative was subsequently N-alkylated with *tert*-butylbromoacetate to obtain the corresponding di-*tert*-butyl ester derivative **4c**, which upon acidic hydrolysis yielded the target ligand **4d**. Spectroscopic data obtained for various compounds are consistent with the expected values.

4.4.2. Radiolabeling, quality control and characterization

Miso-IDA ligand (**4d**) was radiolabeled using $[\text{}^{99\text{m}}\text{Tc}(\text{CO})_3(\text{H}_2\text{O})_3]^+$ precursor to obtain corresponding miso-IDA- $^{99\text{m}}\text{Tc}(\text{CO})_3$ complex. The $[\text{}^{99\text{m}}\text{Tc}(\text{CO})_3(\text{H}_2\text{O})_3]^+$ precursor complex was prepared afresh prior to radiolabeling miso-IDA following the reported protocol briefly mentioned in experimental section in Chapter 1, *Section 1.14.3*. The $[\text{}^{99\text{m}}\text{Tc}(\text{CO})_3(\text{H}_2\text{O})_3]^+$ precursor complex as well as the miso-IDA- $^{99\text{m}}\text{Tc}(\text{CO})_3$ complex was analyzed by HPLC, and the elution profiles obtained are shown in figure 4.8(a) and (b), respectively. The $[\text{}^{99\text{m}}\text{Tc}(\text{CO})_3(\text{H}_2\text{O})_3]^+$ precursor eluted at 3.7 min while the miso-IDA- $^{99\text{m}}\text{Tc}(\text{CO})_3$ complex eluted at 13.9 min.

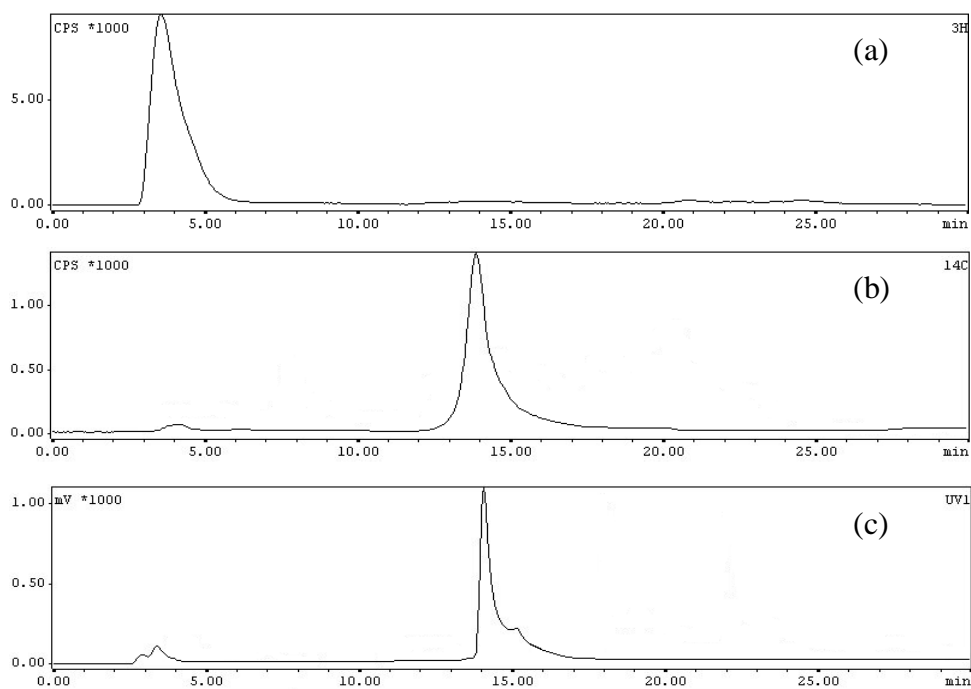


Fig. 4.8. HPLC elution profile of (a) $[\text{}^{99\text{m}}\text{Tc}(\text{CO})_3(\text{H}_2\text{O})_3]^+$ precursor (b) miso-IDA- $^{99\text{m}}\text{Tc}(\text{CO})_3$ complex (c) miso-IDA- $\text{Re}(\text{CO})_3$ complex

The mode of coordination of IDA ligand with $\text{Re}(\text{CO})_3$ core being established in Chapter 2, and then again in Chapter 3, similar spectroscopic study was not carried out for miso-IDA- $\text{Re}(\text{CO})_3$ complex. However, miso-IDA- $\text{Re}(\text{CO})_3$ complex was prepared in macroscopic level, and its UV elution profile was matched with the radioactivity profile of miso-IDA- $^{99\text{m}}\text{Tc}(\text{CO})_3$ complex prepared at nca level to establish their structural equivalence. Figure

4.8(c) shows the HPLC elution profile miso-IDA-Re(CO)₃ complex which matched with the elution profile of corresponding ^{99m}Tc(CO)₃ complex prepared at nca level. This observation clearly indicated similar coordination mode between the ligand and metal core in both the complexes. Proposed structure of miso-IDA-^{99m}Tc(CO)₃ complex is shown in figure 4.9.

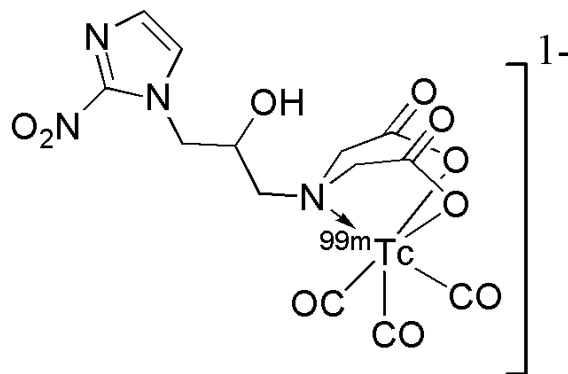


Fig. 4.9. Structure of miso-IDA-^{99m}Tc(CO)₃ complex

LogP_{o/w} of miso-IDA-^{99m}Tc(CO)₃ complex was determined following a reported procedure¹⁹⁰ and it was found to be 0.17. In comparison, the LogP_{o/w} value of [¹⁸F]FMISO was 0.41.²¹² The stability of miso-IDA-^{99m}Tc(CO)₃ complex in serum was assessed, as described in the experimental section, and it did not showed any signs of decomposition during the period of study (3 h).

4.4.3. Biological studies

The miso-IDA-^{99m}Tc(CO)₃ complex was evaluated in Swiss mice bearing fibrosarcoma tumor. The results obtained are compared with that of [¹⁸F]FMISO evaluated in the same tumor bearing animal model. Tumor uptake observed with miso-IDA-^{99m}Tc(CO)₃ complex and [¹⁸F]FMISO at different time points are shown in figure 4.10. It could be seen that [¹⁸F]FMISO showed significantly higher tumor uptake than miso-IDA-^{99m}Tc(CO)₃ complex at all the three time points. Both complexes showed biphasic clearance from tumor, with a relatively faster initial phase, between 30 min and 60 min p.i., followed by a slow clearance phase after 60 min p.i.

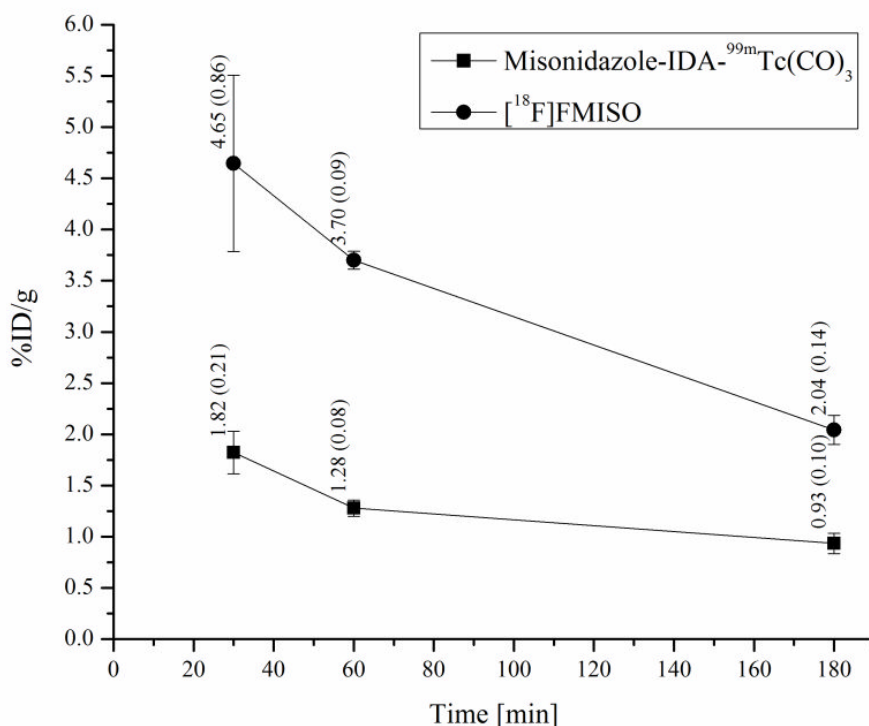


Fig. 4.10. Tumor uptake observed with miso-IDA-^{99m}Tc(CO)₃ complex and [¹⁸F]FMISO at different time points

As discussed in Chapter 2, initial uptake of the radiotracer in tumor by passive diffusion is driven by the concentration gradient developed between blood and intra tumoral environment soon after the administration of the radiotracer in the body. The decrease in tumor activity between 30 min and 60 min p.i. could be attributed to the clearance of unreduced radiotracer from tumor, initiated by the reversal of concentration gradient between blood and intra-tumoral environment. This is evident from the clearance pattern of miso-IDA-^{99m}Tc(CO)₃ complex and [¹⁸F]FMISO from blood at different time points (Fig. 4.11). Miso-IDA-^{99m}Tc(CO)₃ complex showed lower blood activity at 30 min p.i. compared to [¹⁸F]FMISO, which could be attributed to its faster clearance from blood through hepatobiliary route. This is supported by the presence of significant level of activity in intestine as early as 30 min p.i.

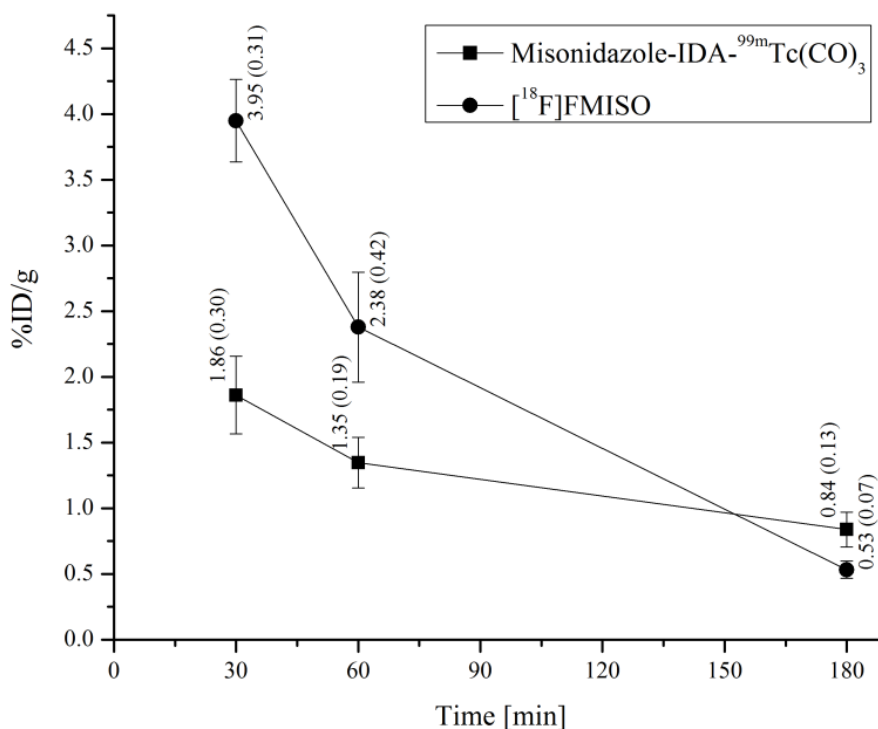


Fig. 4.11. Clearance of miso-IDA-^{99m}Tc(CO)₃ complex and [¹⁸F]FMISO from blood at different time points

From the results obtained in Chapter 2, it is evident that clearance of radiotracer from blood had a significant effect on its uptake and retention in tumor. Presence of higher level of activity in blood facilitated better distribution of the radiotracer in tumor. Faster clearance of radiotracer from blood may lower or reverse the concentration gradient which could result in non-uniform distribution of the radiotracer in the tumor, especially the hypoxic regions, and initiate clearance of the radiotracer from the tumor before it gets reduced and trapped in hypoxic cells.

The SERP of the two radiotracers viz. miso-IDA-^{99m}Tc(CO)₃ complex and [¹⁸F]FMISO being similar, lower tumor uptake of the former compared to the latter could be attributed to its faster blood clearance. Slow clearance of tumor activity after 60 min p.i. could be associated with the radiotracer reduced and trapped in the hypoxic tumor cells. The

steadily decreasing level of activity in muscles is, again, a positive indication of hypoxia specific reduction occurring in tumor.

Though, the tumor associated activity observed with miso-IDA-^{99m}Tc(CO)₃ complex as well as [¹⁸F]FMISO decreased with time, the rate of decrease was higher for the latter than the former. While, ~45% of tumor associated activity observed at 60 min p.i. was cleared at 180 min p.i. for [¹⁸F]FMISO, only ~28% reduction in tumor associated activity was observed with miso-IDA-^{99m}Tc(CO)₃ complex during the same interval. This observation suggests that reduction products of miso-IDA-^{99m}Tc(CO)₃ complex is less permeable across the cell membrane than the reduction products of [¹⁸F]FMISO. However, no attempt was made to analyze the reduction products of either radiotracer.

The variation in TBR observed with miso-IDA-^{99m}Tc(CO)₃ complex and [¹⁸F]FMISO is shown in figure 4.12.

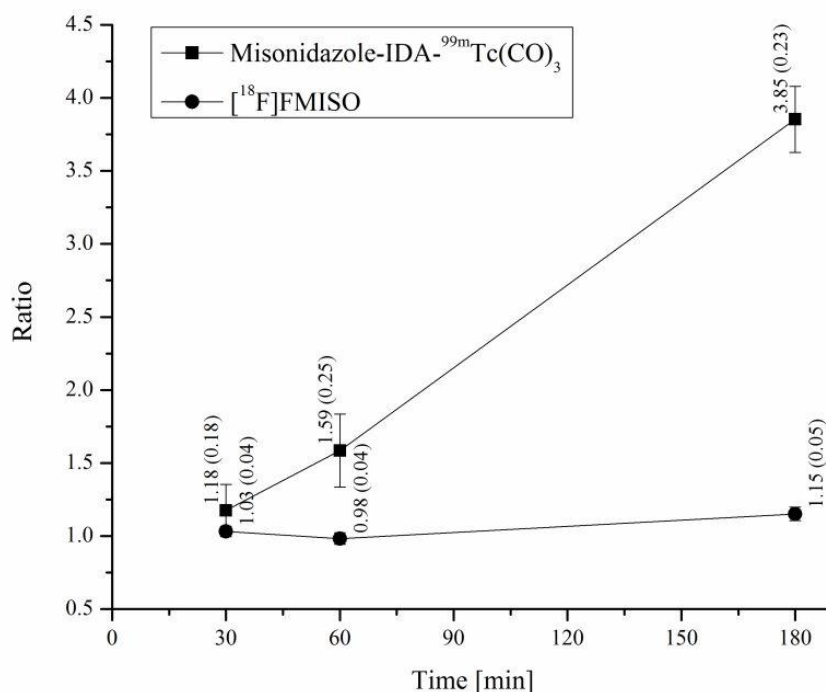


Fig. 4.12. Variation in tumor to blood ratio of miso-IDA-^{99m}Tc(CO)₃ complex and [¹⁸F]FMISO at different time points

While TBR of [^{18}F]FMISO gradually increased with time, that of miso-IDA- $^{99\text{m}}\text{Tc}(\text{CO})_3$ complex showed only marginal improvement, attaining a maximum value of 1.15 (0.05) at 180 min p.i. From figure 4.12, it could be observed that blood clearance of miso-IDA- $^{99\text{m}}\text{Tc}(\text{CO})_3$ complex is slower than that of [^{18}F]FMISO, which adversely affected its TBR. However, it is worth noting that blood clearance of miso-IDA- $^{99\text{m}}\text{Tc}(\text{CO})_3$ complex was better than 2-nitroimidazole-IDA- $^{99\text{m}}\text{Tc}(\text{CO})_3$ complex evaluated in Chapter 2. This could be attributed to the $-\text{OH}$ group present in miso-IDA ligand, which reduced the lipophilicity ($\text{LogP}_{\text{o/w}} = 0.17$ for miso-IDA- $^{99\text{m}}\text{Tc}(\text{CO})_3$ complex, $\text{LogP}_{\text{o/w}} = 0.48$ for 2-nitroimidazole-IDA- $^{99\text{m}}\text{Tc}(\text{CO})_3$ complex) and improved blood clearance. Very high TMR was obtained for miso-IDA- $^{99\text{m}}\text{Tc}(\text{CO})_3$ complex ($\text{TMR} = 93$ at 180 min p.i.), which could be attributed to its fast clearance from muscles. Maximum TMR obtained with [^{18}F]FMISO was 4.7 at 180 min p.i.

Major clearance of miso-IDA- $^{99\text{m}}\text{Tc}(\text{CO})_3$ complex from the animal body was through hepatobiliary route. There was no significant accumulation of activity in other vital organs and the activity initially accumulated cleared with time. Distribution of miso-IDA- $^{99\text{m}}\text{Tc}(\text{CO})_3$ complex and [^{18}F]FMISO in various organs at different time points is shown in figure 4.13(a) and (b), respectively.

4.5. Conclusions

The miso-IDA- $^{99\text{m}}\text{Tc}(\text{CO})_3$ complex evaluated in the present study showed uptake and retention in tumor. Through the tumor uptake value obtained with miso-IDA- $^{99\text{m}}\text{Tc}(\text{CO})_3$ complex was lower than that of [^{18}F]FMISO at every time point studied, the rate of clearance of activity from the tumor after 60 min p.i. was slower for the former. This is an advantage, since imaging protocol could be delayed to obtain better contrast between the hypoxic lesions and the background. Though, significantly high TMR was obtained with miso-IDA- $^{99\text{m}}\text{Tc}(\text{CO})_3$ complex, TBR obtained (~ 1 at 180 min p.i.) was suboptimal for imaging. A hint

for improving tumor uptake as well as TBR of miso-IDA-^{99m}Tc(CO)₃ complex, and in general, for any new radiopharmaceutical for detection of tumor hypoxia, could be obtained from the clearance pattern of [¹⁸F]FMISO from blood. [¹⁸F]FMISO showed high initial blood activity, facilitating better distribution and providing sufficient tumor residence time for the radiotracer to undergo reduction and trapping, followed by gradual clearance, which improved TBR as well as TMR. Structural modifications to misonidazole-^{99m}Tc(CO)₃ complex to modulate its blood clearance to mimic [¹⁸F]FMISO may significantly improve its pharmacokinetics. This is the possible future direction for the development of a ^{99m}Tc-radiopharmaceutical for detection of tumor hypoxia.

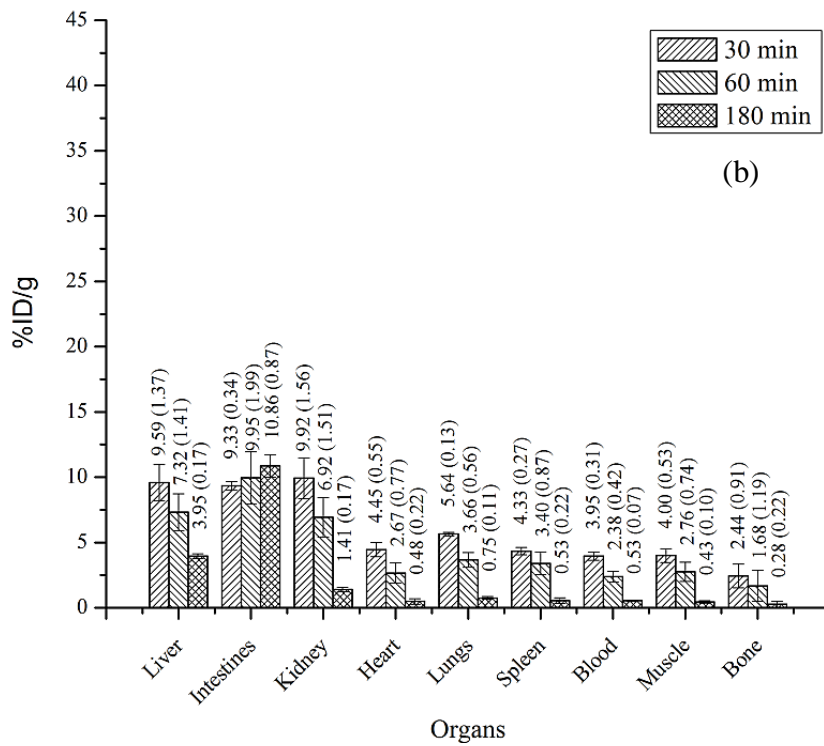
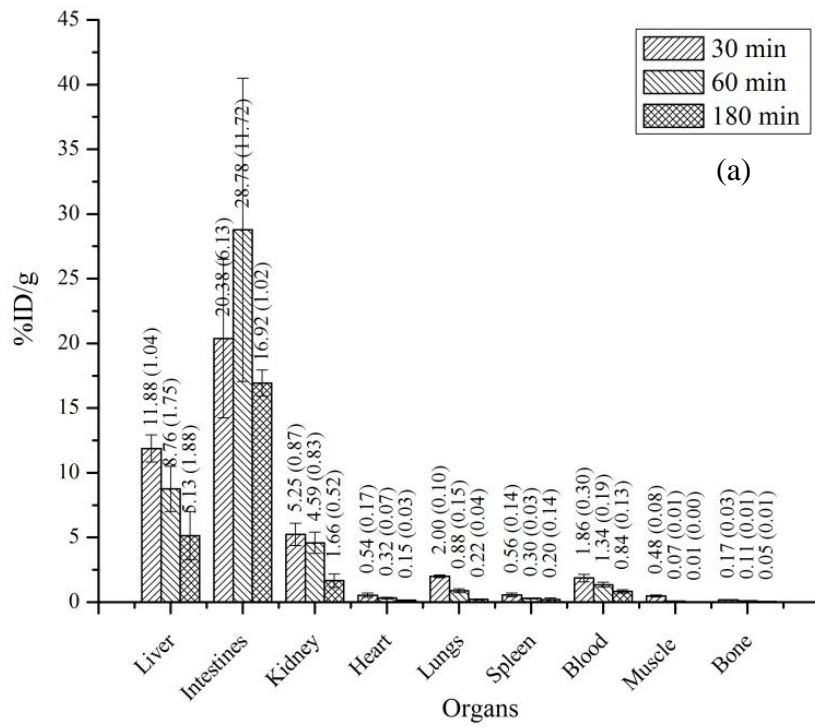


Fig. 4.13. Distribution of (a) miso-IDA-^{99m}Tc(CO)₃ complex and (b) [¹⁸F]FMISO in various organs at different time points

EPILOGUE

While the authors' work has not resulted in a superior ^{99m}Tc -agent for detecting hypoxia, it has provided some useful information for future work. This thesis clearly demonstrated that blood clearance profile of radiopharmaceutical is extremely important in deciding its overall efficacy to detect hypoxic tumor cells. The study also showed that lipophilicity and charge, together decides the clearance pattern of the radiotracer from blood, and hence, cannot be treated individually. This is a new insight, and this aspect should be considered while designing next generation radiopharmaceuticals for detecting hypoxia.

A good hypoxia detecting agent should distribute quickly throughout the tumor mass, reside there for 'sufficient time' to undergo hypoxia specific reduction, and then, clear from blood and other non-target organs in couple of hours, such that an image with acceptable level of contrast between the target and non-target tissue could be achieved. The hitch is to predict the optimal residence time for the radiotracer to undergo reduction in hypoxic cells, and at present, it can only be determined by trials. However, a logical starting point could be to mimic the blood clearance pattern of [^{18}F]FMISO, by appropriate modification of the lipophilicity and charge of the radiotracer. The results obtained could serve as inputs for further modifications to the radiotracer.

In authors' view, few possible directions for developing next generation radiopharmaceuticals for detecting hypoxia, is as follows. Use of bis-nitroimidazoles, reported by Hay et al., is an interesting idea to hasten the reduction of the radiotracer in hypoxic cells.²¹⁷ Recently, couple of studies using radiolabeled bis-nitroimidazoles are reported, where both the nitroimidazole moieties are the same.²¹⁸ The results obtained are encouraging. However, slow blood clearance of the radiotracer resulted in poor tumor to blood ratio. It would be an interesting idea to modify bis-nitroimidazoles with a, tridentate, DETA or AEG ligand, which has shown fast blood clearance in authors work. Thus,

enhanced reduction of bis-nitroimidazoles could be combined with favourable clearance property of DETA and AEG ligands to, possibly, obtain a better hypoxia detecting radiopharmaceutical. Evaluation of radiolabeled bis-nitroimidazoles, containing two differently substituted nitroimidazole (for eg. 2- and 4-, or 2- and 5- nitroimidazole) instead of two same nitroimidazole, is also worth considering.

Another possible direction towards development of better hypoxia imaging agents could be the use of liposomes to carry radiolabeled nitroimidazoles to tumor. Liposomes are expected to accumulate significantly in tumor by virtue of their lipophilicity. There are literature reports which describe the designing and preparation of pH sensitive liposomes, which decompose under acidic condition. Intra-tumoral environment being acidic, such liposomes can be used to transport nitroimidazole radiotracers to the tumor, where they will break and release the radiotracer. Local excess concentration of nitroimidazole radiotracer may enhance its hypoxia specific reduction in tumor. However, blood clearance pattern of the liposome and its effect on target to non-target ratio has to be verified experimentally.

If a nitroimidazole-^{99m}Tc(CO)₃ complex, that significantly accumulates as well as detects all clinically relevant hypoxic regions in a tumor, could be developed, the option of using the corresponding ^{186/188}Re(CO)₃ analogue to deliver therapeutic dose directly to the hypoxic tumor tissues could be explored.

REFERENCES

1. <http://medind.nic.in/haa/t05/i1/haat05i1p10.pdf>.
2. Hockel M., Vaupel P. *J. Natl. cancer Inst.*, **2001**, 93(4), 266.
3. Vaupel P., Harrison L. *The Oncologist*, **2004**, 9(suppl 5), 4.
4. Weibe L.I., Machulla H.J. *Imaging Hypoxia, Kluwer Academic Publishers, Netherlands*, **1999**, 1.
5. Gray L.H., Conger A.D., Ebert M. *Br. J. Radiol.*, **1953**, 26, 683.
6. Höckel M., Schlenger K., Aral B., Mitze M., Schäffer U., Vaupel P. *Cancer Res.*, **1996**, 56, 4509.
7. Gilles M., Rudi D., Christel V., Christophe Van de Wiele. *Eur. J. Nucl. Med. Mol. Imaging*, **2009**, 36, 1674.
8. Fyles A.W., Milosevic M., Wong R., Kavanagh M.C., Pintilie M., Sun A., Chapman W., Levin W., Manchul L., Keane T.J., Hill R.P. *Radiother. Oncol.*, **1998**, 48, 149.
9. Nordmark M., Overgaard M., Overgaard J. *Radiother. Oncol.*, **1996**, 41, 31.
10. Brizel D.M., Sibley G.S., Prosnitz L.R., Scher R.L., Dewhirst M.W. *Int. J. Radiat. Oncol. Biol. Phys.*, **1997**, 38, 285.
11. Nordmark M., Bentzen S.M., Rudat V., Brizel D., Lartigau E., Stadler P., Becker A., Adam M., Molls M., Dunst J., Terris D.J., Overgaard J. *Radiother. Oncol.*, **2005**, 77, 18.
12. Duffy J.P., Eibl G., Reber H.A., Hines O.J. *Molecular Cancer*, **2003**, 2, 12.
13. Brizel D.M., Scully S.P., Harrelson J.M., Layfield L.J., Bean J.M., Prosnitz L.R., Dewhirst M.W. *Cancer Res.*, **1996**, 56, 941.
14. McKeown S.R., Cowen R.L., Williams K.J. *Clin. Oncol.*, **2007**, 19(6), 427.
15. Krohn K.A., Rajendran J.G. *American Society of Clinical Oncology*, **2008**, 538.
16. Arabi M., Piert M. *Q. J. Nucl. Med. Mol. Imaging*, **2010**, 54, 500.

17. Graves E.E., Giaccia A.J. *Oncology*, **2007**, 21(3), 368.
18. Kallinowski F., Zander R., Hoeckel M., Vaupel P. *Int. J. Radiat. Oncol. Biol. Phys.*, **1990**, 19, 953.
19. Höckel M., Schlenger K., Knoop C., Vaupel P. *Cancer Res.*, **1991**, 51, 6098.
20. Vaupel P., Schlenger K., Knoop C., Höckel M. *Cancer Res.*, **1991**, 51, 3316.
21. Griffiths J.R., Robinson S.P. *Br. J. Radiol.*, **1999**, 72, 627.
22. Collingridge D.R., Young W.K., Vojnovic B., Wardman P., Lynch E.M., Hill S.A., Chaplin D.J. *Radiat. Res.*, **1997**, 147, 329.
23. Raleigh J.A., Dewhirst M.W., Thrall D.E. *Semin. Radiat. Oncol.*, **1996**, 6, 37.
24. Kennedy A.S., Raleigh J.A., Perez G.M., Calkins D.P., Thrall D.E., Novotny D.B., Varia M.A. *Int. J. Radiat. Oncol. Biol. Phys.*, **1997**, 37, 897.
25. Koch C.J., Evans S.M., Lord E.M. *Br. J. Cancer*, **1995**, 72, 869.
26. Zhong H., De Marzo A.M., Laughner E., Lim M., Hilton D.A., Zagzag D., Buechler P., Isaacs W.B., Semenza G.L., Simons J.W. *Cancer Res.*, **1999**, 59, 5830.
27. Ivanov S., Liao S.Y., Ivanova A., Danilkovitch-Miagkova A., Tarasova N., Weirich G., Merrill M.J., Proescholdt M.A., Oldfield E.H., Lee J., Zavada J., Waheed A., Sly W., Lerman M.I., Stanbridge E.J. *Am. J. Pathol.*, **2001**, 158, 905.
28. Dunn J.F., O'Hara J.A., Zaim-Wadghiri Y., Lei H., Meyerand M.E., Grinberg O.Y., Hou H., Hoopes P.J., Demidenko E., Swartz H.M. *J. Magn. Reson. Imaging*, **2002**, 16, 511.
29. Baudelet C., Gallez B. *Magn. Reson. Med.*, **2002**, 48, 980.
30. Swartz H.M., Bacic G., Friedman B., Goda F., Grinberg O., Hoopes P.J., Jiang J., Liu K. J., Nakashima T., O'Hara J., et al. *Adv. Exp. Med. Biol.*, **1994**, 361, 119.
31. Le D., Mason R.P., Hunjan S., Constantinescu A., Barker B.R., Antich P.P. *Magn. Reson. Imaging*, **1997**, 15, 971.

32. Hunjan S., Mason R.P., Constantinescu A., Peschke P., Hahn E.W., Antich P.P. *Int. J. Radiat. Oncol. Biol. Phys.*, **1998**, *41*, 161.
33. Rasey J.S., Koh W.J., Grierson J.R., Grunbaum Z., Krohn K.A. *Int. J. Radiat. Oncol. Biol. Phys.*, **1989**, *17*, 985.
34. Rajendran J.G., Mankoff D.A., O'Sullivan F., Peterson L.M., Schwartz D.L., Conrad E.U., Spence A.M., Muzi M., Farwell D.G., Krohn K.A. *Clin. Cancer Res.*, **2004**, *10*, 2245.
35. Sorger D., Patt M., Kumar P., Wiebe L.I., Barthel H., Seese A., Dannenberg C., Tannapfel A., Kluge R., Sabri O. *Nucl. Med. Biol.*, **2003**, *30*, 317.
36. Reischl G., Ehrlichmann W., Bieg C., Solbach C., Kumar P., Wiebe L.I., Machulla H.J. *Appl. Radiat. Isot.*, **2005**, *62*, 897.
37. Ziemer L.S., Evans S.M., Kachur A.V., Shuman A.L., Cardi C.A., Jenkins W.T., Karp J.S., Alavi A., Dolbier W.R.Jr., Koch C.J. *Eur. J. Nucl. Med.*, **2003**, *30*, 259.
38. Lewis J.S., McCarthy D.W., McCarthy T.J., Fujibayashi Y., Welch M.J. *J. Nucl. Med.*, **1999**, *40*, 177.
39. Dehdashti F., Mintun M.A., Lewis J.S., Bradley J., Govindan R., Laforest R., Welch M. J., Siegel B.A. *Eur. J. Nucl. Med. Mol. Imaging*, **2003**, *30*, 844.
40. Zanzonico P., O'Donoghue J., Chapman J.D., Schneider R., Cai S., Larson S., Wen B., Chen Y., Finn R., Ruan S., Gerweck L., Humm J., Ling C. *Eur. J. Nucl. Med. Mol. Imaging*, **2004**, *31*, 117.
41. Olive P.L., Banáth J.P., Aquino-Parsons C. *Acta Oncologica*, **2001**, *40(8)*, 917.
42. Vaupel P., Höckel M., Mayer A. *Antioxid. Redox. Signal*, **2007**, *9(8)*, 1221.
43. Movsas B., Chapman J.D., Greenberg R.E., Hanlon A.L., Horwitz E.M., Pinover W.H., Stobbe C., Hanks G.E. *Cancer*, **2000**, *89(9)*, 2018.

44. Evans S.M., Joiner B., Jenkins W.T., Laughlin K.M., Lord E.M., Koch C.J. *Br. J. Cancer*, **1995**, 72, 875.
45. Varia M.A., Calkins-Adams D.P., Rinker L.H., Kennedy A.S., Novotny D.B., Fowler W.C.Jr., Raleigh J.A. *Gynecol. Oncol.*, **1998**, 71, 270.
46. Zhao D., Constantinescu A., Jiang L., Hahn E.W., Mason R.P. *Am. J. Clin. Oncol.*, **2001**, 24(5), 462.
47. Pacheco-Torres J., López-Larrubia P., Ballesteros P., Cerdán S. *NMR Biomed.*, **2011**, 24(1), 1.
48. Zhao D., Constantinescu A., Hahn E.W., Mason R.P. *Int. J. Radiat. Oncol. Biol. Phys.*, **2002**, 53(3), 744.
49. Zhao D., Ran S., Constantinescu A., Hahn E., Mason R.P. *Neoplasia*, **2003**, 5(4), 308.
50. Zhao D., Constantinescu A., Chang C.H., Hahn E.W., Mason R.P. *Radiat. Res.*, **2003**, 159(5), 621.
51. Liu S., Chakraborty S. *Dalton Trans.*, **2011**, 40(23), 6077.
52. Rösch F., Baum R.P. *Dalton Trans.*, **2011**, 40(23), 6104.
53. Correia J.D., Paulo A., Raposinho P.D., Santos I. *Dalton Trans.*, **2011**, 40(23), 6144.
54. Spitzweg C., Heufelder A.E., Morris J.C. *Thyroid*, **2000**, 10(4), 321.
55. Liu X.H., Chen G.G., Vlantis A.C., van Hasselt C.A. *Crit. Rev. Clin. Lab. Sci.*, **2009**, 46(5-6), 302.
56. Mathiopoulou L., Chrisoulidou A., Boudina M., Mitsakis P., Mandanas S., Pazaitou-Panayiotou K. *Clin. Nucl. Med.*, **2012**, 37(6), 604.
57. Goldenberg D.M., Sharkey R.M. *Ther. Deliv.*, **2011**, 2(6), 675.
58. Türker S., Yekta Özer A. *J. Pharm. Sci.*, **2004**, 29, 145.
59. <http://www.nucmedtutorials.com/dwradiopharm/rad2.html>
60. Fujibayashi Y., Taniuchi H., Yonekura Y., Ohtani H., Konishi J., Yokoyama A. *J. Nucl. Med.*, **1997**, 38, 1155.

61. Dearling J.L., Lewis J.S., Mullen G.E., Rae M.T., Zweit J., Blower P.J. *Eur. J. Nucl. Med.*, **1998**, 25, 788.
62. Dearling J.L., Lewis J.S., Welch M.J., McCarthy D.W., Blower P.J. *Chem. Commun.*, **1998**, 22, 2531.
63. Lewis J.S., McCarthy D.W., McCarthy T.J., Fujibayashi Y., Welch M.J. *J. Nucl. Med.*, **1999**, 40, 177.
64. Lewis J.S., Sharp T.L., Laforest R., Fujibayashi Y., Welch M.J. *J. Nucl. Med.*, **2001**, 42, 655.
65. Dearling J.L., Lewis J.S., Mullen G.E., Welch M.J., Blower P.J. *J. Biol. Inorg. Chem.*, **2002**, 7, 249.
66. Lewis J.S., Herrero P., Sharp T., Engelbach J.A., Fujibayashi Y., Laforest R., Kovacs A., Gropler R.J., Welch M.J. *J. Nucl. Med.*, **2002**, 43, 1557.
67. Maurer R.I., Blower P.J., Dilworth J.R., Reynolds C.A., Zheng Y., Mullen G.E. *J. Med. Chem.*, **2002**, 45, 1420.
68. Dearling J.L., Packard A.B. *Nucl. Med. Biol.*, **2010**, 37, 237.
69. Zhang X., Melo T., Ballinger J.R., Rauth A.M. *Int. J. Radiat. Oncol. Biol. Phys.*, **1998**, 42, 737.
70. Honess D.J., Hill S.A., Collingridge D.R., Edwards B., Brauers G., Powell N.A., Chaplin D.J. *Int. J. Radiat. Oncol. Biol. Phys.*, **1998**, 42(4), 731.
71. Brauers G., Archer C.M., Burke J.F. *Eur. J. Nucl. Med.*, **1997**, 24, 943.
72. Edwards D.I. *Br. J. Vener. Dis.*, **1980**, 56, 285.
73. Edwards D.I., Mathison G.E. *J. Gen. Microbiol.*, **1970**, 63, 297.
74. Edwards D.I., Dye M., Carne H. *J. Gen. Microbiol.*, **1973**, 76, 135.
75. Ings R.M., McFadzean J.A., Ormerod W.E. *Biochem. Pharmacol.*, **1974**, 15, 1421.
76. Nunn A., Linder K., Strauss H.W. *Eur. J. Nucl. Med.*, **1995**, 22(3), 265.

77. Wuest M., Kumar P., Wang M., Yang J., Jans H.S., Wiebe L.I. *Cancer Biother. Radiopharm.*, **2012**, 27(8), 473.
78. Giglio J., Fernández S., Pietzsch H.J., Dematteis S., Moreno M., Pacheco J.P., Cerecetto H, Rey A. *Nucl. Med. Biol.*, **2012**, 39(5), 679.
79. Hoigebazar L., Jeong J.M., Hong M.K., Kim Y.J., Lee J.Y., Shetty D., Lee Y.S., Lee D.S., Chung J.K., Lee M.C. *Bioorg. Med. Chem.*, **2011**, 19(7), 2176.
80. Hoigebazar L., Jeong J.M., Choi S.Y., Choi J.Y., Shetty D., Lee Y.S., Lee D.S., Chung J.K., Lee M.C., Chung Y.K. *J. Med. Chem.*, **2010**, 53(17), 6378.
81. Parliament M.B., Chapman J.D., Urtasun R.C., McEwan A.J., Golberg L., Mercer J.R., Mannan R.H., Wiebe L.I. *Br. J. Cancer*, **1992**, 65(1), 90.
82. Zha Z., Zhu L., Liu Y., Du F., Gan H., Qiao J., Kung H.F. *Nucl. Med. Biol.*, **2011**, 38(4), 501.
83. Lee S.T., Scott A.M. *Semin. Nucl. Med.*, **2007**, 37, 451.
84. Piert M., Machulla H.J., Picchio M., Reischl G., Ziegler S., Kumar P., Wester H.J., Beck R., McEwan A.J., Wiebe L.I., Schwaiger M. *J. Nucl. Med.*, **2005**, 46, 106.
85. Reischl G., Dorow D.S., Cullinane C., Katsifis A., Roselt P., Binns D, Hicks R.J. *J. Pharm. Pharm. Sci.*, **2007**, 10, 203.
86. Yang D.J., Wallace S., Cherif A., Li C., Gretzer M.B., Kim E.E., Podoloff D.A. *Radiology*, **1995**, 194, 795.
87. Rasey J.S., Hofstrand P.D., Chin L.K., Tewson T.J. *J. Nucl. Med.*, **1999**, 40, 1072.
88. Kachur A.V., Dolbier W.R.Jr., Evans S.M., Shiue C.Y., Shiue G.G., Skov K.A., Baird I.R., James B.R., Li A.R., Roche A., Koch C.J. *Appl. Radiat. Isot.*, **1999**, 51, 643.
89. Couturier O., Luxen A., Chatal J.C., Vuillez J.P., Rigo P., Hustinx R. *Eur. J. Nucl. Med. Mol. Imaging*, **2004**, 31, 1182.

90. Dolbier W.R.Jr, Li A.R., Koch C.J., Shiue C.Y., Kachur A.V. *Appl. Radiat. Isot.*, **2001**, 54, 73.
91. Komar G., Seppänen M., Eskola O., Lindholm P., Grönroos T.J., Forsback S., Sipilä H., Evans S.M., Solin O., Minn H. *J. Nucl. Med.*, **2008**, 49, 1944.
92. Mahy P., De Bast M., Gillart J., Labar D., Grégoir V. *Eur. J. Nucl. Med. Mol. Imaging*, **2006**, 33, 553.
93. Rumsey W.L., Cyr J.E., Raju N., Narra R.K. *Biochem. Biophys. Res. Commun.*, **1993**, 193(3), 1239.
94. Ballinger J.R., Judy Wan Mine Kee, Rauth A.M. *J. Nucl. Med.*, **1996**, 37, 1023.
95. Melo T., Jill Duncan, Ballinger J.R., Rauth A.M. *J. Nucl. Med.*, **2000**, 41, 169.
96. Ballinger J.R. *Semin. Nucl. Med.*, **2001**, 31(4), 321.
97. Mallia M.B., Banerjee S., Venkatesh M. *Technetium-99m Labelled Molecules For Hypoxia Imaging. Technetium-99m Radiopharmaceuticals: Status and Trends, Vienna: IAEA*, **2009**, 295.
98. Koh W.J., Rasey J.S., Evans M.L., Grierson J.R., Lewellen T.K., Graham M.M., Krohn K.A., Griffin T.W. **1992**, *Int. J. Radiat. Oncol. Biol. Phys.*, 22, 199.
99. Valk P.E., Mathis C.A., Prados M.D., Gilbert J.C., Budinger T.F. *J. Nucl. Med.*, **1992**, 33, 2133.
100. Rahmim A., Zaidi H. *Nucl. Med. Commun.*, **2008**, 29(3), 193.
101. Banerjee S., Pillai M.R., Ramamoorthy N. *Semin. Nucl. Med.*, **2001**, 31(4), 260.
102. <http://www.world-nuclear.org/info/inf55.html>
103. Jurisson S., Berning D., Jia W., Dangshe M. *Chem. Rev.*, **1993**, 93, 1137.
104. Jurisson S., Lydon J.D. *Chem. Rev.*, **1999**, 99, 2205.
105. Schubiger P.A., Alberto R., Smith A. *Bioconjug. Chem.*, **1996**, 7, 165.
106. Liu S. *Adv Drug Deliv Rev.*, **2008**, 60(12), 1347.

107. <http://www.bnl.gov/bnlweb/history/tc-99m.asp>
108. Eckelman W.C., Coursey B.M. *Int. J. Appl. Radiat. Isot.*, **1982**, 33(10).
109. *Special Issue on 'Radionuclide Generator Technology'*, *Radiochimica Acta* 41(2/3) (1987).
110. *IAEA-TECDOC*, **2003**, 1340, 135.
111. Boyd R.E. *Int. J. Appl. Radiat. Isot.*, **1982**, 33(10), 801.
112. Lebowitz E, Richards P. *Semin. Nucl. Med.*, **1974**, 4(3), 257.
113. Knapp F.F.Jr., Mirzadeh S. *Eur. J. Nucl. Med.*, **1994**, 21(10), 1151.
114. Mazzi U. *Polyhedron*, **1989**, 8, 1683.
115. Maecke H.R., Eisenhut M. *Bioinorg. Chem.*, **1995**, 2, 1079.
116. Mease R.C., Lambert C. *Semin. Nucl. Med.*, **2001**, 31, 278.
117. Schwochau K. *Technetium-Chemistry and Radiopharmaceutical Applications*, Wiley-VCH, Germany, 2000, 1.
118. Banerjee S.R., Maresca K.P., Francesconi L., Valliant J., Babich J.W., Zubieta J. *Nucl. Med. Biol.*, **2005**, 32(1), 1.
119. Blower P. Towards molecular imaging and treatment of disease with radionuclides: The role of inorganic chemistry, *Dalton Trans.*, **2006**, 14, 1705.
120. Weiner R.E., Thakur M.L. *Biodrugs*, **2005**, 19, 145.
121. Level S.Z. *Principles of Nuclear Medicine. Technetium and Rhenium compounds*. Saunders, Philadelphia, **1995**, 213.
122. Liu S., He Z., Hsieh W.Y., Kim Y.S. *Nucl. Med. Biol.*, **2006**, 33(3), 419.
123. Baldas J., Bonnyman J., Pojer P.M., Williams G.A., Mackay M.F. *J. Chem. Soc. Dalton. Trans.*, **1981**, 1798.
124. Baldas J., Bonnyman J. *Int. J. Appl. Rad. Isot.*, **1985**, 36, 133.
125. Pasqualini R., Duatti A. *J. Chem. Soc. Chem. Commun.*, **1992**, 1354.

126. Pasqualini R., Duatti A., Bellande E., Comazzi V., Brucato V., Hoffschir D., Fagret D., Comet M. *J. Nucl. Med.*, **1994**, 35(2), 334.
127. Bolzati C., Boschi A., Uccelli L., Malago E., Bandoli G., Tisato F., Refosco F., Pasqualini R., Duatti A. *Inorg. Chem.*, **1999**, 38, 4473.
128. Pasqualini R., Duatti A. *J. Chem. Soc. Chem. Commun.*, **1992**, 1354.
129. Dehnicke K., Strähle J. *Angew. Chem. Int. Ed. Eng.*, **1992**, 31, 955.
130. Pasqualini R., Comazzi V., Bellande E., Duatti A., Marchi A. *App. Radiat. Isot.*, **1992**, 43, 1329.
131. Pasqualini R., Duatti A., Bellande E., Comazzi V., Brucato V., Hoffschir D., Fagret D., Comet M. *J. Nucl. Med.*, **1994**, 35, 334.
132. Fagret D., Ghezzi C., Vanzetto G. *J. Nucl. Med.*, **2001**, 42, 1395.
133. Refosco R., Bolzati C., Duatti A., Tisato F., Uccelli L. *Recent Rev. Devel. Inorg. Chem.*, **2000**, 2, 89.
134. Bolzati C., Boschi A., Duatti A., Prakash S., Uccelli L., Refosco F., Tisato F., Bandoli G. *J. Am. Chem. Soc.*, **2000**, 122, 4510.
135. Boschi A., Bolzati C., Benini E., Malago E., Uccelli L., Duatti A., Piffanelli A., Refosco F., Tisato F. *Bioconjug. Chem.*, **2001**, 12, 1035.
136. Boschi A., Bolzati C., Uccelli L., Duatti A., Benini E., Refosco F., Tisato F., Piffanelli. *Nucl. Med. Commun.*, **2002**, 23, 689.
137. Bolzati C., Boschi A., Uccelli L., Tisato F., Refosco F., Cagnolini A., Duatti A., Prakash S., Bandoli G., Vittadini A. *J. Am. Chem. Soc.*, **2002**, 124, 11468.
138. Boschi A., Uccelli L., Duatti A., Bolzati C., Refosco F., Tisato F., Romagnoli R., Baraldi P.G., Varani K., Borea P.A. *Bioconjug. Chem.*, **2003**, 14, 1279.
139. Boschi A., Uccelli L., Bolzati C., Duatti A., Sabba N., Moretti E., Di Domenico G., Zavattini G., Refosco F., Giganti M. *J. Nucl. Med.*, **2003**, 44, 806.

140. Boltzati C., Muhmood A., Malago E., Uccelli L., Boschi A., Jones A.G., Refosco F., Duatti A., Tisato F. *Bioconjug. Chem.*, **2003**, *14*, 1231.
141. Boltzati C., Refosco F., Cagnolini A., Tisato F., Boschi A., Duatti A., Uccelli L., Dolmella A., Marotta E., Tubaro M. *Eur. J. Inorg. Chem.*, **2004**, *9*, 1902.
142. Hatada K., Riou L.M., Ruiz M., Yamamichi Y., Duatti A., Lima R.L., Goode A.R., Watson D.D., Beller G.A., Glover D.K. *J. Nucl. Med.*, **2004**, *45*, 2095.
143. Tisato F., Refosco F., Porchia M., Boltzati C., Bandoli G., Dolmella A., Duatti A., Boschi A., Jung C.M., Pietzsch H.J., Kraus W. *Inorg. Chem.*, **2004**, *43*, 8617.
144. Cazzola E., Benini E., Pasquali M., Mirtschink P., Walther M., Pietzsch H.J., Uccelli L., Boschi A., Boltzati C., Duatti A. *Bioconjug. Chem.*, **2008**, *19*, 450.
145. Edwards D.S., Liu S., Barrett J.A., Harris A.R., Looby R.J., Ziegler M.C., Heminway S.J., Carroll T.R. *Bioconjug. Chem.*, **1997**, *8*, 146.
146. Liu S., Edwards D.S., Harris A.R. *Bioconjug. Chem.*, **1998**, *9*, 583.
147. Abrams M.J., Juweid M., Tenkate C.I., Schwartz D.A., Hauser M.M., Gaul F.E., Fuccello A.J., Rubin R.H., Strauss H.W., Fischman A.J. *J. Nucl. Med.*, **1990**, *31*, 2022.
148. Schwartz D.A., Abrams M.J., Hauser M.M., Gaul F.E., Larsen S.K., Rauh D., Zubieta J. *Bioconjug. Chem.*, **1991**, *2*, 333.
149. Ultee M.E., Bridger G.J., Abrams M.J., Longley C.B., Burton C.A., Larsen S., Henson G.W., Padmanabhan S., Gaul F.E., Schwartz D.A. *J. Nucl. Med.*, **1997**, *38*, 133.
150. Babich J.W., Solomon H., Pike M.C., Kroon D., Graham W., Abrams M.J., Tompkins R.G., Rubin R.H., Fischman A.J. *J. Nucl. Med.*, **1993**, *34*, 1967.
151. Babich J.W., Fischman A.J. *Nucl. Med. Biol.*, **1995**, *22*, 25.

152. Babich J.W., Graham W., Barrow S.A., Fischman A.J. *Nucl. Med. Biol.*, **1995**, *22*, 643.
153. Decristoforo C., Mather S.J. *Bioconjug. Chem.*, **1999**, *10*, 431.
154. Decristoforo C., Melendez L., Sosabowski J.K., Mather S.J. *J. Nucl. Med.*, **2000**, *41*, 1114.
155. Decristoforo C., Mather S.J. *Nucl. Med. Biol.*, **1999**, *26*, 389.
156. Decristoforo C., Mather S.J. *Eur. J. Nucl. Med.*, **1999**, *26*, 869.
157. Bangard M., Béhé M., Guhlke S., Otte R., Bender H., Maecke H.R., Birsack H.J. *Eur. J. Nucl. Med.*, **2000**, *27*, 628.
158. Decristoforo C., Mather S.J., Cholewinski W., Donnemiller E., Riccabona G., Moncayo R. *Eur. J. Nucl. Med.*, **2000**, *27*, 1318.
159. Brouwers A.H., Laverman P., Boerman O.C., Oyen W.J.G., Barrett J.A., Harris T.D., Edwards D.S., Corstens F.H.M. *Nucl. Med. Commun.*, **2000**, *21*, 1043.
160. Liu S., Harris A.R., Ziegler M.C., Edwards D.S., Williams N.E. *Bioconjug. Chem.*, **2002**, *13*, 881.
161. Liu S., Edwards D.S., Ziegler M.C., Harris A.R., Hemingway S.J., Barrett B.A. *Bioconjug. Chem.*, **2001**, *12*, 624.
162. Liu S., Hsieh W., Jiang Y., Kim Y., Sreerama S.G., Chen X., Jia B., Wang F. *Bioconjug. Chem.*, **2007**, *18*, 438.
163. Jia B., Shi J., Yang Z., Xu B., Liu Z., Zhao H., Liu S., Wang F. *Bioconjug. Chem.*, **2006**, *17*, 1069.
164. Laverman P., Dams E.T.M., Oyen W.J.G., Storm G., Koenders E.B., Prevost R., van der Meer J.W.M., Corstens F.H.M., Boerman O.C. *J. Nucl. Med.*, **1999**, *40*, 192.
165. Zhang Y., Liu N., Zhu Z.H., Rusckowski M., Hnatowich D.J. *Eur. J. Nucl. Med.*, **2000**, *27*, 1700.

166. Hnatowich D.J., Winnard Jr. P., Virzi F., Fogarasi M., Santo T., Smith C.L., Cantor C.R., Rusckowski M. *J. Nucl. Med.*, **1995**, *36*, 2306.
167. Alberto R., Schibli R., Egli A., Schubiger A. P. *J. Am. Chem. Soc.*, **1998**, *120*(31), 7987.
168. Smith D.P., Baralt E., Morales B., Olmstead M.M., Maestre M.F., Fish R.H. *J. Am. Chem. Soc.*, **1992**, *114* (26), 10647.
169. Top S., Hassane El Hafa , Vessieres A., Quivy J., Vaissermann J., Hughes D.W., McGlinchey M.J., Jean-Paul Mornon , Thoreau E., Jaouen G. *J. Am. Chem. Soc.*, **1995**, *117*(32), 8372.
170. Alberto R., Ortner K., Wheatley N., Schibli R., Schubiger A.P. *J. Am. Chem. Soc.*, **2001**, *123*(13), 3135.
171. Alberto R., Schibli R., Waibel R., Abram U., Schubiger A.P., *Coordination Chemistry Reviews*, **1999**, *190–192*, 901.
172. Schibli R., Katti K.V., Higginbotham C., Volkert W.A., Alberto R. *Nucl. Med. Biol.*, **1999**, *26*, 711.
173. Pak J.K., Benny P., Spingler B., Ortner K., Alberto R. *Chemistry*, **2003**, *9*, 2053.
174. Correia J.D., Domingos A., Santos I., Alberto R., Ortner K. *Inorg. Chem.* **2001**, *40*, 5147.
175. Liu Y., Pak J.K., Schmutz P., Bauwens M., Mertens J., Knight H., Alberto R. *J. Am. Chem. Soc.*, **2006**, *128*, 15996.
176. Agorastos N., Borsig L., Renard A., Antoni P., Viola G., Spingler B., Kurz P, Alberto R. *Chemistry*, **2007**, *13*, 3842.
177. Saw M.M., Kurz P., Agorastos N., Andy Hor T.S, Sundram F.X., Yaw Kai Yan, Alberto R. *Inorganica Chimica Acta*, **2006**, *359*, 4087.

178. Xavier C., Jae-Kyoung Pak, Santos I., Alberto R. *J. Organomet. Chem.*, **2007**, 692, 1332.
179. Alves S., Correia J.D., Gano L., Rold T.L., Prasanphanich A., Haubner R., Rupprich M., Alberto R., Decristoforo C., Santos I., Smith C.J. *Bioconjug. Chem.*, **2007**, 18, 530.
180. Banerjee S.R., Maresca K.P., Francesconi L., Valliant J., Babich J.W., Zubieta J. *Nucl. Med. Biol.*, **2005**, 32, 1.
181. Palma E., João D. G. Correia, Domingos A., Santos I., Alberto R., Spies H. *J. Organomet. Chem.*, **2004**, 689, 4811.
182. Spingler B., Mundwiler S., Ruiz-Sánchez P., Van Staveren D.R., Alberto R. *Eur. J. Inorg. Chem.*, **2007**, 18, 2641.
183. Liu Y., Oliveira B.L., Correia J.D., Santos I.C., Santos I., Spingler B., Alberto R. *Org. Biomol. Chem.*, **2010**, 8, 2829.
184. Xavier C., Giannini C., Dall'Angelo S., Gano L., Maiorana S., Alberto R., Santos I. *J. Biol. Inorg. Chem.*, **2008**, 13, 1335.
185. Kunze S., Zobi F., Kurz P., Spingler B., Alberto R. *Angew. Chem. Int. Ed.*, **2004**, 43, 5025.
186. Peindy N'Dongo H.W., Liu Y., Schmutz P., Spingler B., Alberto R. *J. Organomet. Chem.*, **2009**, 694, 981.
187. Liu Y., Spingler B., Schmutz P. *J. Am. Chem. Soc.*, **2008**, 130(5), 1554.
188. N'Dongo H.W., Raposinho P.D., Fernandes C., Santos I., Can D., Schmutz P., Spingler B., Alberto R. *Nucl. Med. Biol.*, **2010**, 37, 255.
189. Bernard J., Ortner K., Spingler B., Pietzsch H.J., Alberto R. *Inorg. Chem.*, **2003**, 42(4), 1014.

190. Troutner D.E., Volkert W.A., Hoffman T.J., Holmes R.A. *Int. J. Appl. Radiat. Isot.*, **1984**, 35(6), 467.
191. Adam M.F., Dorie M.J., Brown J.M. *Int. J. Radiat. Oncol. Biol. Phys.*, **1999**, 45(1), 171.
192. Zhang X., Su Z.F., Ballinger J.R., Rauth A.M., Pollak A., Thornback J.R. *Bioconjug. Chem.*, **2000**, 11(3), 401.
193. Alberto R., Schibli R., Schubiger P. A., Abram U., Kaden T. A., *Polyhedron*, **1996**, 15, 1079.
194. Itoh M., Hagiwara D., Kamiya, T. *Tetrahedron Lett.*, **1975**, 16(49), 4393.
195. Adams G. E., Flockhart I. R., Smithen C. E., Stratford I. J., Wardman P., Watts M. E. *Radiat Res.*, **1976**, 67(1), 9.
196. Wardman P. *J. Phys. Chem. Ref. Data.*, **1989**, 18(4), 1637.
197. Schibli R., La Bella R., Alberto R., Garcia-Garayoa E., Ortner K., Abram U., Schubiger P.A. *Bioconjug. Chem.*, **2000**, 11, 345.
198. Banerjee S.R., Babich J.W., Zubieta J. *Inorganic Chemistry Communication*, **2004**, 7, 481.
199. Bhujanga Rao A. K. S., Gundu Rao C., Singh B. B. *J. Chem. Soc. Perkin Trans.*, **1994**, 1, 2399.
200. Mallia M. B., Subramanian S., Mathur A., Sarma H. D., Meera V., Banerjee S. *Bioorg. Med. Chem. Lett.*, **2008**, 18(19), 5233.
201. Allali M., Cousinié S., Gressier M., Tessier C., Beauchamp A. L., Coulais Y., Dartiguenave M., Benoist E. *Inorganica Chimica Acta*, **2006**, 359(7), 2128.
202. Lipowska M., He H., Xu X., Taylor A.T., Marzilli P.A., Marzilli L.G. *Inorg. Chem.*, **2010**, 49, 3141.
203. Pauletti G.M., Okumu F.W., Borchardt R.T. *Pharm. Res.*, **1997**, 14, 164.

204. Craig W.A., Welling P.G. *Clin. Pharmacokinet.*, **1977**, 2, 252.
205. W.J. Jusko, M. Gretch, Plasma and tissue protein binding of drugs in pharmacokinetics, *Drug Metab. Rev.* 5 (1976) 43-140.
206. Kedderis G.L., Miwa G.T. *Drug Metab. Rev.*, **1988**, 19, 33.
207. Sasai K., Iwai H., Yoshizawa T., Nishimoto S., Shibamoto Y., Kitakabu Y., Oya N., Takahashi M., Abe M. *Int. J. Radiat. Biol.*, **1992**, 62, 221.
208. Savi A., Gerundini P., Zoli P., Maffioli L., Compierchio A., Colombo F., Matarrese M., Deutsch E. *Eur J Nucl Med.*, **1989**, 15(9), 597.
209. Kelly J.D., Forster A.M., Higley B., Archer C.M., Booker F.S., Canning L.R., Chiu K.W., Edwards B., Gill H.K., McPartlin M, et al. *J. Nucl. Med.*, **1993**, 34(2), 222.
210. Liu S., He Z., Hsieh W.Y., Kim Y.S. *Nucl. Med. Biol.*, **2006**, 33(3), 419.
211. Reischl G., Ehrlichmann W., Bieg C., Kumar P., Wiebe L.I., Machulla H.J. *J. Nucl. Med.*, **2002**, 43(suppl), 364P.
212. Krohn K.A., Link J.M., Mason R.P. *J. Nucl. Med.*, **2008**, 49(suppl), 2, 129S-48S.
213. Kelly C.J., Brady M. *Phys. Med. Biol.*, **2006**, 51(22), 5859.
214. Padhani A.R., Krohn K.A., Lewis J.S., Alber M. *Eur. Radiol.*, **2007**, 17(4), 861.
215. Talbot J.N., Gutman F., Fartoux L., Grange J.D., Ganne N., Kerrou K., Grahek D., Montravers F., Poupon R., Rosmorduc O. *Eur. J. Nucl. Med. Mol. Imaging*, **2006**, 33(11), 1285.
216. Rahmim A., Zaidi H. *Nucl. Med. Commun.*, **2008**, 29(3), 193.
217. Hay M. P., Lee H. H., Wilson W. R., Roberts P. B., Denny W. A. *J. Med. Chem.*, **1995**, 38, 1928.
218. Mei L., Wang Y., Chu T. *Eur. J. Med chem.*, **2012**, 58, 50.

LIST OF PUBLICATIONS

1. On the structural modification of 2-nitroimidazole-^{99m}Tc(CO)₃ complex, a hypoxia marker, for improving in vivo pharmacokinetics
Mallia, M.B., Kumar, C., Mathur, A., Sarma, H.D., Banerjee, S.
(2012) *Nuclear Medicine and Biology*, 39 (8), pp. 1236-1242.
2. Synthesis and evaluation of 2-, 4-, 5-substituted nitroimidazole- iminodiacetic acid-^{99m}Tc(CO)₃ complexes to target hypoxic tumors
Mallia, M.B., Subramanian, S., Mathur, A., Sarma, H.D., Venkatesh, M., Banerjee, S.
(2010) *Journal of Labelled Compounds and Radiopharmaceuticals*, 53 (8), pp. 535-542.
3. Synthesis, radiolabeling and evaluation of ^{99m}Tc(CO)₃-labeled misonidazole analogue to target tumor hypoxia (*Abstract*)
Mallia, M.B., Mathur, A., Banerjee, S., Sarma, H.D., Venkatesh, M.
(2010) *Nuclear Medicine and Biology*, 37 (6), pp. 682-683.
4. On the isolation and evaluation of a novel unsubstituted 5-nitroimidazole derivative as an agent to target tumor hypoxia
Mallia, M.B., Subramanian, S., Mathur, A., Sarma, H.D., Venkatesh, M., Banerjee, S.
(2008) *Bioorganic and Medicinal Chemistry Letters*, 18 (19), pp. 5233-5237.
5. Comparing hypoxia-targeting potential of ^{99m}Tc(CO)₃-labeled 2-nitro and 4-nitroimidazole
Mallia, M.B., Subramanian, S., Mathur, A., Sarma, H.D., Venkatesh, M., Banerjee, S.
(2008) *Journal of Labelled Compounds and Radiopharmaceuticals*, 51 (8), pp. 308-313.
6. Evaluation of ^{99m}Tc(CO)₃ complex of 2-methyl-5-nitroimidazole as an agent for targeting tumor hypoxia
Mallia, M.B., Subramanian, S., Banerjee, S., Sarma, H.D., Venkatesh, M.
(2006) *Bioorganic and Medicinal Chemistry*, 14 (23), pp. 7666-7670.

7. A novel [^{99m}TcN] $^{2+}$ complex of metronidazole xanthate as a potential agent for targeting hypoxia

Mallia, M.B., Mathur, A., Subramanian, S., Banerjee, S., Sarma, H.D., Venkatesh, M.

(2005) *Bioorganic and Medicinal Chemistry Letters*, 15 (14), pp. 3398-3401.